

Carmen Chen

Mutagenesis of Uropathogenic *Escherichia coli* and its Effect on Macrophages

Master's thesis in Biotechnology

Supervisor: Harald Husebye

Co-supervisor: Caroline S. Gravastrand

May 2021

Carmen Chen

Mutagenesis of Uropathogenic *Escherichia coli* and its Effect on Macrophages



Master's thesis in Biotechnology
Supervisor: Harald Husebye
Co-supervisor: Caroline S. Gravastrand
May 2021

Norwegian University of Science and Technology
Faculty of Natural Sciences
Department of Biotechnology and Food Science



Abstract

Sepsis is a systemic inflammatory response to infection, which can lead to organ damage and death. Every year millions of people die from sepsis, yet the underlying mechanisms of sepsis pathophysiology are not well understood. In light of understanding the mechanisms behind bacterial triggered inflammatory cell death in macrophages that may provide new insights into sepsis pathophysiology, we sought to investigate which evasion strategies in a clinical isolated uropathogenic *Escherichia coli* strain (UPEC3) exploits to induce inflammatory cell death in human macrophages and how Rab11 family interacting protein 2 (FIP2) regulates pyroptosis. In the present study we demonstrated that the pore-forming protein, α -hemolysin (HlyA), in UPEC3 is a pivotal toxin that induced rapid inflammatory cell death in human macrophages. Deletion of *hlyA* showed strong decrease of caspase-1 and IL-1 β release from macrophages compared with UPEC3 wild type stimulated cells. In accordance with previous study from our group, FIP2 silencing also decreased the levels of released caspase-1 and IL-1 β in bacterial stimulated macrophages. In support to FIP2 promotes NLRP3 inflammasome activation, our data showed that the virulence factor TIR-domain containing protein C (TcpC) suppresses FIP2 from interacting with NLRP3 and caspase-1.

Acknowledgement

This master's thesis was conducted at Centre of Molecular Inflammation Research (CEMIR), Department of Clinical and Molecular Medicine in cooperation with the Department of Biotechnology and Food Science at the Norwegian University of Science and Technology (NTNU).

I would like to express my deep sense of gratitude to my principal supervisor Dr. Harald Husebye for his constant encouragement and guidance throughout my thesis. I am highly indebted to the PhD candidate, Caroline S. Gravastrand, for investing her time in teaching me and sharing her valuable knowledge and expertise. It was a great honour to be your master student.

I am very thankful to the director of CEMIR, Professor Terje Espevik for giving me the golden opportunity to write my master's thesis at CEMIR, and the help from Dr. Astrid Skjesol and Dr. Mariia Yurchenko in the laboratory. My appreciations also go to the people at CEMIR. Their kind attitude and helpfulness will never be forgotten. It was a pleasure for meeting all of you.

Finally, I would like to take my chance of extending my heartfelt thanks to my family and friends for showing their wholehearted encouragement, support and thoughtfulness.

Sincerely,
Carmen Chen
Trondheim, May 2021

Abbreviations

AIM2:	Absence of melanoma 2
AP-1:	Activator protein-1
ASC:	Apoptosis-associated speck-like protein containing a CARD
ATP:	Adenosine triphosphate
BSA:	Bovine Serum Albumin
CARD:	Caspase recruitment domain
Cas9:	CRISPR-associated protein 9
Caspase:	Cystein-aspartic protease
CLR:	C-type lectinreceptor
CNF1:	Cytotoxic necrotizing factor 1
CRISPR:	Clustered regularly interspaced palindromic repeat
crRNA:	CRISPR RNA
DAMP:	Damage associated pattern
DMSO:	Dimethyl sulfoxide
DNA:	Deoxyribonucleic acid
DsbA:	Thiol disulfide interchange protein
DTT:	Dithiothreitol
ELISA	Enzyme-linked immunosorbent assay
ERC:	Endosomal recycling compartment
ESCRT:	Endosomal sorting complex required for transpor
FADD:	Fas associated death domain
FBS:	Fetal Bovine Serum
FIP2:	Rab11 family interacting protein 2
GAP:	GTPase-activating protein
GDI:	Rab-GDP dissociation inhibitor
GDP:	Guanosine diphosphate
GEF:	Guanine-nucleotide exchange factor
GSDMD:	Gasdermin D
GSDMD-N:	N-terminus of GSDMD
GTP:	Guanosine triphosphate
Hcp:	Hemolysin-coregulated protein
HDAC6:	Histone deacetylase 6
HlyA:	α -Hemolysine
I κ B:	Inhibitor of κ B
IKK α :	Inhibitor of NF- κ B kinase subunit α

IKK β :	Inhibitor of NF- κ B kinase subunit β
IKK ϵ :	Inhibitor of NF- κ B kinase subunit ϵ
IKK:	Inhibitor of NF- κ B kinase
IL-1 β :	Interleukin-1 β
IL-18:	Interleukin-18
IRAK1:	IL-1R associated kinase 1
IRAK4:	IL-1R associated kinase 4
IRF3:	Interferon regulatory factor 3
LB	Lysogeny broth
LPS:	Lipopolysaccharide
MAL/TIRAP:	MyD88-adaptor-lik
MAPK:	Mitogen activated protein kinase
MLKL:	Mixed lineage kinase domaine-like
mRNA:	Messenger RNA
MTOC:	Microtubule organisin centre
MyD88:	Myeloid differentiation factor 8
Myo5b:	Mammalian myosin-5b
NEK7:	NIMA-related kinase 7
NEMO:	NF- κ B essential modulator
NF- κ B:	Nuclear factor- κ B
NLR:	Nucleotide-binding oligomerisation domain leucin rich repeats containing receptor
OmpT:	OmpT
OMV:	Outer membrane vesicle
PAK1:	p21-activated kinases 1
PAM:	Protospacer adjacent motif
PAMP:	Pathogen associated molecular pattern
PBS	Phosphate buffered saline
PCR	Polymerase chain reaction
PMA	Phorbol 12-myristate 13-acetate
PRR:	Pattern recognition receptor
Q-PCR	Quantitative polymerase chain reaction
RBD:	Rab11 binding domain
RIP1:	Receptor interacting protein
RIPK1:	Receptor interacting serine/ threonine kinase 1
RISC:	RNA-induced silencing complex
RLR:	Retinoic acid-inducible gene 1-like receptor
RNA:	Ribonucleic acid
RNAi:	RNA interference
SDS-PAGE:	Sodium dodecyl sulphate–polyacrylamide gel electrophoresis

siRNA:	Short interference RNA
TAK1:	Transforming-growth-factor- β -activated kinase
TBK1:	TANK-binding kinase 1
TBS-T:	Tris buffered saline-tween
TcpC:	TIR-domain containing protein C
TGN:	trans-Golgi network
TIR:	Toll/IL-1R
TLR:	Toll-like receptor
TNF α	Tumour necrosis factor α
TNFR:	Tumour necrosis factor receptor
tracrRNA:	trans-activating crRNA
TRAF3:	Tumor necrosis factor receptor-associated factor 3
TRAF6:	Tumour necrosis factor receptor-associated factor 6
TRAM:	TRIF related adaptor molecule
TRIF:	TIR-domain-containing adaptor protein inducing interferon- β
Tss:	Type six subunit
UBC13:	Ubiquitin-conjugating enzyme13
UEV1A:	Ubiquitin-conjugating enzyme E2 variant 1
UPEC:	uropathogenic <i>E. coli</i>
WT:	UPEC3 wild type
$\Delta cnf1/\Delta hlyA$:	UPEC3 <i>cnf1</i> and <i>hlyA</i> deletion double mutant
$\Delta cnf1/\Delta tcpC$:	UPEC3 <i>cnf1</i> and <i>tcpC</i> deletion double mutant
$\Delta cnf1$:	UPEC3 <i>cnf1</i> deletion mutant
$\Delta hlyA$:	UPEC3 <i>hlyA</i> deletion mutant
$\Delta ompT$:	UPEC3 <i>ompT</i> deletion mutant
$\Delta tcpC$:	UPEC3 <i>tcpC</i> deletion mutant

Table of Contents

1	Introduction	1
1.1	Innate immunity - the first line defence against infectious agents	1
1.2	The pattern recognition Toll-like receptors	2
1.3	Toll-like receptor 4 signalling	3
1.3.1	MyD88-dependent signalling pathway	3
1.3.2	TRIF-dependent signalling pathway	4
1.4	Endosomal trafficking	5
1.4.1	Phagocytosis - uptake of pathogens in phagocytic cells	6
1.4.2	Rab11 and FIP2 regulate phagocytosis	6
1.5	Inflammatory cell death	7
1.5.1	Pyroptosis	7
1.5.2	Canonical inflammasome signalling pathway	8
1.5.3	Non-canonical inflammasome pathway	9
1.5.4	Necroptosis	10
1.6	Immune evasion strategies in uropathogenic <i>Escherichia coli</i>	11
1.6.1	Cytotoxic necrotizing factor 1	11
1.6.2	Type I secretion system and the effector protein α -hemolysine	12
1.6.3	Type VI secretion system	13
1.6.4	TIR-domain containing protein C	14
1.6.5	Outer membrane vesicles	14
1.7	CRISPR-Cas9	14
2	Project Objectives	16
3	Materials and Methods	17
3.1	Bioinformatics	17

3.2	Plasmids isolation	18
3.3	Preparation of chemical and electrocompetent bacteria	19
3.3.1	Chemically competent bacteria	19
3.3.2	Electrocompetent bacteria	19
3.4	Transformation	20
3.4.1	Heat shock	20
3.4.2	Electroporation	20
3.5	Cloning CRISPR-Cas9 systems	21
3.5.1	Primer design	21
3.5.2	Isolation of genomic DNA from gram negative bacteria	22
3.5.3	Cloning CRISPR-constructs	22
3.6	Mutagenesis in UPEC3	23
3.6.1	Transformation of UPEC3	23
3.6.2	Plasmid curing	23
3.7	Growth curve	24
3.8	FIP2 silencing in THP-1 cells	24
3.8.1	Cell seeding	25
3.8.2	Lipofection - FIP2 silencing	25
3.9	Stimulation of THP-1 cells	25
3.9.1	LPS priming and NLRP3 inhibition	26
3.9.2	Preparation of bacteria samples	26
3.9.3	Bacterial and nigericin stimulation of THP-1 cells	26
3.10	LDH assay and supernatant storage	27
3.11	RNA isolation and real time quantitative polymerase chain reaction (Q-PCR)	27
3.11.1	RNA isolation from THP-1 cells	28
3.11.2	cDNA synthesis	28

3.11.3	Quantitative real time polymerase chain reaction (Q-PCR)	29
3.12	Protein isolation and western blot	30
3.12.1	Preparation of bacteria cultures for SDS-PAGE	30
3.12.2	Protein isolation from THP-1 cells and sample preparation for SDS-PAGE	31
3.12.3	SDS-PAGE	31
3.12.4	Protein transfer to membrane	32
3.12.5	Blocking and hybridisation with primary antibodies	32
3.12.6	Secondary antibody hybridisation and blot development	32
3.12.7	Semi-quantitative analysis of proteins by Western blot	33
3.12.8	Blot stripping	33
3.13	Enzyme-linked immunosorbent assay (ELISA)	33
3.13.1	Plate coating with capture antibodies and blocking	34
3.13.2	Serial dilution of IL-1 β standard and sample preparation	34
3.13.3	Hybridisation of enzyme-linked antibodies and signal detection	34
4	Results	35
4.1	Bioinformatic analysis	35
4.1.1	General bioinformatic analysis of <i>cnf1</i> , <i>dsbA</i> , <i>hlyA</i> , <i>ompT</i> and <i>tcpC</i>	35
4.1.2	Potential expression of type VI secretion system in <i>E. coli</i> UPEC3	41
4.2	Generation of uropathogenic <i>E. coli</i> mutants	45
4.2.1	Transformation efficiency	45
4.2.2	Genomic editing efficiency of pCRISPR constructs	45
4.2.3	Verification of gene deletion in UPEC3	48
4.2.4	Number of uptaken plasmids may affect the growth rate of UPEC3 strains	51
4.2.5	Expression and secretion of CNF1 and OmpT in UPEC3 wild type and mutants	54

4.3	Stimulation of THP-1 cells with <i>E. coli</i> strains	57
4.3.1	HlyA expressing UPEC3 strains induce massive cell lysis in THP-1 cells	57
4.3.2	FIP2 silencing and bacterial stimulation affect transcription of inflammatory cytokines in THP-1 cells	59
4.3.3	Post-translational maturation and release of caspase-1 and IL-1 β are affected by bacterial virulence factors	63
4.3.4	FIP2-silencing affects Rac1 stabilisation in UPEC3 stimulated THP-1 cells	68
4.3.5	FIP2-silencing reduces NLRP3 expression	68
4.3.6	FIP2 may involve in inflammasome activation	71
4.3.7	LPS priming enhances NLRP3 inflammasome signalling	72
4.3.8	Effect of FIP2-silencing resembles NLRP3-inhibition in THP-1 cells .	82
4.3.9	CNF1 and HlyA expressing UPEC3 strains upregulate expression of phosphorylated MLKL in THP-1 cells	85
4.3.10	HlyA in UPEC3 mediates degradation of NF- κ B p65 subunit in THP-1 cells	87
4.3.11	HlyA expressed in <i>E. coli</i> CFT073 and in UPEC3 may have different biological activities	89
5	Discussion	94
5.1	Bioinformatics analysis predicted expression of virulence factors in UPEC3 .	94
5.2	UPEC3 is efficiently transformed by electroporation	95
5.3	Editing efficiency increases with homology directed repair	95
5.4	Presence of plasmids in UPEC3 may affect the bacterial metabolism	96
5.5	HlyA induces rapid inflammatory cell death in THP-1 cells	96
5.6	HlyA deficient UPEC3 stimulated THP-1 cells increased cytokine mRNA levels	97
5.7	FIP2 stabilises Rac1 in THP-1 cells	98
5.8	TcpC suppresses FIP2 to promote NLRP3 inflammasome activation	99
5.9	LPS enhances NLRP3 inflammasome signalling	99

5.10	CNF1 promotes Rac1 deamidation and degradation, while HlyA triggers rapid NLRP3 inflammasome degradation	100
5.11	CNF1 and HlyA expressing UPEC3 stimulated cells show tendency to activate necroptosis in THP-1 cells	101
5.12	HlyA triggered protease activation may generate unconventional caspase-1 and IL-1 β intermediates in THP-1 cells	101
5.13	Different protein structures of HlyA expressed in CFT073 and UPEC3 may potentially affect their biological activities	102
5.14	Systemic response may differ from cellular response upon UPEC3 stimulation	102
6	Future Perspectives	104
7	Conclusion	106
	Appendix - Supplementary materials	118
A	Materials	118
A.1	Kits and reagents	118
A.2	Lysogeny broth (LB)	122
A.3	Minimal A medium	122
A.4	Electrophoresis buffer and gel preparation	123
A.5	Tris buffered saline-tween (TBS-T) buffer	123
B	Methods	124
B.1	Database and software	124
B.2	Cloning CRISPR-Cas9 constructs	126
C	Example calculations	134
C.1	Transformation efficiency	134
C.2	Genome editing efficiency	134
C.3	Generation time	135
C.4	Number seeded cells	136

C.5	Bacteria for cell infection	136
C.6	LDH release	137
C.7	Relative quantification value	137
C.8	Relative protein levels	139
C.9	Enzyme-linked immunosorbent assay	140
D	Results	141
D.1	Cloning CRISPR-Cas9 constructs	141
D.2	Genome editing efficiency	146
D.3	Sequence alignment of HlyA expressed in <i>E. coli</i> CFT073 and UPEC3 strains	147
D.4	Post-translational maturation and release of pro-caspase-1 and pro-IL-1 β were affected by bacterial virulence factors	149
D.5	LPS priming enhances NLRP3 inflammasome activation	150

List of Figures

1.1	Cellular location and tertiary structure of Toll-like receptors	3
1.2	Toll-like receptor 4 signalling pathways	5
1.3	FIP2 regulates phagocytosis	7
1.4	The molecular basis of regulation and activation of NLRP3 inflammasome .	10
1.5	Common secretion systems in bacteria	13
1.6	Clustered regularly interspaced palindromic repeats (CRISPR) and the CRISPR-associated protein 9 (Cas9)	15
4.1	Location of genes involved in type I secretion system and <i>cnf1</i>	39
4.2	Location of open reading frames which potentially encode type VI secretion system in UPEC3	43
4.3	Genome editing efficiency of pCRISPR constructs	47
4.4	Verification of <i>cnf1</i> and <i>hlyA</i> deletion in UPEC3 variants	50
4.5	Verification of <i>cnf1</i> and <i>tcpC</i> deletion in UPEC3 variants	51
4.6	Number of plasmids transformed into uropathogenic <i>E. coli</i> affects its growth	53
4.7	Immunoblott of CNF1	54
4.8	Detection of OmpT expressed in different <i>E. coli</i> strains that were cultivated with LB or minimal A medium	55
4.9	Growth curve of uropathogenic and avirulent <i>E. coli</i> in minimal A medium .	56
4.10	LDH release from THP-1 cells stimulated with UPEC3 variants	58
4.11	Pro-inflammatory cytokine mRNA expression level in THP-1 cells stimulated with UPEC3 wild type and different UPEC3 mutant clones	60
4.12	Pro-inflammatory cytokine mRNA expression levels in THP-1 cells stimulated with UPEC3 wild type and mutants	62
4.13	IL-1 β and caspase-1 levels in supernatants of THP-1 cells after 2 h and 4 h stimulation with UPEC3 wild type and mutants	65
4.14	Pro-IL-1 β and β -tubulin protein levels in cell lysates	67

4.15 FIP2, Rac1, NLRP3 and pro-caspase-1 protein levels in THP-1 lysates stimulated with UPEC3 wild type and mutants	70
4.16 GSDMD and cleaved GSDMD protein levels in THP-1 cells stimulated with UPEC3 wild type and mutants	72
4.17 Quantification of released LDH and IL-1 β in supernatants of THP-1 cells stimulated with nigericin, virulent and avirulent <i>E. coli</i>	73
4.18 Pro-caspase-1, caspase-1 p20, pro-IL-1 β and IL-1 β p17 protein levels in supernatants of THP-1 cells stimulated with nigericin or <i>E. coli</i> strains	75
4.19 FIP2, pro-IL-1 β , NLRP3, IFN β and TNF α mRNA levels in LPS primed THP-1 cells stimulated with nigericin, virulent and avirulent <i>E. coli</i> strains .	77
4.20 Western blot of FIP2, Rac1, NLRP3 and β -tubulin in THP-1 cells stimulated with nigericin, virulent and avirulent <i>E. coli</i> strains	80
4.21 Quantification of pro-caspase-1, pro-IL-1 β , GSDMD and N-terminus of GSDMD in THP-1 cells stimulated with nigericin, virulent and avirulent <i>E. coli</i> .	81
4.22 Released LDH, pro-IL-1 β and IL-1 β p17 from THP-1 cells treated with MCC950 and stimulated with nigericin, virulent and avirulent <i>E. coli</i> strains	84
4.23 Quantification of p-MLKL in THP-1 cells stimulated with nigericin, virulent and avirulent <i>E. coli</i>	86
4.24 Quantification of NF- κ B p65 subunit in THP-1 cells stimulated with nigericin, virulent and avirulent <i>E. coli</i> strains	88
4.25 Growth curve of uropathogenic and avirulent <i>E. coli</i> strains	89
4.26 Predicted secondary structures at the C-terminus of α -hemolysine with or without amino acids substitution	93
C.1 Standard curve of IL-1 β	140
D.2 Verification of insertion of oligonucleotides for guide annealing	142
D.3 Designed pCRISPR construct without homology arm	143
D.4 Verification of insertion of homology arms - restriction digestion	144
D.5 Verification of insertion of homology arms - colony PCR	145
D.6 Designed pCRISPR construct with homology arm	146
D.7 Colony PCR of transformed UPEC3	147

D.8	Sequence alignment of α -hemolysin expressed in <i>E. coli</i> CFT073 and UPEC3 strains	148
D.9	Pro-IL-1 β and pro-caspase-1 levels in supernatants of THP-1 cells after 2 h and 4 h of stimulation with UPEC3 wild type and mutants	149
D.10	Quantification of pro-caspase-1 and pro-IL-1 β protein levels in supernatants of THP-1 cells stimulated with nigericin or <i>E. coli</i> strains	150
D.11	Quantification of β -tubulin in THP-1 cells stimulated with nigericin, virulent and avirulent <i>E. coli</i> strains	150

List of Tables

3.1	Summary of parameters for pairwise alignment in LALIGN	18
3.2	Settings for transformation of electrocompetent bacteria	21
3.3	Settings for growth curve measurement	24
3.4	Composition of cDNA synthesis reaction mixture	29
3.5	Composition of reaction mixture for negative control of cDNA synthesis	29
3.6	Thermocycler settings for cDNA synthesis	29
3.7	Composition of reagents for one TaqMan qPCR reaction mixture	30
3.8	Settings for performing Q-PCR	30
4.1	General information of genes of interest	35
4.2	BLAST-analysis of proteins of interest	37
4.3	NCBI Conserved Domain Search	38
4.4	Prediction of operonic expression of genes involved in type I secretion system in UPEC3	39
4.5	BLAST analysis of proteins involved in type I secretion system in UPEC3	40
4.6	Number of curated proteins in different <i>E. coli</i> strains	41
4.7	BLAST analysis of open reading frames in UPEC3 which potentially encodes proteins involved in type VI secretion system	42

4.8	Search for conserved open reading frames in UPEC3 which encodes proteins involved in type VI secretion system	44
4.9	Transformation efficiency of chemical and electrocompetent UPEC3	45
4.10	Pairwise sequence alignment of contigs from whole genome sequencing of UPEC3 mutants with the expected DNA sequences of successful deleted genes	48
4.11	Pairwise sequence alignment of UPEC3 $\Delta cnf1$ bacterial genome with <i>hlyA</i> and the bacterial genome of UPEC3 $\Delta hlyA$ with <i>cnf1</i>	49
4.12	Generation time of UPEC3 variants	54
4.13	Generation time of <i>E. coli</i> strains	90
4.14	Comparison of amino acid residues in α -hemolysin expressed in <i>E. coli</i> CFT073 and UPEC3 strains	91
4.15	Confidence of predicted tertiary structures of α -hemolysin	92
A.1	Reagents	118
A.2	Kits	119
A.3	Primary antibodies	119
A.4	Secondary antibodies	119
A.5	TaqMan primers	120
A.6	Plasmids	120
A.7	Designed primers and guide sequences	121
A.8	Lysogeny broth (LB)	122
A.9	Minimal A medium - Part 1	122
A.10	Minimal A medium - Part 2	123
A.11	50 \times TAE buffer for electrophoresis	123
A.12	1 \times TBS-T buffer for membrane washing in Western blot	123
B.13	Summary of databases	124
B.14	Summary of software	125
B.15	Reagents for annealing and phosphorylating guide oligonucleotides	126

B.16 Reagents for Golden Gate Assembly of guide oligonucleotides and pCRISPR	126
B.17 Thermocycler settings for Golden Gate Assembly	127
B.18 Composition of colony PCR reagents	127
B.19 Thermocycler settings for colony PCR	128
B.20 Composition of reagents for restriction digestion	128
B.21 Reagents for amplification of upstream and downstream regions to target genes.	128
B.22 Thermocycler settings for amplification of upstream and downstream regions to <i>cnf1</i> and <i>tcpC</i>	129
B.23 Reagents for amplification of upstream and downstream regions to <i>dsbA</i> and <i>ompT</i>	129
B.24 Thermocycler settings cloning upstream and downstream regions to <i>dsbA</i> and <i>ompT</i>	129
B.25 Composition of reagents for overlap extension PCR	130
B.26 Settings for enrichment of overlap extension PCR products.	131
B.27 Composition of reagents for fusing upstream and downstream sequences of <i>dsbA</i>	131
B.28 Thermocycler settings for fusing upstream and downstream sequences of <i>dsbA</i>	131
B.29 Reagents for enrichment of homology arms of <i>dsbA</i>	132
B.30 Thermocycler settings for enrichment of homology arms of <i>dsbA</i>	132
B.31 Restriction digestion of overlap extension PCR product	132
B.32 Overnight ligation	133
C.33 Blot densities	139

1 Introduction

Sepsis is clinically defined as systemic inflammatory response to infection and is associated with high mortality [1, 2, 3]. In some cases, sepsis can lead to septic shock, which is collapse of the circulatory and the respiratory system and has a mortality rate of 90 % [4]. Often, sepsis occurs from infection of Gram-negative bacteria in blood, where macrophages, monocytes, neutrophils and vascular endothelial cells are stimulated and produce cytokines, chemokines, adhesion molecules and blood clotting factors [1, 2, 5]. Production of pro-inflammatory molecules and blood clotting factors can further leads to elevated body temperature, increased heartbeat and breathing rate, low blood pressure, tissue damage and compromised organ function. Moreover, immunosuppression and imbalanced homeostasis are also associated with sepsis pathogenesis [1, 4]. Every year, millions of people die from sepsis and currently there are no therapies available for sepsis treatment [2, 3]. As sepsis is considered as a global health burden, new insights into underlying mechanism(s) that drives sepsis pathophysiology are important for future development of accurate diagnosis and efficient therapies.

1.1 Innate immunity - the first line defence against infectious agents

Innate immune system is the first line of defence against pathogens, which includes cellular immunity and anatomical barrier that protects the body from invasion of microorganisms[1, 6]. Innate cellular immune responses are important for defending against pathogen invasion, clearance and initiate activation of the adaptive immune system by presenting antigen and production of cytokines [7, 8]. Cells derived from the myeloid lineage, such as monocytes, dendritic cells, neutrophils, etc., are the first responses to pathogen invasion. Unlike the innate immune system, adaptive immunity provides antigen-specific response at later stage of pathogen elimination. To activate naïve T-cells in the adaptive immune system, dendritic cells and differentiated monocytes, macrophages, are considerable for presenting derivatives of the microorganism and secreting cytokines that induce differentiation and maturation of T-cells [1, 7]. Mature T-cells can in turn induce B-cell maturation, proliferation, immunoglobulin class switching and differentiation into plasma cells [9, 10]. Nevertheless, activated B- and T-cells can create memory, which provides faster and stronger response to secondary infection [1, 11, 12].

1.2 The pattern recognition Toll-like receptors

Innate immune cells primary recognise invasive agents through pattern recognition receptors (PRRs) [1]. In general there are four major subfamilies of PRRs, namely, the Toll-like receptors (TLRs), the retinoic acid-inducible gene 1-like receptors (RLRs), the nucleotide-binding oligomerisation domain leucine rich repeats containing receptors (NLR) and C-type lectin receptors (CLRs) [13, 14]. These PRRs recognise pathogen associated molecular patterns (PAMPs), which are conserved motifs that are derived from pathogens. PRRs also bind to molecules from damaged cells or tissues, collectively defined as damage associated patterns (DAMPs) [1, 14].

The single transmembrane TLRs can be found on the plasma membrane or within endosomes [15]. The human cell surface TLRs are TLR1, TLR2, TLR4, TLR5, TLR6 and TLR10, while TLR3, TLR7, TLR8 and TLR9 are located in endosomes (Figure 1.1A) [16, 17]. In general, TLRs that are located on the plasma membrane recognise conserved surface ligands on the pathogens, such as lipopolysaccharides (LPS) and peptidoglycans in bacteria. On the other hand, the endosomal TLRs usually detect viral and bacterial nucleic acids [1].

TLRs are type I integral glycoproteins and have two unique domains. The N-terminus of TLRs is characterised with its horseshoe-shaped structure, that is composed with leucine rich repeats, decorated with N-linked glycans (Figure 1.1B) [15]. The N-terminus ectodomain is either facing to extracellular environment or endosome, where the glycan free region of N-terminus interacts with PAMPs or DAMPs. Across the transmembrane helix, the C-terminus at the cytosolic side, has a conserved Toll/IL-1R (TIR) domain, which serves as a docking site for adaptor proteins [16, 18]. Upon interaction between the ligand and the ectodomain, TLRs dimerise and bring two TIR domains to close proximity which further induce activation of downstream signalling pathways [15, 16]. Depending on adaptor proteins that interact with the TIR domains and formation of TLR homodimers or heterodimers, different signalling pathways become activated.

A

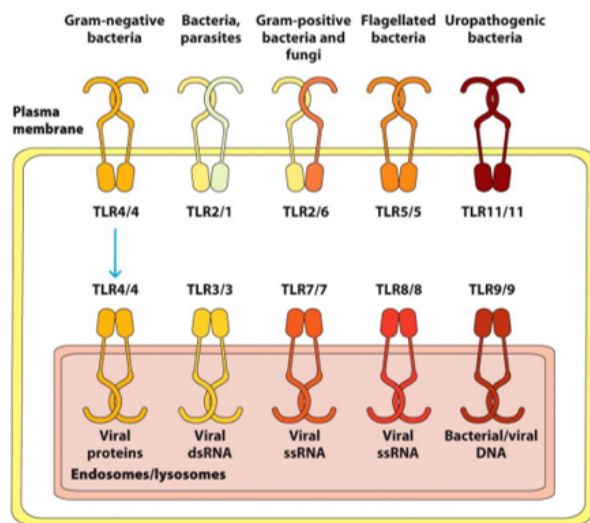


Figure 5-12
Kuby Immunology, Seventh Edition
© 2013 W.H. Freeman and Company

B

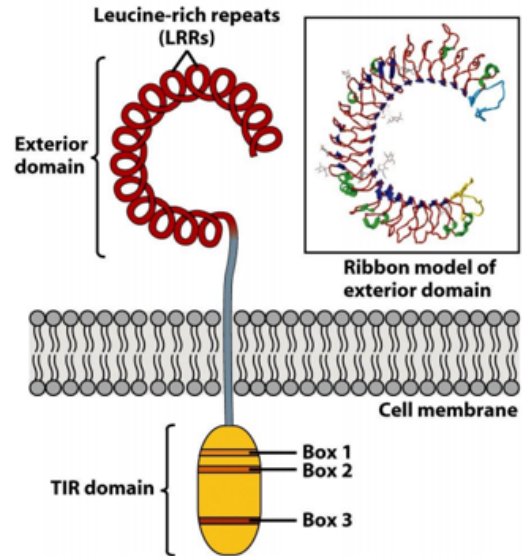


Figure 3-10
Kuby IMMUNOLOGY, Sixth Edition
© 2007 W.H. Freeman and Company

Figure 1.1: Cellular location and tertiary structure of Toll-like receptors. Human TLRs that are located on the plasma membrane are TLR1, TLR2, TLR4, TLR5, TLR6 and TLR10 (not shown on the figure), while TLR3, TLR7, TLR8 and TLR9 are found in endosomes (A). Representative tertiary structure of TLRs that has a horseshoe-shaped ectodomain with leucine-rich-repeats, and a cytoplasmic TIR domain (B). [Part (A) from *Judith Owen. Kuby immunology. Freeman, New York, 7th ed. edition, 2013.* Part (B): from *Judith Owen. Kuby immunology. Freeman, New York, 6th ed. edition, 2007*].

1.3 Toll-like receptor 4 signalling

To activate downstream signalling pathways to TLRs, recruitment of adaptor proteins with TIR domain are necessary. The adaptor proteins which bridge the TLRs and downstream kinases are myeloid differentiation factor 88 (MyD88), MyD88-adaptor-like (MAL/TIRAP), TIR-domain-containing adaptor protein inducing interferon- β (TRIF) and TRIF related adaptor molecule (TRAM) [19]. Intriguingly, each TLR recruits a specific combination of the adaptor proteins, which in turn activate different transcription factors that upregulate expression of inflammatory cytokines and type I interferons [20].

1.3.1 MyD88-dependent signalling pathway

Remarkably, myeloid differentiation 2 (MD-2) associated TLR4 can activate both MyD88- and TRIF-dependent pathways upon LPS stimulation [17, 20, 21]. To activate signalling proteins in the MyD88-dependent pathway in TLR4, association with MAL is indispensable for recruiting MyD88 to the TIR domain of TLR4. After MAL and MyD88 adaptors are associated with TLR4, IL-1R associated kinase 4 (IRAK4) is recruited immediately to MyD88 followed with IRAK1. IRAK1 and IRAK4 further activate tumour necrosis factor

receptor-associated factor 6 (TRAF6) which complexes with ubiquitin-conjugating enzyme 13 (UBC13) and ubiquitin-conjugating enzyme E2 variant 1 (UEV1A), resulting ubiquitination and activation of transforming-growth-factor- β -activated kinase (TAK1). Activated TAK1 further leads to phosphorylation of inhibitor of NF- κ B kinase (IKK) complex, which consist of NF- κ B essential modulator (NEMO), inhibitor of NF- κ B kinase subunit α (IKK α) and IKK β kinases. Subsequently, IKK complex phosphorylates inhibitor of κ B (I κ B), which in turn becomes ubiquitinated and degraded by proteasome [19, 20]. Degradation of I κ B releases nuclear factor- κ B (NF- κ B) from inhibition and can be proteosomal processed that allows the transcription factors to translocate into the nucleus as dimers and induce transcription of pro-inflammatory cytokines, such as pro-interleukin-1 β (pro-IL-1 β) [22, 23, 24]. Nevertheless, upon activation of TAK1, mitogen activated protein kinase (MAPK) pathway becomes activated, where kinases undergo phosphorylation cascade and finally activate the transcription factor activator protein-1 (AP-1) [19, 20].

1.3.2 TRIF-dependent signalling pathway

Alternatively, TRAM and TRIF adaptor proteins can be recruited to the TIR domain of TLR4. Like MAL, TRAM also binds to the plasma membrane and requires phosphorylation to be activated. Active TRAM recruits TRIF and activate tumor necrosis factor receptor-associated factor 3 (TRAF3). TRAF3 will in turn activate TANK-binding kinase 1 (TBK1) and IKK ϵ that phosphorylates the transcription factor interferon regulatory factor 3 (IRF3). IRF3 translocates into the nucleus and the IRF3 dimer binds to the DNA, resulting upregulation of transcription of IFN β [19, 20]. Interestingly, IRF3 induced gene expression through TLR4-TRAM-TRIF signalling is regulated by Rab11 family interacting protein 2 (FIP2) [25]. In addition to TRAF3 association with TRIF, TRAF6 and receptor interacting protein 1 (RIP1) can be recruited to TRIF, which activate NF- κ B signalling and possibly apoptosis via fas associated death domain (FADD) [19, 20].

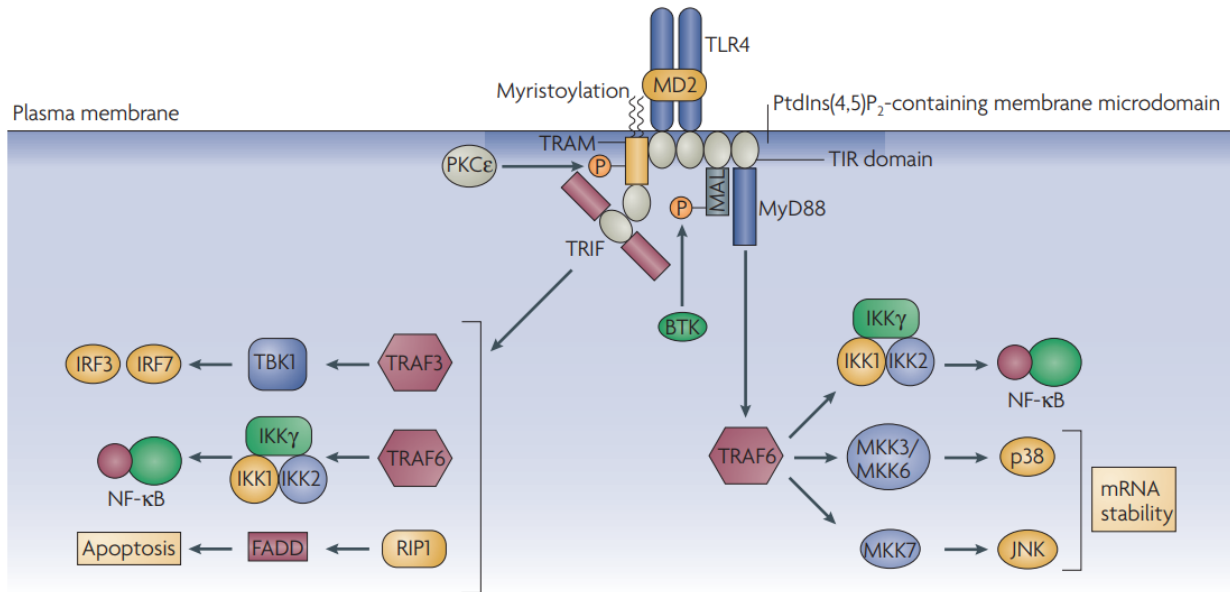


Figure 1.2: Toll-like receptor 4 signalling pathways. TLR4 signalling pathways can either be MyD88-dependent or TRIF-dependent. The MyD88-dependent signalling activate kinases in NF- κ B and MAPK signalling pathways and subsequently induce expression of IFN β and pro-inflammatory cytokines. TRIF-signalling pathway is activated through recruitment and phosphorylation of TRAM and TRIF to TLR4, which leads to upregulation of IFN β . TRIF- dependent signalling can also activate FADD and NF- κ B that are respectively involved in apoptosis and NF- κ B signalling pathway. [from: Luke A J O'Neill and Andrew G Bowie. *The family of five: Tir-domain-containing adaptors in toll-like receptor signalling. Nature Reviews Immunology*, 7(5):353–364,2007]

1.4 Endosomal trafficking

Endosomal trafficking is a dynamic, interconnected network of various of proteins that sort, transport and tether membranes during vesicle fusion. Endocytosed vesicles fuse to early endosomes, can undergo two distinct pathways, lysosomal degradation or retrieval to plasma membrane. In early endosomes, endosomal sorting complex required for transport (ESCRT) machinery sorts cargoes for degradation or recycling [26]. Cargoes sorted for degradation in early endosomes matures to late endosomes and forms multivesicular bodies by inward budding, which fuse with lysosomes. Cargoes that undergo the retrieval fate can be transported to the plasma membrane from the early endosome, endosomal recycling compartment (ERC) or Golgi [27].

During maturation of endosomes, the pH decreases and allows for directional transportation by altering membrane phosphatidylinositol phospholipids compositions, recruitment and activation of the small GTPases, Rab [28]. The human genome encodes more than 60 Rabs and is the largest family within monomeric GTPase subfamily [6, 29]. Rab GTPases are mainly involved in intracellular trafficking and it contributes defining endomembrane identity, where each Rab protein is associated with one or more organelles. Nevertheless Rab

regulates vesicle formation, vesicle fusion and guides cargo trafficking to its destination by recruiting unique sets of effector proteins upon activation. Inactive Rab is bound to Rab-GDP dissociation inhibitor (GDI) and keeps the small GTPase in the cytosol. Similar to other small GTPase families, Rab becomes activated when guanosine diphosphate (GDP) is exchanged with guanosine triphosphate (GTP) by guanine-nucleotide exchange factor (GEF). Active Rab binds to membrane of organelles or vesicles and recruits Rab effectors, such as phosphatidylinositol kinases, motor proteins that walk on actin filaments or microtubules and tethering proteins that are involved in vesicle fusion. Upon association with GTPase-activating protein (GAP) GTP is hydrolysed to GDP and Rab is back to its inactive state [6, 28].

1.4.1 Phagocytosis - uptake of pathogens in phagocytic cells

Phagocytosis is one of the multiple molecule uptake mechanisms of endocytosis. Pathogens that have breached the anatomical barrier, encounter phagocytic cells, e.g. macrophages, neutrophils, dendritic cells etc., that engulf microorganisms through phagocytosis. Phagocytic cells recognise PAMPs via PRRs, which triggers remodelling of cytoskeleton and evaginate the plasma membrane to form a phagocytic cup that facilitate the uptake of the pathogen [1]. In addition to PRRs, opsonic receptors, such as Fc receptors also mediate uptake of microorganisms by recognising soluble proteins, opsonins, that binds to conserved domains on the surface of the pathogens [1, 30]. Pathogen that has been fully ingested in enclosed vacuole (phagosome) is transported inside the cell and gradually mature to phagolysosome. During the maturation process of phagosome, the membrane composition of phagosome changes with a series of vesicle fusion and fission. Finally, fusion with lysosome allows lysosomal enzymes, reactive oxygen species and antimicrobial agents to disintegrate the microorganism [30].

1.4.2 Rab11 and FIP2 regulate phagocytosis

In addition to Rab4, Rab11 has been found in ERC and it is an important small GTPase for trafficking of TLR4 and TRAM from ERC to *E. coli* phagosomes, allowing TRIF signalling activation and upregulation of IRF3 induced gene expression [6, 25, 31]. Nevertheless, FIP2 has been shown to bridge Rab11 and TRAM, which is critical for transportation of TRAM and TLR4 to phagosomes [25]. There are three characterised domains in FIP2, Rab11 binding domain (RBD) at the C-terminus, C2 domain at the N-terminus and the central Myo5b domain. FIP2 links Rab11 to TRAM by interacting with Rab11 at the C-terminus and TRAM that binds between the C2 domain and Myo5b domain [25, 32]. The C2 domain is a calcium ion-binding domain, which induce interaction with phospholipids, whereas Myo5b domain binds the motor protein, mammalian myosin-5b (Myo5b) that propels on actin

filaments and delivers cargo to its destination [32, 33, 34]. Upon bacterial stimulation, FIP2 complexes with Rab11 and TRAM and the complex is transported from ERC to the plasma membrane. FIP2 stabilises the small GTPases, Rac1 and Cdc42, and induce actin polymerisation that facilitate formation of the phagocytic cup (Figure 1.3) [25].

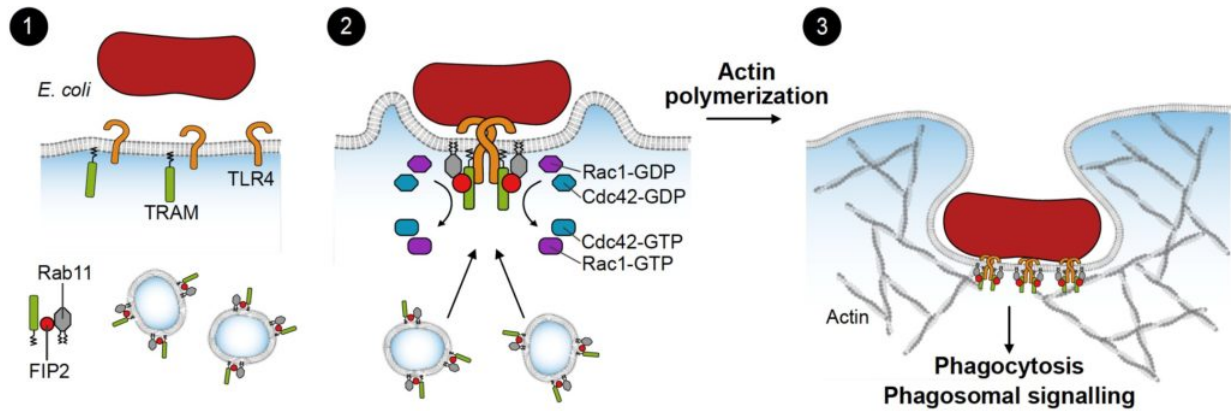


Figure 1.3: FIP2 regulates phagocytosis. FIP2 bridges Rab11 and TRAM and are trafficked to the plasma membrane upon bacterial stimulation. FIP2 stabilises Rac1 and Cdc42 and mediate formation of phagocytic cup. [from: Sporsheim, Bjørnar. "Model describing molecules involved in bacterial uptake (phagocytosis) in an immune cell." *En fagblogg om medisin og helse ved NTNU*. 21 June 2019. <https://blog.medisin.ntnu.no/en/new-protein-may-control-serious-inflammatory-reactions/>].

1.5 Inflammatory cell death

In multicellular organisms, homeostasis of cell number, organ differentiation and elimination of damaged or infected cells are tightly controlled by cell death programs. Among the various types of cell death mechanism, the inflammatory death modes, pyroptosis and necroptosis are often activated in infected cells [14].

1.5.1 Pyroptosis

Activation of pyroptosis upregulates expression of pro-inflammatory cytokines and chemokines as an inflammatory response to fight back invasive pathogens. However, activation of inflammatory signalling pathways can also leads to the infected cells to commit suicide. Pyroptotic cell death is characterised by activation of the inflammatory caspase-1 and caspase-4/5 in human. In general, the canonical model of activating pyroptosis involves formation of inflammasome which usually consist a sensor, adaptor and an effector proteins. There are two main type of sensors, NLRs or those that only contain a pyrin domain, such as absence of melanoma 2 (AIM2) and pyrin. The sensors usually associate with adaptor protein apoptosis-associated speck-like protein containing a CARD (ASC), which interacts with pro-caspase-1 through the caspase recruitment domain (CARD) [35]. The NLR, AIM2 and pyrin

sensors are also cytosolic PRRs, which recognise PAMPs, DAMPs or small molecules such as adenosine triphosphate (ATP) [36]. Among the inflammasomes, NLRP3 is the best characterised inflammasome. NLRP3 contains a leucine rich repeat domain, a pyrin domain at the N-terminus that interacts with the pyrin domain in ASC. The central nucleotide binding domain is crucial for oligomerisation upon activation [37].

1.5.2 Canonical inflammasome signalling pathway

To activate NLRP3 inflammasome, two signals are required (Figure 1.4). Signal 1, priming the cells with pathogen derivatives, such as LPS, upregulates the expression of pro-inflammatory cytokines and NLRP3 by activating NF- κ B signalling pathway through TLR4. Moreover, NLRP3 is also deubiquitinated and phosphorylated as well as ASC and caspase-1 during the priming step [37, 38]. Signal 2, is necessary for activating NLRP3 assembly to a functional inflammasome. During the activation step, potassium efflux triggers NLRP3 inflammasome activation. Furthermore, some studies have shown that calcium release from the endoplasmic reticulum also induces NLRP3 oligomerisation, while another study demonstrated that increase of the cytosolic calcium concentration is dispensable. Release of oxidised mitochondrial DNA, reactive oxygen species and lysosomal destabilisation have also been proposed for involving NLRP3 activation [37].

Importantly, it has been revealed that NIMA-related kinase 7 (NEK7) plays an essential role in NLRP3 activation, where it oligomerises with NLRP3 and it is important for ASC speck formation [35, 37]. During the activation step, different domains within NLRP3 undergo phosphorylation and dephosphorylation, while the CARD domain of ASC is phosphorylated [38]. All of these events trigger NLRP3 oligomerisation and association with ASC, which further recruits pro-caspase-1. Cleavage of pro-caspase-1 generates caspase-1 p20 which processes pro-IL-1 β to IL-1 β p17 and released to the environment. Caspase-1 p20 also cleaves gasdermin D (GSDMD), and cleaved GSDMD N-terminus translocates to the plasma membrane where it oligomerises and forms pores, causing potassium efflux, influx of water and cytokine release. As a result, the cells swell and die due to osmotic lysis [35].

Interestingly, studies have shown Golgi is involved in docking NLRP3 and regulate NLRP3 activation. For instance, protein kinase D at the Golgi has been shown to be critical for NLRP3 phosphorylation that facilitate self-oligomerised NLRP3 to dissociate from endoplasmic reticulum membrane and assembles to NLRP3 inflammasome [39]. It has also been observed that NLRP3 was recruited to disassembled trans-Golgi network (TGN), where it serves as a platform for NLRP3 aggregation and polymerisation with ASC [40]. From a recent publication, small aggregates of NLRP3 were found in TGN and the data showed that these aggregates were transported from TGN to microtubule organising centre (MTOC), which is mediated by dynein adaptor, histone deacetylase 6 (HDAC6). HDAC6 bound to

dynein transports cargo with NLRP3 components to MTOC, where NLRP3 interacts with NEK7, forms single speck and cleaves pro-IL-1 β and GSDMD [41]. Recent unpublished data from our group have shown that FIP2 frequently associates with trans-Golgi network, MTOC as well as ASC specks. Intriguingly, FIP2 also interacts with NLRP3 and caspase-1. THP-1 cells treated with FIP2 siRNA impaired ASC specks formation and decreased release of cleaved caspase-1 20 and IL-1 β 17 [42].

1.5.3 Non-canonical inflammasome pathway

In contrast to the canonical inflammasome pathway, in the non-canonical inflammasome pathway, intracellular LPS can directly interact and activate caspase-4 or caspase-5 without any receptor proteins. Caspase-4 and caspase-5 cleave GSDMD which subsequently can activate the canonical inflammasome pathway by inducing efflux of potassium through GSDMD pores on the plasma membrane (Figure 1.4) [35, 37].

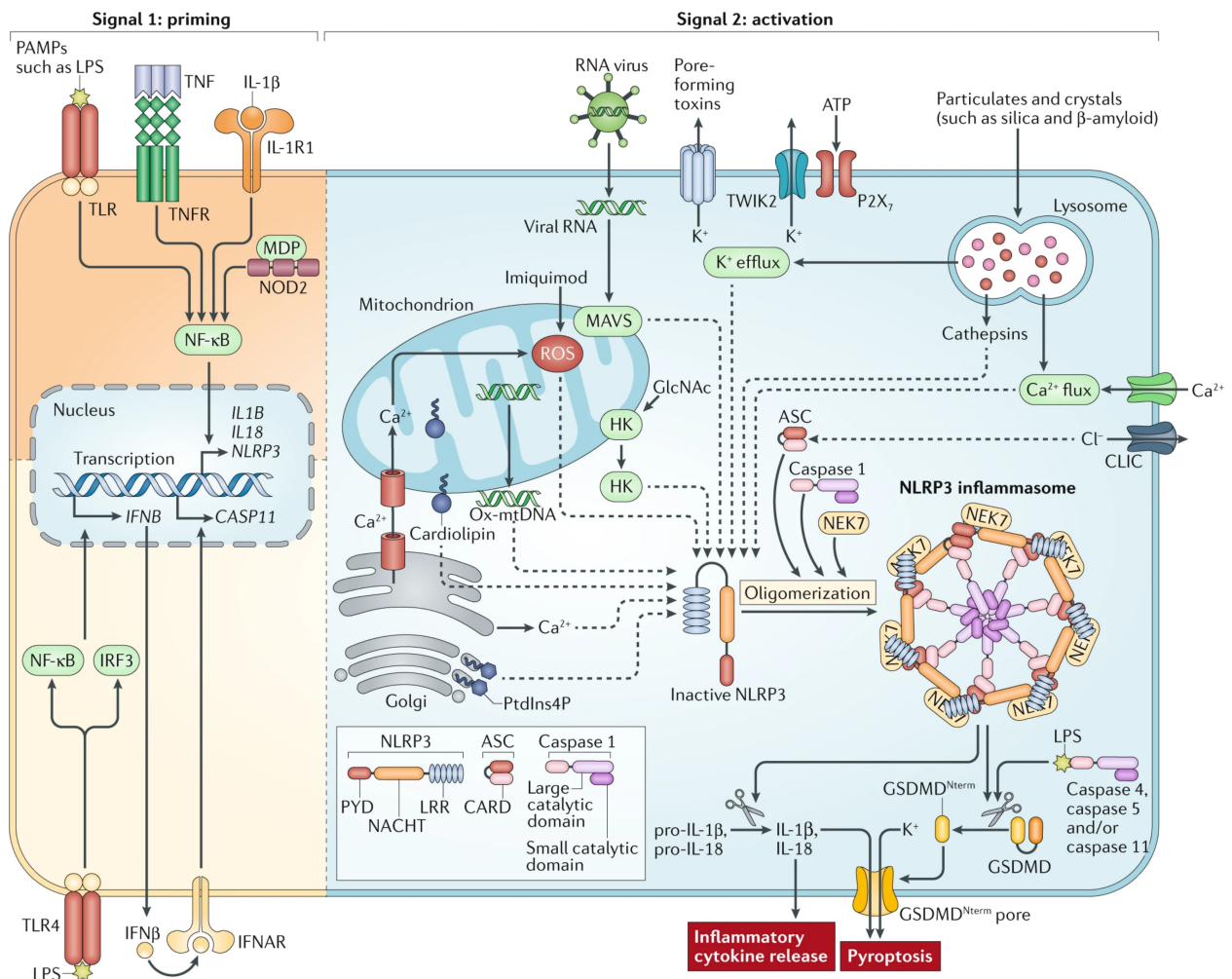


Figure 1.4: The molecular basis of regulation and activation of NLRP3 inflammasome. Signal 1: the priming step, stimulation of TLRs with PAMPs, activates NF- κ B which upregulates expression of pro-inflammatory cytokines, such as pro-IL-1 β , pro-interleukin-18 (pro-IL-18) and NLRP3. Efflux of potassium, increased intracellular calcium concentration, lysosome degradation, release of reactive oxygen species are among the events that induce assembly and activation of NLRP3 inflammasome in the canonical pathway (signal 2). Active NLRP3 inflammasome cleaves pro-IL-1 β and GSDMD. IL-1 β are released to the extracellular environment, while oligomerisation of GSDMD N-terminal on the plasma membrane accelerates efflux of potassium and release of cytokines. In the non-canonical pathway, GSDMD can be cleaved by active caspase-4 or caspase-5 upon direct LPS stimulation. [from Karen V Swanson, Meng Deng, and Jenny P-Y Ting. *The nlrp3 inflammasome: molecular activation and regulation to therapeutics. Nature Reviews Immunology*, 19(8):477-489, 2019]

1.5.4 Necroptosis

Activation of necroptosis can be triggered by dissociation of receptor interacting serine/threonine kinase 1 (RIPK1) from tumour necrosis factor receptor (TNFR) and formation of complex IIb, which is composed by FADD, RIPK1 and RIKP3. Phosphorylated RIKP1 and RIKP3 activate mixed lineage kinase domain-like (MLKL) that oligomerise to pores on the plasma membrane. Interestingly, active caspase-8 cleaves RIPK1 and RIPK3, shifting

toward apoptotic signalling pathway [43, 44, 45]. Furthermore, TLR4 and TRAM can activate RIPK3 directly via TRIF, which further induce MLKL phosphorylation. Remarkably, damaged plasma membrane caused by MLKL oligomers, can be shedded out by ESCRT-III machinery. Repairing the damaged cell membrane and potentially rescuing the cell from lysis [14, 43].

1.6 Immune evasion strategies in uropathogenic *Escherichia coli*

Escherichia coli (*E. coli*) are rod-shaped Gram-negative bacteria. The cell wall of *E. coli* consist of two membrane layers, an inner and outer membrane. Between the outer and inner membrane, there is a peptidoglycan layer. The outer membrane is also decorated with lipopolysaccharides (LPS), which are composed by lipid A, core polysaccharide and an O-antigen. The core polysaccharide is attached to lipid A, and it is a chain of non-repeating oligosaccharide. Unlike the core polysaccharide, O-antigen is composed of repeating oligosaccharide and is the most diverse component of LPS. Lipid A is relatively conserved which is often recognised by TLR4 [46]. Upon stimulation of TLR4, *E. coli* can be phagocytosed and subsequently activate MyD88-dependent or TRIF-dependent signalling pathway that induce transcription of pro-inflammatory cytokines [25]. Eliminating the pathogen and attract leukocytes to the infection site. As the bacteria strive to survive from being eliminated by immune cells, the bacteria have evolved with several different evasion strategies to counteract host's immune system.

1.6.1 Cytotoxic necrotizing factor 1

The cytotoxic necrotizing factor 1 (CNF1) is a deamidating toxin which is secreted from the bacteria and it is often expressed in uropathogenic *E. coli* (UPEC). CNF1 has a conserved domain at the C-terminus that is responsible for catalysing deamidation of glutamine 61 in Rac1 and Cdc42, and glutamine 63 in RhoA [47]. Study has shown that constitutive activation of Rac1 triggers ubiquitin-proteasomal degradation of the small GTPase protein, which facilitate *E. coli* host invasion [48]. The the N-terminal has been characterised for its importance of receptor binding and internalisation of the toxin into the target cell [49]. Interestingly, decreased pH induces conformational change of CNF1 which facilitate its release from endosomes to cytosol [50]. Deamidation of Rho GTPases leads to actin polymerisation which can activate NLRP3 inflammasome through p21-activated kinases 1 (PAK1). PAK1 phosphorylates threonine 659 of NLRP3 which is important for recruitment of NEK7 and NLRP3 inflammasome assembly [51].

1.6.2 Type I secretion system and the effector protein α -hemolysine

Interestingly, *cnf1* is localised downstream to hlyCABD operon and these genes are often co-expressed [52]. The hlyCABD operon encodes type I secretion system with α -hemolysine (HlyA) as effector protein (Figure 1.5). N-terminus of HlyA has a hydrophobic α -helical structure that binds to the target cell membrane and regulate its activity [53, 54]. The RTX motif with a consensus sequence GGXGXDXUX (G: Glycine, X: any residue, U: hydrophobic residue), is located close to the C-terminus. This motif binds to calcium ions that stabilise the protein structure, which is important for recognition of target cell. Finally, the C-terminus region of HlyA serves as a secretion signal, but the protein is not cleaved upon release [53]. Nevertheless, myristylation of lysine 564 and lysine 690 residues are essential post-translational modifications for HlyA activity.

Secreted HlyA can bind to the target cell and subsequently oligomerise to form pores on the plasma membrane. High concentration of HlyA can directly lead to cell lysis, whereas sublytic concentration of HlyA can stimulate inflammasome signalling by increasing the membrane permeability that leads to efflux of calcium and potassium ions. Low concentration of HlyA can stimulate superoxide production as well as IL-1 synthesis [53]. According to a publication, HlyA showed inhibition of CNF1 induced inflammatory response [55]. The study demonstrated the concept by infecting mice with *E. coli* wild type, *cnf1*, *hlyA* single deletion mutants and *cnf1* and *hlyA* double deletion mutant. Interestingly, mice that were subjected to *hlyA* single deletion mutant had a higher sera concentration of IL-1 β than *E. coli* wild type, *cnf1* single deletion and *cnf1* and *hlyA* double deletion mutant.

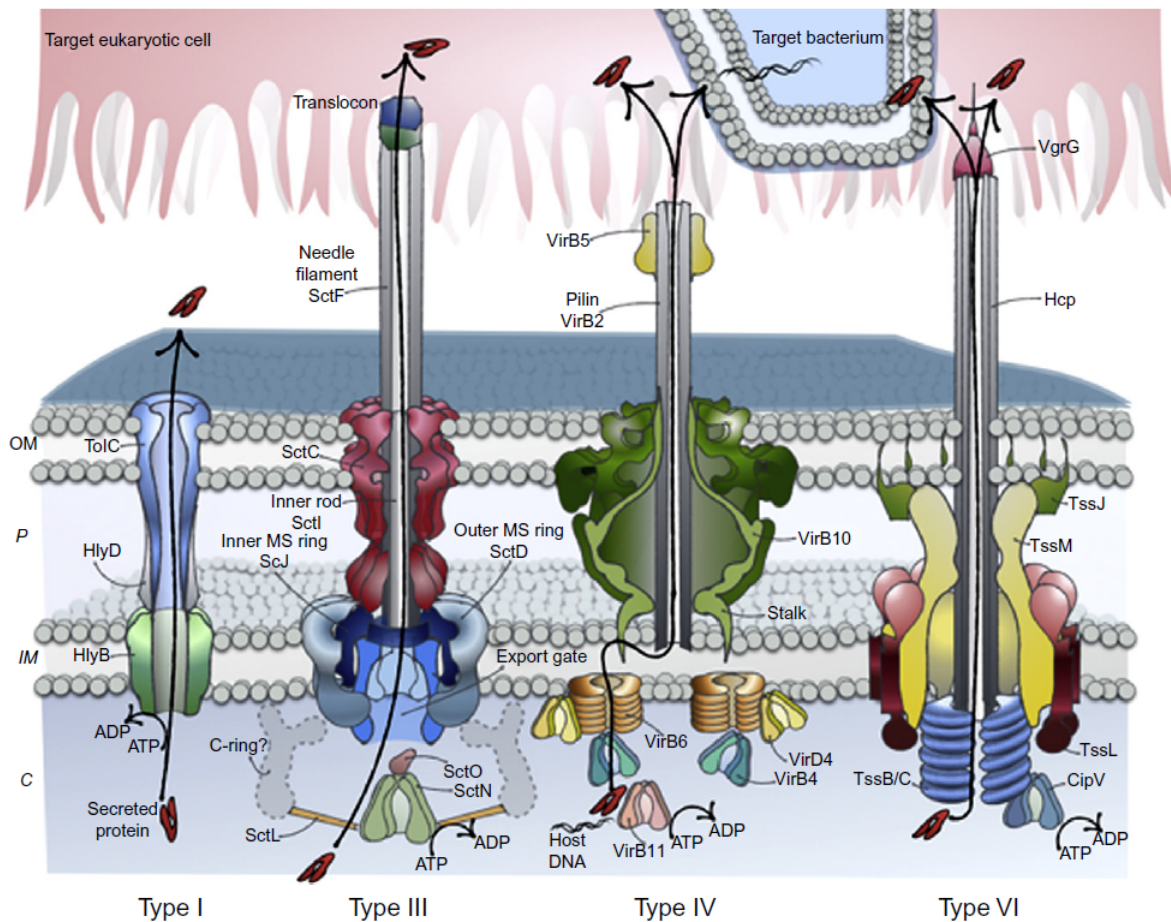


Figure 1.5: Common secretion systems in bacteria. Type I, III, IV and VI secretion systems are illustrated with their respective subunits and effector proteins. OM: Outer membrane. P: Periplasm. IM: Inner membrane. C: cytoplasm. [from: *Alexandre Chenal, AC Sotomayor-Perez, and Daniel Ladant. The Comprehensive Sourcebook of Bacterial Protein Toxins. Elsevier Amsterdam, 4th edition, 2015.*]

1.6.3 Type VI secretion system

Type VI secretion system (T6SS) is a bacterial self defence mechanism to distinguish and protect from non-self, but it has also been identified in many pathogenic Gram-negative bacteria [56, 57, 58, 59, 60]. T6SS may impair the innate immunity by inhibiting phagocytosis and production of pro-inflammatory cytokines and chemokines, induce expression of immunosuppressive cytokines and facilitate bacterial spread in organs [58].

T6SS is composed by several protein subunits (Figure 1.5). In short, type six subunit (Tss), TssJ, TssL and TssM associate to form a channel between the bacterial outer and inner membrane, where the baseplate complex and the effector proteins get through. TssE and TssK form the baseplate complex as a platform for loading effector proteins, such as VgrG and PAAR domain containing proteins. The effector proteins are delivered through a contraction mechanism, which involves hemolysin-coregulated protein (Hcp) tube poly-

merisation, followed with association of TssB/TssC (VipA/VipB) around the Hcp tube [56]. The Hcp tube associated with polymerised VipA/VipB, contracts and delivers effector proteins. Finally, TssH (ClpV) consumes ATP to disassemble the contracted sheet, which allows reassembly of Hcp tube and association with VipA/VipB [56]. Interestingly, Hcp family proteins are also secretory proteins and can stimulate release of cytokines from human brain microvascular endothelial cells and murine macrophages [58, 59].

1.6.4 TIR-domain containing protein C

(TcpC) has been observed to suppress innate immunity by impairing the TLR signalling pathway and inhibit activation of NLRP3 inflammasome [61, 62]. TLR signalling pathway can be inhibited by TcpC, where it directly interacts with MyD88 and TLR4, suppressing transcription of NF- κ B, IRF7, IL-1 α , IL-1 β , TNF- α , IL-8 and IL-6 [61]. In addition to suppressing transcription of pro-inflammatory cytokines, TcpC also interferes assembly of NLRP3 inflammasome by binding to NLRP3 and caspase-1 via its TIR-domain [62].

1.6.5 Outer membrane vesicles

Outer membrane vesicles (OMVs) are often secreted from Gram-negative bacteria and are important for the bacteria to detoxify toxic compounds and misfolded proteins. Interestingly, bacterial DNA, RNA and plasmids have also been reported in OMVs, but the mechanism of incorporating nucleic acids into OMVs is not yet well understood [63]. Currently, there is no unified mechanism of OMV biogenesis, but studies have shown deletion of OmpT (*ompT*) and thiol disulfide interchange protein (*dsbA*) decreased OMV production in *E. coli* [63, 64, 65]. In addition to regulation of OMVs, DsbA is an important protein in the periplasma of Gram-negative bacteria, where it catalyses disulfide bonds in proteins [66]. Moreover, OMVs can also serve as a delivery system of toxins, such as CNF1 [67]. A recent study showed HlyA can be transported with LPS in OMVs. Endocytosed OMVs can release LPS when HlyA disrupts the vesicles [68]. Released LPS into cytosol activate human caspase-4 and murine caspase-11 in the non-canonical inflammasome signalling pathway [68, 69].

1.7 CRISPR-Cas9

Clustered regularly interspaced palindromic repeats (CRISPRs) and the CRISPR-associated protein 9 (Cas9) originated from bacterial adaptive immune defence against bacteriophages and has now become a gene editing tool to edit the genome of a desired organism (Figure 1.6). Cas9 is a nuclease with HNH and RuvC-like domains that induce double strand break of the DNA. To direct Cas9 to the target site (protospacer), the nuclease complexes with the

antirepeat-repeat RNA duplex, which consist of CRISPR RNA (crRNA) and trans-activating crRNA (tracrRNA). When the 20 nucleotides (spacer) of crRNA basepair with the target site, Cas9 induces site specific double strand DNA break next to the protospacer adjacent motif (PAM), which is NGG (N: any nucleotide, G: guanine) [70].

Despite CRISPR-Cas9 has been a breakthrough in genome editing, the editing efficiency is one of the aspects which require further improvement. Studies have shown by cloning homology arm into CRISPR-Cas9 plasmid, the editing efficiency was improved. The homology arm is a fused product of upstream and downstream regions of the target gene, which allows homology directed repair of the genome after DNA cleavage by Cas9 [71, 72, 73]. Furthermore, designing the spacer with high guanine and cytosine (GC) content also increases editing efficiency of CRISPR-Cas9 [74].

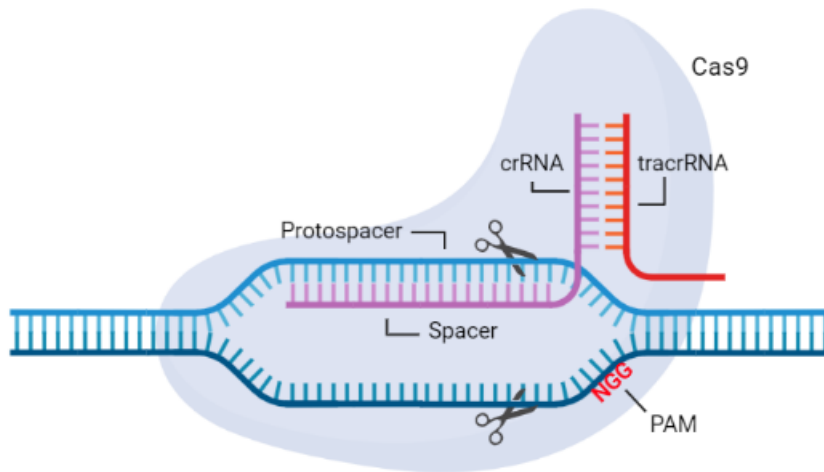


Figure 1.6: Clustered regularly interspaced palindromic repeats (CRISPR) and the CRISPR-associated protein 9 (Cas9). Cas9 is guided by 20 nucleotide long spacer of the antirepeat-repeat RNA complex (tracrRNA:crRNA). Spacer basepairs with the protospacer next to the NGG (N: any nucleotide, G: guanine) protospacer adjacent motif (PAM) and induces Cas9 to cleave double stranded DNA at the target site. [Made with [BioRender](#)].

2 Project Objectives

The Gram-negative bacteria *E. coli* is the most common isolated pathogen from urosepsis patients. Similar to other types of sepsis, urosepsis can be life-threatening due to activation of systemic inflammatory response that leads to organ failure [75, 76, 77]. Over time, pathogenic bacteria have evolved with various of evasion strategies to cope the host's immune response. Thus, understanding the fundamental mechanisms behind evasion strategies and interaction between pathogen and innate immune cells will provide insights into sepsis pathophysiology.

Previously, our group has reported phagocytosis of bacteria in human macrophages depends on FIP2 and TRAM [25]. Recent unpublished data have also shown that FIP2 interacts with NLRP3 and caspase-1 [42]. Nevertheless, our group has also observed FIP2 frequently co-localises with ASC specks, MTOC and trans-Golgi network (TGN) [42]. In light of FIP2 has an essential role in phagocytosis and pyroptosis, we speculate regulating FIP2 expression may affect inflammatory cell death in macrophages upon stimulation with Gram-negative bacteria.

Within our scope of study, we will investigate how Gram-negative bacteria stimulate inflammatory cell death in macrophages and the effect of FIP2 silencing has on bacterial stimulated cells. To accomplish the goals of our study, we will focus on the following objectives:

Objective 1: Identify and localise virulent genes of interest in the genome of a clinical isolated uropathogenic *E. coli* strain (UPEC3).

Objective 2: Establish CRISPR-Cas9 constructs which specifically target genes of interest in UPEC3.

Objective 3: Establish UPEC3 mutants by utilising CRISPR-Cas9 and validate successful gene deletion.

Objective 4: Stimulate human macrophages, THP-1 cells, with UPEC3 wild type and mutants and analyse cytokine expression level and activation of NLRP3 inflammasomes.

Objective 5: Investigate the effect of FIP2 in context of NLRP3 induced cell death by using RNA interference gene silencing technology.

3 Materials and Methods

All reagents, kits, antibodies and media used in this study are attached to Appendix, [section A.1](#).

3.1 Bioinformatics

Basic local alignment tool and conserved domain search are bioinformatics tools, which quickly predict protein homology, detect characteristic and functional domains within an open reading frame by comparing the query sequences with the existing sequences in databases [78, 79]. Modelling tertiary structure of the protein of interest also provides information about the effect of amino acids variation and its biological activity [80].

The genomic DNA of the clinical isolate of uropathogenic *Escherichia coli* strain 3 (UPEC3) was sequenced and most of the genes were previously annotated. Location of the genes of interest *cnf1*, *hlyA*, *ompT* and *tcpC* were identified from the annotation file obtained from Jostein Johansen in Jan Egil Afset research group at St. Olavs hospital, Clinic of Laboratory Medicine. In addition to *cnf1*, *hlyA* and *tcpC*, *ompT* and *dsbA* were also investigated in this study. The location of *dsbA* was performed by multiple peptide sequence alignment. First, nucleotide sequences of the contigs were translated into peptide sequences by [EMBOSS Transeq](#) in all frames, which consist three frames in the forward and reverse direction. Moreover, the codon table for bacteria was selected. The output from EMBOSS Transeq was then used to align with the reference peptide sequence of DsbA from UniProt (entry: [P0AEG4](#)). After *dsbA* was localised, the peptide sequence was further analysed with NCBI basic local alignment tool ([BLASTP](#)) and [NCBI Conserved Domain Search](#) to predict the sequence similarity and identity of DsbA that is expressed by UPEC3. Similarly, CNF1, HlyA, OmpT and TcpC were analysed with the same bioinformatics software.

The database [UniProtKB](#) or [Protein Data Bank](#) were selected for the [BLASTP](#)-analysis, where the query sequences were searched against the library sequences in these databases. Moreover, position-specific-iterative BLAST (PSI-BLAST) was chosen as the algorithm for the BLAST-analysis in case the databases did not have the sequences characterised in *E. coli* but have sequences that are distantly related to the query sequences. For the [NCBI Conserved Domain Search](#), the parameters by default were chosen and the CDD v3.19 - 582353 PSSMs database was selected in this analysis.

To analyse whether some of the genes were expressed in operon. A continues sequence with the genes of interest were submitted to [Softberry FGENESB](#). The genetic code 11 for bacterial and archaeal and plant plastid code and *Escherichia coli* K-12 as the closest organism were selected. In addition to evaluate whether the query contains operons, this

software also predicts potential coding sequences in the microbial genome.

Verification of successful gene deletion and comparison of peptide sequences were performed by [LALIGN](#) with default settings ([Table 3.1](#)). Protein tertiary structures were predicted by Protein Homology/analogY Recognition Engine V 2.0 ([Phyre²](#)) by uploading the peptide sequences to the online platform. The predicted protein models were visualised in [NCBI iCn3D](#).

Table 3.1: Summary of parameters for pairwise alignment in LALIGN

Parameters	Setting
Alignment method	Local
Number of reported subalignments	3
E-value threshold	10
Scoring matrix	BLOSUM50
Opening gap penalty	-12
Extending gap penalty	-2

3.2 Plasmids isolation

Plasmids are small circular DNA, which are commonly used for gene manipulation and gene expression in a organism of interest. The general structure of a plasmid vector contains an origin for its replication in host, multiple cloning sites for incorporating a DNA fragment of interest and a selectable marker gene for selection of organisms which harbour the plasmid [[81](#), [82](#)].

All plasmids were isolated from *Escherichia coli* (*E. coli*) DH5 α in order to performe *in vitro* plasmid manipulation. Plasmids were isolated according to the protocol for PureYield™ Plasmid Miniprep System ([Promega](#)) with some modifications to increase the yield of plasmids. The volume of the buffers that were used to isolate the plasmids was the same as given in the protocol provided by the manufacturer.

The pellet from 2 mL of overnight bacteria culture was resuspended with 600 μ L of deionised water. 100 μ L of lysis buffer was added to the bacteria suspension and incubated at room temperature for 2 min. The lysate was neutralised with 350 μ L cold neutralisation solution before incubation on ice for 3 min. The cell lysate was centrifuged at 16 000 \times g for 5 min. The supernatant was mixed with an equal volume of 96 % ethanol before the solution was loaded on a minicolumn and centrifuged at 16 000 \times g for 1 min. This step was repeated until all the sample was loaded on to the column. The column was washed with 200 μ L of endotoxin removal wash and centrifuged at 16 000 \times g for 1 min, followed with 400 μ L of column wash solution and centrifuging for 2 min. The plasmids were eluted from the column

after adding 40 μL of elution buffer and incubation for 2 min before centrifuging the column at $16\,000 \times g$ for 1 min. To increase the yield, an additional amount of 30 μL elution buffer was added to the column and the previous step was repeated.

3.3 Preparation of chemical and electrocompetent bacteria

Competent bacteria are able to take up exogenous DNA, however, not all bacteria are naturally competent. In order to induce artificial competency, the bacteria must be exposed to high Ca^{2+} concentration and heat shock or electric shock. Depending on type of artificial competence, the bacteria are prepared differently [83].

1 mL of uropathogenic *E. coli* 3 (UPEC3) of overnight culture was diluted with 100 mL LB. The bacteria culture was incubated at 37°C with shaking until $\text{OD}_{600} = 0.3 - 0.4$ and incubated on ice for 30 min. Cold bacteria culture was transferred to sterile 50 mL tubes. The cultures were centrifuged at $2280 \times g$ for 20 min at 4°C . After centrifuging, the supernatant was discarded. Chemical and electrocompetent bacteria were made after following [section 3.3.1](#) and [section 3.3.2](#), respectively.

3.3.1 Chemically competent bacteria

Chemically competent UPEC3 was prepared as follows. The pellet was resuspended with filtered cold 0.1 M CaCl_2 (25 mL). The culture was centrifuged, and the supernatant was removed as described earlier. 5 mL of cold 0.1 M CaCl_2 in 15 % glycerol was added to the pellet. The pellet was resuspended before centrifuging at $2280 \times g$ for 10 min at 4°C . After the supernatant was removed, the pellet was resuspended with 400 μL of cold 0.1 M CaCl_2 in 15 % glycerol. Aliquots (50 μL) of bacteria were frozen with liquid nitrogen and immediately stored at -80°C .

3.3.2 Electrocompetent bacteria

Electrocompetent bacteria were made by resuspending the pellet with cold, filtered and deionised water (25 mL). The bacteria solution was centrifuged at $2280 \times g$ for 10 at 4°C and the supernatant was removed. 5 mL of cold 10 % glycerol was used to wash the pellet, followed with centrifuging the bacteria solution. After removal of the supernatant, 400 μL of cold 10 % glycerol was added to the pellet. Bacteria aliquots (50 μL) were frozen with liquid nitrogen and immediately stored at -80°C .

3.4 Transformation

Transformation is a basic method for artificially inducing plasmid uptake, where heat shock and electroporation are two common techniques for transforming *E. coli* [84, 85].

3.4.1 Heat shock

Bacteria were thawed on ice for 10 min. An amount of 2 μ L plasmids were added to chemical competent UPEC 3 and further incubated on ice for 20 min. The bacteria were heat shocked at 42°C for 2 min, which increases permeability of the bacteria cells. Immediately after heat shock, the tube was placed on ice to cool for 2 min. 1 mL LB medium was added to the bacteria and incubated in an incubator at 37°C with shaking for 1.5 h to let the bacteria recover and develop antibiotic resistance. Thereafter, the bacteria culture was pelleted by centrifuging for 4 min at 3300 \times g. 150 μ L of the remaining supernatant was used to resuspend the pellet before plating on LB plates with suitable antibiotics for selection of clones with the desired plasmids. The bacteria were incubated at 37°C overnight.

3.4.2 Electroporation

Electrocompetent bacteria were thawed on ice for 5 min. pCRISPR (2 μ L) was added to the bacteria and further incubated on ice for 10 min. The bacteria were transferred to a pre-cooled electroporation cuvette (BTX) with 1mm or 2 mm distance between the electrodes. The cuvette was placed into the electroporator (BTX ECM 830), and the electroportation was executed with the settings listed in Table 3.2. By introducing electrical pulse, the membrane becomes permeable for plasmid uptake. Immediately after the pulse, 1 mL of 37°C LB was added to the cuvette and mixed by pumping with a pipette. The bacteria solution was transferred to a sterile 1.5 mL tube and incubated at 37°C in a shaker for 1.5 h. The bacteria were centrifuged at 3300 \times g for 4 min, before 150 μ L remaining supernatant was used to resuspend the pellet and subsequently plated on LB plate with suitable antibiotics.

Table 3.2: Settings for transformation of electrocompetent bacteria. The indicated settings were used for transformation with electroporation cuvette that has a 1 mm or 2 mm distance between the electrodes. For 1 mm and 2 mm cuvettes, 1.8 kV and 2.5 kV were selected, respectively

Parameter	Setting
Voltage	1.8 kV or 2.5 kV
Pulse length	119 μ s
Number of pulses	7
Pulsing interval	100 ms
Polarity	Unipolarity

3.5 Cloning CRISPR-Cas9 systems

To clone CRISPR-Cas9 systems, polymerase chain reaction (PCR) and restriction enzymes were used. PCR is a technique to amplify DNA sequence of interest upon repeated cycles of DNA template denaturation, primer annealing and polymerase DNA extension. By increasing the temperature in each cycle the DNA template becomes denatured, which allows DNA oligoes (primers) to anneal with the template upon decreased temperature. The temperature is then elevated to activate DNA polymerase that adds nucleotides and extends the primer to a DNA strand [86]. Amplified DNA fragments can be inserted into a vector by generating compatible sticky ends with restriction enzymes that recognise consensus sequence in the DNA and induce cleavage. DNA fragments with cohesive ends is then joined and ligated by ligases [87].

3.5.1 Primer design

Primers and guide RNAs (spacer) for generating the desired CRISPR constructs were designed *in silico* by using the online platform, [Benchling](#). The spacer sequences, which either target *cnf1*, *dsbA*, *hlyA*, *ompT* or *tcpC*, primers for cloning upstream and downstream sequences of the target genes as well as primer for sequencing the final constructs are attached to Appendix ([Table A.7](#)). In general, the spacer sequences (sgRNA) with a length of 20 bp, were selected regarding to 40-60 % GC-content and the off- and on-target values, which were predicted by Benchling. To insert the sgRNA into CRISPR plasmid (pCRISPR), the bases AAAC were added to the 5' end and a G at the 3' end of the forward sgRNA, whereas AAAAC were added to the 5' end of the reverse sgRNA. These bases at the end of the sgRNAs are compatible with the sticky ends in pCRISPR after digestion with *BsaI*, which can be ligated into the plasmid after enzymatic restriction.

For amplification of upstream and downstream sequences to the target genes, the primers

were designed for overlap extension PCR and a restriction site for *XbaI* was incorporated at the end of the primers. Primers designed for overlap extension PCR with *XbaI* restriction site, were named with suffices `_XbaI_Rev` or `_XbaI_For`. Six random nucleotides were added after the *XbaI* restriction sites in the `_XbaI_Rev` or `_XbaI_For` primers which serve as a binding site for *XbaI*. The primers for overlap extension PCR with the suffixes `_OE_For` and `_OE_Rev` were designed accordingly. A part of the primer (20-25 bp) must anneal with the upstream region and the second part of the primer (20-25 bp) must anneal with the downstream region of the target gene. The first part of the `_OE_For` primers and `_XbaI_Rev` primers were also designed with regard to their melting point, which should be within 50-60°C and the melting temperature between these two primers should not differ more than 4°C. Further more, secondary structures of `_OE_For` primers were also considered to avoid possible primer dimer formation, which potentially affect DNA amplification. The primer pairs `_OE_Rev` and `_XbaI_For` were designed with similar approach.

3.5.2 Isolation of genomic DNA from gram negative bacteria

DNeasy Blood & Tissue Kit from [QIAGEN](#) was used to isolate genomic DNA from UPEC3 strain. The genomic DNA was isolated according to manufacturer's instructions. Briefly, 2 mL of overnight culture was harvested by centrifuging for 2 min at 16 000 ×g. The pellet was resuspended with 180 µL ATL buffer after removal of supernatant. Proteinase K (20 µL) was added to the mixture before incubation at 56°C for 1 h to lyse the bacteria. After incubation AL buffer (200 µL) and 200 µL of ethanol (96-100 %) was added and mixed with the lysate by vortexing the solution. The lysate was loaded to a mini-column and centrifuged at 6000 ×g for 1 min. The column was washed with 500 µL AW1 buffer by centrifuging as described earlier. 500 µL of AW2 buffer was added to the column and centrifuged at 16 000 ×g for 4 min. Before elution, the empty column was centrifuged at 16 000 ×g for 1 min to remove residual ethanol in the column. 200 µL AE buffer was added to the column and incubated at room temperature for 1 min. The DNA was eluted by centrifuging the column at 6000 ×g for 1 min.

3.5.3 Cloning CRISPR-constructs

The cloning procedure of CRISPR-Cas9 has been described elsewhere [72]. Briefly, oligonucleotides for guide annealing (sgRNA) were inserted into the the vector, pCRISPR, via the cloning approach, Golden Gate Assembly. In short, *BsaI* was used to digest pCRISPR and the annealed and phosphorylated sgRNA was ligated into the vector by T4 DNA ligase. The assembly products (5 µL) were used to transform chemical competent *E. coli* DH5a as described in [section 3.4.1](#). Bacteria carrying plasmids with correct insert, were verified with colony PCR and digestion with the restriction enzymes, *BsaI* and *SpeI*. Enzymatic digested

plasmids which potentially have the single guide oligonucleotides, were further dephosphorylated with antarctic phosphatase. The homology arms were created after amplification of downstream and upstream regions of the target genes by using the isolated genomic DNA of UPEC3 as template. Downstream and upstream DNA segments were fused via overlap extension PCR. Finally, the ends of the homology arms were digested with *XbaI* to generate sticky ends which are compatible with the cohesive ends of the *SpeI*-digested pCRISPR with sgRNA, and inserted into the vector after an overnight ligation with T4 DNA ligase at 16°C. A more detailed description of the cloning procedures is attached to Appendix ([section B.2](#)).

3.6 Mutagenesis in UPEC3

3.6.1 Transformation of UPEC3

UPEC3 were mutated after sequential transformation of pCas9 and pCRISPR construct, which target a gene of interest. Electrocompetent UPEC3 ([section 3.3](#)) was transformed with 2 µL of pCas9 (417 ng) according to the description in [section 3.4.2](#), but with adjustment of the voltage to 1.8 kV due to usage of 1 mm cuvettes. After recovering the bacteria by incubation in LB medium for 1.5 h, the bacteria were pelleted and resuspended with the remaining 100 µL of supernatant. The resuspended bacteria were plated on LB agar plate with chloramphenicol for selection of pCas9 transformed bacteria.

A transformed UPEC3 colony which grew on the chloramphenicol plate, was inoculated in LB medium with corresponding antibiotic. The overnight culture was used to prepare electrocompetent UPEC3 strain which harbour pCas9 by inoculating 100 µL of the overnight culture in 100 mL LB medium with chloramphenicol (25 µg/mL), and followed the same procedures as described in [section 3.3](#).

Electrocompetent UPEC3 harbouring pCas9 was transformed with pCRISPR constructs by electroporation ([section 3.4.2](#)). After 41 to 45 h of incubation at 37°C of UPEC3 pCas9 transformed with equal mole of pCRISPR_cnf1_sg2 or pCRISPR_Harm_cnf1_sg2, the genomic editing efficiency between the two plasmids were compared by colony PCR with the designed primer pairs cnf1_For and cnf1_Rev ([Table A.7](#)). Example calculation of genome editing efficiency is attached to Appendix, [section C.2](#).

3.6.2 Plasmid curing

To remove pCRISPR from the bacteria, colonies with positive knockout of the target gene were inoculated into LB medium (3 mL) with chloramphenicol (25 µg/mL). The bacteria culture was incubated at 37°C in a shaker overnight. 3 µL of the culture were diluted in 3 mL of LB with chloramphenicol (25 µg/mL) and were incubated overnight with shaking at

37°C. The overnight bacteria culture was also plated on LB agar plates with chloramphenicol and incubated overnight at 37°C. Colonies that were formed on the plate, after overnight incubation, were picked and prepared for colony PCR to verify loss of pCRISPR construct. The primer pairs CRISPR_FF_For and CRISPR_FF_Rev (Table A.7) were used for colony PCR and verification of curing pCRISPR. As a second control of curing pCRISPR constructs, a colony was inoculated into 3 mL LB medium with kanamycin (50 µg/mL) and incubated overnight at 37°C in a shaker.

3.7 Growth curve

Single bacteria colony was picked and inoculated into 3 mL of LB medium or minimal A medium with or without chloramphenicol (50 µg/mL). The bacteria were incubated at 37°C with shaking overnight. Overnight cultures were diluted ten times in LB or in minimal A medium before measuring the absorbance at 600 nm (Abs_{600}). The ten times diluted bacteria cultures were further diluted to obtain a final $Abs_{600} = 0.01$. Each of the diluted sample with a volume of 150 µL was distributed to a well of a flat bottom 96-well plate in triplicates. The surrounding wells were filled with 150 µL of medium to reduce evaporation of the samples during incubation and absorbance measurement. The absorbance of the samples was measured for 24 h by a plate reader (Bioscreen C) with the settings that are given in Table 3.3.

Table 3.3: Settings for growth curve measurement. Overnight *E. coli* cultures were diluted in LB to Abs_{600} was 0.01. The absorbance of the cultures was measured with the following settings in BioScreener C.

Parameter	Setting
Temperature	37°C
Experiment length	23 h 59 min
Measurement interval	30 min
Start measurement	Immediately
Shaking type	Continuous
Shaking amplitude	Maximum
Shaking speed	Normal
Stop shaking before measurement	5 s
Filter	600 nm, Brown

3.8 FIP2 silencing in THP-1 cells

RNA interference (RNAi) technology can be used to repress gene expression in eukaryotes by transfecting the cells with synthetic small interfering RNAs (siRNAs) [88]. Eukaryotic cells

can be transfected with siRNA through lipofection by delivering siRNAs in liposomes [89]. Cytosolic siRNA associated with RNA-induced silencing complex (RISC), guides RISC to target mRNA. Perfect complementarity between siRNA and mRNA induces mRNA degradation by RISC, while imperfect complementarity results translational repression [6, 88].

3.8.1 Cell seeding

THP-1 cells were transferred from flask to a 50 mL tube. The cells were centrifuged at $170 \times g$ for 7 min and the pellet was resuspended with the remaining 5 to 10 mL of the supernatant. 20 μ L cell solution was diluted into 10 mL of isotone and the number of cells were counted with profile C for THP-1 cells by Beckman Z2 Coulter Particle Count and Size Analyzer. The cells were diluted with RPMI supplemented with pre-warmed 10 % FBS and 680 μ M L-glutamine to the desired concentration. Example calculation of cell dilution can be found in Appendix, [section C.4](#). To differentiate and let the cells adhere on the plate, PMA was added to the cell solution to obtain a final concentration of 60 nM before the cells were distributed to a well of a 6 well plate. The cells were incubated for 24 h at 37°C with a CO₂ level of 5 % .

3.8.2 Lipofection - FIP2 silencing

After 24 h of incubation of cells seeded on a multiwell plate, the cells were either treated with 16 nM AllStars non-silencing (NS) RNA or FIP2-5 silencing oligos. The oligos were prepared by mixing 490 μ L of pre-warmed Opti-MEM with 10 μ L of RNAiMax and the mixture was incubated at room temperature for 5 min to let the liposomes develop. In a second tube, 496 μ L of Opti-MEM was mixed with 4 μ L of NS RNA or FIP2-5 silencing oligos. The mixtures in the two tubes were combined, mixed and incubated at room temperature for 15 min to let the oligoes pack inside the liposomes. After incubation, 495 μ L of the liposomes with oligoes were dripped over each well with THP-1 cells. The cells were incubated at 37°C with 5 % CO₂ for 48 h. The cell medium was changed to RPMI with 10 % FBS and 680 μ M L-glutamine and further incubated for 48 h.

3.9 Stimulation of THP-1 cells

The medium was aspirated from the THP-1 cells that have been incubated for two days, and new RPMI medium with 1 % FBS was added to the cells (900 μ L). The cells were incubated at 37°C with 5 % CO₂ until LPS priming and stimulation with bacteria.

3.9.1 LPS priming and NLRP3 inhibition

A LPS stock 1 mg/mL from *E. coli* K-12 were vortexed for 15 s before it was sonicated in ultrasonic bath for 1 min at level 5. The LPS stock was then vortexed for another 15 s, centrifuged with a tabletop centrifuge before diluting 1 μ L of the LPS stock in 999 μ L RPMI with 1 % FBS. Except for the cells that were only treated with medium, the diluted LPS solution (100 μ L) was added to each well with THP-1 cells to obtain a final LPS concentration of 100 ng/mL. The cells were incubated with LPS at 37°C for 2 hours.

NLRP3 inhibition in THP-1 cells was proceeded accordingly. Following priming, LPS containing medium was aspirated and the cells were treated with DMSO or 10 μ M MCC950 for 30 min before bacterial stimulation. Otherwise, this step was omitted.

3.9.2 Preparation of bacteria samples

Overnight cultures of *E. coli* CFT073, DH5 α , UPEC3 variants (200 μ L) were diluted into 4 mL of LB medium under sterile condition. The cultures were incubated for 30 to 40 min until the OD₆₀₀ reached between 0.3 and 0.4. The required volumes of bacteria for a certain multiplicity of infection (MOI) value were calculated aided with [Agilent Genomics: Tools - Bio Calculators](#), which provides an estimate of *E. coli* concentration from OD₆₀₀ values. The number of bacteria for THP-1 infection was calculated with regard of MOI = 2, N + 1 wells times 10. Example calculations are attached to Appendix, [section C.5](#). After the desired volumes of bacteria were taken out from the cultures, the bacteria were centrifuged at 16 000 \times g, 4°C for 2 min. The supernatants were discarded and the pellets were washed with 1 mL of filter sterilised PBS twice. After the last washing step and centrifugation, the supernatants were discarded and the pellets were resuspended with 500 μ L of PBS. Before stimulation, 1/10 of the bacteria solution was taken out and opsonized after incubation with RPMI and 10 % A⁺ on 37°C water bath for 5 min. Opsonized bacteria were stored on ice until stimulation.

3.9.3 Bacterial and nigericin stimulation of THP-1 cells

Opsonized bacteria were vortexed before 100 μ L of the bacteria solution was dripped over LPS primed or non-primed THP-1 cells. The cells were incubated at 37°C with 5 % CO₂ for 2 or 4 h. Nigericin stock was diluted hundred times in RPMI with 1 % FBS, before 111 μ L of the diluted nigericin solution was dripped over LPS-primed THP-1 cells. The cells that were stimulated with nigericin were incubated for 1 h at 37°C with 5 % CO₂.

3.10 LDH assay and supernatant storage

Damaged plasma membrane releases lactate dehydrogenase (LDH) from cells and is an indicator of cell toxicity. Release of LDH can colourimetrically quantified when LDH oxidates lactate to pyruvate by reducing nikotinamid adenine dinucleotide (NAD⁺) to NADH + H⁺. Tetrasodium salt is a colourless agent and is converted to a red colour product, formazan, when NADH + H⁺ is reduced by diaphorase [90].

To measure the maximal cell lysis, 100 μ L of lysis buffer provided in CyQUANT™ LDH Cytotoxicity Assay Kit, was added to a well with cells that only have been treated with medium and incubated at 37°C with CO₂ for 30 min. After 2 and 4 h of stimulation with bacteria, the supernatants were transferred from the wells to 1.5 mL tubes. The samples were centrifuged at 10 000 \times g for 1 min to pellet cell debris and bacteria. 190 μ L of supernatant was transferred to a well of a 96-well plate with round bottom. The plate with supernatants were stored at -20°C for short term storage or long term storage at -80°C for later analysis (section 3.12). Duplicates of 50 μ L supernatants were added to a 96-well flat bottom plate. Subsequently, 50 μ L of reaction mixture was added to the samples and the plate was gently tapped to mix the samples with the reaction solution. The plate was incubated at room temperature for 20 to 30 min protected from light, before the reaction was terminated by adding 50 μ L of stopping buffer. Both reaction mixture and stopping buffer are from CyQUANT™ LDH Cytotoxicity Assay Kit. The absorbance was measured at 490 nm and 680 nm by a microplate reader (BMG LABTECH). The difference between the absorbance at 490 nm and 680 nm provides the activity of LDH. Calculation of LDH release can be found in Appendix, section C.6.

3.11 RNA isolation and real time quantitative polymerase chain reaction (Q-PCR)

Quantification of mRNA can be performed with Q-PCR. Among the various Q-PCR methods, TaqMan assay provides relative and absolute quantification of mRNA. Similar with PCR, Q-PCR requires primers which anneals with a template. By varying the temperature in each cycle, the primer anneals with a template, allowing Taq DNA polymerase to extend the DNA strand and moves toward a probe with a reporter and quencher fluorophore. Due to the close proximity between the reporter and quencher fluorophore, the emitted energy from reporter is absorbed by quencher, thus no signal is detected. When Taq DNA polymerase reaches to the probe, the polymerase degrades the probe and releases the reporter from quencher fluorophore. Free reporter fluorophore emits light and accumulates from each cycle. Real signal is detected when the intensity of emitted light is above a threshold value. This signal is also defined as threshold cycle (Ct) [91]. In fact that a DNA polymerase is

employed in Q-PCR, quantification of mRNA levels requires reverse transcription of mRNA to synthesise complementary DNA (cDNA) that is used as a template in Q-PCR [92].

3.11.1 RNA isolation from THP-1 cells

After the supernatants of stimulated THP-1 cells were collected for Western blot analysis and LDH assay (section 3.10), the remaining supernatants were discarded. The cells were lysed by incubating the cells with 0.5 mL QIAzol lysis reagent at room temperature for 2-3 min. The lysates were transferred to 1.5 mL tube and stored at -80°C . Frozen lysates were thawed on ice and subsequently incubated at room temperature for 5 min. To precipitate RNA, 100 μL of chloroform was added to each sample and mixed for 15 s vigorously. The homogenised samples were centrifuged at $11\,600 \times g$ for 15 min at 4°C . Carefully, the aqueous phase containing RNA (approximately 200 μL), was collected into a new 1.5 mL tube. The organic phase was stored on ice for later protein isolation (section 3.12.2). To each sample, 100 μL of 100 % ethanol was added and the samples were mixed by inverting the tubes before loading the solution to a mini column and centrifuged at $9600 \times g$ for 30 s at room temperature. The flow through was discarded. An amount of 80 μL of diluted DNAase (RNase-Free DNase Set) was added directly to the membrane of each column with samples. The columns were incubated at room temperature for 15 min to let the DNAase degrade DNA residuals bounded to the column. The DNAase and other impurities, such as proteins, carbohydrates and fatty acids, were washed after adding 350 μL RW1 buffer (RNeasy Kits) to the column and centrifuged at $9600 \times g$ for 30 s. After discarding the flow through, 500 μL of RPE buffer (RNeasy Kits) was added to the column and centrifuged at $9600 \times g$ for 30 s to wash traces of salts. This step was repeated one more time. To remove the ethanol residuals from the column, the mini-column was transferred to a new collection tube and centrifuged at $16\,000 \times g$ for 2 min. RNA was eluted from the column after incubating the column membrane with 51 μL of RNase- free water for 1-2 min and subsequently centrifuged at $9600 \times g$ for 30 s. After quantification of RNA concentration with NanoDrop ND-1000 (Thermo Scientific), the samples were stored at -80°C .

3.11.2 cDNA synthesis

Isolated RNA samples were reverse transcribed to cDNA by preparing a master mix for each sample using Maxima First Strand cDNA Synthesis Kit for RT-qPCR (Table 3.4). RNA samples with a concentration higher than 50 ng/ μL were diluted with RNAase free water. In addition, a negative control was prepared (Table 3.5). The cDNA was synthesised after incubating the samples in a thermocycler (C1000 TouchTM, Bio-Rad) with the program given in Table 3.6. The cDNA was frozen at -20°C for later use.

Table 3.4: Composition of cDNA synthesis reaction mixture. Maxima First Strand cDNA Synthesis Kit for RT-qPCR was used to prepare master mix for cDNA synthesis.

Reagent	Volume [μL]
5 \times Reaction mix	4
Maxima enzyme mix	2
RNA	9
Nuclease free water	5

Table 3.5: Composition of reaction mixture for negative control of cDNA synthesis. Maxima First Strand cDNA Synthesis Kit for RT-qPCR was used to prepare master mix a negative control for cDNA synthesis.

Reagent	Volume [μL]
5 \times Reaction mix	4
RNA	9
Nuclease free water	7

Table 3.6: Thermocycler settings for cDNA synthesis

Step	Temperature [$^{\circ}\text{C}$]	Time [min]
Primer annealing	25	10
cDNA synthesis	50	30
Reaction termination	85	5
Hold	4	∞

3.11.3 Quantitative real time polymerase chain reaction (Q-PCR)

The expression level of human pro-IL-1 β , TNF α , NLRP3, IFN β and FIP2 were analysed with quantitative polymerase chain reaction (Q-PCR). The cDNA were thawed at room temperature. For each TaqMan probe for FIP2, pro-IL-1 β , TNF α , TBP, NLRP3 and IFN β , a reaction solution was prepared as listed in [Table 3.7](#). For several samples, the volume of the reagents in the Q-PCR reaction mixture was scaled up with regard to the number of samples. A volume of 15 μL of the reaction mixture was distributed to a well of a MicroAmpTM Optical 96-Well Reaction Plate on a cooling rack. The ten times diluted cDNA (5 μL) was then added to the well. After sealing the plate with MicroAmpTM Optical Adhesive Film, the samples were mixed and collected at the bottom of the plate by centrifuging at 133 $\times g$ for 2 min before real time quantitative PCR was performed on StepOnePlusTM Real-Time PCR System. The program settings for the Q-PCR are summarised in [Table 3.8](#). Example

calculation of relative quantification (RQ) value is attached to Appendix (section C). All RQ values were calculated with regard to Ct mean values of technical duplicates and the standard deviation between the replicates was negligible.

Table 3.7: Composition of reagents for one TaqMan qPCR reaction mixture.

Reagent	Volume [μ L]
2 \times PerfeCTa qPCR FastMix	10
Primer	1
cDNA (10 \times diluted)	5
Deionised water	4

Table 3.8: Settings for performing Q-PCR. Q-PCR was performed on StepOnePlus™ Real-Time PCR System with the following settings.

Step	Temperature [$^{\circ}$ C]	Time [s]	Cycle
Initial polymerase activation	95	20	1
Polymerase activation	95	1	40
Elongation	60	20	

3.12 Protein isolation and western blot

Sodium dodecyl sulphate–polyacrylamide gel electrophoresis (SDS-PAGE) is a protein separation technique, where linearised and negatively charged proteins are separated by their molecular weight [6]. The proteins of interest can be detected and semi-quantified by Western blotting which is a method for transferring the proteins from a gel to a membrane and incubate the membrane with antibodies. Primary antibodies specifically hybridise with the protein of interest on the membrane, while secondary antibodies interact with primary antibodies. To visualise the protein bands, horseradish peroxidase conjugated to secondary antibodies, catalyses a chemical reaction that emits light as a byproduct that can be recorded with an imaging device [6, 93].

3.12.1 Preparation of bacteria cultures for SDS-PAGE

1 mL of overnight bacteria cultures were centrifuged at 2300 \times g for 15 min at 4 $^{\circ}$ C. To remove residual bacteria, the supernatants were sterile filtered with a syringe filter that has a pore size of 0.46 μ m. 200 μ L of overnight bacteria culture was centrifuged with the same settings given above, and the supernatant was discarded. The filtered supernatants and bacteria

pellets were stored at -80°C for later use, or on ice for analysis on the same day. Samples that were stored at -80°C , were thawed on ice before preparing them with LDS buffer. The supernatants (20 μL) were mixed with 6 μL of 3.6 x LDS + 0.1 M DTT and boiled at 80°C for 7 min. The bacteria pellet was lysed after incubating the samples at 80°C in 320 μL of 2 x LDS + 0.1 M DTT for 10 min and sonication in ultrasonic baths (VWR) for 5 min at maximum level. The lysates were sheared with a syringe needle ten times to reduce the viscosity of the samples.

3.12.2 Protein isolation from THP-1 cells and sample preparation for SDS-PAGE

Any residues of the aqueous phase were aspirated from the organic phase of the phenol-chloroform solution from RNA isolation ([section 3.11.1](#)). A volume of 150 μL of 100 % ethanol was added to the organic solution and mixed by inverting to prevent shearing of DNA. The samples were incubated for 2-3 min at room temperature before centrifugation at $2000 \times g$ for 5 min at 4°C to pellet the DNA. The supernatant containing the proteins, were collected in a new 1.5 mL tube and mixed with 750 μL of isopropanol. The samples were incubated for 10 min at room temperature before centrifugation at $12\,000 \times g$ for 10 min at 4°C to pellet the protein. After discarding the supernatant, 1 mL of wash solution (0.3 M guanidine hydrochloride in 95 % ethanol) was added to the protein pellet and stored at -20°C for later preparation.

The protein pellet in wash solution was incubated at room temperature for 20 min before centrifuging at $7500 \times g$, 4°C for 5 min. The washing step was repeated two more times. After the last wash of the protein pellet, the supernatant was discarded and 1 mL of 100 % ethanol was added to the pellet, vortexed and incubated at room temperature for 20 min. Finally, after centrifugation at $7500 \times g$, 4°C for 5 min and removal of supernatant, the pellet was air dried to remove ethanol residual for 2 to 5 min. Depending on the size of the protein pellet, 100 μL or 200 μL of 4 M urea in 1 % SDS was used to resuspend the pellet. After complete dissociation of protein pellet, 3.6 x LDS with 0.1 M DTT was added to the samples and denatured at 95°C for 5 min. Furthermore, the collected supernatants ([section 3.10](#)) were thawed and 20 μL of supernatants were boiled in 6 μL 3.6 x LDS with 0.1 M DTT for 80°C for 7 min.

3.12.3 SDS-PAGE

After assembly of 4-12 % Bis-Tris NuPage acrylamide gels in the SDS-PAGE apparatus, the chambers were filled either with $1 \times$ MOPS or $1 \times$ MES buffer. In general, $1 \times$ MOPS buffer has a higher pKa value than $1 \times$ MES, which allows slower migration of proteins and

give a better resolution for proteins with a size above 50 kDa. On the other hand, $1 \times$ MES buffer allows proteins to migrate faster and is more suitable for separating smaller proteins that are below 50 kDa.

The samples that have been linearised after boiling in LDS + DTT buffer, were loaded to the wells. SeeBlue™ Plus2 Pre-stained Protein Standard (4 μ L) and MagicMark™ XP Western Protein Standard (1.5 μ L) were added into the same well. Because the proteins in MagicMark contain a IgG binding site, these proteins can hybridize with primary or secondary antibodies, making them detectable on the membrane during development of the blots. On the other hand, SeeBlue marker is visible on the gel and membrane which is necessary for controlling protein transfer efficiency from the gel to the membrane and quick evaluation of migration of the proteins of interest. The proteins were separated after running the gels first at 80 V for 30 min and subsequently at 180 V for 1 h.

3.12.4 Protein transfer to membrane

The acrylamide gels were removed from the cassette after separation and rinsed in deionised water before placing on top of the membrane of iBlot2 transfer stack. A pre-wetted separation filter paper was placed on top of the gel, followed with a top stack and an absorbent pad on top of the top stack. Air bubbles were removed between each step of assembly of the iBlot2 transfer stack. The transfer stack was placed on iBlot2 gel transfer device and the proteins were transferred to the membrane after running the P0 program that runs at 20 V for 1 min, followed with 4 min at 23 V and finally 2 min at 25 V. The P0 program is recommended for transfer of proteins with a size between 30 kDa to 150 kDa.

3.12.5 Blocking and hybridisation with primary antibodies

After transferring the proteins to the membrane, the stack was disassembled. The membrane was blocked with 5 % BSA at room temperature with agitation for 1 h. BSA solution was discarded after blocking the membrane, and proteins of interest were hybridised with primary antibodies by incubating the membrane overnight at 4°C with shaking.

3.12.6 Secondary antibody hybridisation and blot development

On the next day, the membrane was washed five times with $1 \times$ TBS-T for 5 min, before incubation with secondary antibodies for 1 h. Subsequently, residual antibodies were washed away from the membrane with $1 \times$ TBS-T for 5 min five times. The proteins of interest were detected after incubating the membrane with SuperSignal substrate, which is consumed by horseradish peroxidase to generate emission signal that can be detected by LI-COR Odessey

Fc. After incubating the membrane for 3 min with super signal, the membrane was placed between two x-ray films, and the blots were developed and captured by LI-COR Odessey Fc Imaging System by selecting the Chemi channels and an exposure time for 2 min.

3.12.7 Semi-quantitative analysis of proteins by Western blot

The densities of the protein bands were quantified by using the analysis tool in LI-COR software, Image Studio version 5.0. Quantified blot densities were used to calculate relative protein levels in cell lysates with regard to β -tubulin protein levels. An example calculation of relative protein levels is attached to Appendix, [section C.8](#).

3.12.8 Blot stripping

The membrane with primary and secondary antibodies was rinsed in deionised water. A volume of 350 μ L of β -mercaptoethanol was added to 50 mL of stripping buffer (62.5 mM Tris-HCl, 2 % SDS). The membrane was incubated with stripping buffer in a water bath at 55°C for 30 min with shaking. After stripping the membrane, the membrane was rinsed with deionised water followed with washing in 1 \times TBS-T once for 5 min, then twice for 10 min. The membranes were blocked with 5 % BSA for 1 h. To ensure the primary antibodies were completely removed from the membrane, the blots were developed by incubating the membrane with secondary antibodies and addition of SuperSignal as described in [section 3.12.6](#). The excess of secondary antibodies and SuperSignal were washed away with 1 \times TBS-T before the membranes were incubated with primary antibodies at 4°C overnight. The blots were developed on the next day as described in [section 3.12.6](#).

3.13 Enzyme-linked immunosorbent assay (ELISA)

ELISA is immunoassay that quantitatively detects a protein of interest. Among the various of developed ELISA methods, sandwich ELISA is characterised by immobilised antibodies in wells, which recognise and capture the protein (antigen) of interest in a complex sample. To quantify the protein of interest, enzyme-linked antibodies bind to another epitope of the antigen and convert a substrate to a coloured product which can be colourimetrically measured. The concentration of the antigen in the samples is determined from a standard curve which describes the relationship between known antigen concentration and the optical density of the coloured product [1].

3.13.1 Plate coating with capture antibodies and blocking

The total amount of pro-IL-1 β and IL-1 β in the collected supernatants ([section 3.10](#)) were quantified with Enzyme-linked immunosorbent assay (ELISA), Human IL-1 beta/IL-1F2 DuoSet. A 96-well plate was coated with 50 μ L of capture antibodies diluted in PBS at 4°C overnight. The day after, the plate was washed with 0.05 % Tween in PBS by TECAN HydroSpeed plate washer trice to remove excess of capture antibodies. After the last washing step, the plate was inverted and tapped on tissue paper to remove residual washing buffer on the plate. Each well of the plate was blocked with 5 % FBS in PBS for 1 h to prevent unspecific binding of IL-1 β in the wells. The plate was washed trice as described above.

3.13.2 Serial dilution of IL-1 β standard and sample preparation

Recombinant human IL-1 β standard (45 ng/mL) was serially diluted with 5 % FBS in PBS with a final concentration 204.75 pg/mL, 102.38 pg/mL, 51.19 pg/mL, 25.59 pg/mL, 12.80 pg/mL, 6.40 pg/mL and 3.20 pg/mL. The 120 μ L of the IL-1 β standards and 5 % FBS in PBS, used as blank, were transferred to a 96-well round bottom plate and put on ice until use. All of the supernatants were diluted 10 and 50 times on a 96-well round bottom plate. Samples observed with large amount of LDH and IL-1 β release in the supernatant, were further diluted 100 times in 5 % FBS in PBS. The washed ELISA plate was incubated with 50 μ L of diluted IL-1 β standards, supernatants or 5 % FBS in PBS for 2 h.

3.13.3 Hybridisation of enzyme-linked antibodies and signal detection

After incubation with samples and standard reagents, the plate was washed five times with 0.05 % Tween in PBS before adding diluted detection antibodies (50 μ L) to each well and incubated at room temperature for 1 h. The plate was washed with 0.05 % Tween in PBS five times, before adding 50 μ L of diluted streptavidin-HRP per well and further incubated the plate at room temperature for 30 min. After washing the plate seven times with 0.05 % Tween in PBS, pre-room tempered substrate mixtures were mixed together in 1:1 ratio and 100 μ L of the mixed substrate solution was added to each well. The plate was incubated at room temperature for 20 to 30 min, protected from light. A volume of 50 μ L of 1 M H₂SO₄ was added to each well to stop the colour development reaction. The absorbance was measured at 450 nm and 570 nm by a microplate reader (BMG LABTECH). Estimation of pro-IL-1 β and IL-1 β concentration in the supernatants were calculated from the standard curve. Example calculation is attached to Appendix, [section C.9](#).

4 Results

4.1 Bioinformatic analysis

The genome of the clinical uropathogenic *E. coli* isolate, UPEC3, was previously sequenced and the virulence factors were annotated by Jostein Johansen in Jan Egil Afset research group. *cnf1*, *hlyA* and *tcpC* have earlier been characterised and are known for their importance for invading the host upon infection [94, 61, 95]. According to previous publications, *ompT* and *dsbA* affect production of outer membrane vesicles, which potentially deliver toxins to target cells [67, 68]. Therefore, we chose to focus on these genes in this study. The location of *cnf1*, *dsbA*, *hlyA*, *ompT* and *tcpC* in UPEC3 is summarised in Table 4.1.

Table 4.1: General information of genes of interest. The genes are located in different contigs and the size of the genes are given in base pairs (bp). The molecular weight of the protein encoded by the gene was obtained from ProtParam.

Gene	Name	Contig nr.	Start	End	Length [bp]	Molecular weight [kDa]
<i>cnf1</i>	Cytotoxic necrotizing factor type 1	19	18632	21676	3045	113
<i>dsbA</i>	Thiol:disulfide interchange protein	9	2736	3362	627	23
<i>hlyA</i>	α -hemolysin	19	10963	14037	3075	110
<i>tcpC</i>	Tir domain containing protein	3	411416	412339	924	36
<i>ompT</i>	Omptin outer membrane protease	1	183854	182901	954	36

4.1.1 General bioinformatic analysis of *cnf1*, *dsbA*, *hlyA*, *ompT* and *tcpC*

We further performed BLAST- and conserved domain search analysis to investigate whether the peptide sequences have the functional domains that have been previously characterised. According to the PSI-BLAST result (Table 4.2), CNF1, DsbA, HlyA, OmpT and TcpC obtained 100 % overlap with the reference sequences and an identity > 97 %, indicating the query sequences were highly similar with the reviewed proteins in the Universal Protein Resource database, UniProt. Nonetheless, the hit results from PSI-BLAST have a relatively high confidence, given that the E-values were less than 5e-154.

Indeed, the total query cover of CNF1 was only 29 %, but the catalytic domain in the C-terminus in our query sequence is highly similar (identity: 99 %) with the sequence in Protein Data Bank. Likewise, the C-terminus of the CNF1 query sequence matched with the catalytic site of CNF1 that was obtained from the conserved domain search with a very significant E-value of 1.2e-52. In addition to the catalytic domain, part of the domain with unknown function 4765 (DUF4765) was detected in the CNF1 query. According to the Pfam database, the function of DUF4765 is currently unknown.

Summarised in Table 4.3, the query sequence of DsbA matched with the thioredoxin like

superfamily architecture with a very significant E-value of $2.3e-147$, indicating that the output result is highly confident and that the DsbA encoded by UPEC3 is very likely to be functional. As expected, HlyA was found to belong to the RTX superfamily, with the characteristic repeats of GGxGxDxZ (x: any amino acid, Z: hydrophobic amino acid) in the central part of the peptide sequence. Moreover, calcium binding repeats were also detected at the C-terminus of HlyA. Query sequence of OmpT also had 100 % overlap with the reference sequence in the conserved domain search with a significant E-value. Consistent with previous publication [96], the query sequence of TcpC contains a Toll-like receptor domain at the C-terminus. Combining the results obtained from PSI-BLAST and conserved domain search, it is probable that UPEC3 expresses functional CNF1, DsbA, HlyA, OmpT and TcpC proteins, which may interfere or stimulate the inflammatory signalling pathways in macrophages.

Table 4.2: BLAST-analysis of proteins of interest. The sequence similarity between the existing peptide sequence in the databases and the query peptide sequence of CNF1, DsbA, HlyA, OmpT or TcpC were analysed with position-specific iterated BLAST (PSI-BLAST) algorithm. Either [Protein Data Bank](#) or [UniProt](#) were selected as database as reference proteins source. The coverage and the identity between the query and the reference sequences are given in percentage with an E-value for confidence evaluation of the search result. All reference proteins originated from *E. coli* and can be accessed through the provided accession code.

Query	Hit description	Query cover [%]	E-value	Identity [%]	Accession Code	Database
CNF1	Catalytic domain of Cytotoxic Necrotizing Factor Type 1	29	0	99.7	1HQ0_A	Protein data base
DsbA	Thiol:disulfide interchangeable protein	100	5.0e-154	99.5	P0A4L5.1	UniProt
HlyA	Hemolysin	100	0	97.5	P09983.1	UniProt
OmpT	OmpT	100	0	99.0	P09169.1	UniProt
TcpC	Tir containing protein	100	0	99.6	A0A0H2V8B5.1	UniProt

Table 4.3: Conserved Domain Search of proteins of interest. The peptide sequence of CNF1, DsbA, HlyA, OmpT and TcpC from *E. coli* UPEC3 were analysed for conserved domains within the sequences. The default settings with CDD v3.19 - 582353 PSSMs database were selected in [NCBI Conserved Domain Search](#). Conserved domains that were found within the peptide sequences are given with the amino acid position with accession code and the superfamily they belong to. The confidence of the the search results are provided as E-value.

Query	Hit type	Total Amino acid residues	From	To	E-Value	Accession	Short name	Incomplete	Superfamily	Database
CNF1	specific	1014	828	995	1.2e-52	cd16834	CNF1-like	-	cl28892	CCD
CNF1	non-specific	1014	521	698	1.1e-19	pfam15962	DUF4765	N	cl24513	CCD
DsbA	superfamily	208	1	208	2.3e-147	cl00388	Thioredoxin-like superfamily	-	-	CCD
DsbA	specific	208	24	203	6.5e-66	cd03019	DsbA_DsbA	-	cl00388	CCD
HlyA	specific	1024	292	600	4.6e-129	pfam02382	RTX	-	cl10587	CCD
HlyA	superfamily	1024	292	600	4.6e-129	cl10587	RTX superfamily	-	-	CCD
HlyA	specific	1024	751	785	7.0e-10	pfam00353	HemolysinCabind	-	cl15317	Pfam
HlyA	specific	1024	769	803	3.2e-08	pfam00353	HemolysinCabind	-	cl15317	Pfam
HlyA	specific	1024	732	767	8.2e-07	pfam00353	HemolysinCabind	-	cl15317	Pfam
HlyA	specific	1024	817	850	5.4e-07	pfam00353	HemolysinCabind	-	cl15317	Pfam
HlyA	superfamily	1024	724	908	7.870-08	COG2931	Ca2+-binding protein, RTX toxin-related	C	cl26960	CCD
OmpT	superfamily	317	1	317	0	cl01886	OmpT superfamily	-	-	CCD
OmpT	specific	317	1	317	7.3e-171	COG4571	OmpT	-	cl01886	CCD
TcpC	superfamily	307	173	260	2.5e-17	cl23749	TIR_2 superfamily	C	-	CCD
TcpC	non-specific	307	171	304	7.2e-12	smart00255	TIR	-	cl23749	CCD

According to an earlier study, it has been demonstrated that *cnf1* can be co-expressed with hlyCABD operon [52]. As [Figure 4.1](#) illustrates, *hlyA* is located 7669 bp upstream to *cnf1* in contig 19. Despite *hlyA* and *cnf1* are relatively close, the distance between *hlyD* and *cnf1* is 945 bp, which is larger than the average intrinsic distance between genes that are expressed in an operonic manner. Moreover, according to the prediction by [Softberry FGENESB](#), *cnf1* was not predicted as a part of the hlyCABD operon, but rather as a single transcription unit ([Table 4.4](#)). Altogether, these observations indicate that *cnf1* does not belong to the hlyCABD operon.

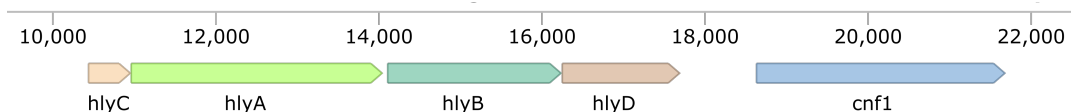


Figure 4.1: Location of genes involved in type I secretion system and *cnf1*. The genes *hlyC*, *hlyA*, *hlyB* and *hlyD*, which are involved in type I secretion system are located upstream to *cnf1* in contig 19 of UPEC3.

Table 4.4: Prediction of operonic expression of genes involved in type I secretion system in UPEC3. Potential operonic expression of close consecutive genes in contig number 19 was analysed by [Softberry FGENESB](#). *hlyC*, *hlyA*, *hlyB* and *hlyD* are transcribed as an operon (Op), whereas *cnf1* is transcribed as a single transcription unit (Tu). The location of the predicted genes is given with their respective start and end positions. All the predicted coding sequences (CDS) are located in the + strand. Number of amino acids (aa) of the predicted genes that are similar to the proteins in the [cluster of Orthologous Groups](#) (COG) database. The confidence of the predicted CDS is given as score values, which was obtained from running BLASTP by FGENESB. According the [BLAST course](#), the larger the score value is, the higher is the sequence similarity. An open reading frame was partially predicted to encode the protein urea transporter (UT).

Name	Gene number	Tu/ Op	Strand	Feature type	Start	End	Number of aa	Score
<i>hlyC</i>	1	1 Op 1	+	CDS	10439	10948	170	21
<i>hlyA</i>	2	1 Op 2	+	CDS	10963	14038	1024	922
<i>hlyB</i>	3	1 Op 3	+	CDS	14108	16231	707	76
<i>hlyD</i>	4	1 Op 4	+	CDS	16250	17686	478	615
UT	5	2 Tu 1	+	CDS	18127	18354	75	98
<i>cnf1</i>	6	3 Tu 1	+	CDS	19661	21673	671	290

Although *hlyC* was predicted as a coding sequence, the BLASTP score of this protein was relatively low, indicating the query sequence and the reference sequence in the [COG](#) database were relatively dissimilar. However, based on the results from the conserved domain search and the BLASTP with the UniProt as selected database, the query sequence obtained a higher score and identity values ([Table 4.5](#)). Nonetheless, HlyC had a significant E-value,

reflecting a high degree of similarity with the reference sequence in UniProt database. According to Table 4.4, the complete query sequence of CNF1 was not detected. However, since the alignment covered the conserved domain of CNF1 at the C-terminal, the confidence of this alignment was relatively high, which obtained a significant score value of 290 (Table 4.4). Between *hlyD* and *cnf1*, an open reading frame was found, which partially encodes the urea transporter (UT) protein.

Table 4.5: BLAST analysis of proteins involved in type I secretion system in UPEC3. The protein sequences of HlyC, HlyA, HlyB and HlyD were respectively analysed with BLASTP algorithm and the UniProt database was selected.

Protein	Score	Coverage [%]	E-value	Identity [%]	Strain
HlyC	347	100	1.0E-123	98.2	<i>E. coli</i>
HlyA	2001	100	0.0	97.5	<i>E. coli</i>
HlyB	1439	100	0.0	100	<i>E. coli</i>
HlyD	949	100	0.0	99.2	<i>E. coli</i>

Despite HlyC obtained a lower BLASTP score value when the COG database was used (Table 4.4) in comparison with the BLAST analysis (Table 4.5), it is important to note that the COG and UniProt databases are designed differently regarding their purposes. In general, COG is a database with complete genomes of bacteria and archaea and it is mainly used for comparative and evolutionary analysis of prokaryote genomes, quality control of genome sequences and examination of the consistency of phyletic patterns based on the presence or absence of certain protein families [97]. In contrast to COG, UniProt database provides users up-to-date and comprehensive information of proteins, such as subcellular location of proteins, description of protein function, protein sequence and structure. In addition to the collection of bacterial and archaeal protein collection, UniProt also includes proteins in eukaryotes and viruses. A closer comparison between these two databases, showed that the number of reviewed proteins expressed in *E. coli* strains is larger in UniProt than in COG database (Table 4.6).

Nonetheless, the protein collection in UniProt contains curated proteins from various *E. coli* strains in contrast to the COG database, which only includes genes that are expressed in *E. coli* O157:H7 strain Sakai substrain RIMD 0509952 and *E. coli* strain K12 substrain MG1655. Three UPEC strains and the extraintestinal pathogenic *E. coli* (ExPEC) S88 are among the documented *E. coli* strains in UniProt, which in theory are more phylogenetic related to our experimental UPEC3 strain according to the Pathosystems Resource Integration Center, PATRIC, compared with the enterohemorrhagic *E. coli* (EHEC) O157:H7 strain Sakai substrain RIMD 0509952 or the non-pathogenic *E. coli* K12 substrain MG1655. Thus, one may expect that the coverage and the identity of the query sequences HlyC, HlyA,

HlyB and HlyD are relatively higher from the BLASTP analysis against the proteins in the UniProt database compared with the results obtained from FGENESB when the queries were searched against the COG database. In contrast to COG database, a BLASTP search against UniProt database does not provide any information about conservation of neighbouring genes, which is one of the important features that were implemented in the algorithm for prediction of operon by FGENESB. To sum up, it is very unlikely that *cnf1* belongs to the hlyCABD operon.

Table 4.6: Number of curated proteins in different *E. coli* strains. The data of the proteins from COG database were obtained from the 2020 release, whereas the data from UniProt were from the UniProtKB/Swiss-Prot 2020.06 released in October 2020.

<i>E. coli</i> strain	Number of genes	Database
UTI89 (UPEC)	825	UniProt
O6:H1 strain CFT073/ ATCC 700928 (UPEC)	1697	UniProt
O6:K15:H31 strain 536 (UPEC)	894	UniProt
O45:K1 strain S88 (ExPEC)	758	UniProt
O157:H7 str. Sakai (EHEC)	3904	COG
K12 substr. MG1655	3544	COG

4.1.2 Potential expression of type VI secretion system in *E. coli* UPEC3

According to the gene annotation file of UPEC3 strain, Hcp, Clp ATPase and CLPA/B type chaperon protein which are among the proteins involved in type VI secretion system (T6SS), were found. These genes have previously been mapped by Jostein Johansen from Jan Egil Afset's group. This observation further led to a more profound analysis of neighbouring open reading frames (ORFs) which potentially encode essential proteins for establishing T6SS. Position specific iterated BLAST and conserved domain search were utilised to analyse the ORFs. Location of ORFs which potentially are involved in T6SS is summarised in [Table 4.5](#) and illustrated in [Figure 4.2](#).

Summarised in [Table 4.7](#), the open reading frames in the neighbourhood of Hcp, Clp ATPase and ClpA/B type chaperon protein were analysed with PSI-BLAST and the most essential genes in T6SS were detected. As shown, the channel forming proteins, TssL, TssJ and TssM were found in UPEC3. The predicted identities of these proteins were below 45.4 %, while the coverage of the sequences was 71 %, 100 % and 99 %, respectively. The baseplate proteins of T6SS, TssE and TssK, obtained coverly above 97 % and identities of 55.8 % and 56.5 %, respectively. Other proteins that are involved in T6SS, such as the ClpV (TssH), TssA and TssG were also found in the query sequences. Interestingly, TssH and TssA were predicted

Table 4.7: BLAST analysis of open reading frames in UPEC3 which potentially encodes proteins involved in type VI secretion system (T6SS). Protein Data Bank was selected as database for the PSI-BLAST of the query peptide sequences translated from the open reading frames (ORFs). The locations of the ORFs which encodes the essential proteins for T6SS in UPEC3 are given. The query cover and the identity between the reference and query sequences are in percentage, and the confidence of each search is given as an E-value. The origin of the reference peptide sequences are noted under reference strain.

Query	ORF location	Contig	Protein	Name	Identiy [%]	E-value	Query cover [%]	Reference strain
1	97303-97803	7	TssB	Contractile sheath small subunit	44.9	3.00E-25	70	<i>V. cholerae</i>
2	97862-99400	7	TssC	Contractile sheath large subunit	42.5	7.00E-119	82	<i>P. aeruginosa</i>
3	99418-100755	7	TssK/ VasE	Baseplate subunit TssK	56.5	3.00E-172	100	<i>E. coli</i>
4	100752-101417	7	TssL	DotU family	28.9	2.00E-11	71	<i>A. baumannii</i>
5	101430-103080	7	OmpA	OmpA family	66.7	3.00E-48	21	<i>E. coli</i>
6	103140-103631	7	Hcp	Heamolysin co-regulated protein (Hcp)	35.9	1.00E-28	87	<i>P. aeruginosa</i>
7	103823-106459	7	TssH	Chaperone protein ClpB	43.5	0.0	76	<i>E. coli</i>
8	106471-108960	7	TssI	VgrG-like protein	97.9	0.0	57	<i>E. coli</i>
9	110496-113015	7	TssI	VgrG-like protein	93.8	0.0	57	<i>E. coli</i>
10	116329-119655	7	TssM/ VasK	Type IV secretion system protein IcmF	45.4	0.0	99	<i>E. coli</i>
11	119822-121258	7	TssA/VasJ	Type IV secretion system protein TssA	60.9	2.00E-60	32	<i>E. coli</i>
12	124890-125969	7	TssG	Type VI secretion system protein TssG	53.7	4.00E-108	94	<i>E. coli</i>
13	121264-122694	7		PAAR domain containing protein	N/A	N/A	N/A	N/A
14	123166-124926	7	TssF/ VasA	Baseplate subunit TssF	66.7	0.0	100	<i>E. coli</i>
15	125950-126486	7	TssJ/ VasD	Lipoprotein TssJ	43.8	2.00E-54	100	<i>E. coli</i>
16	126490-126918	7	TssE	Baseplate subunit TssE	55.8	1.00E-52	97	<i>E. coli</i>
17	9519-12281	21	TssH/ ClpV	Chaperone protein ClpB	39.4	4.00E-157	78	<i>E. coli</i>
18	13932-14468	21	TssA	Type IV secretion system protein TssA	35.5	2.00E-26	99	<i>V. cholerae</i>

in both contig 7 and 21. Tube forming protein, Hcp and the contractile sheath forming proteins, VipA (TssB), VipB (TssC) and the VgrG-like (TssI) proteins were predicted from the queries with a relatively low identity and coverage. All queries obtained very significant low E-values.

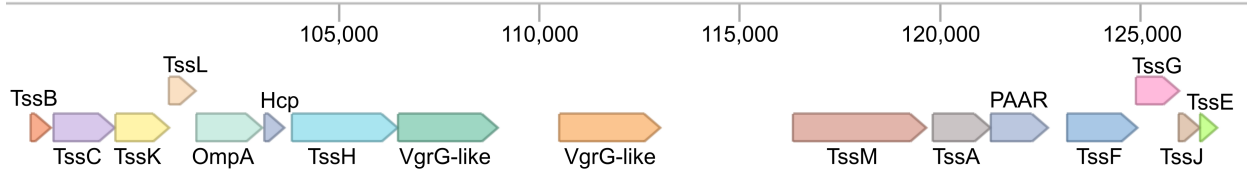


Figure 4.2: Location of open reading frames which potentially encode type VI secretion system in UPEC3. The open reading frames were found in contig 7 of the genomic DNA of UPEC3.

In support of the PSI-BLAST results (Table 4.7), conserved domain search of the open reading frames were performed. Characteristic domains of the baseplate complex proteins, contractile sheath and effector proteins were found in the queries (Table 4.8). The prediction of the conserved domains within the queries obtained high confidence, given these had low E-values. As shown in Table 4.8 the N-terminus of TssA was omitted in the query sequences in contig 7 and 21 during the analysis. In summary, the predictions of the ORFs in UPEC3, show a high likelihood of encoding proteins that are involved in forming a functional T6SS.

Table 4.8: Search for conserved open reading frames in UPEC3 which encodes proteins involved in type VI secretion system. Open reading frames (ORFs) in contig 7 and 21 were translated and the peptide sequences were submitted to [NCBI Conserved Domain Search](#) with the default settings. The version of the database by default was CDD v3.1.9 - 523353 PSSMs used. The hit of the conserved domains within the queries are summarised with their short name and the predicted locations are given as amino acid positions with respective E-value. The predicted conserved domains can be accessed through the PSSM-ID or the accession codes.

Query	ORF location	Contig	Hit type	PSSM-ID	From	To	E-Value	Accession	Short name	Incomplete	Superfamily
1	97303-97803	7	specific	377529	6	156	2.43E-64	pfam05591	T6SS_VipA	-	cl01402
2	97862-99400	7	superfamily	384129	21	508	0	cl05484	VipB superfamily	-	-
3	99418-100755	7	specific	377569	24	440	8.00E-142	pfam05936	T6SS_VasE	-	cl01406
4	100752-101417	7	specific	274532	20	198	4.23E-52	TIGR03349	IV_VLDotU	-	cl01370
5	101430-103080	7	specific	225439	386	542	2.67E-35	COG2885	OmpA	-	cl34510
6	103140-103631	7	specific	213799	2	160	9.01E-68	TIGR03344	VI.effect_Hcp1	-	cl01226
7	103823-106459	7	superfamily	274528	13	864	0	cl37250	VI.ClpV1 superfamily	-	-
8	106471-108960	7	superfamily	273730	22	509	1.48E-155	cl36942	vgr_GE superfamily	-	-
8	106471-108960	7	specific	226704	563	804	1.55E-71	COG4253	COG4253	-	cl01733
9	110496-113015	7	superfamily	273730	25	512	4.21E-155	cl36942	vgr_GE superfamily	-	-
9	110496-113015	7	specific	226704	566	827	3.32E-70	COG4253	COG4253	-	cl01733
10	116329-119655	7	superfamily	226054	1	1090	6.38E-118	cl34628	IcmF superfamily	-	-
11	119822-121258	7	specific	274543	137	433	1.70E-89	TIGR03362	VI_chp_7	-	cl11880
11	119822-121258	7	specific	377715	7	81	5.76E-13	pfam06812	ImpA_N	N	cl19907
12	124890-125969	7	specific	377755	22	319	2.70E-95	pfam06996	T6SS_TssG	-	cl01404
12	124890-125969	7	superfamily	382521	22	319	2.70E-95	cl01404	T6SS_TssG superfamily	-	-
13	121264-122694	7	specific	269829	5	84	8.30E-25	cd14744	PAAR_CT_2	-	cl21497
14	123166-124926	7	specific	377574	1	583	0	pfam05947	T6SS_TssF	-	cl15462
15	125950-126486	7	specific	378947	47	165	1.05E-30	pfam12790	T6SS_SciN	-	cl01405
16	126490-126918	7	specific	274540	3	129	2.02E-29	TIGR03357	VI_zyme	-	cl01403
17	9519-12281	21	superfamily		13	892	0	cl37250	VI.ClpV1 superfamily		
18	13932-14468	21	superfamily	386221	1	175	1.23E-57	cl11880	T6SS_VasJ superfamily	N	-

4.2 Generation of uropathogenic *E. coli* mutants

4.2.1 Transformation efficiency

The most efficient method for transforming UPEC3 strain was investigated by transforming equal amount of plasmids via electroporation or heat shock. Transformation efficiency of chemical and electrocompetent UPEC3 was calculated and summarised in Table 4.9. An example calculation of transformation efficiency is attached to Appendix, section C.1. As shown in Table 4.9, 25 colonies were transformed in the chemical competent UPEC3. In contrary, the number of transformed UPEC3 upon electroporation was estimated to be 908. Given that the transformation efficiency is proportional to colony forming units, electrocompetent UPEC3 obtained a higher transformation efficiency relatively to chemical competent UPEC3. Thus, electroporation was concluded as the most efficient method for transforming UPEC3.

Table 4.9: Transformation efficiency of chemical and electrocompetent UPEC3. A volume of 2 μL of pCRISPR (76 ng/ μL) was used to transform 50 μL of UPEC3 and plated on kanamycin agar plates. On the next day, the colonies grown on the plates were counted (cfu) and the transformation efficiency was calculated according to the amount of plasmids that were used to transform the bacteria.

UPEC3	cfu	Transformation efficiency [cfu/ μg]
Chemical competent	25	164
Electrocompetent	908	5974

4.2.2 Genomic editing efficiency of pCRISPR constructs

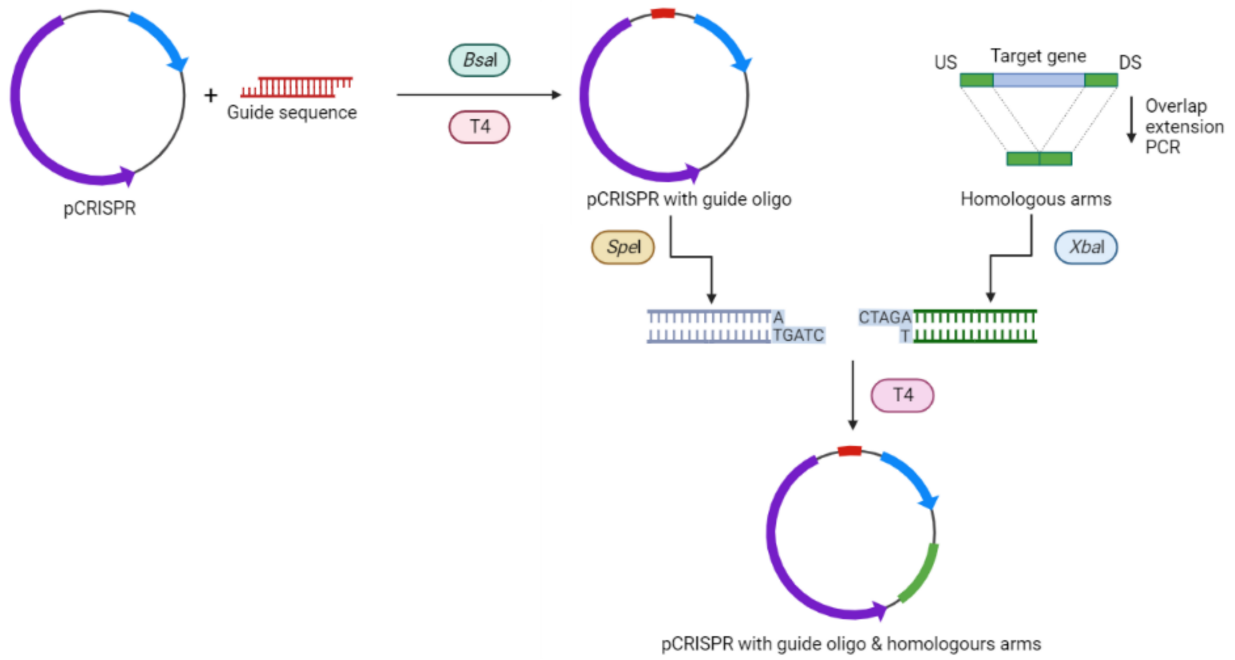
In order to delete the genes of our interest, both pCas9 and the designed pCRISPR constructs must be taken up by UPEC3. The plasmids were electroporated, but neither of the chemical nor the electrocompetent UPEC3 were able take both plasmids simultaneously. Therefore, the transformation approach was modified, where the uropathogenic *E. coli* strain was first transformed with pCas9 by electroporation and subsequently made these bacteria electrocompetent. The pCRISPR constructs were then transformed into the pCas9 harbouring UPEC3 strain by electroporation. After antibiotic selection, the colonies were screened for positive mutants by colony PCR.

In general, all the designed pCRISPR constructs contain the following features, a high copy number origin (ColE) and kanamycin resistance gene (NeoR/KanR) followed with a lambda t0 terminator. The PLtetO-1 promoter and tet operators are located upstream to direct repeats (DR) and crRNA leader, which controls expression of downstream elements, whereas

the *rrnB* T1 terminator is located downstream to the DRs and crRNA leader. Restriction enzyme digestion with *Bsa*I, generated linearised pCRISPR and sticky ends that were compatible to ligate with the guide RNA. Afterwards, the homology arms were inserted between the lambda t0 terminator and the origin after digestion with *Spe*I (Figure 4.3A). A list of single guide RNA and primers for generating the homology arms are listed in Table A.7.

To compare the genomic editing efficiency between the pCRISPR constructs without and with the homology arms, the pCRISPR_cnf1_sg2 (Figure D.3) and the pCRISPR_Harm_cnf1_sg2 (Figure D.6) were used as a demonstration of the concept. After the UPEC3 harbouring pCas9 were transformed with either pCRISPR_Harm_cnf1_sg2 or pCRISPR_cnf1_sg2 and incubated for 41-45 h at 37°C, 19 colonies were picked from each clone for verification of successful deletion of *cnf1* by PCR. The expected size of the amplicon of successful deleted *cnf1* is 1859 bp, while colonies with *cnf1* are expected to obtain an amplicon of 4904 bp, when the primer pairs *cnf1*_For and *cnf1*_Rev were used (Figure D.7). The primer pairs that were used for screening positive clones can be found in Table A.7. The editing efficiency of the pCRISPR constructs was calculated by dividing number of clones with total number of colonies that were picked for screening (Figure 4.3B).

A



B

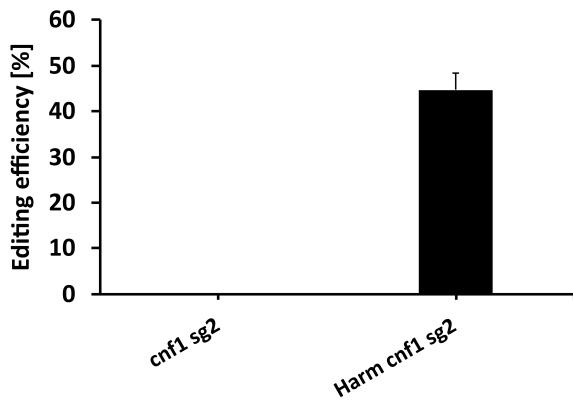


Figure 4.3: Genome editing efficiency of pCRISPR constructs. Electrocompetent UPEC3 strain harbouring pCas9 was either transformed with pCRISPR_cnf1_sg2 (cnf1 sg2), which does not contain homology arms or pCRISPR_Harm_cnf1_sg2 (Harm cnf1 sg2) with homology arms. The transformed bacteria, were incubated at 37°C for 41 to 45 hours before picking single colonies for PCR. The primer pairs *cnf1_For* and *cnf1_Rev* were used to amplify the local region of *cnf1*. General cloning procedure of pCRISPR constructs with or without homologous arms (A). Average editing efficiency and standard deviation from two independent experiments (B). US: Upstream region of the target gene. DS: Downstream region of the target gene. [Part A: Made with [BioRender](#)]

The genome editing efficiency of pCRISPR-construct with homologous arms was 44 %, while none of the colonies picked from bacteria transformed with pCRISPR without homology arms obtained an amplicon which corresponds to successful deletion of *cnf1*. According to the result from this demonstration, by including an additional DNA fragment into the CRISPR plasmid, which is a fragment of fused upstream and downstream region to the target gene, the editing efficiency increased significantly compared with pCRISPR without homology arms. Thus, pCRISPR-constructs which target *dsbA hlyA*, *ompT* or *tcpC* were also designed and cloned with a similar approach as pCRISPR_Harm_cnf1_sg2.

4.2.3 Verification of gene deletion in UPEC3

To verify mutation made in the UPEC3 genome, the mutants were sequenced and assembled by Christina Gabrielsen in Jan Egil Afset's research group. The assembled sequences in contigs were then aligned with the expected DNA sequence of successful deleted genes by [EMBOSS Matcher](#), which identify local similarities of two sequences. The identity, similarity and number of gaps that were introduced to align the DNA sequences are summarised in [Table 4.10](#). According to the alignment result, all the UPEC3 mutants have a high identity and similarity with zero gaps introduced into the sequences. The scores were above 5000, showing that the DNA sequences were aligned with a high confidence and that *cnf1*, *hlyA*, *ompT* and *tcpC* mutants were made in the UPEC3 strains. The bacterial genome of the *cnf1* and *hlyA* double deletion mutant ($\Delta cnf1/\Delta hlyA$) was also sequenced, but the DNA sequence downstream to *hlyC* was unfortunately not detected. Since the $\Delta cnf1/\Delta hlyA$ mutant was derived from the UPEC3 $\Delta hlyA$ mutant, we believe at least *hlyA* was successfully deleted. However, no commercial antibodies towards HlyA could be found and Western blotting could not be performed to confirm deletion.

Table 4.10: Pairwise sequence alignment of contigs from whole genome sequencing of UPEC3 mutants with the expected DNA sequences of successful deleted genes. The predicted DNA sequences after deletion of genes of interest were aligned with the contigs from whole genome sequencing by [EMBOSS Matcher](#). The identity, similarity and gaps that are introduced to align two sequences are given in percentage. The confidence of the sequence alignment is given with a score value.

UPEC3 strain	Identity [%]	Similarity [%]	Gaps [%]	Score
$\Delta cnf1$	100	100	0	19886
$\Delta hlyA$	100	100	0	5910
$\Delta ompT$	100	100	0	7653
$\Delta tcpC$	100	100	0	8918

According to the results in [section 4.1.1](#), *hlyA* is located 7669 bp upstream to *cnf1*. Due to the close location between *hlyA* and *cnf1*, it is possible that *hlyA* may be eliminated from the bacterial genome if the DNA reparation occurred randomly after DNA cleavage by Cas9. To investigate whether *hlyA* remained intact in the genomic DNA after *cnf1* has been deleted or vice versa, pairwise sequence alignment of the contigs from sequenced bacterial genome were aligned with *cnf1* or *hlyA* sequences from the original UPEC3. Summarised in [Table 4.11](#), the whole *hlyA* sequence was detected with high identity and similarity. Furthermore, no gaps were introduced into the sequences for the alignment. The score of the alignment between *hlyA* in UPEC3 Δ *cnf1* and *hlyA* was relatively high, indicating the alignment had a high confidence. Similar with the alignment of UPEC3 Δ *hlyA* and *cnf1*, the identity and confidence were relatively high, however, part of *cnf1* was not sequenced.

Table 4.11: Pairwise sequence alignment of UPEC3 Δ *cnf1* bacterial genome with *hlyA* and the bacterial genome of UPEC3 Δ *hlyA* with *cnf1*. Sequence alignment was performed by [EMBOSS Matcher](#). The identity, similarity and gaps that were introduced for the alignment of two sequences are in percentages. The confidence of the alignment are given in score values. Incomplete alignment of the gene sequence with the bacterial genome is given with the position within the gene.

UPEC3 strain	Gene	Identity [%]	Similarity [%]	Gaps [%]	Score	Incomplete
Δ <i>cnf1</i>	<i>hlyA</i>	100	100	0	17968	-
Δ <i>hlyA</i>	<i>cnf1</i>	100	100	0	25750	515-3045

In addition to whole genome sequencing, the local region of *cnf1* and *hlyA* were amplified by colony PCR, to verify that *cnf1* and *hlyA* remained intact in the bacterial genome of Δ *hlyA* and Δ *cnf1* single mutants, respectively. The local regions were amplified with the PCR primer pairs *cnf1*_For and *cnf1*_Rev or *hlyA*_For and *hlyA*_Rev ([Table A.7](#)). Amplicons generated from PCR with *cnf1*_For and *cnf1*_Rev primers will have a size of 4905 bp if *cnf1* was not deleted and 1859 bp upon successful *cnf1* deletion. Similarly, PCR primer pairs *hlyA*_For and *hlyA*_Rev will give an amplicon of 4933 bp if *hlyA* remained intact, while 1858 bp if deleted. Moreover, the double deletion mutant Δ *cnf1*/ Δ *hlyA* were also verified with colony PCR with the respective primer pairs.

According to [Figure 4.4](#), UPEC3 wild type obtained two DNA fragments with a size around 5000 bp, when amplified with PCR primer pairs *cnf1*_For and *cnf1*_Rev or *hlyA*_For and *hlyA*_Rev, respectively. Showing that *cnf1* and *hlyA* were not deleted. On the other hand, an amplicon at 2000 bp was obtained in Δ *cnf1* upon amplification with the *cnf1* forward and reverse primers ([Figure 4.4A](#)), while Δ *cnf1* with *hlyA* primer pairs gave an amplicon of 5000 bp ([Figure 4.4B](#)). Supporting successful *cnf1* deletion, while *hlyA* remained intact in Δ *cnf1*. With the same reasoning, *cnf1* was not removed from Δ *hlyA* mutant, while both *cnf1* and *hlyA* were deleted in the double mutant Δ *cnf1*/ Δ *hlyA*.

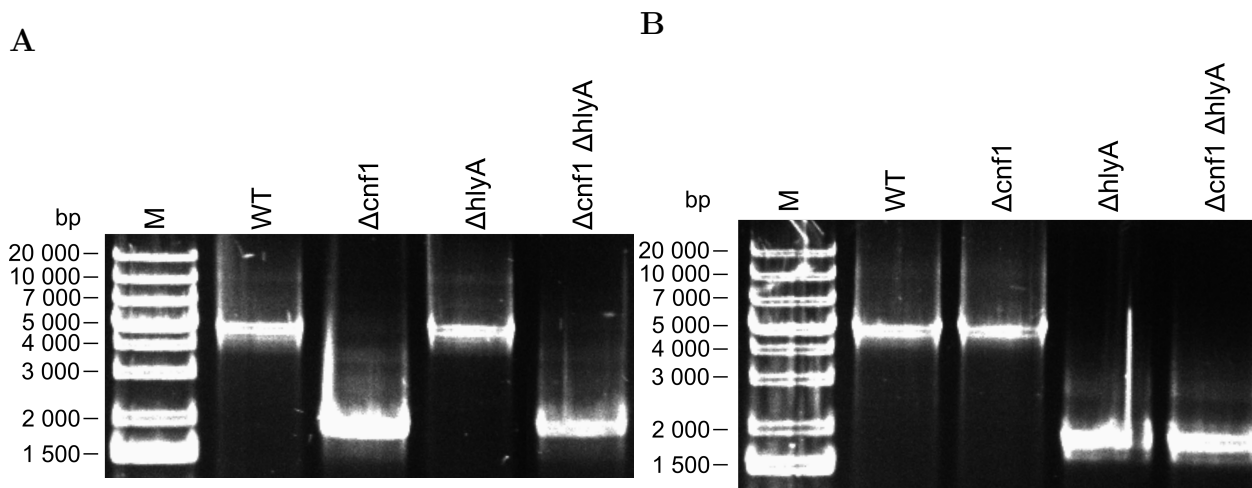


Figure 4.4: Verification of *cnf1* and *hlyA* deletion in UPEC3 variants. UPEC3 wild type and mutants were picked for colony PCR that either had the primer pair *cnf1*_For and *cnf1*_Rev (**A**), or *hlyA*_For and *hlyA*_Rev primer pairs (**B**). The expected size of amplicon with successful *cnf1* and *hlyA* deletion are 1859 bp and 1858 bp, respectively. Unsuccessful deletion of *cnf1* or *hlyA* gives an amplicon with a length of 4905 bp and 4933 bp, respectively. M: GeneRuler 1kb Plus DNA ladder. WT: UPEC3 wild type. $\Delta cnf1$: UPEC3 *cnf1* deletion mutant. $\Delta hlyA$: UPEC3 *hlyA* deletion mutant. $\Delta cnf1/\Delta hlyA$: UPEC3 *cnf1* and *hlyA* double deletion mutant.

Furthermore, the *cnf1* and *tcpC* double deletion mutant ($\Delta cnf1/\Delta tcpC$) was also verified by colony PCR with the same approach as described above. Again the primer pairs *cnf1*_For and *cnf1*_Rev were used to verify deletion of *cnf1*, while *tcpC*_For and *tcpC*_Rev were used to amplify the local region to *tcpC*. The expected size of the amplicon from a successful deletion of *tcpC* is 1382 bp, and 2306 bp if the gene was not deleted. Consistent with the expected sizes of successful knockout of *cnf1* and *tcpC*, [Figure 4.5](#) shows that *cnf1* and *tcpC* were successfully deleted from UPEC3.

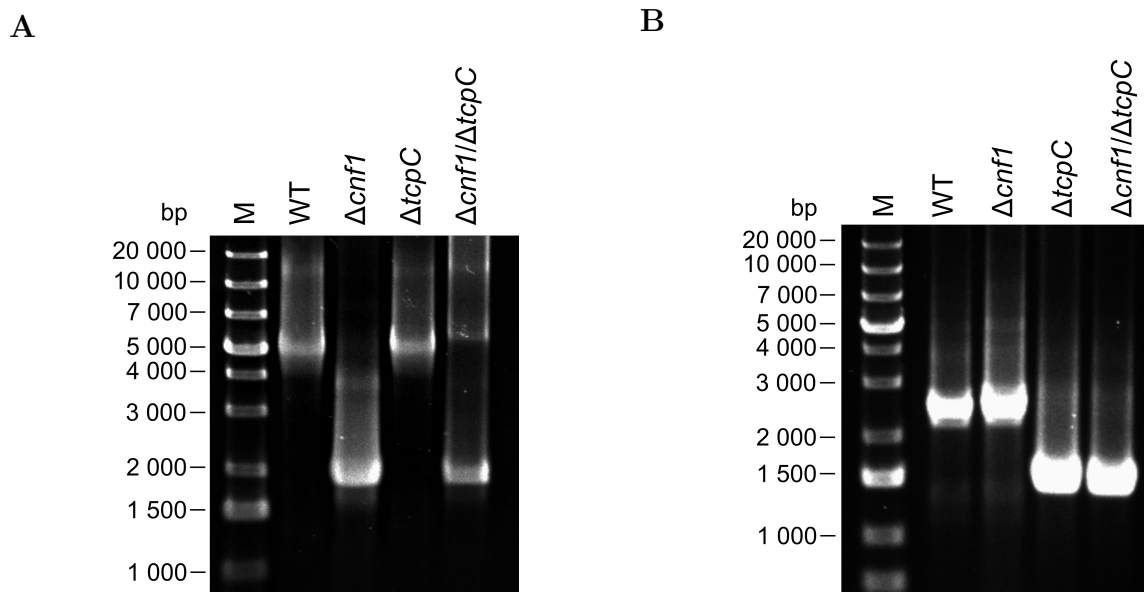


Figure 4.5: Verification of *cnf1* and *tcpC* deletion in UPEC3 variants. UPEC3 wild type and mutants were picked for colony PCR that either had the primer pair *cnf1*_For and *cnf1*_Rev (A), or the primer pairs *tcpC*_For and *tcpC*_Rev (B). The expected size of amplicon with successful *cnf1* and *tcpC* deletion is 1859 bp and 1382 bp, respectively. Unsuccessful deletion of *cnf1* or *tcpC* gives an amplicon with a length of 4905 bp and 2306 bp, respectively. M: GeneRuler 1kb Plus DNA ladder. WT: UPEC3 wild type. $\Delta cnf1$: UPEC3 *cnf1* deletion mutant. $\Delta tcpC$: UPEC3 *tcpC* deletion mutant. $\Delta cnf1/\Delta tcpC$: UPEC3 *cnf1* and *tcpC* double deletion mutant.

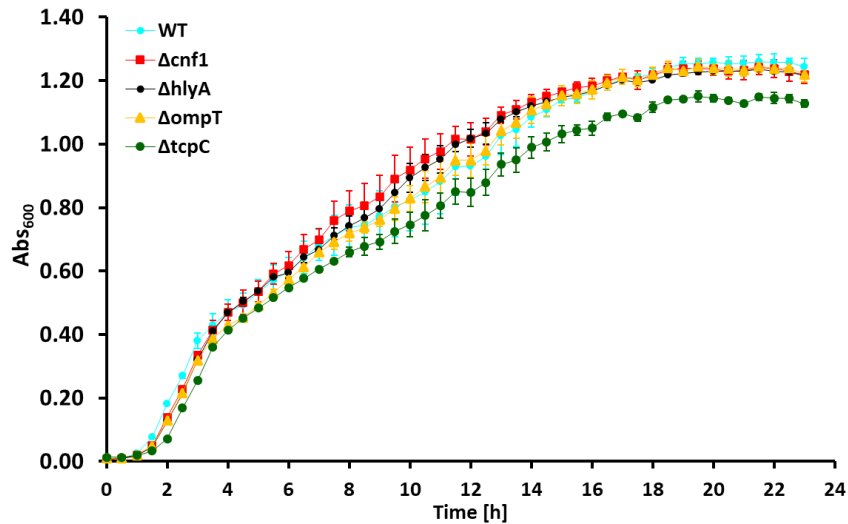
4.2.4 Number of uptaken plasmids may affect the growth rate of UPEC3 strains

Before starting infecting THP-1 cells with UPEC3 wild type and mutants, the growth curves of the bacteria were measured to ensure that deletion of the genes of interest did not change the bacterial growth rate. As illustrated in [Figure 4.6A](#), UPEC3 wild type seems to grow a bit faster than the mutants strains, while $\Delta tcpC$ which still harboured pCRISPR construct, grew slower. According to the calculated generation time of the bacteria at their exponential phase ([Table 4.12](#)), the bacteria were not growing with a significantly different rate. Despite, the generation time of $\Delta tcpC$ was relatively similar to other UPEC3 variants, its growth curve points that it has a longer lag phase than the other bacteria strains, where the early exponential phase began after 2 h of incubation, while other UPEC3 variants have already entered this phase after 1.5 h of incubation. Nevertheless, UPEC3 wild type seems to have the shortest lag phase among the bacteria strains. Example calculation of generation time is attached to appendix, [section C.3](#).

The growth curve of UPEC3 transformed with pCas9 was measured and compared with growth curves of the mutants. Moreover, the avirulent, DH5 α strain transformed with pCas9, was also included to the growth curves measurement, to investigate its growing pattern with the same condition as the UPEC3 strain. As shown in [Figure 4.6B](#), the growth curve of the

pCas9 transformed UPEC3 overlapped with the growth curves of the mutants at log phase and at the exponential phase. After the pCRISPR construct was cured from $\Delta tcpC$ mutant, the lag phase was shortened to a similar interval as the other UPEC3 strains. The lag phase of the pCas9 transformed DH5 α was relatively similar as UPEC3 strains. However, after two hours of incubation, DH5 α seems to grow slower than the UPEC3 strains, and reached to stationary phase earlier than UPEC3 variants. In summary, the growth curves demonstrated that the number of uptaken plasmids in UPEC3 strains may affect their growth. For later THP-1 bacterial stimulation experiments, UPEC3 harbouring pCas9 will be used to compare with mutants stimulated cells. pCas9 transformed UPEC3 will be denoted as UPEC3 wild type for easier comparison purpose.

A



B

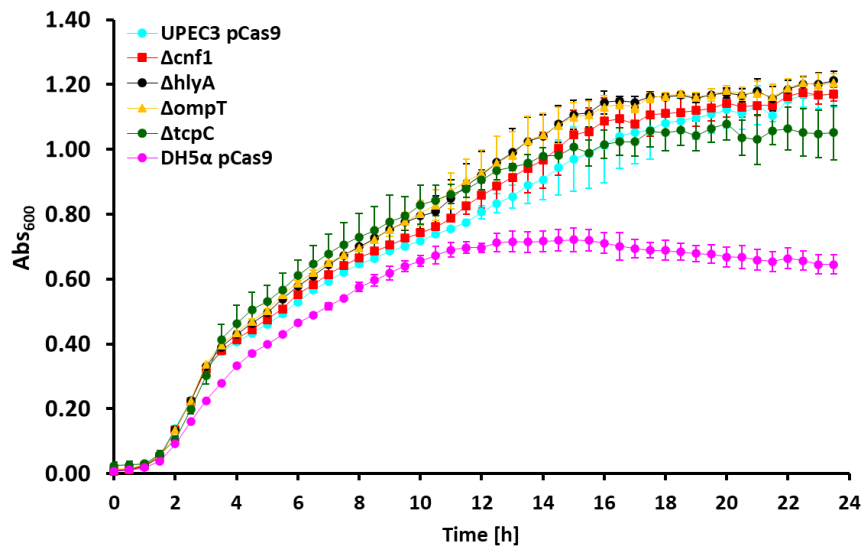


Figure 4.6: Number of plasmids transformed into uropathogenic *E. coli* affects its growth. An overnight culture of each strain was diluted to the absorbance at 600 nm was 0.01 in LB medium. The bacteria were grown at 37 °C with aeration. The mean absorbance at 600 nm and standard deviation were calculated from technical triplicates. **A:** UPEC3 wild type (WT) did not harbour any plasmids, while the $\Delta cnf1$, $\Delta hlyA$, $\Delta ompT$ only carried pCas9. Both pCas9 and pCRISPR_Harm_tcpC_sg4 were not cured from the *tcpC* UPEC3 knockout strain ($\Delta tcpC$). **B:** All UPEC3 variants only harboured pCas9. DH5α pCas9: pCas9 transformed *E. coli* DH5α strain.

Table 4.12: Generation time of UPEC3 variants. The generation time (t_g) of the UPEC3 variants were predicted from the absorbance when the bacteria were at their exponential phase. For UPEC3 wild type, $\Delta cnf1$, $\Delta hlyA$ and $ompT$ deletion mutant ($\Delta ompT$), the generation time was calculated from 1.5 to 3 h of incubation, while the generation time of $\Delta tcpC$ was calculated between the time interval 2 and 3.5 h of incubation. Only the mutants harboured pCas9, while $\Delta tcpC$ harboured the high copy number pCRISPR construct, in addition to the low copy number pCas9.

UPEC3 strain	t_g [min]
WT	39
$\Delta cnf1$	33
$\Delta hlyA$	32
$\Delta ompT$	33
$\Delta tcpC$	39

4.2.5 Expression and secretion of CNF1 and OmpT in UPEC3 wild type and mutants

In addition to colony PCR and whole genome sequencing, deletion of $cnf1$ and $ompT$ were verified by Western blotting. Apparently, neither $\Delta cnf1$, $\Delta cnf1/\Delta hlyA$ nor DH5 α expressed CNF1 (Figure 4.7), which coincide with earlier observations from whole genome sequencing (section 4.2.3). On the other hand, UPEC3 wild type, $\Delta hlyA$, $\Delta ompT$ and $\Delta tcpC$ single mutants express and secrete CNF1. Indeed, only a small amount of CNF1 was secreted to the supernatant, while most of the toxin remained within the bacteria.

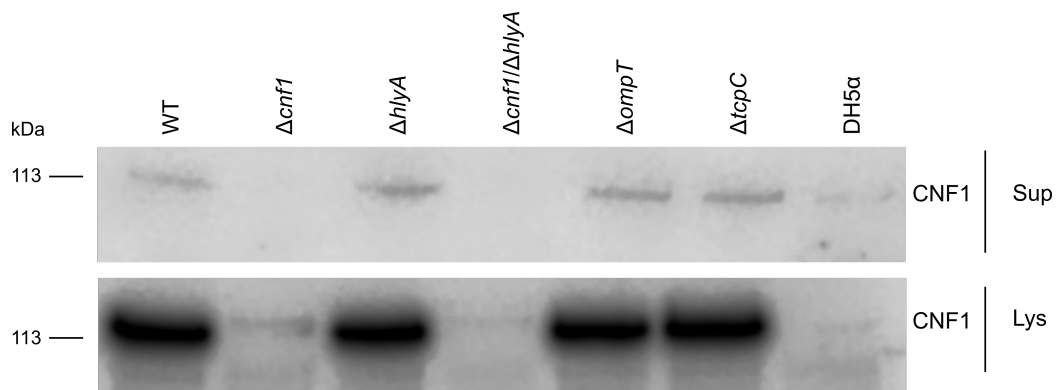
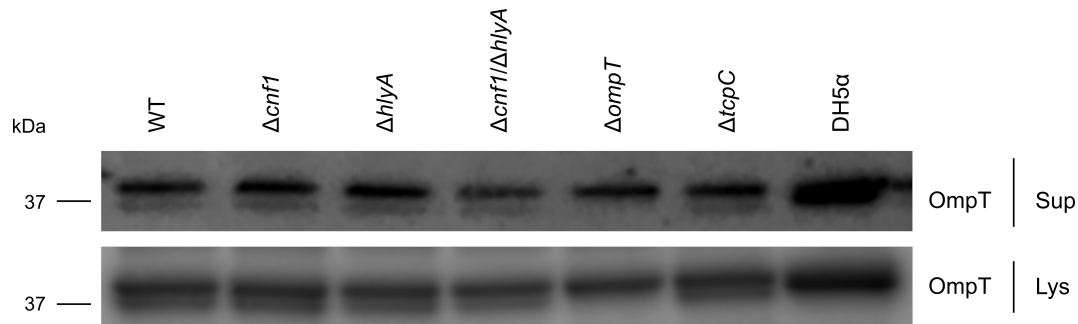


Figure 4.7: Immunoblot of CNF1. Expression and secretion of CNF1 in UPEC3 variants and in the avirulent DH5 α strain were detected with immunoblot. All bacteria strains were cultivated in LB medium with chloramphenicol at 37°C overnight with agitation. The supernatant (sup) and the lysate (lys) were separated after centrifuging the samples. The supernatants were sterile filtered to remove bacteria residues.

In the same way, protein expression level of OmpT in different UPEC3 mutants and DH5 α were measured by Western blotting the supernatants and the lysates of overnight bacteria cultures that were cultivated in LB medium (Figure 4.8A). The bands which correspond to OmpT (37 kDa) appeared weakly on the membrane and the resolution between OmpT and a background band was initially poor. To improve the resolution of the OmpT band, the bacteria were cultivated with minimal A medium instead of LB. As illustrated in Figure 4.8B, OmpT was not detected in the lysate nor in the supernatant of the UPEC3 *ompT* knockout strain. Indicating *ompT* was successfully deleted, which corresponds with the results from pairwise sequence alignment (Table 4.10). Furthermore, the growth curves of UPEC3 variants in minimal A medium confirmed that the $\Delta ompT$ grew with a similar growth rate as the UPEC3 wild type (Figure 4.9), ensuring that deletion of *ompT* did not affect the growth rate.

A



B

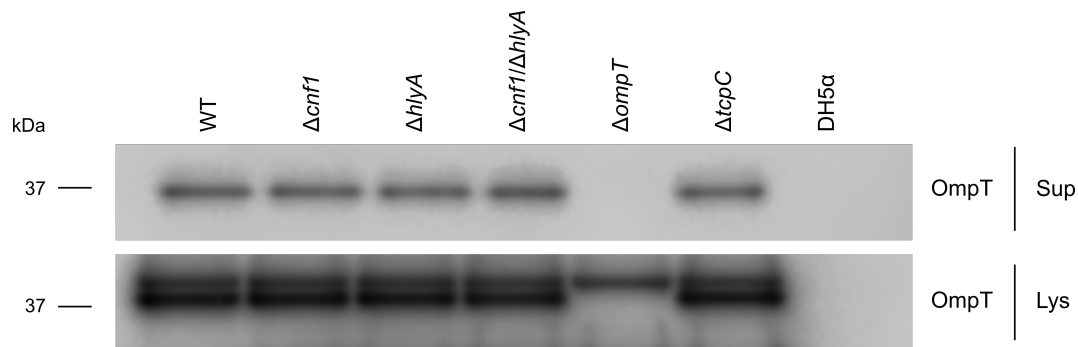


Figure 4.8: Detection of OmpT expressed in different *E. coli* strains that were cultivated with LB or minimal A medium. Bacteria cultures in LB (A) and minimal A medium (B) were incubated in parallel for 21 h at 37°C. A volume of 1 mL of each culture was prepared for the supernatant (sup) sample, while 200 μ L of culture was pelleted and lysed (lys).

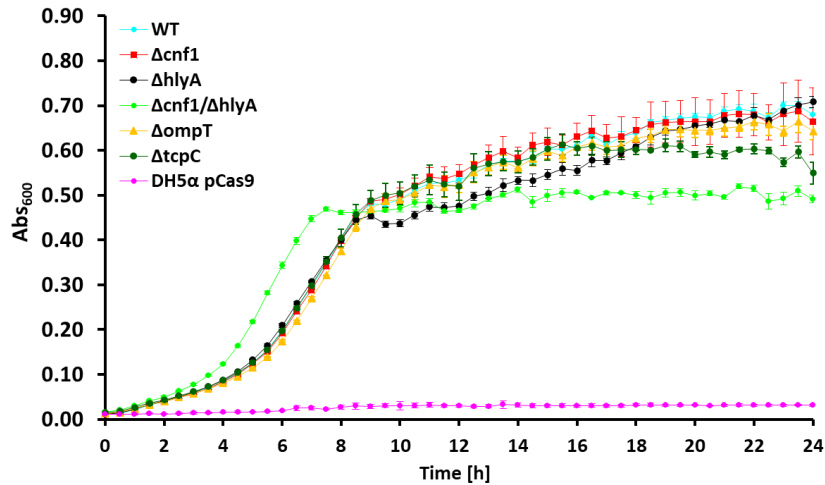


Figure 4.9: Growth curve of uropathogenic and avirulent *E. coli* in minimal A medium. Overnight cultures of UPEC3 variants and DH α were diluted so the initial absorbance at 600 nm was 0.01. The bacteria were incubated at 37°C with agitation, and the turbidity was measured. The mean absorbance and the standard deviation were calculated from technical triplicates.

Although, the $\Delta cnf1/\Delta hlyA$ double deletion mutant grew relatively faster after three hours of incubation in minimal A medium and reached the stationary phase earlier than other UPEC3 strains, the amount of detected OmpT in the supernatant and in the lysate was comparable as other OmpT expressing UPEC3 strains. Unfortunately, DH5 α did not grow well in minimal A medium so we cannot conclude whether this strain expresses OmpT or not from the Western blot. However, sequence data obtained from GeneBank ([GenBank:CP017100.1](#)) shows that DH5 α encodes OmpT. Together with the whole genome sequencing results ([Table 4.10](#)), the immunoblots also confirmed that *cnf1* and *ompT* were successfully deleted from the respective UPEC3 strains. Moreover, the UPEC3 strains seem to cope with rough growing conditions much better than the avirulent DH5 α ([Figure 4.9](#)).

4.3 Stimulation of THP-1 cells with *E. coli* strains

The clinical isolates of uropathogenic *E. coli* expresses several virulence factors, where CNF1 and HlyA and TcpC are among these factors that have been demonstrated to activate or inhibit inflammatory signalling pathways [94, 61, 95]. In this study, we selected THP-1 cells as a model cell line for studying the cell death mechanisms in macrophages upon stimulation with different *E. coli* strains. Also, we used siRNA technology to target the expression of Rab11 family interacting protein 2 (FIP2). First, we stimulated THP-1 cells with bacteria without LPS priming and investigated the effect of CNF1, HlyA and TcpC on inflammatory cell death. As already shown in [section 4.2.3](#) and [section 4.2.5](#), we have generated several UPEC3 mutants. Due to time limitation, we chose to focus on stimulation of THP-1 cells with UPEC3 strains with *cnf1*, *hlyA* single and *cnf1/hlyA* double mutants in later infection experiments. The *ompT* single mutant and *cnf1/tcpC* double deletion mutant were not inspected in this study.

4.3.1 HlyA expressing UPEC3 strains induce massive cell lysis in THP-1 cells

Prior to bacterial stimulation, the THP-1 cells were treated with either Allstar non-silencing RNA (NS RNA) control or FIP2 silencing siRNA (FIP2 siRNA), to investigate the effect of FIP2 silencing has on inflammatory signalling pathways in THP-1 cells. Upon activation of inflammatory signalling pathways, THP-1 cells release pro-inflammatory cytokines as well as lactate dehydrogenase (LDH) due to damaged plasma membrane [90]. As LDH is an important marker of cell lysis, LDH released from THP-1 cells upon bacterial stimulation was measured. The percentage of LDH released from the cells were calculated using THP-1 cells lysed with lysis buffer as control ([Figure 4.10](#)). An example of the calculation of LDH release is attached to Appendix, [section C.6](#).

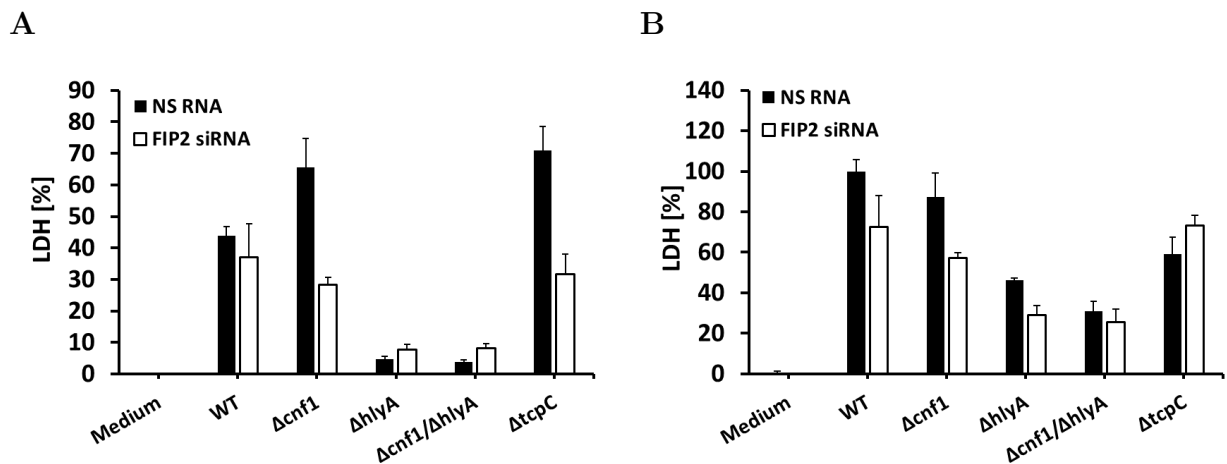


Figure 4.10: LDH release from THP-1 cells stimulated with UPEC3 variants. THP-1 cells treated with NS RNA or FIP2 siRNA before stimulation with UPEC3 wild type and mutants with a multiplicity of infection (MOI) of 2 for 2 h (A) and 4 h (B). The LDH level in the supernatants were colorimetrically quantified. The error bars illustrate the standard deviation of technical duplicates. The percentage of released LDH were normalised to NS RNA treated cells in medium.

According to Figure 4.10A, THP-1 cells that were either stimulated with the single mutant $\Delta cnf1$ or $\Delta tcpC$ for 2 h, the amount of LDH release was higher than cells that were stimulated with UPEC3 wild type. Intriguingly, the LDH release was dramatically decreased in THP-1 cells that were stimulated with $\Delta hlyA$ or $\Delta cnf1/\Delta hlyA$ relatively to UPEC3 wild type stimulated cells. The amount of LDH released from THP-1 cells that were stimulated with $\Delta cnf1/\Delta hlyA$ was significantly lower than cells that were stimulated with $\Delta cnf1$, but has an equivalent LDH level as cells stimulated with $\Delta hlyA$. After 4 h of stimulation, the amount of released LDH was increased in all THP-1 cells stimulated with bacteria (Figure 4.10B).

Indeed, it is noticeable that there was an effect of FIP2 silencing in THP-1 cells that were stimulated with $\Delta cnf1$ or $\Delta tcpC$ for 2 h, where the LDH release was reduced by 50 % relative to the NS RNA treated THP-1 cells. Interestingly, after 4 h of stimulation, the effect of FIP2 silencing disappeared in cells stimulated with UPEC3 wild type and mutants (Figure 4.10B). Altogether, these observations indicate that HlyA expressed in UPEC3 damages the plasma membrane and subsequently induce cell lysis in THP-1 cells.

4.3.2 FIP2 silencing and bacterial stimulation affect transcription of inflammatory cytokines in THP-1 cells

The expression level of pro-inflammatory cytokines was further analysed with Q-PCR to address whether FIP2 silencing and treatment with UPEC3 wild type or mutant strains would affect the mRNA levels of the pro-inflammatory cytokines of interest. Before analysing mRNA levels of pro-inflammatory cytokines, the efficiency of FIP2 silencing was controlled by Q-PCR. As shown in [Figure 4.11A](#) and [Figure 4.12A](#), FIP2 mRNA levels were reduced by approximately 80 % compared to the NS RNA treated cells without stimulation. Bacterial stimulation in NS RNA THP-1 cells seem to down-regulate FIP2 mRNA expression relatively to unstimulated THP-1 cells. Moreover, the expression of FIP2 in bacterial stimulated THP-1 cells was reduced to a similar level as the unstimulated THP-1 cells when treated with FIP2 siRNA. Indicating FIP2 was successfully silenced.

In general, THP-1 cells that were treated with the $\Delta hlyA$ or $\Delta cnf1/\Delta hlyA$ mutants have the highest expression level of mRNA for the tumour necrosis factor- α (TNF α), pro-interleukin-1 β (pro-IL-1 β), NLR family pyrin domain containing 3 (NLRP3) and interferon- β (IFN β) after 2 h ([Figure 4.11](#)) and 4 h ([Figure 4.12](#)). Compared with cells that were treated with UPEC3 wild type for 2 h, $\Delta hlyA$ single and $\Delta cnf1/\Delta hlyA$ double mutants stimulated THP-1 cells increased the expression levels of pro-IL-1 β and NLRP3 approximately by 42 % and 54 %, respectively ([Figure 4.11B](#) and [Figure 4.11C](#)). On the other hand, expression of TNF α in NS RNA THP-1 cells stimulated with $\Delta hlyA$ increased by 60 % and 72 % in $\Delta cnf1/\Delta hlyA$ relatively to UPEC3 wild type stimulated NS RNA cells ([Figure 4.11E](#)). Compared with UPEC3 wild type, IFN β was increased by 52 % in $\Delta cnf1$ mutant stimulated NS RNA cells. More strikingly, the relative levels of IFN β mRNA were increased by more than 90 % in $\Delta hlyA$ and $\Delta cnf1/\Delta hlyA$ mutants compared to UPEC3 wild type, while the mRNA levels decreased approximately with 50 % when the cells were treated with FIP2 siRNA ([Figure 4.11D](#)). Nevertheless, the FIP2 siRNA treated THP-1 cells showed a modest reduction (approximately 25 %) in the transcription level of NLRP3 ([Figure 4.11C](#)). Similar observations are seen in [Figure 4.11E](#), where the RQ values of TNF α between NS RNA and FIP2 siRNA treated THP-1 cells showed a similar reduction.

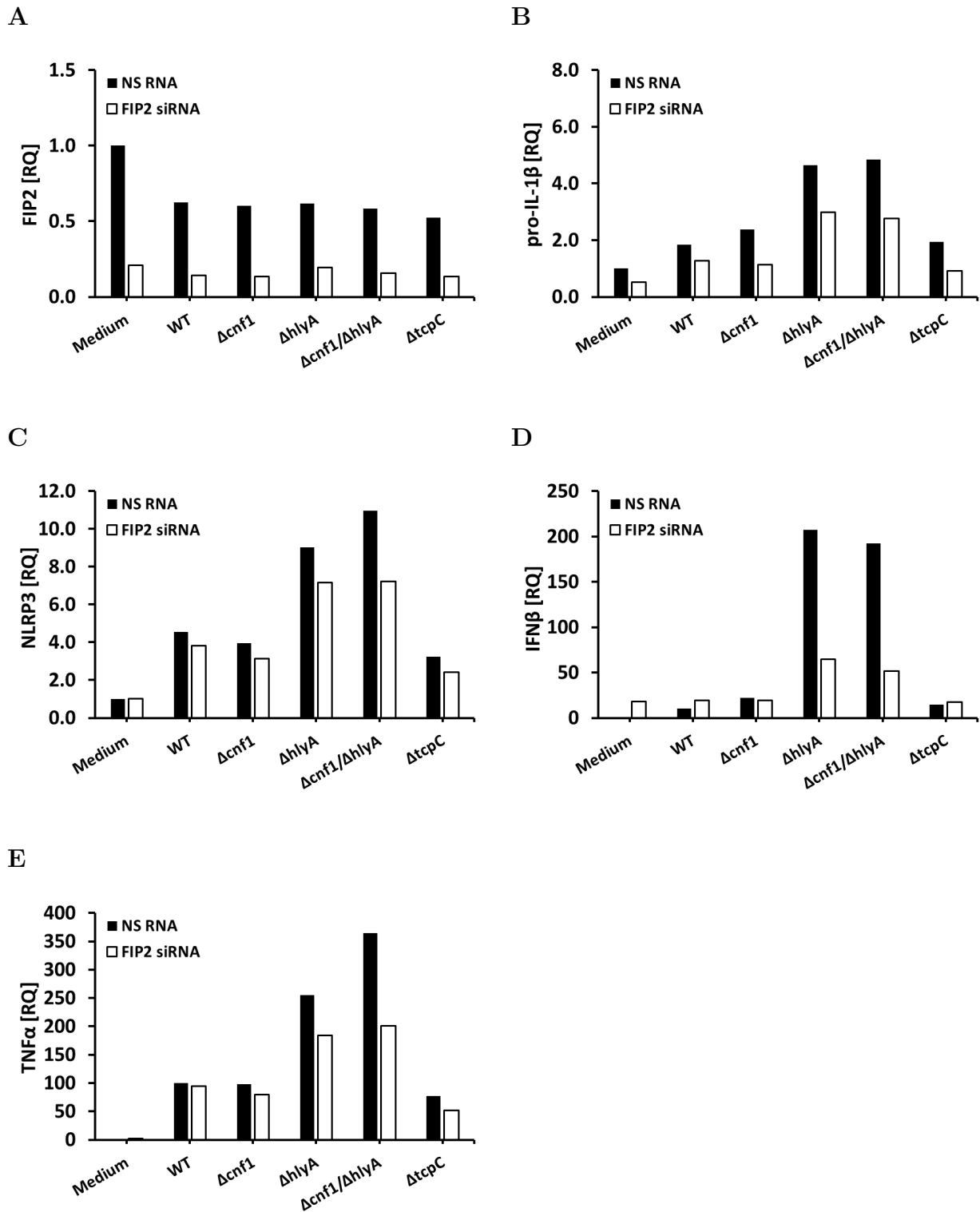


Figure 4.11: Pro-inflammatory cytokine mRNA expression level in THP-1 cells stimulated with UPEC3 wild type and mutants. THP-1 cells were treated with NS RNA or FIP2 siRNA before stimulation with UPEC3 wild type and mutants for 2 h (MOI = 2). FIP2 mRNA expression levels (**A**), pro-IL-1 β mRNA levels (**B**), NLRP3 mRNA levels (**C**), IFN- β mRNA levels (**D**), TNF α mRNA levels (**E**). The values are given as relative quantification (RQ). The RQ values were normalised against the TATA-box binding protein (TBP).

Likewise, the same trend of the relatively high cytokine expression in THP-1 cells stimulated with $\Delta hlyA$ single mutant and $\Delta cnf1/\Delta hlyA$ double mutants seems to persist after 4 h of stimulation (Figure 4.12). In general, FIP2 silencing gave a modest reduction in mRNA levels of pro-IL-1 β and TNF α mRNAs (Figure 4.12B and Figure 4.12A). Except for the $\Delta tcpC$ stimulated cells, FIP2 silencing showed approximately 50 % reduction of IFN β mRNA levels relatively to NS RNA treated cells (Figure 4.12A). As observed from 2 h of bacterial stimulation, NLRP3 mRNA levels in FIP2 siRNA treated THP-1 did not decrease after 4 h (Figure 4.12C).

Overall, stimulation with UPEC3 strains up-regulated transcription of pro-IL-1 β , NLRP3, IFN β and TNF α in THP-1 cells, while FIP2 silencing gave a modest reduction of mRNA levels of pro-inflammatory cytokines.

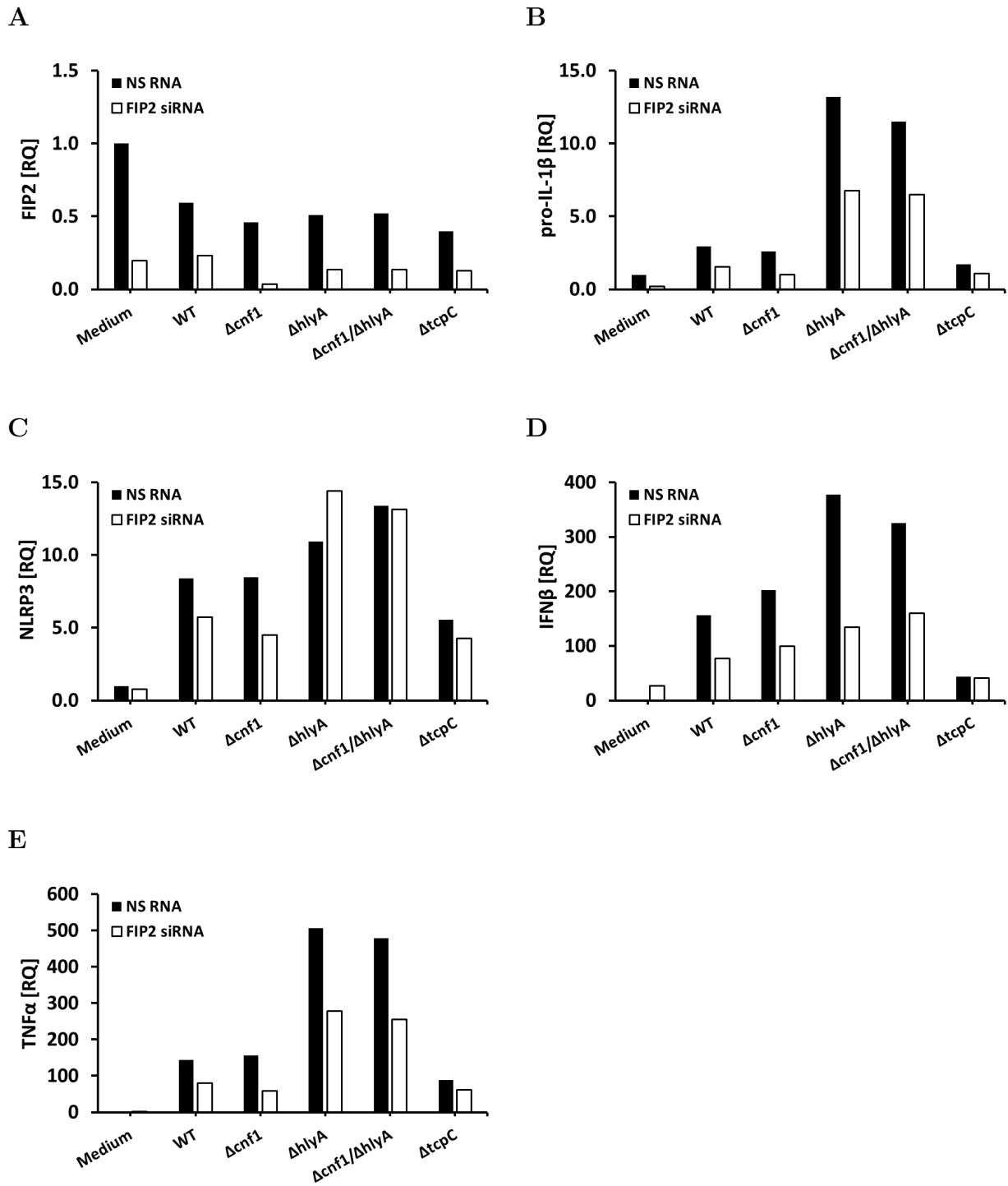


Figure 4.12: Pro-inflammatory cytokine mRNA expression levels in THP-1 cells stimulated with UPEC3 wild type and mutants . THP-1 cells were treated with NS RNA or FIP2 siRNA, before stimulation with UPEC3 wild type and mutants (MOI = 2) for 4 h. FIP2 mRNA levels (**A**). pro-IL-1 β mRNA levels (**B**). NLRP3 mRNA levels (**C**) IFN β (**D**). and TNF α mRNA levels (**E**). The RQ values were normalised against TATA-box binding protein (TBP).

4.3.3 Post-translational maturation and release of caspase-1 and IL-1 β are affected by bacterial virulence factors

As illustrated in [Figure 4.13A](#), immunoblots of THP-1 cell supernatants stimulated with UPEC3 wild type or mutants for 2 h, both pro-caspase-1 and cleaved caspase-1 p20 were detected. Shown in [Figure D.9A](#), pro-caspase-1 was increased at least by 60 % in NS RNA cells stimulated with UPEC3 wild type, $\Delta cnf1$ and $\Delta tcpC$ compared with the unstimulated cells. Relative to UPEC3 wild type stimulated NS RNA cells, the level of caspase-1 p20 protein was increased by 61 % in $\Delta cnf1$ and 73 % in $\Delta tcpC$ stimulated cells ([Figure 4.13C](#)). On the other hand, $\Delta hlyA$ single mutant and the $\Delta cnf1/\Delta hlyA$ double mutant stimulated cells released similar amount of pro-caspase-1 as the unstimulated cells, while release of caspase-1 p20 was decreased by at least 70 % relative to UPEC3 wild type stimulated NS RNA cells. As shown in [Figure 4.13E](#), release of caspase-1 also reflected the trend observed for released IL-1 β p17 in the supernatants, where $\Delta cnf1$ and $\Delta tcpC$ showed at least 50 % increase of IL-1 β p17, while it was decreased by 80 % in $\Delta hlyA$ and $\Delta cnf1/\Delta hlyA$ relatively to UPEC3 wild type stimulated cells. Due to large background of IL-1 β p17 in UPEC3 wild type stimulated cells, only half of the IL-1 β p17 bands were quantified.

After 4 h, the pattern of released pro-caspase-1 from UPEC3 wild type, $\Delta cnf1$ and $\Delta tcpC$ single mutants stimulated NS RNA cells persisted ([Figure 4.13B](#) and [Figure D.9B](#)). Unlike the 2 h of bacterial stimulation, release of caspase-1 p20 and IL-1 β p17 were the lowest in cells stimulated with $\Delta tcpC$ ([Figure 4.13D](#) and [Figure 4.13F](#)), while cells stimulated with UPEC3 wild type or $\Delta cnf1$ released the largest amount of caspase-1 p20 and pro-caspase-1 ([Figure D.9B](#)). Interestingly, UPEC3 wild type and the $\Delta cnf1$ stimulated NS RNA cells released the largest amount of pro-IL-1 β ([Figure D.9D](#)), yet these cells released less IL-1 β p20 compared with cells stimulated with $\Delta hlyA$ and $\Delta cnf1/\Delta hlyA$ ([Figure 4.13F](#)). Interestingly, immunoblots also showed an intermediate form of caspase-1 (37 kDa) and IL-1 β (28 kDa) in the supernatants of UPEC3 wild type, $\Delta cnf1$ and $\Delta tcpC$ stimulated THP-1 cells, but not in cells treated with medium ([Figure 4.13A](#) and [Figure 4.13B](#)). Unconventional caspase-1 and IL-1 β intermediates were not observed in NS RNA cells that were stimulated with $\Delta hlyA$ or $\Delta cnf1/\Delta hlyA$ for 2 h ([Figure 4.13A](#)), while these intermediates were weakly detected after 4 h of stimulation [Figure 4.13B](#)).

Indeed, FIP2 silencing did not decrease pro-caspase-1 and caspase-1 p20 in the supernatants of 2 h stimulation with UPEC3 wild type or the $\Delta cnf1/\Delta hlyA$ double mutant ([Figure D.9A](#) and [Figure 4.13C](#)). FIP2 silencing slightly reduced release of pro-caspase-1 (30 % <) in $\Delta cnf1$, $\Delta hlyA$ and $\Delta tcpC$ mutants stimulated cells. However, relative to NS RNA cells, the levels of caspase-1 p20 in the supernatants of $\Delta cnf1$ and $\Delta tcpC$ stimulated FIP2 siRNA THP-1 cells were reduced by 62 % and 71 %, respectively ([Figure 4.13C](#)). After 2 h of stimulation, pro-IL-1 β was also reduced in FIP2 siRNA cells stimulated with $\Delta cnf1$ and $\Delta tcpC$ mutants at least by 68 % ([Figure D.9C](#)). Strikingly, after 2 h, the amount of IL-1 β

in the supernatants of $\Delta cnf1$ and $\Delta tcpC$ mutants stimulated FIP2 siRNA cells decreased by 80 %. FIP2 silencing also decreased the release of pro-caspase-1 slightly after 4 h stimulation with UPEC3 wild type, $\Delta hlyA$ single mutant, $\Delta cnf1/\Delta hlyA$ double mutant and $\Delta tcpC$ single mutant (Figure D.9B). In contrast, release of caspase-1 p20 was decreased by 45 % in FIP2 siRNA cells stimulated UPEC3 wild type and approximately by 70 % in cells treated with $\Delta cnf1$ or $\Delta hlyA$ (Figure 4.13D). Except $\Delta tcpC$ mutant stimulated cells, FIP2 siRNA treatment also reduced release of pro-IL-1 β at least 62 % (Figure D.9D) and IL-1 β p20 by 77 % (Figure 4.13F) after 4 h.

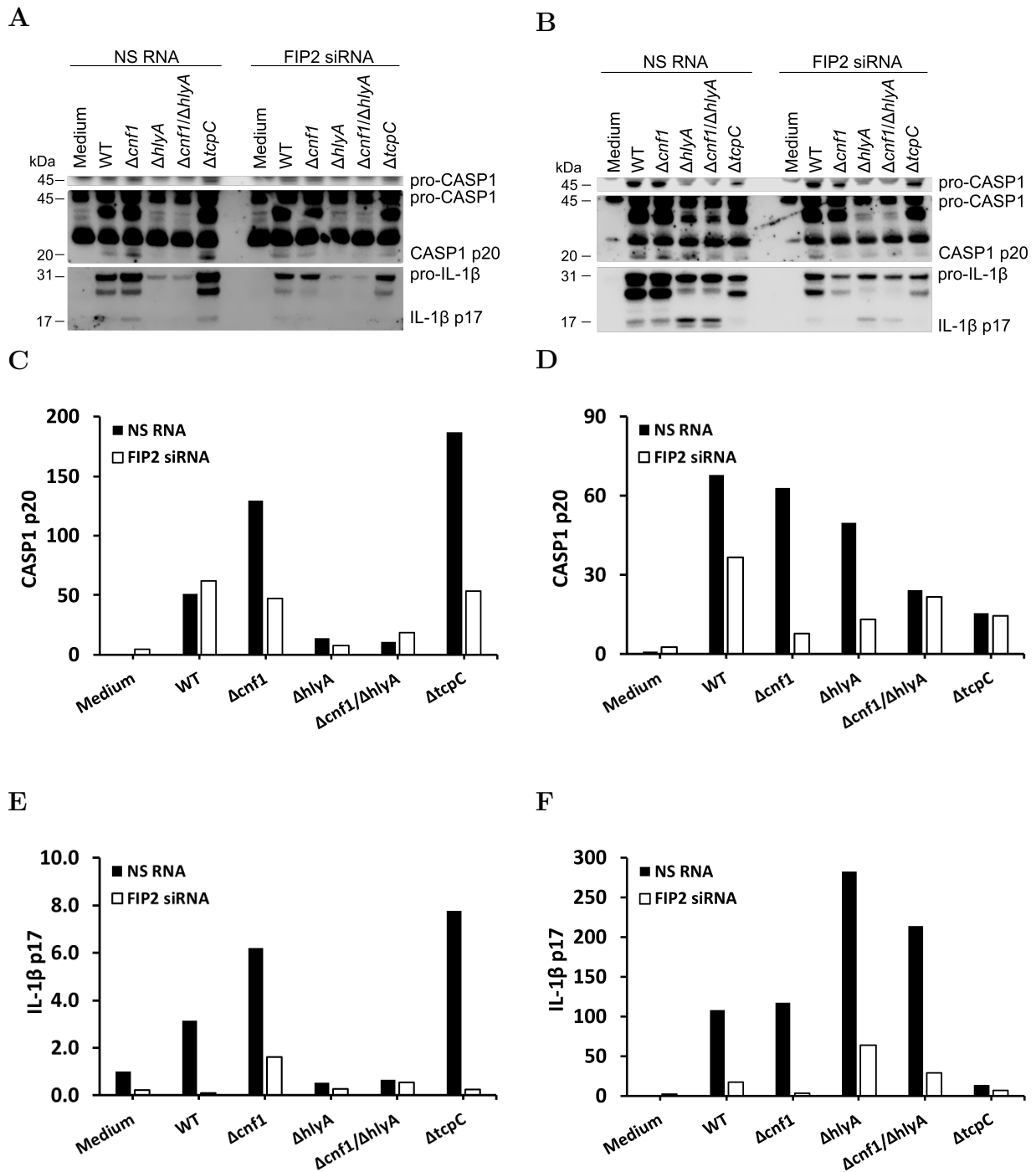


Figure 4.13: IL-1 β and caspase-1 levels in supernatants of THP-1 cells after 2 h and 4 h stimulation with UPEC3 wild type and mutants. THP-1 cells treated with NS RNA or FIP2 siRNA before stimulation with UPEC3 wild type or mutants for 2 h and 4 h (MOI = 2). Immunoblot of pro-caspase-1, caspase-1 p20, pro-IL-1 β and IL-1 β p17 after 2 h (**A**) and 4 h (**B**) stimulation. Quantification of caspase-1 p20 protein level after 2 h (**C**) and 4 h (**D**) stimulation. Quantification of IL-1 β p17 protein level after 2 h (**E**) and 4 h (**F**) stimulation. Quantified protein levels were normalised to unstimulated NS RNA THP-1 cells.

To investigate activation of components in pyroptosis, a more profound analysis of the cell lysates was performed by Western blotting. To control that the amount of proteins was loaded equally to the gel, the sample volume was adjusted regarding to β -tubulin in the lysates. As illustrated in [Figure 4.14A](#) and in [Figure 4.14C](#), after 2 h of bacterial stimulation, β -tubulin was detected in the lysates and the amount was relatively similar as in the unstimulated cells. Moreover, the level pro-IL-1 β protein increased in NS RNA cells that were stimulated with UPEC3 strains and more strikingly in cells that were stimulated with the $\Delta tcpC$ mutant, a 70 % increase was observed ([Figure 4.14E](#)).

After 4 h of stimulation, β -tubulin was reduced approximately by 93 % in NS RNA cells that were treated with UPEC3 wild type, $\Delta cnf1$ or $\Delta tcpC$ single mutant clones relatively to unstimulated cells ([Figure 4.14B](#) and [Figure 4.14D](#)). Furthermore, pro-IL-1 β was also much less in UPEC3 wild type, $\Delta cnf1$ or $\Delta tcpC$ mutants stimulated NS RNA cells. Indicating, massive cell death after 4 h and intracellular components may have released to the extracellular environment due to cell lysis. Therefore, samples from 4 h of stimulation were not further analysed. Nevertheless, FIP2 siRNA only had a moderate impact on β -tubulin protein level ([Figure 4.14C](#) and [Figure 4.14D](#))

Comparing with NS RNA THP-1 cells, pro-IL-1 β was reduced by 65 % and 85 % in FIP2 siRNA cells that were stimulated with $\Delta cnf1/\Delta hlyA$ double mutant and $\Delta tcpC$ single mutant, respectively ([Figure 4.14E](#)). After 4 h of stimulation, decrease of pro-IL-1 β in FIP2 siRNA cells persisted ([Figure 4.14F](#)). Due to weak detected signals from IL-1 β p17 after 2 h of bacterial stimulation, IL-1 β p17 in the lysates was not quantified ([Figure 4.14A](#)).

In summary, THP-1 cells stimulated with UPEC3 wild type, $\Delta cnf1$ and $\Delta tcpC$ mutants for 2 h released the largest amount of pro-caspase-1, caspase-1 p20, pro-IL-1 β and IL-1 β p17. After 4 h, $\Delta hlyA$ single mutant and $\Delta cnf1/\Delta hlyA$ double mutant stimulated NS RNA cells released the largest amount of IL-1 β p17. FIP2 siRNA did not affect β -tubulin protein level, but pro-IL-1 β was reduced in the supernatants and in the cell lysates, which coincide with the pro-IL-1 β mRNA level. The protein level of IL-1 β p17 in the supernatants and lysates was also reduced in FIP2 siRNA treated cells.

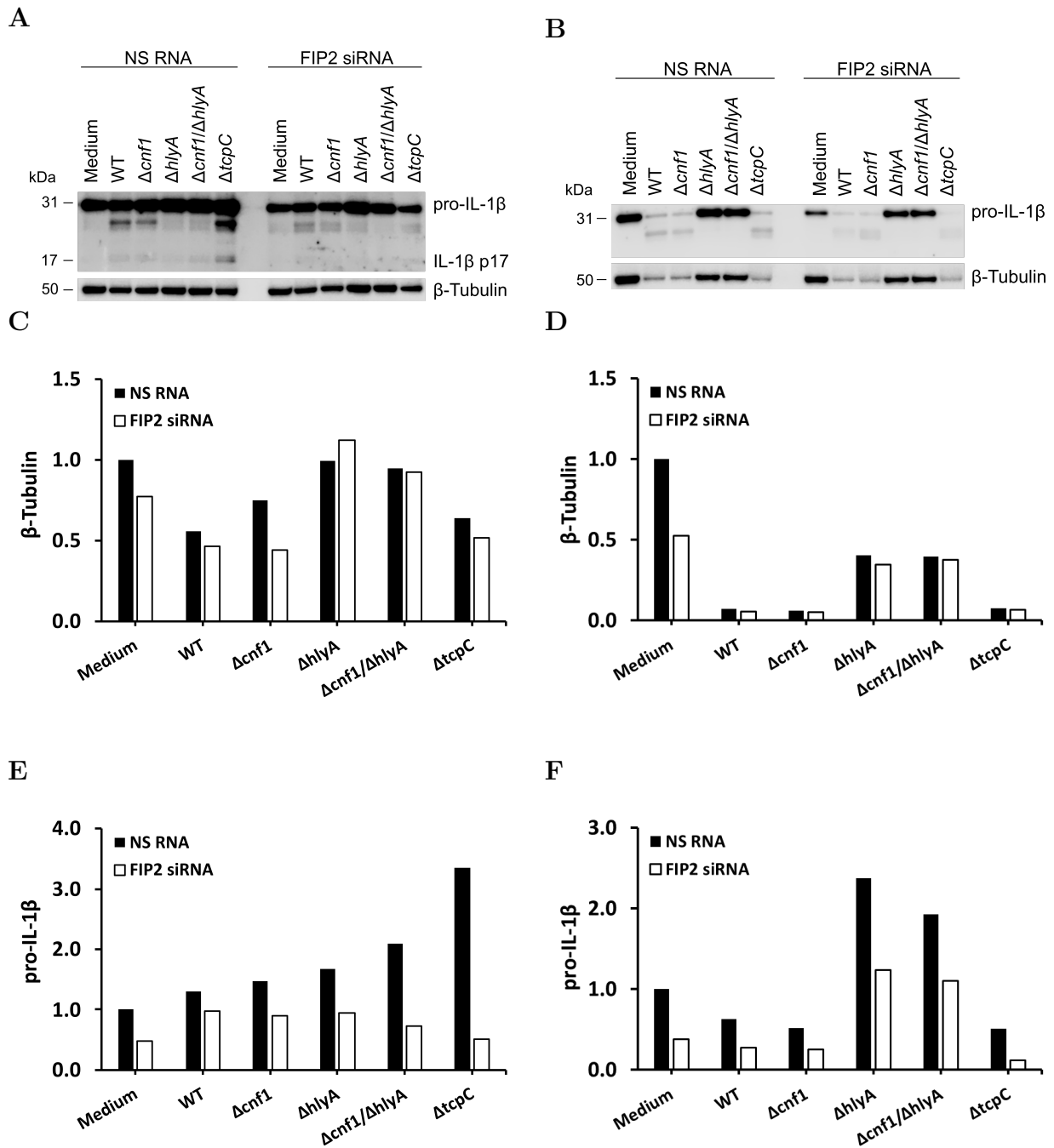


Figure 4.14: Pro-IL-1 β and β -tubulin protein levels in cell lysates. THP-1 cells were treated with NS RNA or FIP2 siRNA before stimulation with UPEC3 wild type or mutants for 2 h or 4 h (MOI = 2). Immunoblot of pro-IL-1 β , IL-1 β p17 and β -tubulin after 2 h (**A**). Immunoblot of pro-IL-1 β and β -tubulin after 4 h stimulation (**B**). Quantification of β -tubulin protein level after 2 h (**C**) and 4 h (**D**) stimulation. Quantification of pro-IL-1 β protein level after 2 h (**E**) and 4 h (**F**) stimulation. Except β -tubulin protein level, semi-quantified protein levels are given in units of fold change. β -Tubulin protein levels were normalised to unstimulated NS RNA cells.

4.3.4 FIP2-silencing affects Rac1 stabilisation in UPEC3 stimulated THP-1 cells

According to previous publication from our group, FIP2 has been demonstrated that it stabilises Rac1 and Cdc42, which facilitate actin polymerisation and phagocytosis [25].

Before investigating the expression level of Rac1, the protein level of FIP2 was controlled by Western blotting. As shown in [Figure 4.15A](#) and [Figure 4.15B](#), FIP2 was only detected in NS RNA cells stimulated with $\Delta cnf1$, $\Delta hlyA$, $\Delta cnf1/\Delta hlyA$ and $\Delta tcpC$ and were moderately upregulated in NS RNA cells relatively to unstimulated cells. FIP2 was weakly expressed in unstimulated cells and UPEC3 wild type stimulated cells. Except for $\Delta hlyA$ stimulated FIP2 siRNA cells, FIP2 was not detected in FIP2 siRNA treated cells, indicating FIP2 silencing was successful. Most strikingly, FIP2 was reduced approximately by 90 % in FIP2 siRNA cells relatively to NS RNA cells that were stimulated with $\Delta tcpC$ mutant.

[Figure 4.15C](#) shows that UPEC3 wild type, $\Delta cnf1$ and $\Delta hlyA$ mutants stimulated NS RNA cells expressed Rac1 in a moderate level as the unstimulated cells. Compared with NS RNA unstimulated cells, Rac1 was increased approximately by 50 % and 85 % in NS RNA cells that were stimulated with $\Delta cnf1/\Delta hlyA$ and $\Delta tcpC$ mutants, respectively. In accordance with previous publication, the protein level of Rac1 correlated with the expression level of FIP2. As illustrated in [Figure 4.15C](#), Rac1 decreased in FIP2 siRNA unstimulated cells and UPEC3 wild type, $\Delta cnf1$, $\Delta cnf1/\Delta hlyA$ and $\Delta tcpC$ stimulated cells. Indeed, Rac1 was not reduced in $\Delta hlyA$ stimulated FIP2 siRNA cells, which correlated with the FIP2 protein level ([Figure 4.15B](#)). Similarly, Rac1 decreased by 96 % in $\Delta tcpC$ mutant FIP2 siRNA stimulated cells relatively to NS RNA cells. Overall, the amount of Rac1 correlated with the FIP2 protein level and that FIP2 silencing destabilised Rac1.

4.3.5 FIP2-silencing reduces NLRP3 expression

[Section 4.3.2](#) showed the mRNA level of NLRP3 increased in cells that were stimulated with UPEC3 wild type and mutants, while FIP2 siRNA treatment gave a modest reduction of mRNA level of NLRP3. According to [Figure 4.13](#), caspase-1 p20 and IL-1 β p17 were released from the cells upon stimulation with bacteria. Reflecting inflammasomes were activated. To investigate the protein level of NLRP3, Western blotting was performed.

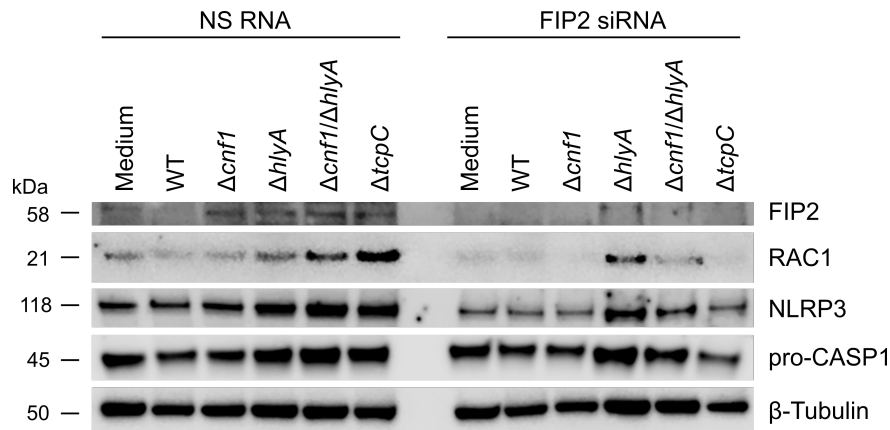
After 2 h of stimulation, NLRP3 increased moderately in UPEC3 wild type, $\Delta cnf1$ and $\Delta hlyA$ stimulated NS RNA cells relatively to unstimulated cells. NS RNA cells that were stimulated with $\Delta cnf1/\Delta hlyA$ and $\Delta tcpC$ increased NLRP3 by 55 % and 63 %, respectively, which indeed showed some correlation with Rac1 protein level ([Figure 4.15C](#)). In contrast to the protein level of pro-caspase-1 in the supernatants ([Figure D.9A](#)), the lysates showed the protein level of pro-caspase-1 in UPEC3 wild type and mutants stimulated cells were

relatively similar to the unstimulated cells (Figure 4.15E). Caspase-1 p20 was not detected in the cell lysates, which reflects on its release to the extracellular environment (Figure 4.13).

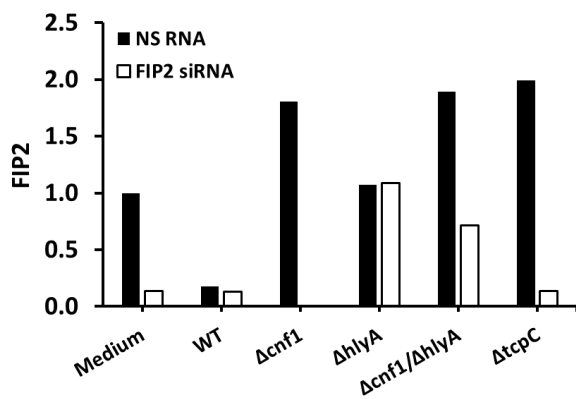
Treatment with FIP2 siRNA showed a small reduction of NLRP3 monomer in unstimulated cells, as well as cells stimulated with $\Delta cnf1$ and $\Delta hlyA$. Interestingly, FIP2 siRNA treatment reduced the NLRP3 protein level by 52 % in cells that were stimulated with UPEC3 wild type or $\Delta cnf1/\Delta hlyA$, and 68 % in $\Delta tcpC$ relatively to the NS RNA treated cells. As shown in Figure 4.15E, FIP2 siRNA gave a modest up-regulation of pro-caspase-1 in cells that were treated with UPEC3 wild type, $\Delta cnf1$ and $\Delta hlyA$, while pro-caspase-1 was reduced moderately in $\Delta cnf1/\Delta hlyA$ and $\Delta tcpC$ stimulated cells.

Taking all together, NLRP3 protein level correlated with the protein level of Rac1. Pro-caspase-1 in lysates of UPEC3 wild type and mutants stimulated cells were relatively similar to unstimulated cells independent of FIP2 siRNA treatment.

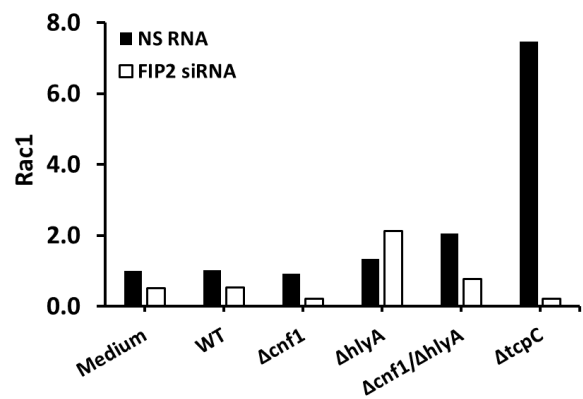
A



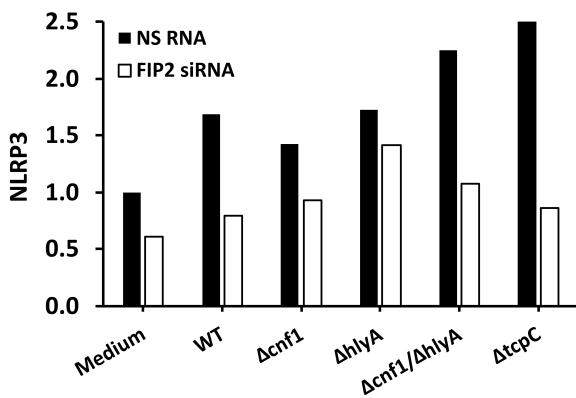
B



C



D



E

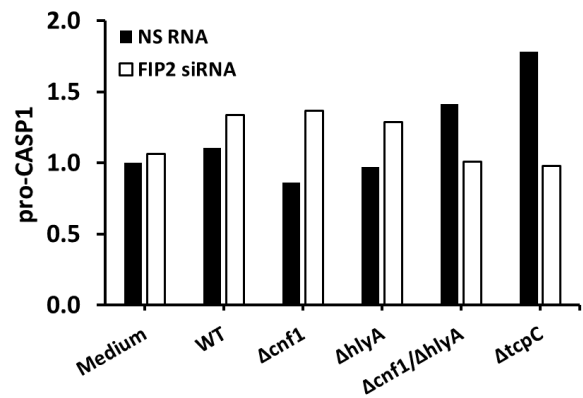


Figure 4.15: FIP2, Rac1, NLRP3 and pro-caspase-1 protein levels in THP-1 lysates stimulated with UPEC3 wild type and mutants. THP-1 cells were treated with NS RNA or FIP2 siRNA before stimulation with UPEC3 wild type or mutants for 2 h (MOI = 2). Immunoblot of FIP2, Rac1, NLRP3 pro-caspase-1 and β -tubulin in cell lysates (A). Quantification of FIP2 protein level (B). Quantification of Rac1 protein level (C). Quantification of NLRP3 protein level (D). Quantification of pro-caspase-1 protein level (E). Quantified protein levels are given in units of fold change.

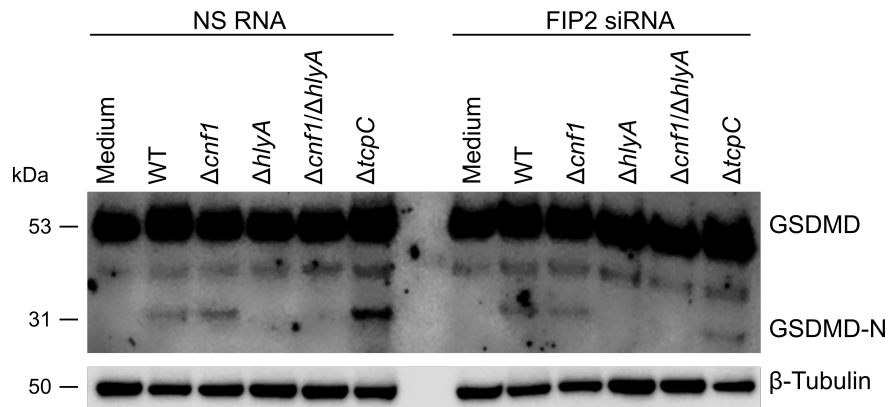
4.3.6 FIP2 may involve in inflammasome activation

In addition to cleavage of pro-IL-1 β , gasdermin D (GSDMD) can also be processed by NLRP3 inflammasome. Western blotting was conducted to investigate cleavage of GSDMD by active NLRP3 inflammasome and the effect of FIP2 silencing.

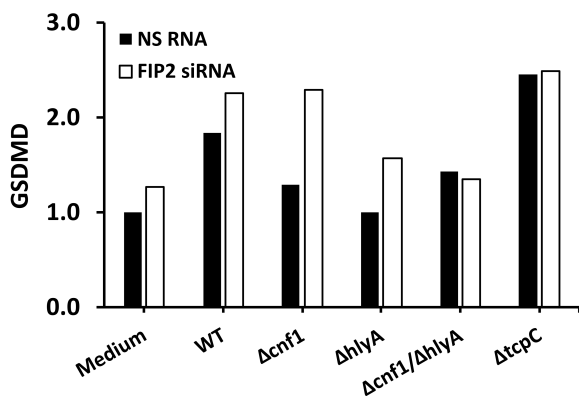
As illustrated in [Figure 4.16A](#) and [Figure 4.16B](#), GSDMD was moderately upregulated in NS RNA THP1 cells stimulated with UPEC3 wild type and $\Delta cnf1 / \Delta hlyA$, while it was relatively similar between unstimulated cells and cells that were stimulated with $\Delta cnf1$ and $\Delta hlyA$. In contrast, $\Delta tcpC$ stimulated cells increased GSDMD approximately by 60 % relatively to unstimulated cells. The amount of GSDMD in NS RNA treated THP-1 cells stimulated with UPEC3 wild type, $\Delta cnf1$ and $\Delta tcpC$ showed increased levels of GSDMD cleavage relative to the medium control ([Figure 4.16C](#)). While cells stimulated with the $\Delta hlyA$ single mutant and the $\Delta cnf1 / \Delta hlyA$ double mutant showed no detectable GSDMD cleavage.

Treatment with FIP2 siRNA showed moderate increase of GSDMD ([Figure 4.16B](#)). Remarkably, FIP2 silencing caused indifferent GSDMD cleavage relative to NS RNA cells, except for the cells stimulated with $\Delta tcpC$. In these cells, FIP2 silencing caused a 85 % reduction in GSDMD cleavage ([Figure 4.16C](#)).

A



B



C

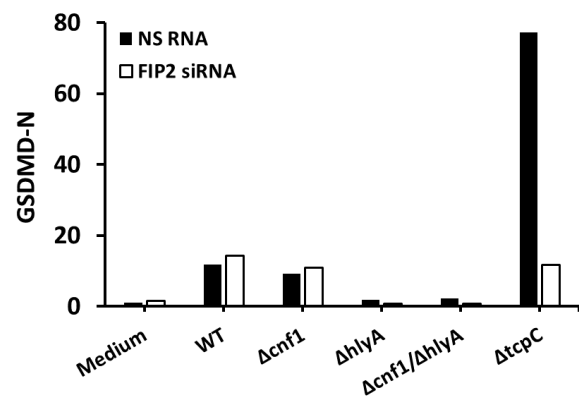


Figure 4.16: GSDMD and cleaved GSDMD protein levels in THP-1 cells stimulated with UPEC3 wild type and mutants. THP-1 cells were treated with NS RNA or FIP2 siRNA before stimulation with UPEC3 wild type or mutants for 2 h (MOI = 2). Immunoblot of β -tubulin, gasdermin D (GSDMD) and GSDMD N-turminus (GSDMD-N) following GSDMD cleavage (A). Quantification of GSDMD protein level (B). Quantification of GSDMD-N protein level (C). Quantified protein levels are given in units of fold change.

4.3.7 LPS priming enhances NLRP3 inflammasome signalling

In the previous demonstration (section 4.3.3), signal of released IL-1 β p17 in UPEC3 wild type and mutants stimulated THP-1 cells was relatively weak, probably due to omittance of priming the cells. To enhance the signal from activated NLRP3 inflammasome, THP-1 cells were primed with LPS for 2 h before the cells were stimulated with UPEC3 wild type, $\Delta cnf1$, $\Delta hlyA$, $\Delta cnf1/\Delta hlyA$, *E. coli* CFT073 and the avirulent DH5 α strain. The cells were only stimulated for 2 h, since 4 h of stimulation caused severe cell death (section 4.3.3). Nigericin is a bacterial toxin causing potassium ion efflux and subsequent activation of the NLRP3 inflammasome, was used to stimulate THP-1 cells for 1 h as a positive control. LDH release and the total concentration of IL-1 β in the supernatants were measured after 2 h of

bacterial stimulation (Figure 4.17).

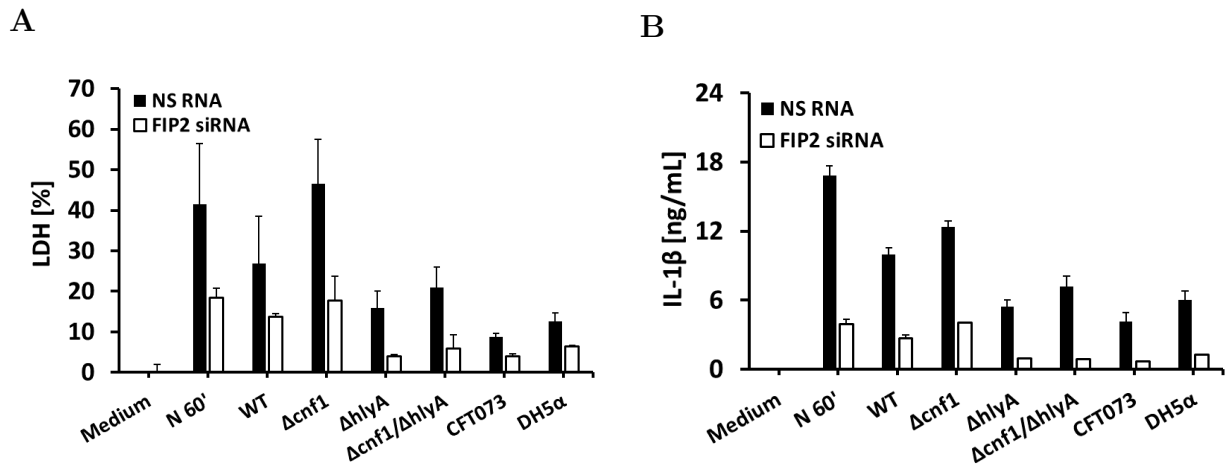


Figure 4.17: Quantification of released LDH and IL-1 β in supernatants of THP-1 cells stimulated with nigericin, virulent and avirulent *E. coli*. THP-1 cells were treated with NS RNA or FIP2 siRNA before the cells were primed with LPS for 2 h, then the cells were stimulated with nigericin for 1 h (N 60') or UPEC3 wild type, UPEC3 mutants, CFT073 and DH5 α for 2 h (MOI = 2). The LDH level in the supernatants were colorimetrically quantified (A). Total concentration of released pro-IL-1 β and IL-1 β p17 was quantified in technical duplicates using an enzyme-linked immunosorbent assay (B). The error bars show the standard deviation of duplicates.

Figure 4.17 shows that LDH release largely resembling the amount of IL-1 β released into supernatants. Nigericin and $\Delta cnf1$ stimulated NS RNA cells released the largest amount of LDH and IL-1 β , with an increase approximately by 40 % of LDH and 99 % of IL-1 β relatively to unstimulated cells. Due to large standard deviation in Figure 4.17A, the level of released LDH results from nigericin, UPEC3 wild type and $\Delta cnf1$ are not significant. Remarkably, FIP2 siRNA treatment decreased IL-1 β release by 67 % in $\Delta cnf1$ stimulated cells, while it was reduced at least by 72 % in cells that were treated with nigericin, UPEC3 wild type, $\Delta hlyA$, $\Delta cnf1/\Delta hlyA$, CFT073 and DH5 α (Figure 4.17B).

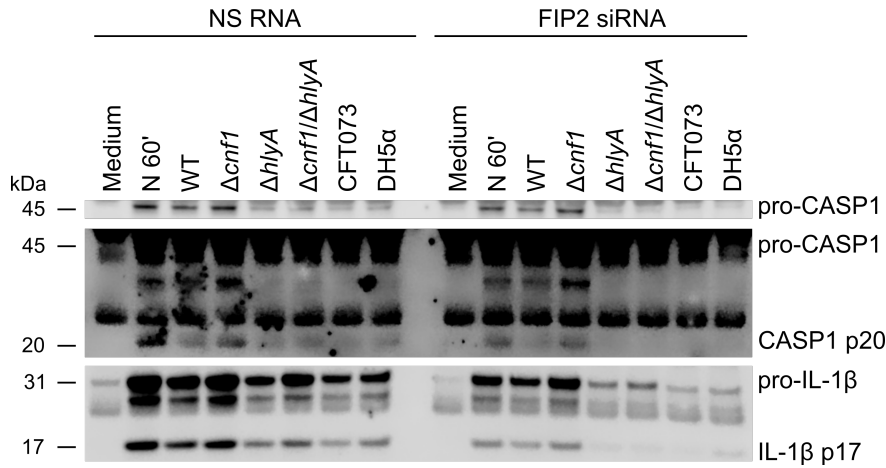
As illustrated in Figure 4.17B, amount of released IL-1 β is consistent with the immunoblot of caspase-1 and IL-1 β (Figure 4.18). Strikingly, when the cells were primed with LPS for 2 h, released pro-caspase-1 was increased by 84 % in nigericin and $\Delta cnf1$ stimulated NS RNA cells and 79 % in UPEC3 wild type relatively to unstimulated cells (Figure D.10A). The protein level of pro-caspase-1 was elevated approximately by 55% in $\Delta hlyA$, $\Delta cnf1/\Delta hlyA$ and DH5 α stimulated cells, while CFT073 moderately increased pro-caspase-1 release. In contrast, NS RNA cells without LPS priming, stimulation with UPEC3 wild type, $\Delta cnf1$ and $\Delta hlyA$, pro-caspase-1 was only increased by 60 %, 67 % and 15 %, respectively (Figure D.9A). As shown in Figure 4.18B, nigericin stimulated NS RNA cells released the largest amount of caspase-1 p20 with an increase by 98 % compared to unstimulated cells. Relative to UPEC3 wild type stimulated cells, released caspase-1 p20 only decreased moderately in $\Delta hlyA$ and

$\Delta cnf1/\Delta hlyA$ stimulated cells, while $\Delta cnf1$ increased capsase-1 p20 release by 48 %.

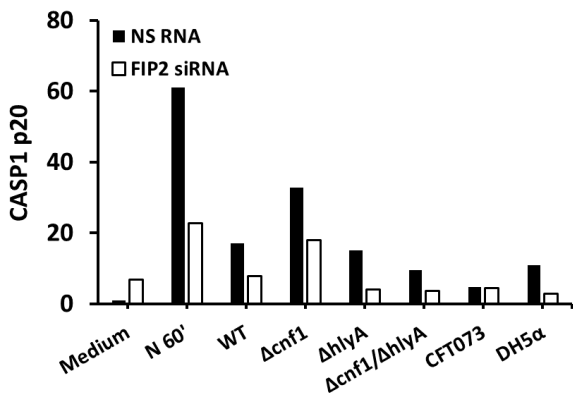
Similar to [Figure 4.17](#), [Figure D.10B](#) shows increased pro-IL-1 β release in nigericin, UPEC3 variants, CFT073 and DH5 α treated NS RNA cells. Interestingly, compared with UPEC3 wild type stimulated NS RNA cells, less pro-IL-1 β was released in $\Delta hlyA$ and $\Delta cnf1/\Delta hlyA$ stimulated cells without LPS priming and the reduction of pro-IL-1 β was approximately by 86 % ([Figure D.9C](#)). In contrast, pro-IL-1 β was only reduced by 58 % in LPS primed NS RNA cells that were stimulated with $\Delta hlyA$ and 9 % in $\Delta cnf1/\Delta hlyA$ relatively to UPEC3 wild type ([Figure D.10B](#)). Although $\Delta hlyA$, $\Delta cnf1/\Delta hlyA$ and DH5 α stimulated NS RNA cells only gave a moderate reduction of total concentration of pro-IL-1 β and IL-1 β p17 in the supernatants relative to UPEC3 wild type ([Figure 4.17B](#)), IL-1 β p17 was reduced by 50 % in $\Delta hlyA$ and DH5 α stimulated cells ([Figure 4.18C](#)). Indicating, LPS priming stimulates release of pro-IL-1 β from THP-1 cells.

According to [Figure D.10A](#), FIP2 silencing only moderately decreased pro-caspase-1 release, while capsase-1 p20 was reduced by 62 % in nigericin and $\Delta cnf1/\Delta hlyA$ stimulated cells relatively to NS RNA cells [Figure 4.18B](#). Furthermore, $\Delta hlyA$ stimulated FIP2 siRNA cells showed reduction of caspase-1 release by 72 %. FIP2 silencing also reduced pro-IL-1 β release by at least 58 % ([Figure D.10B](#)). More strikingly, IL-1 β p17 was reduced by 77 % in nigericin stimulated cells and at least 71 % in cells that were stimulated with UPEC3 wild type and mutants. Compared with NS RNA cells, FIP2 siRNA cells treated with CFT073 and DH5 α decreased IL-1 β p17 release by 92 % and 83 %, respectively.

A



B



C

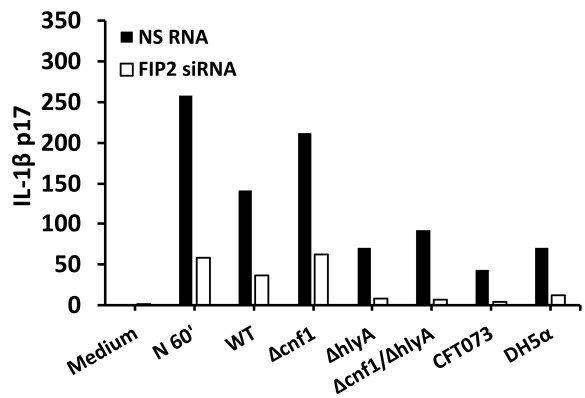


Figure 4.18: Pro-caspase-1, caspase-1 p20, pro-IL-1 β and IL-1 β p17 protein levels in supernatants of THP-1 cells stimulated with nigericin or *E. coli* strains. THP-1 cells were treated with NS RNA or FIP2 siRNA, before LPS priming for 2 h. Primed cells were stimulated with nigericin for 1 h (N 60') or UPEC3 variants, CFT073 and DH5 α for 2 h (MOI = 2). Immunoblot of pro-caspase-1, caspase-1 p20, pro-IL-1 β and IL-1 β p17 (A). Quantification of caspase-1 p20 protein level (B). Quantification of IL-1 β p17 protein level (C). Quantified protein levels were normalised to unstimulated NS RNA THP-1 cells.

Levels of pro-inflammatory cytokines mRNA were measured in LPS primed THP-1 cells stimulated with nigericin or virulent and avirulent *E. coli* strains and FIP2 silencing were controlled with Q-PCR. As shown in Figure 4.19A, NS RNA cells treated with nigericin, UPEC3 wild type and $\Delta cnf1$, FIP2 mRNA level was reduced approximately by 25 %, while $\Delta hlyA$ showed a small increase of FIP2 mRNA (17 %) relative to unstimulated cells. Treatment with FIP2 siRNA, decreased the FIP2 mRNA levels approximately by 90 %. Indicating FIP2 silencing was successful.

Consistent with previous observation (Figure 4.11), $\Delta hlyA$ and $\Delta cnf1/\Delta hlyA$ stimulated NS RNA cells showed the highest level of pro-IL-1 β mRNA, which increased by 86 % relative to unstimulated cells (Figure 4.19B). Interestingly, LPS primed NS RNA cells stimulated with

UPEC3 wild type and $\Delta cnf1$, showed increased levels of pro-IL-1 β mRNA approximately by 22 % compared with cells without LPS priming, while $\Delta hlyA$ and $\Delta cnf1/\Delta hlyA$ only increased 7 % (Figure 4.19B and Figure 4.11). LPS priming elevated NLRP3 mRNA level by 89 % in UPEC3 wild type relatively to unstimulated cells (Figure 4.19C), while NLRP3 mRNA level was only increased by 78 % in unprimed cells (Figure 4.11C). Stimulation with nigericin, UPEC3 mutants, CFT073 and DH5 α also increased NLRP3 mRNA (> 77 %). Interestingly, comparing with UPEC3 wild type stimulated NS RNA cells, IFN β mRNA levels were increased at least by 75 % in $\Delta cnf1$, $\Delta hlyA$, $\Delta cnf1/\Delta hlyA$, CFT073 and DH5 α stimulated cells (Figure 4.19D). IFN β mRNA was slightly decreased in UPEC3 wild type stimulated cells compared with nigericin stimulated NS RNA cells. Remarkably, relative to UPEC3 wild type stimulated NS RNA cells, LPS priming only increased TNF α mRNA levels by 40 % in $\Delta hlyA$ and 32 % in $\Delta cnf1/\Delta hlyA$ NS RNA stimulated cells, while NS RNA cells without LPS priming showed an increase of TNF α by 60 % and 73 % in $\Delta hlyA$ and $\Delta cnf1/\Delta hlyA$, respectively (Figure 4.19E and Figure 4.11E).

Strikingly, pro-IL-1 β mRNA levels were decreased at least by 67 % in FIP2 siRNA cells compared with LPS primed NS RNA cells (Figure 4.19B), while THP-1 cells without LPS priming only showed a moderate decrease (45 % <) of pro-IL-1 β mRNA levels (Figure 4.11B). Except for DH5 α stimulated cells, FIP2 silencing also decreased NLRP3 mRNA levels at least by 56 % and TNF α by 49 %, whereas unprimed cells only showed a modest reduction of NLRP3 and TNF α mRNA (Figure 4.11). Furthermore, UPEC3 $\Delta cnf1$ stimulated FIP2 siRNA cells showed a reduction of IFN β by 84 % (Figure 4.19D). On the other hand, cells without LPS priming stimulated with $\Delta cnf1$ only gave 10 % reduction of IFN β (Figure 4.11D).

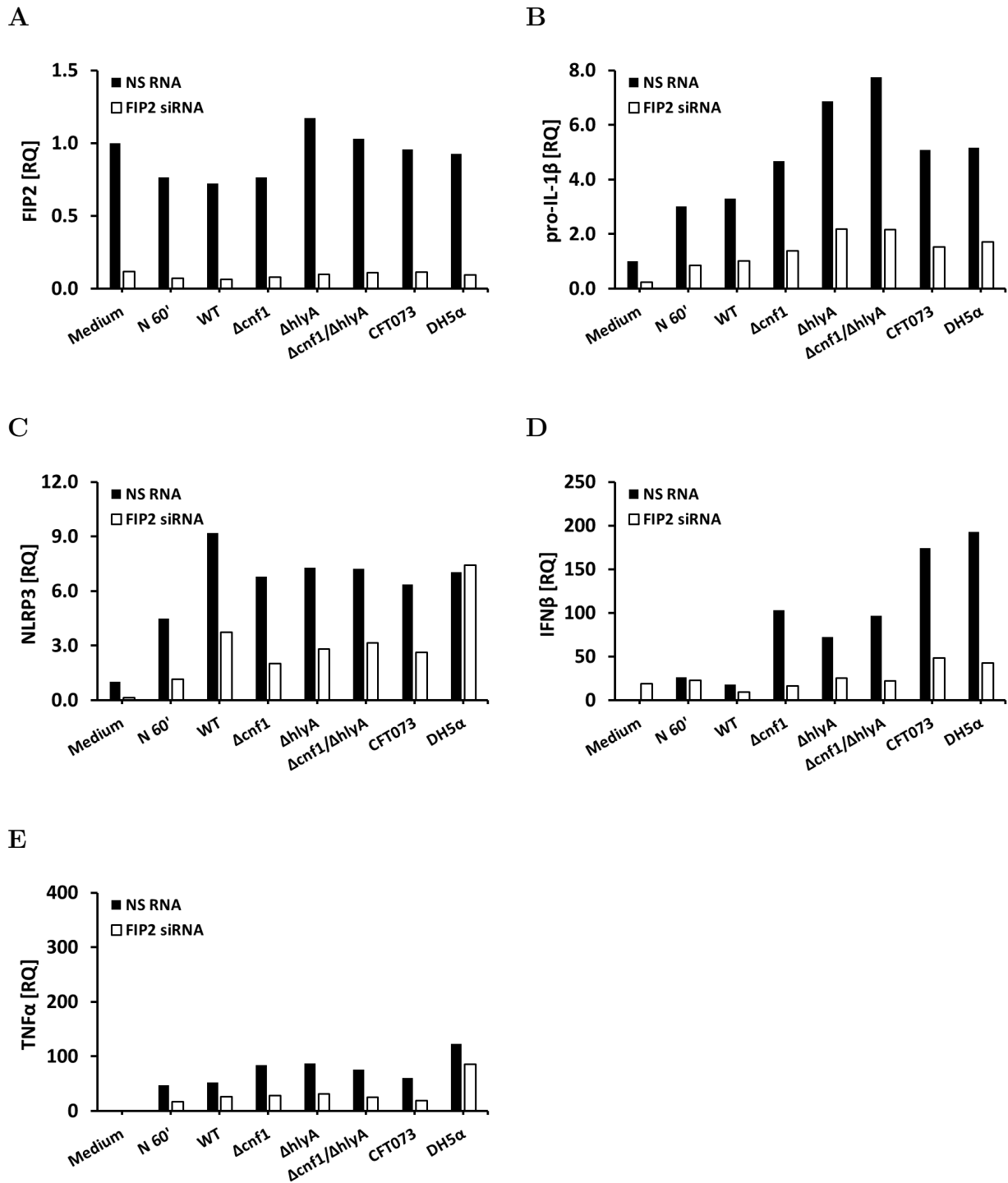


Figure 4.19: FIP2, pro-IL-1 β , NLRP3, IFN β and TNF α mRNA levels in LPS primed THP-1 cells stimulated with nigericin, virulent and avirulent *E. coli* strains. THP-1 cells lipofected with NS RNA or FIP2 siRNA were primed with LPS for 2 h before the cells were stimulated with nigericin for 1 h or with UPEC3 variants, CFT073 and DH5 α for 2 h (MOI = 2). Quantified mRNA levels of FIP2 (A), pro-IL-1 β (B), NLRP3, (C), IFN β (D) and TNF α (E).

After 2 h of LPS priming followed with 1 h of nigericin treatment or 2 h of stimulation with UPEC3 variants, CFT073 and DH5 α , the β -tubulin protein levels were relatively equivalent in the lysates (Figure 4.20A and Figure D.11). As a second control of FIP2 silencing, Western blotting of FIP2 in the cell lysates was performed. Figure 4.20A shows FIP2 protein level was relatively similar between NS RNA cells stimulated with UPEC3 wild type, $\Delta hlyA$, $\Delta cnf1/\Delta hlyA$, CFT073 and DH5 α . Furthermore, unstimulated NS RNA cells showed a weak band of FIP2. FIP2 was slightly decreased in nigericin and $\Delta cnf1$ stimulated cells relative to unstimulated NS RNA cells. Both the unstimulated and UPEC3 wild type stimulated FIP2 siRNA cells showed a small decrease of FIP2, while FIP2 increased slightly in nigericin FIP2 siRNA cells relative to NS RNA cells (Figure 4.20B). FIP2 protein level was decreased at least by 60 % in $\Delta cnf1$, $\Delta hlyA$, $\Delta cnf1/\Delta hlyA$, CFT073 and DH5 α stimulated FIP2 siRNA cells (Figure 4.20B).

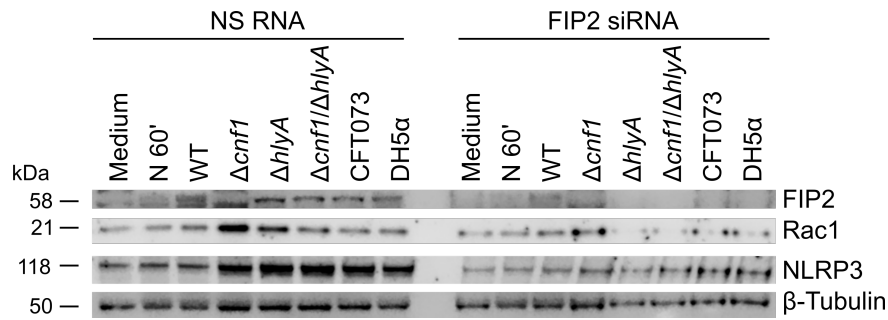
Interestingly, Rac1 protein level was increased by 70 % in $\Delta cnf1$ and 60 % in $\Delta hlyA$ stimulated NS RNA cells, relative to unstimulated cells (Figure 4.20C). In contrast, when the cells were not primed with LPS, Rac1 in $\Delta cnf1$ and $\Delta hlyA$ stimulated cells were at a similar level as the unstimulated cells (Figure 4.15C). LPS primed cells that were stimulated with nigericin, UPEC3 wild type, $\Delta cnf1/\Delta hlyA$, CFT073 and DH5 α only showed a small increase of Rac1. Furthermore, NLRP3 protein levels were modestly elevated in nigericin, UPEC3 wild type and $\Delta cnf1$ stimulated NS RNA cells relative to unstimulated cells, while CFT073 and DH5 α showed an increase by 62 % and 56 %, respectively (Figure 4.20D). Strikingly, relative to UPEC3 wild type stimulated NS RNA cells, $\Delta hlyA$ increased NLRP3 protein level by 55 % and 61 % in $\Delta cnf1/\Delta hlyA$ stimulated cells, while NS RNA cells without LPS priming only showed small increase of NLRP3 protein levels in cells that were stimulated with $\Delta hlyA$ (3 %) and $\Delta cnf1/\Delta hlyA$ (25 %).

Illustrated in Figure 4.21B, NS RNA cells stimulated with nigericin, UPEC3 wild type and CFT073 showed tendencies of modest decrease of pro-caspase-1 relatively to unstimulated cells, while pro-caspase-1 was decreased approximately by 54 % in cells stimulated with $\Delta cnf1$, $\Delta hlyA$, $\Delta cnf1/\Delta hlyA$ and DH5 α . In contrast, NS RNA cells without LPS priming, pro-caspase-1 was slightly reduced when stimulated with $\Delta cnf1$ or $\Delta hlyA$ (16 % <) and a small increase (29 %) in $\Delta cnf1/\Delta hlyA$ (Figure 4.15E). Nevertheless, NS RNA cells showed a moderate increase of pro-IL-1 β when stimulated with the *E. coli* strains and small decrease in nigericin stimulated cells (Figure 4.21C). IL-1 β p17 was observed in the lysates, however, due to weak detected signal, it was not quantified (Figure 4.21A). GSDMD was reduced by 52 % in nigericin stimulated NS RNA cells, while GSDMD was moderately decreased in cells that were stimulated with bacteria relatively to unstimulated cells (Figure 4.21D). Interestingly, GSDMD-N protein levels in UPEC3 wild type and $\Delta cnf1$ stimulated NS RNA cells were comparable to nigericin treated cells (Figure 4.21E). In contrast to non-primed cells (Figure 4.16C), GSDMD-N was detected in LPS primed NS RNA cells stimulated with $\Delta hlyA$ and $\Delta cnf1/\Delta hlyA$. More strikingly, relative to UPEC3 wild type stimulated

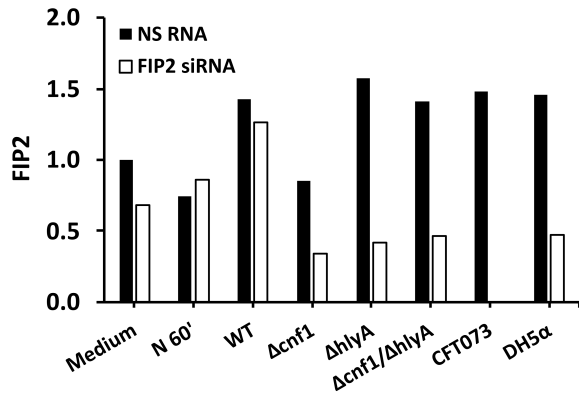
NS RNA cells, $\Delta hlyA$, $\Delta cnf1/\Delta hlyA$, CFT073 and DH5 α showed a decrease of GSDMD-N approximately by 80 %.

In contrast to previous observation of Rac1 in cells without LPS priming (Figure 4.15C), FIP2 siRNA cells primed with LPS showed a decrease of Rac1 by 83 % in $\Delta hlyA$ and 65 % in $\Delta cnf1/\Delta hlyA$ relative to NS RNA cells. NLRP3 protein levels were moderately decreased in FIP2 siRNA cells (33-47 %), except $\Delta hlyA$ and $\Delta cnf1/\Delta hlyA$ FIP2 siRNA cells, which showed a decreased NLRP3 protein level by 69 % and 57 %, respectively. FIP2 silencing only gave a modest decrease of pro-caspase-1 in nigericin, UPEC3 wild type and $\Delta cnf1$ stimulated cells, and a small increase in cells that were stimulated with $\Delta hlyA$, $\Delta cnf1/\Delta hlyA$, CFT073 and DH5 α . Pro-IL-1 β protein level in the lysates were at least reduced by 49 % in FIP2 siRNA compared with NS RNA cells (Figure 4.21C). Consistent with previous observation of GSDMD (Figure 4.16), FIP2 silencing slightly increased GSDMD (Figure 4.21D). Nevertheless, GSDMD-N was modestly decreased in UPEC3 wild type and $\Delta cnf1$ stimulated FIP2 siRNA cells, which has been observed earlier (Figure 4.16C). Remarkably, GSDMD-N was reduced at least by 85 % in $\Delta hlyA$, $\Delta cnf1/\Delta hlyA$, CFT073 and DH5 α stimulated FIP2 siRNA relative to NS RNA cells (Figure 4.21E). Overall, LPS priming enhances NLRP3 inflammasome signalling in THP-1 cells by increasing pro-IL-1 β and NLRP3 expression.

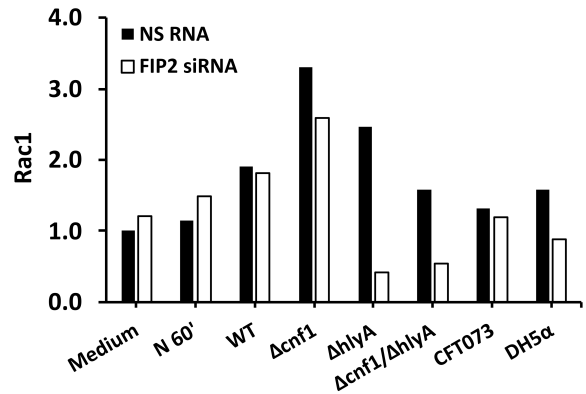
A



B



C



D

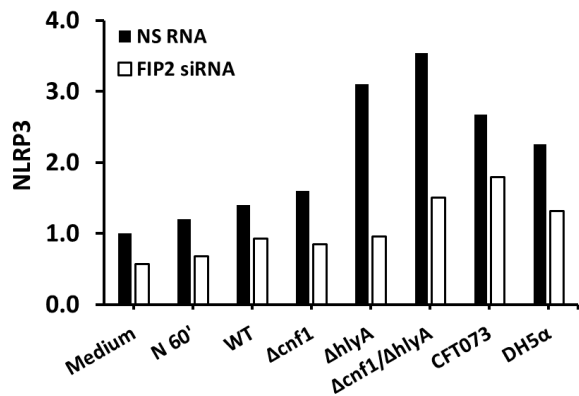
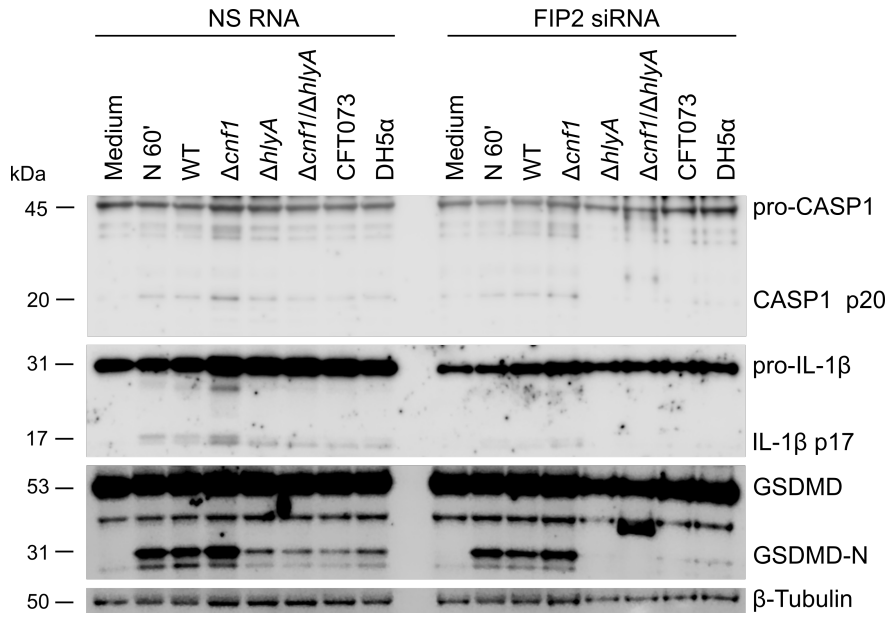
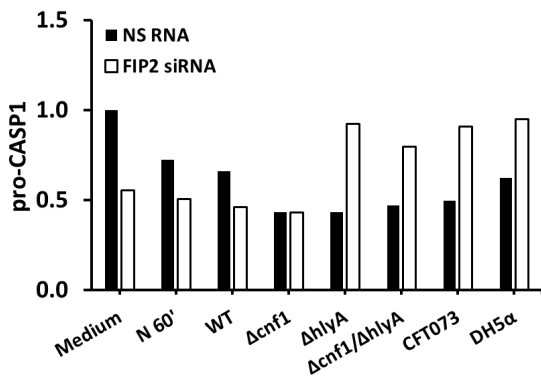


Figure 4.20: Western blot of FIP2, Rac1, NLRP3 and β -tubulin in THP-1 cells stimulated with nigericin, virulent and avirulent *E. coli* strains. THP-1 cells were lipofected with NS RNA or FIP2 siRNA before LPS priming for 2 h. Primed cells were stimulated with nigericin for 1 h or with UPEC3 variants, CFT073 and DH5 α for 2 h (MOI = 2). Immunoblot of FIP2, Rac1, NLRP3 and β -tubulin (**A**). Quantified protein levels of FIP2 (**B**), Rac1 (**C**), and NLRP3 (**D**). Quantified protein levels are given in units of fold change.

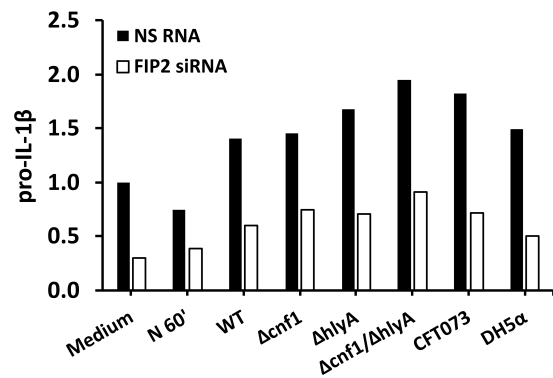
A



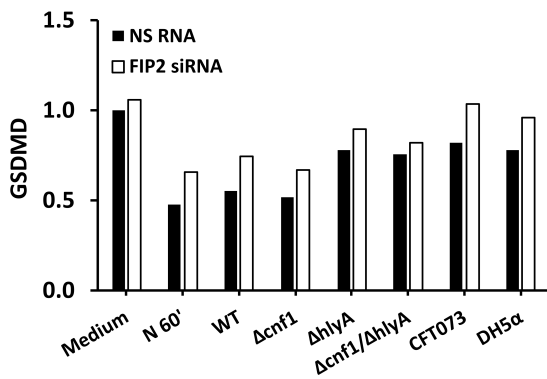
B



C



D



E

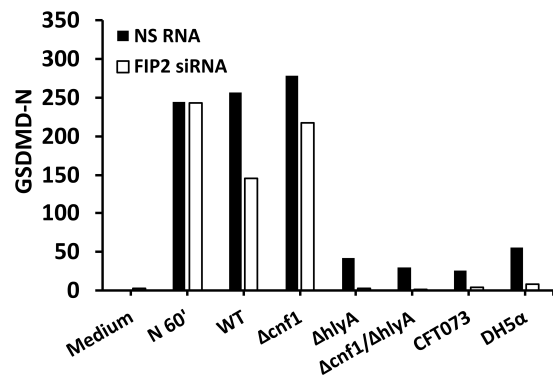


Figure 4.21: Quantification of pro-caspase-1, pro-IL-1 β , GSDMD and N-terminus of GSDMD in THP-1 cells stimulated with nigericin, virulent and avirulent *E. coli*. THP-1 cells were treated with NS RNA or FIP2 siRNA before LPS priming for 2 h. Primed THP-1 cells were stimulated with nigericin for 1 h or with UPEC3 mutants, CFT073 and DH5 α for 2 h (MOI = 2). Immunoblot of pro-caspase-1, caspase-1 p20, pro-IL-1 β , IL-1 β p17, GSDMD, GSDMD-N and β -tubulin (A). Quantified protein levels of pro-caspase-1 (B), pro-IL-1 β (C), GSDMD (D) and GSDMD-N (E). Quantified protein levels are given in units of fold change.

4.3.8 Effect of FIP2-silencing resembles NLRP3-inhibition in THP-1 cells

To investigate whether FIP2 regulates NLRP3 inflammasome signalling pathway, LPS primed THP-1 cells were treated with the NLRP3-inhibitor, MCC950, before stimulation with nigericin, virulent and avirulent *E. coli* strains. Cells without MCC950 treatment were treated with DMSO. In [section 4.3.7](#), LPS priming showed tendency of stimulating THP-1 cells to release pro-IL-1 β and pro-caspase-1. Therefore, we included LPS as an additional treatment to inspect its potential for stimulating release of pro-IL-1 β and pro-caspase-1 from THP-1 cells. Due to time limitation, only the supernatants were analysed in this study.

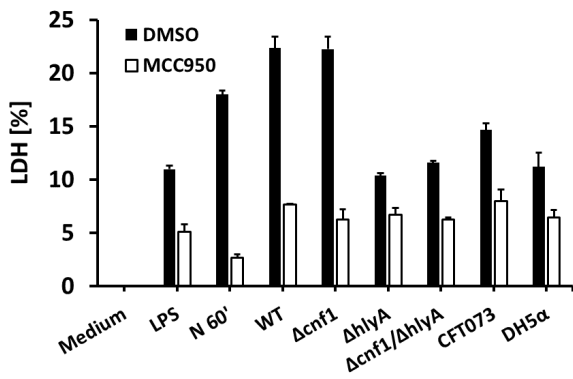
Consistent with previous observation of LDH release ([Figure 4.17A](#)), nigericin, UPEC3 wild type and $\Delta cnf1$ released the largest amount of LDH ([Figure 4.22A](#)). Interestingly, LPS stimulated DMSO cells also induced release of LDH (11 %). Compared with LPS stimulated DMSO cells, LDH release was increased by 51 % in UPEC3 wild type and $\Delta cnf1$ stimulated cells, while nigericin stimulation increased LDH release by 40 %. Remarkably, $\Delta hlyA$, $\Delta cnf1/\Delta hlyA$ and DH5 α stimulated DMSO cells released a similar LDH level as the LPS stimulated cells, while CFT073 stimulated cells showed a small increase of LDH release (25 %).

NLRP3 inflammasome activation was further investigated by Western blotting caspase-1 and IL-1 β in the supernatants. Unfortunately, neither pro-caspase-1 nor caspase-1 p20 were detected in the supernatants, probably due to its instability and were degraded. Like previous observations, pro-IL-1 β , IL-1 β p17 and the intermediate IL-1 β were detected in nigericin, UPEC3 wild type and $\Delta cnf1$ stimulated DMSO cells ([Figure 4.22B](#)). Relatively to LPS treated DMSO cells, cells that were stimulated with nigericin, UPEC3 wild type and $\Delta cnf1$ increased pro-IL-1 β and IL-1 β p17 release approximately by 83 %. Compared with UPEC3 wild type stimulated DMSO cells, pro-IL-1 β was reduced approximately by 75 % in $\Delta hlyA$, $\Delta cnf1/\Delta hlyA$ and DH5 α stimulated DMSO cells ([Figure 4.22C](#)). Furthermore, IL-1 β p17 was reduced by 83 % in $\Delta hlyA$, 69 % in $\Delta cnf1/\Delta hlyA$ and 74 % in DH5 α stimulated DMSO cells relatively to UPEC3 wild type stimulated DMSO cells ([Figure 4.22D](#)). CFT073 stimulated DMSO cells showed 60 % decrease of pro-IL-1 β and IL-1 β p17 relatively to UPEC3 wild type.

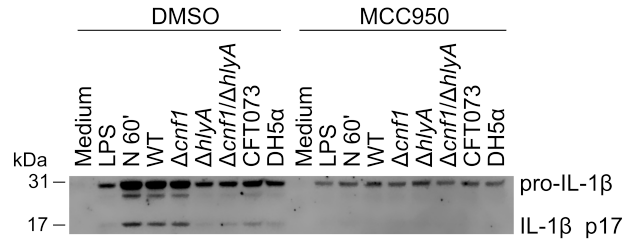
Intriguingly, MCC950 decreased LDH release by 54 % in LPS stimulated cells ([Figure 4.17A](#)). More strikingly, MCC950 decreased LDH release by 85 %, 66 % and 72 % in nigericin, UPEC3 wild type and $\Delta cnf1$ stimulated cells, respectively, which resemble the reduction of LDH release when FIP2 was silenced ([Figure 4.10A](#) and [Figure 4.17A](#)). LDH release was moderately decreased in MCC950 cells that were stimulated with $\Delta hlyA$, $\Delta cnf1/\Delta hlyA$ CFT073 and DH5 α (35-46 %). Nevertheless, pro-IL-1 β was reduced by 50 % in MCC950 cells only treated with LPS. Further more, treatment with MCC950 reduced pro-IL-1 β release approximately by 87 % and IL-1 β p17 by 92 % in nigericin, UPEC3 wild type and $\Delta cnf1$ stimulated

cells relatively to DMSO cells (Figure 4.22). On the other hand, FIP2 silencing decreased pro-IL-1 β approximately by 66 % and IL-1 β p17 by 74 % in cells that were stimulated with nigericin, UPEC3 wild type and $\Delta cnf1$ (Figure D.10B and Figure 4.18C). $\Delta cnf1/\Delta hlyA$, CFT073 and DH5 α stimulated cells also showed decreased levels of pro-IL-1 β at least by 61 % and IL-1 β p17 approximately by 85 % in MCC950 cells. Similarly, FIP2 siRNA cells stimulated with $\Delta cnf1/\Delta hlyA$, CFT073 and DH5 α showed a decrease of pro-IL-1 β approximately by 84 % and at least 83 % decrease of IL-1 β p17 relatively to NS RNA cells. $\Delta hlyA$ stimulated MCC950 only showed 37 % decrease of pro-IL-1 β and 67 % in IL-1 β p17 relatively to DMSO cells, while FIP2 silencing reduced pro-IL-1 β and IL-1 β p17 release by 77 % and 89 %, respectively. In summary, reduction of LDH, pro-IL-1 β and IL-1 β p17 release from FIP2 siRNA cells resembles the effect of MCC950 treatment.

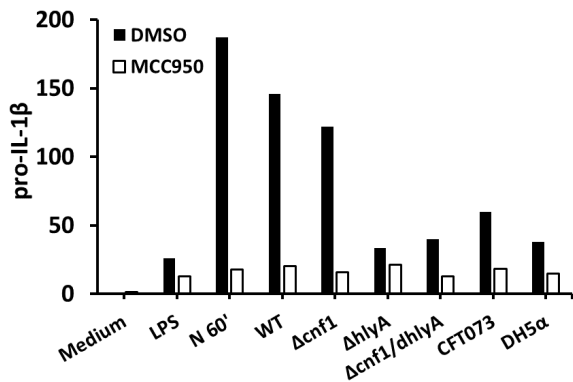
A



B



C



D

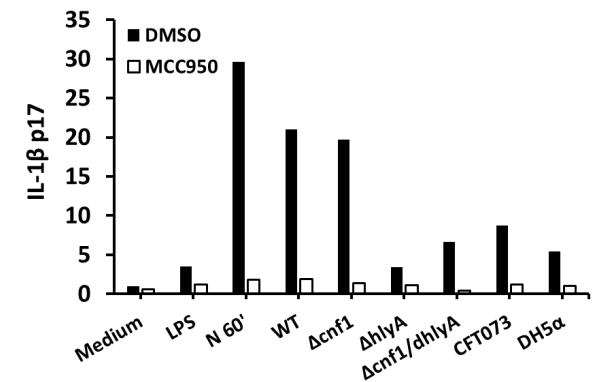


Figure 4.22: Released LDH, pro-IL-1 β and IL-1 β p17 from THP-1 cells treated with MCC950 and stimulated with nigericin, virulent and avirulent *E. coli* strains. THP-1 cells were primed with LPS for 2 h before treatment with with NLRP3 inhibitor, MCC950, or DMSO for 30 min. THP-1 cells were stimulated with nigericin for 1 h or with UPEC3 variants, CFT073 and DH5 α for 2 h (MOI = 2). Average and standard deviation of LDH release calculated from technical duplicates (A). Immunoblot of pro-IL-1 β and IL-1 β p17 in supernatants of THP1 cells (B). Quantified protein levels of pro-IL-1 β (C) and IL-1 β p17 (D). Quantified protein levels were normalised to unstimulated DMSO cells.

4.3.9 CNF1 and HlyA expressing UPEC3 strains upregulate expression of phosphorylated MLKL in THP-1 cells

To address whether other cell death signalling pathways were activated during bacterial stimulation, the initiator caspase-8 and the executioner caspase-3 in apoptosis signalling pathway [98], were investigated. Moreover, phosphorylated MLKL (p-MLKL) which is the terminal protein in necroptosis [14], was also analysed by Western blotting.

Due to technical issues, caspase-3 and caspase-8 were unfortunately not detected. As [Figure 4.23A](#) and [Figure 4.23B](#) show, p-MLKL was increased by 71 % in UPEC3 wild type and $\Delta tcpC$ stimulated cells relatively to unstimulated cells. Interestingly, compared to UPEC3 wild type stimulated NS RNA cells, $\Delta cnf1$ and $\Delta cnf1/\Delta hlyA$ showed an reduction of p-MLKL by 52 %, while p-MLKL decreased by 69 % in $\Delta hlyA$ ([Figure 4.23B](#)). [Figure 4.23C](#) also shows that LPS primed cells stimulated with nigericin and UPEC3 wild type increased p-MLKL by 55 % and 69 %, respectively ([Figure 4.23D](#)). Relative to UPEC3 wild type stimulated NS RNA cells, $\Delta cnf1$ and $\Delta hlyA$ stimulated cells decreased p-MLKL approximately by 65 %, whereas $\Delta cnf1/\Delta hlyA$ reduced p-MLKL by 80 %. Furthermore, CFT073 and DH5 α showed a decrease of p-MLKL by 76 % and 49 % relative to UPEC3 wild type NS RNA cells, respectively.

Indeed, FIP2 silencing showed moderate increase of p-MLKL in unstimulated cells, UPEC3 wild type, $\Delta cnf1$ and $\Delta tcpC$ stimulated cells ([Figure 4.23B](#)). This was also observed in LPS primed FIP2 siRNA cells ([Figure 4.23D](#)), where the unstimulated cells and cells treated with nigericin and $\Delta cnf1$ moderately increased p-MLKL (44 % <).

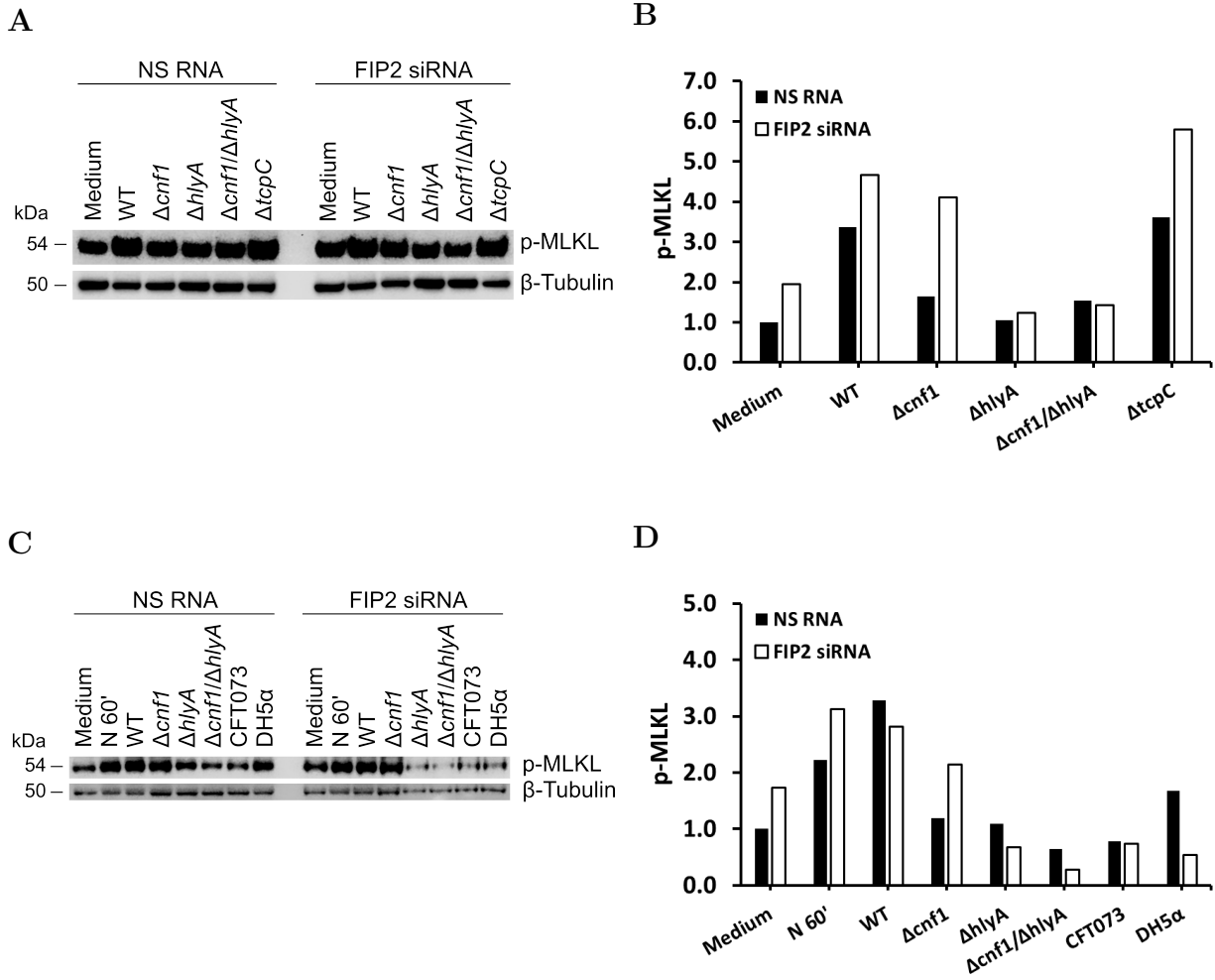


Figure 4.23: Quantification of p-MLKL in THP-1 cells stimulated with nigericin, virulent and avirulent *E. coli*. Immunoblot of p-MLKL (A) and quantified p-MLKL (B) in NS RNA or FIP2 siRNA treated THP-1 cells before stimulation with UPEC3 wild type and mutants for 2 h (MOI = 2). Immunoblot of p-MLKL (C) and quantified p-MLKL (D) in THP-1 cells treated with NS RNA or FIP2 siRNA before LPS priming for 2 h, then stimulated with nigericin for 1 h or with UPEC3 wild type, UPEC3 variants, CFT073 and DH5α for 2h (MOI = 2). Quantified protein levels are given in units of fold change.

4.3.10 HlyA in UPEC3 mediates degradation of NF- κ B p65 subunit in THP-1 cells

According to a previous publication, HlyA has been demonstrated that it induces degradation of NF- κ B p65 subunit in human bladder cells and mouse macrophages [95]. To examine whether HlyA expressed in UPEC3 also mediates degradation of NF- κ B p65 in THP-1 cells, Western blot was conducted.

Figure 4.24A and Figure 4.24B illustrate NF- κ B p65 in UPEC3 wild type and mutants stimulated cells showed a modest reduction relatively to unstimulated cells after 2 h. Strikingly, after 4 h of stimulation, NF- κ B p65 was reduced by 77 % in UPEC3 wild type, 92 % in $\Delta cnf1$ and 89 % in $\Delta tcpC$ stimulated NS RNA cells compared with unstimulated cells (Figure 4.24D). Moreover, intense bands below 65 kDa were detected in UPEC3 wild type, $\Delta cnf1$ and $\Delta tcpC$ stimulated cells, whereas these bands were not observed in unstimulated cells and weakly detected in NS RNA cells that were stimulated with $\Delta hlyA$ and $\Delta cnf1/\Delta hlyA$ (Figure 4.24C). Similar to 2 h of bacterial stimulation without LPS priming (Figure 4.24B), LPS primed NS RNA cells that were stimulated with UPEC3 wild type and $\Delta cnf1$, showed a small decrease of NF- κ B p65 after 2 h (Figure 4.24E and Figure 4.24F).

As shown in Figure 4.24B, FIP2 silencing only gave a small increase of NF- κ B in $\Delta cnf1$, $\Delta hlyA$ and $\Delta tcpC$ stimulated cells. After 4 h of stimulation, FIP2 silencing only showed a modest increase of NF- κ B p65 in $\Delta cnf1$, $\Delta hlyA$ and $\Delta cnf1/\Delta hlyA$ stimulated cells. Indeed, LPS primed FIP2 siRNA cells also showed a moderate increase of NF- κ B p65 in nigericin, UPEC3 wild type and $\Delta cnf1$ stimulated cells (Figure 4.24F).

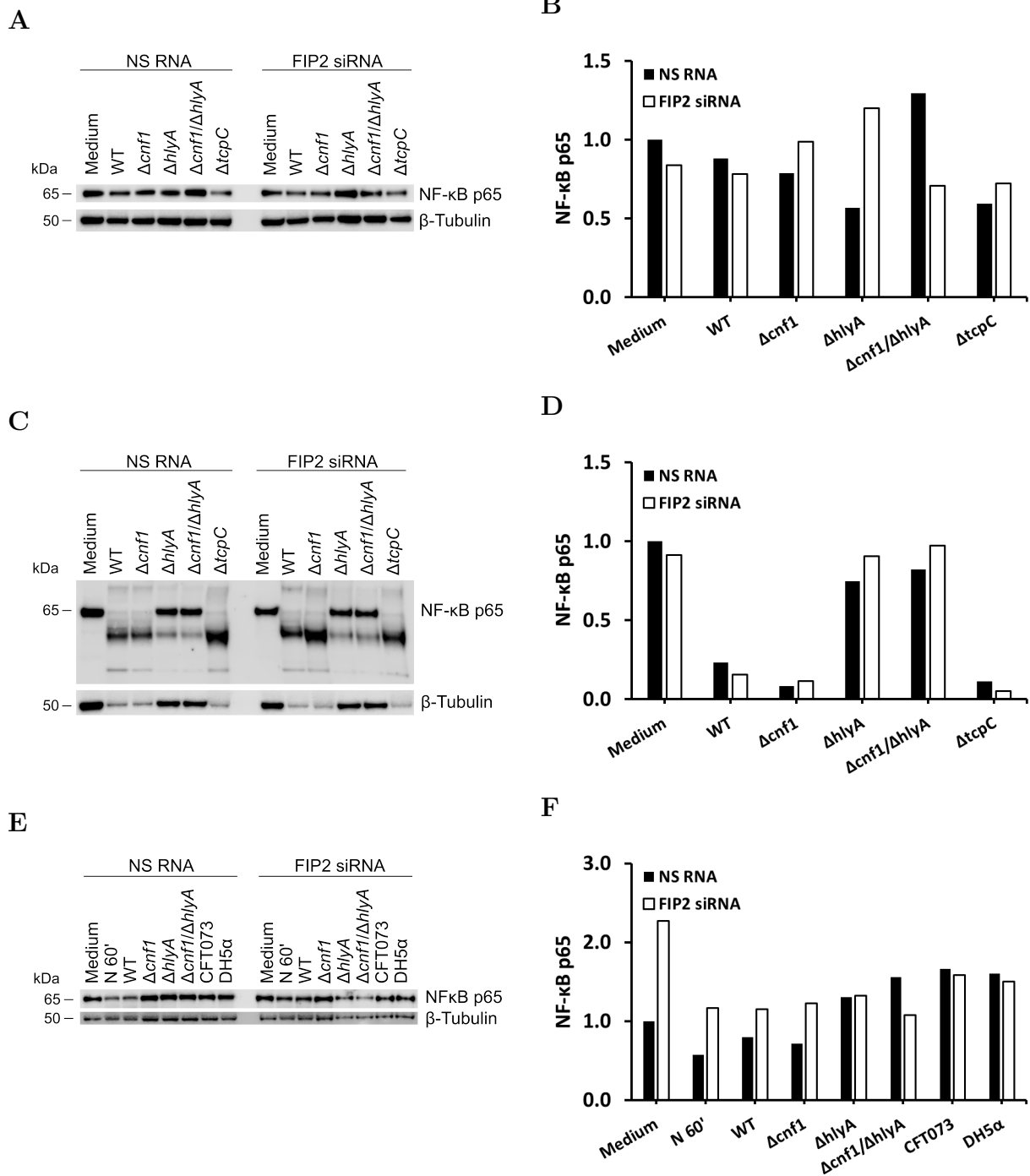


Figure 4.24: Quantification of NF- κ B p65 subunit in THP-1 cells stimulated with nigericin, virulent and avirulent *E. coli* strains. Immunoblot of NF- κ B p65 subunit and β -tubulin in THP-1 cells treated with NS RNA or FIP2 siRNA before stimulation with UPEC3 variants (MOI = 2) for 2 h (A) or 4 h (C). Quantified NF- κ B p65 protein levels in THP-1 cells after 2 h (B) and 4 h (D) of UPEC3 variants stimulation. Immunoblot of NF- κ B p65 subunit in THP-1 cells treated with NS RNA or FIP2 siRNA before LPS priming, then stimulation with nigericin for 1 h or with virulent and avirulent *E. coli* (MOI = 2) for 2 h (E). Quantification of NF- κ B p65 protein levels in LPS primed THP-1 cells after 1 h of nigericin and 2 h of *E. coli* stimulation (F). Quantified protein levels were normalised to unstimulated DMSO cells.

4.3.11 HlyA expressed in *E. coli* CFT073 and in UPEC3 may have different biological activities

From [section 4.3.7](#) to [section 4.3.10](#) two uropathogenic *E. coli* strains, UPEC3 and CFT073, were used to stimulate THP-1 cells. Both strains express HlyA and TcpC, while CFT073 lacks CNF1. Therefore, one may expect UPEC3 $\Delta cnf1$ and CFT073 stimulated THP-1 cells may respond relatively similar. Surprisingly, we observed CFT073 showed decreased pro-IL-1 β and IL-1 β p17 release by 80 %, 85 % reduction in pro-caspase-1 and 75 % reduction in caspase-1 p20 release relative to $\Delta cnf1$ stimulated NS RNA cells ([Figure 4.18](#)). Strikingly, GSDMD-N was decreased by 90 %, while GSDMD was increased by 34 % in CFT073 stimulated NS RNA cells relative to $\Delta cnf1$ ([Figure 4.21](#)). Furthermore, compared with $\Delta cnf1$ stimulated NS RNA cells, NF- κ B p65 was increased by 57 % in CFT073 stimulated cells ([Figure 4.24F](#)).

To investigate whether the response from bacterial stimulated THP-1 cells may have been affected by different bacterial growth rates, growth curves of UPEC3 wild type, $\Delta cnf1$, $\Delta hlyA$, $\Delta cnf1/\Delta hlyA$, CFT073 and DH5 α were measured. As shown in [Figure 4.25](#), UPEC3 variants, CFT073 and DH5 α have a relative similar growth rate in the first 8 h of incubation. Thereafter, CFT073 and DH5 α approached the stationary phase much earlier than UPEC3 wild type, $\Delta cnf1$ and $\Delta hlyA$. However, the deviation of growth rate after 8 h of bacteria incubation is not applicable during stimulation of THP-1 cells, since the bacteria were probably at the late lag phase and early exponential phase after dilution of the bacteria cultures. Indeed, the lag phase of CFT073 lasted approximately 30 min longer compared with UPEC3 wild type and mutants, while the generation time of CFT073 was relatively similar to UPEC3 wild type and $\Delta cnf1$ ([Table 4.13](#)).

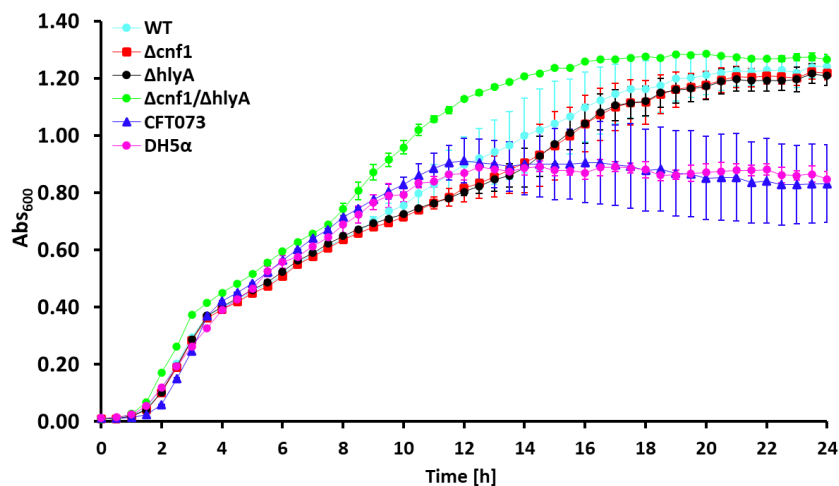


Figure 4.25: Growth curve of uropathogenic and avirulent *E. coli* strains. The bacteria were grown in LB medium at 37 °C for 24 h with shaking in a plate reader. The turbidity of three replicates of each culture was measured at 600 nm. WT: UPEC3 wild type.

Table 4.13: Generation time of *E. coli* strains. UPEC3 wild type (WT), UPEC3 mutants, CFT073 and DH5 α were grown in LB medium at 37 °C for 24 h with shaking, and the turbidity of three replicates was measured at 600 nm by a plate reader. The generation times (t_g) were calculated when the bacteria were at their exponential phase. For UPEC3 WT, $\Delta cnf1$, $\Delta hlyA$ and DH5 α , the exponential phase was considered between the time frame 2-3 h after start of incubation. The exponential phase of $\Delta cnf1/\Delta hlyA$ and CFT073 were respectively within 1.5-2.5 h and 2.5-3.5 h after incubation initiation.

<i>E. coli</i> strain	t_g [min]
WT	44.4
$\Delta cnf1$	40.4
$\Delta hlyA$	40.7
$\Delta cnf1/\Delta hlyA$	31.1
CFT073	46.1
DH5 α	52.6

Although, the level of HlyA expression could be different, we could not address this due to lack of proper antibodies. Indeed, the response from THP-1 cells that were stimulated with CFT073 was similar to $\Delta hlyA$ and $\Delta cnf1/\Delta hlyA$ than $\Delta cnf1$ (section 4.3.7 - section 4.3.10). Therefore, we speculate that the structure of HlyA expressed in CFT073 (HlyA^{CFT073}) may differ from HlyA expressed in UPEC3 strains (HlyA^{UPEC3}). To compare the protein structure of HlyA^{CFT073} with HlyA^{UPEC3}, the peptide sequences were aligned by using LALIGN to compare the primary structures. The peptide sequence of HlyA^{CFT073} was obtained from NCBI (GenBank ID: AAN82018.1). According to the summary from LALIGN, the identity between the two sequences was 97.9 % with 100 % overlap. Indicating these two peptide sequences are highly similar, but with some variation of amino acids residues. A detailed alignment result is attached to Appendix, section D.3. Amino acid residues that were found in HlyA^{UPEC3} different from HlyA^{CFT073}, are summarised in Table 4.14. Interestingly, serine 20 (Ser 20), threonine 482 (Thr 482), aspartate 518 (Asp 518), leucine (965) and alanine 966 (Ala 966) in HlyA^{CFT073} were substituted to alanine 20 (Ala 20), methionine 482 (Met 482), lysine 518 (Lys 518), serin 965 (Ser 965) and threonine 996 (Thr 966) in HlyA^{UPEC3}.

To investigate the impact of Ala 20, Met 482, Lys 518, Ser 965 and Thr 966 have on the tertiary structure of HlyA, the amino acid sequence of HlyA^{CFT073} with or without substitution of amino acids were uploaded to Phyre² to predict the structures. The predicted tertiary structure of wild type HlyA^{CFT073} obtained a relatively high confidence, where 95 % of the peptide sequence was predicted with a confidence above 90 % (Table 4.15). Except substitution of Leu 965 with serine and Ala 966 with threonine in HlyA^{CFT073}, the predicted structures of the local region with amino acid substitution had a relatively low confidence. Therefore, these predicted models were not considered for further analysis. As illustrated in Figure 4.26, the local structure of HlyA with Leu 965 and Ala 966 was relatively less organised compared with the structure with Ser 965 and Thr 966 substitution. Before sub-

stitution of amino acids, the peptide sequence from position 944 to 947 is localised on the opposite side of the peptide sequences at position 963 to 966, 980 to 984 and 1001 to 1004 (Figure 4.26A and Figure 4.26C). After amino acid substitution, small β -sheets were formed from 963 to 966, 981 to 983 and 1001 to 1004 (Figure 4.26B and Figure 4.26D). These small β -sheets are stacking under the β -sheet with amino acid residues from 944 to 947, forming a barrel-like structure (Figure 4.26F).

Table 4.14: Comparison of amino acid residues in α -hemolysin expressed in *E. coli* CFT073 and UPEC3 strains. Pairwise sequence alignment of α -hemolysin (HlyA) expressed in *E. coli* CFT073 and in UPEC3 strains was performed by LALIGN. The sequence alignment had a 100 % overlap and an identity of 97.9 %. Amino acid residues (aa) that are different in the HlyA sequences are noted with their respective location and the function of the domain.

Location	aa in HlyA ^{CFT073}	aa in HlyA ^{UPEC3}	Domain	Function
20	Ser	Ala	N-terminal	Target cell binding
223	Thr	Asn	N-terminal	-
482	Thr	Met	N-terminal	Facilitate hemolysis
489	Gly	Ser	N-terminal	Facilitate hemolysis
515	Lys	Arg	N-terminal	Facilitate hemolysis
516	Lys	Arg	N-terminal	Facilitate hemolysis
518	Asp	Lys	N-terminal	Facilitate hemolysis
522	Lys	Gln	N-terminal	Facilitate hemolysis
524	Val	Ile	N-terminal	Facilitate hemolysis
865	Asp	Glu	Ca ²⁺ binding	Folding/ Ca ²⁺ binding
885	Arg	Lys	Ca ²⁺ binding	Folding/ Ca ²⁺ binding
912	Arg	Lys	C-terminal	Secretion signal
920	Gly	Arg	C-terminal	Secretion signal
922	Ile	Leu	C-terminal	Secretion signal
947	Leu	Phe	C-terminal	Secretion signal
956	Ala	Val	C-terminal	Secretion signal
962	Asn	His	C-terminal	Secretion signal
965	Leu	Ser	C-terminal	Secretion signal
966	Ala	Thr	C-terminal	Secretion signal

Table 4.15: Confidence of predicted tertiary structures of α -hemolysin. The tertiary structures of HlyA expressed in CFT073 with or without substituted amino acids were predicted by [Phyre²](#). The net confidence of the predicted structures are given in percentage of amino acid residues (aa residues) modelled with a confidence above 90 %. Regions that were predicted with low confidence are listed with amino acid positions. WT: wild type HlyA^{CFT073}. Ser20Ala: substitution of serine with alanine at position 20. Thr482Met: Substitution of threonine with methionine at position 482. Asp518Lys: Sustitution of aspartate with lysine at position 518. Leu965Ser / Ala966Thr: substitution of leucine with serine at position 965 and alanine with threonine at position 966.

Substituted aa	aa residues [%]	Low confidence regions
WT	95	1-4 / 418-500 / 577-616
Ser20Ala	40	1-617
Thr482Met	89	1-4 / 467-577
Asp518Lys	86	1-24 / 494-613 / 1014-1024
Leu965Ser / Ala966Thr	94	1-17 / 526-577

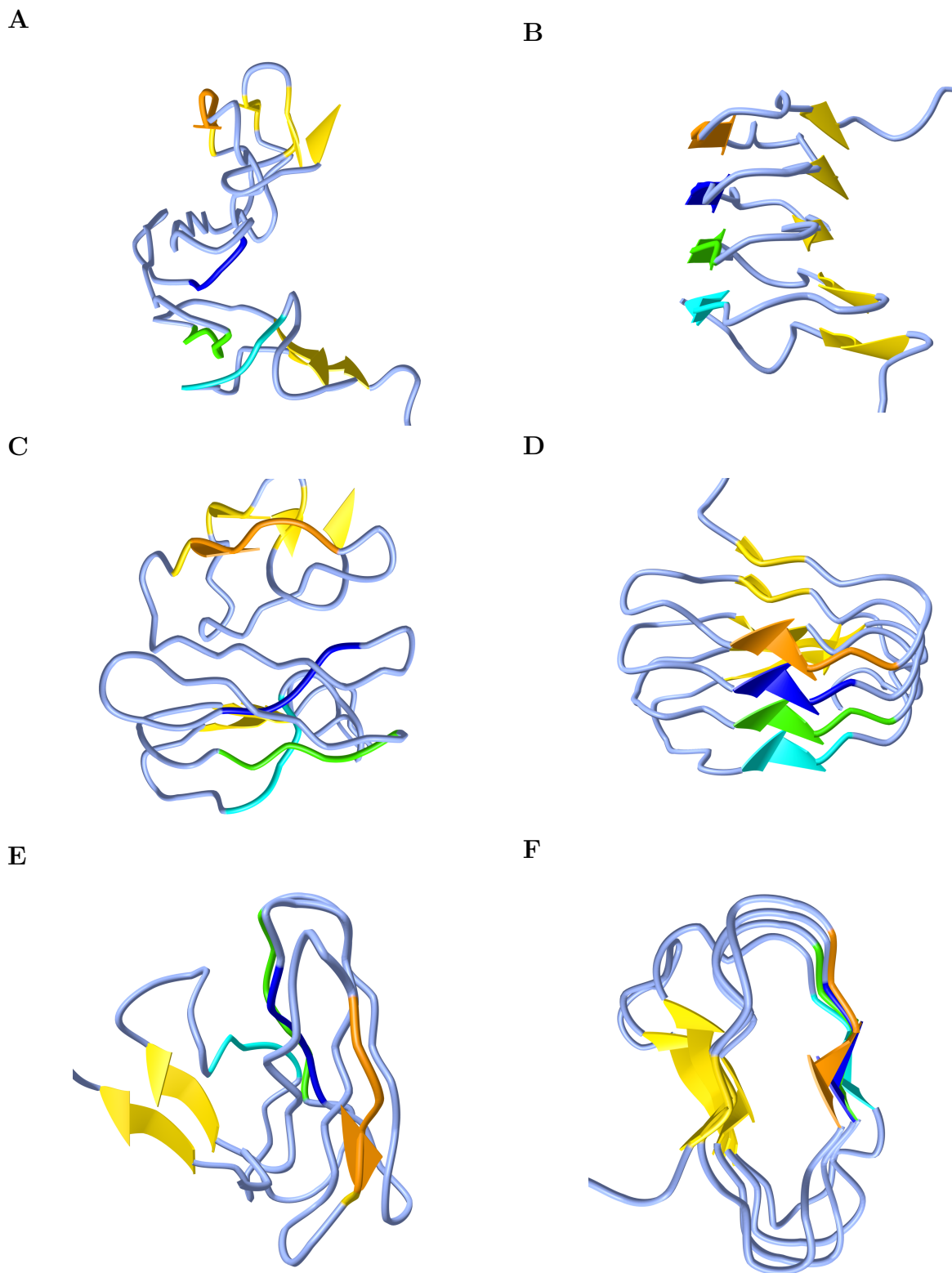


Figure 4.26: Predicted secondary structures at the C-terminus of α -hemolysine with or without amino acids substitution. The tertiary structure of HlyA expressed in CFT073 was predicted by [Phyre²](#) after submitting the peptide sequence with or without substitution of amino acid residues. **(A)** and **(C)**: Side view of HlyA at the proximity to Leu 965 and Ala 966. **(B)** and **(D)**: Side view of HlyA close to Ser 965 and Thr 966. Top view of HlyA with Leu 965 and Ala 966 **(E)**. Top view of HlyA with Ser 965 and Thr 966 **(F)**. Yellow sheet: β -sheets. Orange: peptide sequence from position 944 to 947. Blue: peptide sequence from position 963 to 966. Green: peptide sequence from position 980 to 984. Cyan: peptide sequence from position 1001 to 1004.

5 Discussion

In this study we aim to identify the pivotal virulence factor in UPEC3 which causes inflammatory cell death in THP-1 cells and examine how FIP2 regulates NLRP3 inflammasome signalling pathway. To achieve our goals we established UPEC3 mutants, which we then used to stimulate THP-1 cells with or without FIP2 silencing.

5.1 Bioinformatics analysis predicted expression of virulence factors in UPEC3

Earlier reports have shown CNF1, HlyA and TcpC are common evasion strategies which uropathogenic *E. coli* utilises to counteract host's immunity [61, 94, 95]. In addition to various secretion systems, OMVs may serve as cargo for delivery of bacterial nucleic acids as well as HlyA and CNF1 to target cells [63, 67, 68]. OmpT and DsbA have been characterised for regulating OMVs biogenesis in *E. coli* [63, 64, 65]. In the present study, *cnf1*, *dsbA*, *hlyA*, *ompT* and *tcpC* were mapped in the genome of a clinical isolated uropathogenic *E. coli* strain, UPEC3. According to our bioinformatics analysis of CNF1, DsbA, HlyA, OmpT and TcpC, the peptide sequences showed high similarity with reference sequences in databases (Table 4.2). Importantly, the functional domains of these proteins were also found with high confidence (Table 4.3). Indicating that UPEC3 expresses functional *cnf1*, *dsbA*, *hlyA*, *ompT* and *tcpC* genes. Moreover, analysis of hlyCABD operon also showed that UPEC3 most likely has a functional type 1 secretion system for the secretion of HlyA (Table 4.4 and Table 4.5).

Furthermore, BLAST-analysis and conserved domain search revealed that UPEC3 encodes all essential subunits of T6SS (Table 4.7 and Table 4.8). Although some queries obtained relatively low sequence identities but high overlap percentages and significantly low E-values from BLAST analysis. This fact can be explained by the reference sequences have a relatively distant phylogenetic relationship to UPEC3. Despite TssJ and TssM reference sequences originated from *E. coli* and these sequences completely overlapped with the queries, the identities between reference and query sequences were only at moderate levels (Table 4.7). Perhaps, these proteins are homologs with conserved domains but have some variations in primary structure (Table 4.8). Interestingly, *tssA* and *tssH* were predicted in both contig 7 and 21, suggesting two copies of these genes may exist in UPEC3. According to previous studies, Hcp protein families can be secreted and stimulate production of inflammatory cytokines in macrophages [58]. Also it has important structural functions for delivering toxins [56]. Currently, the functional domains of Hcp is poorly characterised. Whether the protein structure of secreted and non-secreted Hcp differs remains enigmatic. Thus, we cannot conclude whether Hcp is secreted from UPEC3. Altogether, our analyses of the open

reading frames indicate that UPEC3 has the potential of expressing a functional T6SS.

5.2 UPEC3 is efficiently transformed by electroporation

According to earlier studies, polysaccharide chain and phosphorylation of lipopolysaccharide core affect transformation efficiency in *E. coli* [99, 100]. Since the structure of LPS varies in different *E. coli* phylogroups and serogroups [101], the plasmid uptake efficiency in UPEC3 may also be affected by chemical and electroporation transformation. Based on transformation efficiency of chemical and electrocompetent UPEC3, electroporation was clearly the most efficient transformation method for UPEC3 (Table 4.9).

5.3 Editing efficiency increases with homology directed repair

As UPEC3 failed to take up pCas9 and pCRISPR construct simultaneously, electrocompetent UPEC3 harbouring pCas9 was generated and subsequently transformed with pCRISPR by electroporation. Previously, the genomic editing efficiency of CRISPR-Cas9 was enhanced by cloning homologous arms into the plasmid [71, 72, 73]. Consistent with earlier studies, the genomic editing efficiency of CRISPR-Cas9 was improved and the gene of our interest was successfully deleted in approximately 40 % of transformed UPEC3 (Figure 4.3B). Due to time limitation, we only compared editing efficiency of pCRISPR constructs with and without homology arms that targeted *cnf1*. Since pCRISPR constructs with homology arms gave the highest editing efficiency, same approach was used to delete *hlyA*, *ompT* and *tcpC* in UPEC3. Moreover, $\Delta cnf1/\Delta hlyA$ and $\Delta cnf1/\Delta tcpC$ double deletion mutants were also generated. Unfortunately, we failed to induce *dsbA* knockout in UPEC3. Probably, the designed spacers annealed poorly with the the proto-spacers or that the homology arms were too short for efficient homology directed repair after double strand break was induced by Cas9. However, we cannot exclude the fact that DsbA is an important protein for catalysing disulphide bonds of proteins in periplasma [66], which probably may be essential for UPEC3 to survive.

We have verified the mutants by colony PCR, Western blot and whole genome sequencing. In line with our *in silico* simulations, whole genome sequencing showed *cnf1*, *hlyA*, *ompT* and *tcpC* were successfully deleted in single mutants and the genome was repaired as expected (Table 4.10). According to the result from whole genome sequencing, the local region of hlyCABD operon and *cnf1* was missing in $\Delta cnf1/\Delta hlyA$ double mutant. However, colony PCR showed $\Delta cnf1/\Delta hlyA$ obtained amplicons that were similar to $\Delta cnf1$ and $\Delta hlyA$ single mutants (Figure 4.4). Indicating that *cnf1* and *hlyA* were deleted in $\Delta cnf1/\Delta hlyA$ and the upstream and downstream regions to these genes probably remained intact. The likelihood of *cnf1* and *tcpC* deletion is high, given the amplicons from colony PCR had a similar size

as $\Delta cnf1$ and $\Delta tcpC$ single mutants (Figure 4.5). Because $\Delta cnf1/\Delta tcpC$ double mutant was obtained at the later stage in this study, gene deletion and reparation in $\Delta cnf1/\Delta tcpC$ double mutant were only verified by colony PCR. However, the deletion of *cnf1* and *ompT* were confirmed by Western blotting using specific antibodies towards both proteins. The results from the other UPEC3 deletions made were consistent with the results from whole genome sequencing. Initially we had some problem detecting OmpT band using Western blotting, due to several background bands blending into the real band. This issue was resolved by incubation of UPEC3 in minimal medium A before lysis and analysis of the $\Delta ompT$ clone by immuno-blotting (Figure 4.8).

5.4 Presence of plasmids in UPEC3 may affect the bacterial metabolism

After the target genes were deleted, pCRISPR-constructs were cured, since the presence of ColE replication origin in plasmids have shown to affect the metabolism in *E. coli* [102], which potentially can affect the response from THP-1 cells in later stimulation experiments. However, we decided to keep pCas9 in UPEC3 mutants due to our desire to generate multiple gene knockout mutants. Growth curve measurements revealed UPEC3 wild type without harbouring any plasmids had a relatively shorter lag phase than mutants with pCas9 (Figure 4.6A). Interestingly, this difference was abolished when UPEC3 was transformed with pCas9 (Figure 4.6B). We emphasise variation of growing conditions could impact duration of lag phase and growth rate [103]. Nevertheless, previous publications have shown that expression of foreign protein and the plasmid size also affected the bacterial metabolism and the growth rate [104, 105]. Thus, harbouring pCas9 might be energy demanding so the bacteria grew slower, given the fact that this plasmid has a size of 9326 bp. We reasoned by transforming UPEC3 wild type with pCas9, we can eliminate the metabolic differences between UPEC3 wild type and the mutant clones. This way, we also avoid different responses from THP-1 cells which is caused by metabolic discrepancy between UPEC3 with and without pCas9.

5.5 HlyA induces rapid inflammatory cell death in THP-1 cells

To investigate which virulence factors expressed in UPEC3 are pivotal for inducing inflammatory cell death in human macrophages, we generated UPEC3 mutant clones that we used to stimulate THP-1 cells. Detection of released LDH, caspase-1 p20 and IL-1 β p17 are important indicators for inflammatory cell death in THP-1 cells, since LDH release is often resulted by damaged plasma membrane [90], while caspase-1 p20 and IL-1 β p17 are hallmarks of inflammasome activation in the pyroptotic signalling pathway [35, 37, 38]. Our data

showed a correlation between LDH release and the decreased levels of released caspase-1 p20 and IL-1 β p17 after 2 h of bacterial stimulation (Figure 4.10A and Figure 4.13A), indicating that the cell death observed was caused by inflammasome activation and subsequent pyroptotic cell death. Remarkably, deletion of *hlyA* gene, both in the single knockout with *hlyA* only and in the double gene knockout with *cnf1* showed a strong decrease in cellular LDH release, caspase-1 p20 and IL-1 β p17 release after 2 h of stimulation (Figure 4.13E). Showing that *hlyA* deletion in UPEC3 markedly reduced inflammatory cell death in stimulated THP-1 cells. Interestingly, deleting *cnf1* had an opposite effect, increasing the level of released LDH, caspase-1 p20 and IL-1 β p17 after 2 h of stimulation. After 4 h of stimulation, the cells stimulated with Δ *cnf1* showed similar levels of released IL-1 β p17 with the wild type cells but markedly lower than the cells stimulated with the Δ *hlyA* and Δ *cnf1*/ Δ *hlyA*, yet these cells showed a lower LDH release than wild type and Δ *cnf1* stimulated cells (Figure 4.10B and Figure 4.13F). Suggesting that deletion of *hlyA* in UPEC3 delayed inflammasome activation in THP-1 cells. Indeed, the immunoblot of caspase-1 p20 in the supernatants after 4 h stimulation, have a relatively large background (Figure 4.13B), especially in Δ *hlyA* and Δ *cnf1*/ Δ *hlyA* mutants stimulated cells, which made the semi-quantification of caspase-1 p20 very challenging.

Recently, a study showed phospho-PAK1 (p-PAK1) phosphorylated NLRP3 downstream to active Rac1 [51]. Despite Rac1 protein level correlated with the level of NLRP3 monomer after 2 h of stimulation (Figure 4.15), we cannot conclude whether Rac1 was in its active or in active state. We attempted to detect p-PAK1, but we were not able to observe p-PAK1 in our immunoblots. Furthermore, our protein samples were not cross-linked, so we could not detect NLRP3-oligomers. However, detection of caspase-1 p20 and IL-1 β p17, which are hallmarks of active inflammasomes, supports inflammasome was assembled. Nevertheless, levels of GSDMD-N also correlated with caspase-1 p20 and IL-1 β p17, and were only observed in UPEC3 wild type, Δ *cnf1* and Δ *tcpC* stimulated THP-1 cells (Figure 4.16). Due to massive cell lysis after 4 h of bacterial stimulation (Figure 4.14), these cell lysates were not profoundly analysed.

5.6 HlyA deficient UPEC3 stimulated THP-1 cells increased cytokine mRNA levels

We further investigated transcription level of cytokines in THP-1 cells upon bacterial stimulation. Remarkably, when compared to the wild type UPEC3 and the other deletion mutants the mRNA levels of pro-IL-1 β , NLRP3 and TNF α were the highest in Δ *hlyA* and Δ *cnf1*/ Δ *hlyA* mutants stimulated THP-1 cells. Strikingly, IFN β was increased by more than 90 % in Δ *hlyA* and Δ *cnf1*/ Δ *hlyA* relative to UPEC3 wild type stimulated cells (Figure 4.11D). The reason for IFN β mRNA levels increase in *hlyA* deletion mutants is unknown,

but one might speculate that when the pore forming toxin HlyA is removed, the plasma membrane remains intact and an increase in phagocytosis may drive IFN β mRNA expression. A relationship between macrophage *E. coli* phagocytes and IFN β mRNA induction has been described [25] and will be addressed in future experiments.

According to previous study, TcpC has shown to inhibit MyD88- and TRIF-dependent signalling pathways [61]. Thus, one would expect increased mRNA levels of cytokines in THP-1 cells that were stimulated with $\Delta tcpC$ relatively to UPEC3 wild type. Surprisingly, cytokine mRNA levels in $\Delta tcpC$ stimulated cells contradicted this expectation. However, the protein levels involved in pyroptotic cell death, pro-IL-1 β and NLRP3, were highest in $\Delta tcpC$ stimulated cells (Figure D.9C and Figure 4.15). Perhaps, these observations correlate with degradation of transcription factor NF- κ B p65 in UPEC3 wild type, $\Delta cnf1$ and $\Delta tcpC$ stimulated cells, that is apparent in non-LPS-primed cells following 4 h of UPEC3 stimulations (Figure 4.24D). We also envision that HlyA triggered proteolysis of proteins in TRIF-dependent signalling pathway in UPEC3 wild type, $\Delta cnf1$ and $\Delta tcpC$ mutants stimulated THP-1 cells could explain our observation of decreased IFN β mRNA relatively to *hlyA* deletion mutants after 2 h and 4 h stimulation as indicated in Figure 4.11D and Figure 4.12D. Consistent with previous study, NF- κ B was degraded after 4 h of stimulation [95]. Our observation of NF- κ B degradation led us to speculate whether HlyA released from UPEC3 also induced proteolysis of PAK1 and HDAC6 in THP-1 cells, which was observed in HlyA expressing *E. coli* UTI89 stimulated human bladder cells [95]. In light of PAK1 and HDAC6 are critical proteins in NLRP3 activation and endosomal trafficking to MTOC [41, 51], HlyA triggered proteolysis has the potential of shutting down NLRP3-inflammasome signalling pathway in THP-1 cells, which further lead to fewer IL-1 β p17 release. In fact, reduced IL-1 β p17 release over time was observed after 4 h of stimulation, where $\Delta hlyA$ and $\Delta cnf1 / \Delta hlyA$ clearly released more IL-1 β p17 than UPEC3 wild type, $\Delta cnf1$ and $\Delta tcpC$ (Figure 4.13).

5.7 FIP2 stabilises Rac1 in THP-1 cells

FIP2 has shown to play an essential role in phagocytosis and regulation of NLRP3 inflammasome [25, 42]. In this study we also investigated the effect of FIP2 silencing has on non-LPS primed THP-1 cells when stimulated with UPEC3 wild type and mutants. Consistent with unpublished data from our group [42], FIP2 silencing showed decreased levels of caspase-1 p20 and IL-1 β p17 release from cells that were stimulated with UPEC3 variants (Figure 4.13). Indicating, FIP2-silencing has the potential of suppressing inflammasome activation. Moreover, FIP2 silencing also showed tendency to reduce LDH release and moderately downregulate pro-IL-1 β , NLRP3, IFN β and TNF α mRNA levels (Figure 4.10A, Figure 4.11 and Figure 4.12). Indeed, the effect of FIP2 silencing was less clear on LDH release and transcriptional levels of cytokine, which probably reflects on omitting LPS-priming. Interestingly, FIP2 protein levels correlated with Rac1, coinciding with earlier demonstra-

tion of FIP2 in phagocytosis [25], yet we cannot exclude the fact that UPEC3 may not be phagocytosed, since *kpsD* and *kpsM* were found in UPEC3. These genes are involved in group 2 capsule protein synthesis and studies have shown that encapsulated *E. coli* blocks complement fixation and phagocytosis [106, 107]. Despite Q-PCR showed FIP2 silencing was successful (Figure 4.11A), semi-quantification of FIP2 protein levels was difficult due to high background (Figure 4.15A). Hence, Western blot toward FIP2 must be optimised in the future.

5.8 TcpC suppresses FIP2 to promote NLRP3 inflammasome activation

Furthermore, we have also shown that FIP2 silencing decreased pro-IL-1 β and NLRP3 protein levels (Figure 4.14E and Figure 4.15D). Interestingly, FIP2 silencing did not decrease GSDMD, nor did it reduce GSDMD cleavage in UPEC3 wild type and $\Delta cnf1$ stimulated THP-1 cells (Figure 4.16). However, when THP-1 cells were stimulated with $\Delta tcpC$, FIP2 siRNA showed 85 % reduction of cleaved GSDMD. These led us to hypothesise that FIP2 does not affect the expression level of GSDMD in THP-1 cells, but rather activation and assembly of inflammasomes upon bacterial stimulation, based on the fact that TcpC inhibits inflammasome assembly by interacting with NLRP3 and caspase-1 [62]. Since FIP2 also binds to NLRP3 and caspase-1 [42], deletion of TcpC from UPEC3 would allow FIP2 to promote inflammasome activation that cleaves GSDMD and cytokines. On the other hand, the presence of TcpC could have diminished the effect of FIP2 siRNA on GSDMD cleavage, by competing against FIP2 for interacting with NLRP3 and caspase-1. Interestingly, FIP2 silencing resembles NLRP3 inhibitor treatment, where less LDH and IL-1 β p17 were released (Figure 4.22), in support of FIP2 serving an important role in regulating both LPS priming and the activation of the NLRP3 inflammasome.

5.9 LPS enhances NLRP3 inflammasome signalling

In this study, we investigated the effect caused by bacterial stimulation without LPS priming in THP-1 cells. However, the signal intensities of proteins downstream to NLRP3 inflammasome were relatively weak when LPS priming was omitted (Figure 4.13 and Figure 4.16). This may be explained by other types of cell death were operating. However, it is also clear that 4 h of stimulation may cause general proteolysis of proteins. Therefore we chose to prime the cells for 2 h with LPS before 2 h of stimulation with bacteria variants. Nevertheless, pro-caspase-1 and pro-IL-1 β release were elevated as well as caspase-1 p20 and IL-1 β p17 (Figure D.10 and Figure 4.18), which is consistent with the fact that LPS priming stimulate transcription of pro-inflammatory cytokines and licensing NLRP3 inflammasome

signalling pathway giving subsequent pyroptotic cell death [37, 38]. In contrast to unprimed THP-1 cells, GSDMD-N was detectable in $\Delta hlyA$ and $\Delta cnf1/\Delta hlyA$ stimulated cells that were primed with LPS (Figure 4.21A).

Compared with non-LPS primed cells, LPS priming caused the wild type and $\Delta cnf1$ stimulated cells to induce comparable NLRP3 mRNA levels to those stimulated with clones deficient in *hlyA* expression (Figure 4.11D and Figure 4.19C). While pro-IL-1 β showed a marginal increase (Figure 4.11B and Figure 4.19B), the induction of IFN β mRNA stimulated by the $\Delta cnf1$ increased to the level of $\Delta hlyA$ (Figure 4.11D and Figure 4.19D). Nevertheless, LPS priming caused a marked decrease in TNF α mRNA levels compared with unprimed cells in all UPEC3 variant stimulations (Figure 4.11E and Figure 4.19E). Intriguingly, LPS priming enhanced the effect of FIP2 silencing, where total amount of IL-1 β in supernatants (Figure 4.17B) and mRNA levels of pro-IL-1 β , NLRP3 and TNF α were strongly reduced in UPEC3 wild type and mutants stimulated cells in contrast to cells without LPS priming (Figure 4.11 and Figure 4.19). Collectively, LPS priming enhanced NLRP3 signalling by increasing expression of pro-IL-1 β and NLRP3.

5.10 CNF1 promotes Rac1 deamidation and degradation, while HlyA triggers rapid NLRP3 inflammasome degradation

Furthermore, in LPS primed cells, the $\Delta cnf1$ mutants stimulated the highest Rac1 protein levels, in contrast to UPEC3 wild type stimulated cells (Figure 4.20C). This observation led us to speculate $\Delta cnf1$ could not deamidate Rac1, hence Rac1 was not ubiquitinated and degraded [48]. On the other hand, UPEC3 wild type which expresses CNF1, can induce constitutive activation of Rac1 which triggers NLRP3 inflammasome activation via p-PAK1 [51] but also proteosomal degradation of Rac1 [48]. Previous study has shown that HDAC6 is important for NLRP3 activation by transporting NLRP3 components to MTOC, where NLRP3 interacts with NEK7 and mediate autophagosomal degradation of NLRP3 inflammasome [41]. Interestingly, the NLRP3 protein levels in UPEC3 wild type and $\Delta cnf1$ stimulated cells were comparable to unstimulated cells (Figure 4.20D). Together with the observation of the relatively high amount of GSDMD-N and released caspase-1 p20 and IL-1 β p17 in UPEC3 wild type and $\Delta cnf1$ stimulated cells (Figure 4.18 and Figure 4.21E), we believe autophagosomal degradation of NLRP3 inflammasome could have taken place in UPEC3 wild type and $\Delta cnf1$ stimulated cells after processing pro-IL-1 β and GSDMD. Based on the fact that less GSDMD-N, caspase-1 p20 and IL-1 β p17 were observed in cells stimulated with *hlyA* deficient mutants but these cells showed increased NLRP3 protein levels (Figure 4.18, Figure 4.21E and Figure 4.20D), we speculate that fewer NLRP3 inflammasomes were activated and autophagosomal degraded.

5.11 CNF1 and HlyA expressing UPEC3 stimulated cells show tendency to activate necroptosis in THP-1 cells

Bacterial stimulation may induce additional cell death signalling pathways. To address whether apoptotic or necroptotic signalling pathways were activated, we performed Western blot to detect caspase-3, caspase-8 and phosphorylated MLKL at serin 358 (p-MLKL). Unfortunately, we failed to detect caspase-3 and caspase-8 in THP-1 cells. However, according to the vast amount of LDH, caspase-1 and IL-1 β release in nigericin, UPEC3 wild type, $\Delta cnf1$ and $\Delta tcpC$ stimulated cells, we reasoned that inflammatory signalling pathways were the primary activated pathways. Strikingly, our data showed increased p-MLKL in nigericin, UPEC3 wild type and $\Delta tcpC$ stimulated cells relatively to unstimulated cells (Figure 4.23). Surprisingly, FIP2 siRNA treatment increased p-MLKL modestly, yet these cells did not show increased LDH release compared with NS RNA cells. Indicating, necroptosis may not be the primary activated signalling pathway in early stimulation. However, we cannot exclude the possibility of ESCRT-III machinery activation that shred out p-MLKL from the plasma membrane [14]. Recently, a study revealed that endosomal trafficking of p-MLKL (phosphorylated serin 358) is the rate limiting checkpoint and accumulation of p-MLKL at hotspots on the plasma membrane must surpass a threshold for execution of necroptosis in epithelial cells [108]. Thus, detection of p-MLKL in whole cell lysates in our study does not imply p-MLKL aggregated on the plasma membrane in THP-1 cells nor can we be certain that necroptosis has been executed.

5.12 HlyA triggered protease activation may generate unconventional caspase-1 and IL-1 β intermediates in THP-1 cells

Interestingly, in addition to the conventional pro-caspase-1 and pro-IL-1 β , unconventional caspase-1 (37 kDa) and IL-1 β (28 kDa) intermediates were detected in supernatants and in cell lysates. Strikingly, unconventional caspase-1 and IL-1 β were only observed in nigericin, UPEC3 wild type, $\Delta cnf1$ and $\Delta tcpC$ stimulated cells (Figure 4.13, Figure 4.14, Figure 4.18, Figure 4.21 and Figure 4.22). Unpublished data from our group has also shown the intermediate pro-caspase-1 are common isoforms and over-expression of these intermediates may induce apoptosis. The underlying mechanisms of forming these intermediates in THP-1 cells are currently not well characterised and documented. Until now, it has been proposed that neutrophil elastase and lysosomal enzyme cathepsin D are responsible for cleavage of pro-IL-1 β to 20 kDa unconventional IL-1 β (p20) [109, 110, 111]. Previous study has shown unconventional IL-1 β has a lower bioactivity relative to mature IL-1 β p17 [112]. Given the fact that HlyA expressing UPEC [95] triggers degradation of NF- κ B due to activation of serine proteases in human bladder cells and similar observations were seen in our study, we speculate HlyA expressing UPEC3 may induce activation of an unknown protease that

cleaves pro-caspase-1 and pro-IL-1 β to unconventional isoforms.

5.13 Different protein structures of HlyA expressed in CFT073 and UPEC3 may potentially affect their biological activities

In this study we have also noticed that the uropathogenic CFT073 *E. coli* stimulated THP-1 cells responded differently from $\Delta cnf1$ UPEC3 mutant. Both bacteria express HlyA and TcpC, but not CNF1, yet CFT073 showed decreased release of LDH, capase-1 p20 and IL-1 β p17 relatively to $\Delta cnf1$ mutant stimulated cells. Growth curve measurement of these two *E. coli* strains showed the generation time at the exponential phase was relatively similar. On the other hand, we noticed a small difference in the lag phase of CFT073 relatively to $\Delta cnf1$. Whether the difference of lag phase duration contributed to different responses from THP-1 cells is not likely. We further investigated the primary structure of HlyA^{CFT073} and HlyA^{UPEC3} to identify possible amino acid substituents that may give different secondary and tertiary structures. Our bioinformatic analysis revealed the primary structures of HlyA^{CFT073} and HlyA^{UPEC3} were indeed nonidentical. Local region with amino acid residues substituted by residues that belong to the same classification group, have relatively similar properties, were less susceptible for protein conformational changes (Table 4.14). Interestingly, Ser 20, Thr 482, Asp 518, Leu 965 and Ala 966 in HlyA^{CFT073} were substituted by Ala 20, Met 482, Lys 518, Ser 965 and Thr 966 in HlyA^{UPEC3}.

Except HlyA^{CFT073} wild type and HlyA^{CFT073} Leu965Ser / Ala966Thr, the confidence of the predicted tertiary structures was relatively poor and were not profoundly analysed in this study (Table 4.15), but we should not neglect that these substituted amino acids can still give different HlyA conformations. Remarkably, the polar amino acids, Ser 965 and Thr 966 in HlyA^{CFT073} obtained more structured C-terminus and induced stabilisation of neighbouring β -sheets to form a barrel like-shaped structure, while these were not observed in HlyA^{CFT073} wild type with Leu 965 and Ala 966 (Figure 4.26). Perhaps, Ser 965 and Thr 966, which both have a hydroxyl group, supported the neighbouring β -sheets by forming hydrogen bonds with the amino acids in the closely located β -sheets. The effect of this conformational change at C-terminus remains elusive. However, we speculate it may regulate HlyA secretion based on the fact that the C-terminus of the toxin serves as a secretion signal [53].

5.14 Systemic response may differ from cellular response upon UPEC3 stimulation

So far, our data suggest expression of HlyA in UPEC3 causes rapid inflammatory cell death in THP-1 cells. However, previous publication has shown that deletion of *hlyA* in UPEC strain, UTI89, reduced bacteremia in mice, while IL-1 β level in mice sera was increased

compared with wild type, *cnf1* deletion mutant and *cnf1* and *hlyA* double deletion mutant after 3 h of intravenous infection [55]. Despite our data is not consistent with earlier demonstration, it is important that we emphasise our study used different experimental setups, which potentially could give different observations. First, our study focused on single cell line response, which is less complex than mouse model that provides information about systemic response upon infection. Second, THP-1 cells are human macrophages, and we cannot exclude the possibility that human and murine macrophages may respond differently upon bacterial stimulation. Third, in this study we used a clinical isolated *E. coli* strain and may phylogenetically differ from *E. coli* UTI89. Perhaps, these two *E. coli* strains express additional virulent factors which may give different responses. As we have shown in the present study, deletion of *hlyA* seems to delay pyroptosis in THP-1 cells, where released IL-1 β p17 was relatively low after 2 h of stimulation, while it was markedly increased after 4 h of stimulation compared with wild type and Δ *cnf1* stimulated cells (Figure 4.13). Therefore, we believe sampling of sera at multiple time points is critical for observing and determining the relationship between *hlyA* deficient bacteria and released IL-1 β in sera, which was not conducted in previous study [55].

6 Future Perspectives

By employing CRISPR-Cas9 we aimed to establish clinical isolated uropathogenic *E. coli* mutants. Stimulating THP-1 cells with UPEC3 wild type and mutants revealed the pore forming protein, HlyA, is a pivotal virulence factor for inducing rapid inflammatory cell death in human macrophages, while deletion of *hlyA* showed delayed activation of pyroptosis. In accordance with unpublished data from our group [42], FIP2 silencing reduced release of caspase-1 and IL-1 β in nigericin and bacterial stimulated THP-1 cells. Moreover, our data suggest FIP2 has an essential role in regulating pro-IL-1 β and NLRP3 expression and promote NLRP3 inflammasome assembly. Nonetheless, our pilot study of TcpC suggest it competes against FIP2 for interacting with NLRP3 and caspase-1. However, there are still many unanswered questions that need to be addressed in the future.

Indeed, UPEC3 has a high likelihood of expressing T6SS. As studies have shown, Hcp seems to have a dual function in T6SS. Hcp is indispensable for forming a tube-like platform for loading and delivering T6SS effector proteins to the target cell [56]. On the other hand, Hcp can also be secreted and induce expression of inflammatory cytokines of the target cell [58, 59]. Currently, the functional domains within Hcp are not well characterised, so we could not address its function based on our bioinformatics analysis. Clearly, experimental demonstrations are necessary to verify whether UPEC3 is capable to form functional T6SS and its role in context of inflammatory cell death in macrophages.

We have generate several UPEC3 mutants in this study and the mutants were verified by colony PCR, whole genome sequencing and Western blot. However, large DNA fragments were missing in the genome of $\Delta cnf1/\Delta hlyA$ double mutant, which we believe technical issues could have affected whole genome sequencing. Therefore, repeated whole genome sequencing is necessary to pinpoint whether the bacterial genome of $\Delta cnf1/\Delta hlyA$ double mutant was repaired as expected. Moreover $\Delta cnf1/\Delta tcpC$ double mutant should also be sequenced in the future to ensure target genes were deleted.

Consistent with previous publication [62], our data suggest TcpC binds to NLRP3 and caspase-1. Unexpectedly, the mRNA levels of cytokines showed a modest reduction in $\Delta tcpC$ mutant stimulated cells relatively to UPEC3 wild type, which contradicts previous study [61]. However, we acknowledge that experimental repeats are necessary to increase the confidence of our observations. Moreover, establishing *hlyA* and *tcpC* double knockout mutants and stimulating THP-1 cells with this mutant, may unravel the fact that HlyA could possibly mask over the effect of *tcpC* deletion. Furthermore, we also intrigued by examining how $\Delta ompT$ and $\Delta cnf1/\Delta tcpC$ mutants stimulated cells respond in the future.

Deletion of *hlyA* indeed increased expression levels of pro-inflammatory cytokines which can be interpreted by prevention of NF- κ B p65 degradation. However, rescuing NF- κ B p65 from

proteolysis does not explain the observation of increased IFN β mRNA levels in $\Delta hlyA$ and $\Delta cnf1/\Delta hlyA$ stimulated THP-1 cells. Future investigations of protein expression levels in TRIF-dependent signalling pathway may provide new insights into the relationship between HlyA deficient bacterial stimulation and expression level of IFN β in THP-1 cells. Indeed, our pilot study of structural differences between HlyA^{CFT073} and HlyA^{UPEC3} was only based on bioinformatics analysis, which does not provide great certainty of the HlyA structure compared with x-ray crystallography. Unfortunately, we were not able to investigate the haemolytic activity of HlyA^{CFT073} and HlyA^{UPEC3} due to time restriction. We believe testing the haemolytic activity of HlyA^{CFT073} and HlyA^{UPEC3} in the future can provide answers whether structural differences may affect the biological functions of HlyA. Nevertheless, whole blood models or animal models are necessary to address whether the systemic response differs upon stimulation with UPEC3 wild type versus $\Delta hlyA$ mutant.

Previously, our group has shown that FIP2 stabilises Rac1, which is important for *E. coli* phagocytosis [25]. Indeed, Rac1 levels correlated with FIP2 protein levels in the present study. However, unpublished demonstration from our group has shown that fewer UPEC3 were phagocytosed by human macrophages relatively to the avirulent variant DH5 α . The fact that UPEC3 encodes two important proteins involved in group 2 capsule biosynthesis, led us speculate whether UPEC3 synthesises this capsule to prevent phagocytosis by THP-1 cells. Currently, other essential genes involved in group 2 capsule biosynthesis have not been annotated in UPEC3. Further bioinformatics analysis can be expected to address whether UPEC3 has the potential of synthesising group 2 capsule to avoid being phagocytosed.

Nevertheless, THP-1 cells that were stimulated with nigericin, UPEC3 wild type, $\Delta cnf1$ and $\Delta tcpC$ upregulated p-MLKL expression, but we cannot conclude whether the detected p-MLKL resided in cytosol or in the plasma membrane. As shown in recent study, p-MLKL trafficking and accumulation in plasma membrane are two important check points for executing necroptosis [108]. Moreover, ESCRT-III machinery could also have been activated, which can shred out p-MLKL. Thus, further investigations of necroptosis kinetics in THP-1 cells upon bacterial stimulation are required. Furthermore, it would be interesting to examine whether FIP2 suppresses the necroptotic signalling pathway over time, given that FIP2 silencing showed increased levels of p-MLKL after 2 h of stimulation.

7 Conclusion

UPEC exploits various virulence factors to counteract the host's immune system and activate inflammatory cell death. Upon bacterial stimulation, FIP2 also plays a central role in inflammasome activation in human macrophages. Like other types of sepsis, urosepsis shows high mortality rate, yet there are no available therapies for treating the patients. Systemic inflammation, immunosuppression and imbalanced homeostasis are critical factors that are associated with sepsis pathogenesis. However, the underlying mechanisms that drive sepsis pathophysiology remain elusive. Therefore, it is important to continue expanding our knowledge of UPEC virulence and how it interacts with infected cells. In light of FIP2 is essential in inflammasome activation, further research may support FIP2 targeted treatment to suppress overactive inflammatory response in urosepsis patients.

References

- [1] Judith Owen. *Kuby immunology*. Freeman, New York, 7th edition, 2013. ISBN 9781464137846.
- [2] Christina Nedeva, Joseph Menassa, and Hamsa Puthalakath. Sepsis: inflammation is a necessary evil. *Frontiers in cell and developmental biology*, 7:108, 2019.
- [3] Hallie C Prescott and Derek C Angus. Enhancing recovery from sepsis: a review. *Jama*, 319(1):62–75, 2018.
- [4] Tom van der Poll, Frank L van de Veerdonk, Brendon P Scicluna, and Mihai G Netea. The immunopathology of sepsis and potential therapeutic targets. *Nature Reviews Immunology*, 17(7):407, 2017.
- [5] Richard S Hotchkiss, Lyle L Moldawer, Steven M Opal, Konrad Reinhart, Isaiah R Turnbull, and Jean-Louis Vincent. Sepsis and septic shock. *Nature reviews Disease primers*, 2(1):1–21, 2016.
- [6] Tim Hunt Bruce Alberts, John H. Wilson. *Molecular biology of the cell*. Garland Science, New York, 6th edition, 2015. ISBN 9780815344322.
- [7] Stephen J Gaudino and Pawan Kumar. Cross-talk between antigen presenting cells and t cells impacts intestinal homeostasis, bacterial infections, and tumorigenesis. *Frontiers in immunology*, 10:360, 2019.
- [8] DAVID L Dunn, Roderick A Barke, Napoleon B Knight, Edward W Humphrey, and Richard L Simmons. Role of resident macrophages, peripheral neutrophils, and translymphatic absorption in bacterial clearance from the peritoneal cavity. *Infection and immunity*, 49(2):257–264, 1985.
- [9] Shane Crotty. A brief history of t cell help to b cells. *Nature Reviews Immunology*, 15(3):185–189, 2015.
- [10] Roza I Nurieva, Yeonseok Chung, Gustavo J Martinez, Xuexian O Yang, Shinya Tanaka, Tatyana D Matskevitch, Yi-Hong Wang, and Chen Dong. Bcl6 mediates the development of t follicular helper cells. *Science*, 325(5943):1001–1005, 2009.
- [11] Anna-Karin E Palm and Carole Henry. Remembrance of things past: long-term b cell memory after infection and vaccination. *Frontiers in immunology*, 10:1787, 2019.
- [12] Kyla D Omilusik and Ananda W Goldrath. The origins of memory t cells, 2017.
- [13] Osamu Takeuchi and Shizuo Akira. Pattern recognition receptors and inflammation. *Cell*, 140(6):805–820, 2010.

-
- [14] Gustavo P Amarante-Mendes, Sandy Adjemian, Laura Migliari Branco, Larissa C Zanetti, Ricardo Weinlich, and Karina R Bortoluci. Pattern recognition receptors and the host cell death molecular machinery. *Frontiers in immunology*, 9:2379, 2018.
- [15] Istvan Botos, David M Segal, and David R Davies. The structural biology of toll-like receptors. *Structure*, 19(4):447–459, 2011.
- [16] Nicholas J Gay, Martyn F Symmons, Monique Gangloff, and Clare E Bryant. Assembly and localization of toll-like receptor signalling complexes. *Nature Reviews Immunology*, 14(8):546–558, 2014.
- [17] Maximiliano Javier Jiménez-Dalmaroni, M Eric Gerswhin, and Iannis E Adamopoulos. The critical role of toll-like receptors—from microbial recognition to autoimmunity: a comprehensive review. *Autoimmunity reviews*, 15(1):1–8, 2016.
- [18] Suprabhat Mukherjee, Sahel Huda, and Santi P Sinha Babu. Toll-like receptor polymorphism in host immune response to infectious diseases: A review. *Scandinavian journal of immunology*, 90(1):e12771, 2019.
- [19] Luke AJ O’Neill and Andrew G Bowie. The family of five: Tir-domain-containing adaptors in toll-like receptor signalling. *Nature Reviews Immunology*, 7(5):353–364, 2007.
- [20] Taro Kawai and Shizuo Akira. Tlr signaling. In *Seminars in immunology*, volume 19, pages 24–32. Elsevier, 2007.
- [21] Yoshinori Nagai and Kiyoshi Takatsu. Chapter 26 - role of the immune system in obesity-associated inflammation and insulin resistance. In Ronald Ross Watson, editor, *Nutrition in the Prevention and Treatment of Abdominal Obesity*, pages 281–293. Academic Press, San Diego, 2014. ISBN 978-0-12-407869-7. doi: <https://doi.org/10.1016/B978-0-12-407869-7.00026-X>. URL <https://www.sciencedirect.com/science/article/pii/B978012407869700026X>.
- [22] Chen-Ming Fan and Tom Maniatis. Generation of p50 subunit of nf- κ b by processing of p105 through an atp-dependent pathway. *Nature*, 354(6352):395–398, 1991.
- [23] Paul P Tak, Gary S Firestein, et al. Nf- κ b: a key role in inflammatory diseases. *The Journal of clinical investigation*, 107(1):7–11, 2001.
- [24] Ting Liu, Lingyun Zhang, Donghyun Joo, and Shao-Cong Sun. Nf- κ b signaling in inflammation. *Signal transduction and targeted therapy*, 2(1):1–9, 2017.
- [25] Astrid Skjesol, Mariia Yurchenko, Korbinian Bösl, Caroline Gravastrand, Kaja Elisabeth Nilsen, Lene Melsæther Grøvdal, Federica Agliano, Francesco Patane, Germana

-
- Lentini, Hera Kim, et al. The tlr4 adaptor tram controls the phagocytosis of gram-negative bacteria by interacting with the rab11-family interacting protein 2. *PLoS pathogens*, 15(3):e1007684, 2019.
- [26] Amber L Schuh and Anjon Audhya. The escrt machinery: from the plasma membrane to endosomes and back again. *Critical reviews in biochemistry and molecular biology*, 49(3):242–261, 2014.
- [27] Saroja Weeratunga, Blessy Paul, and Brett M Collins. Recognising the signals for endosomal trafficking. *Current opinion in cell biology*, 65:17–27, 2020.
- [28] Sarah R Elkin, Ashley M Lakoduk, and Sandra L Schmid. Endocytic pathways and endosomal trafficking: a primer. *Wiener Medizinische Wochenschrift*, 166(7):196–204, 2016.
- [29] Ferdi Ridvan Kiral, Friederike Elisabeth Kohrs, Eugene Jennifer Jin, and Peter Robin Hiesinger. Rab gtpases and membrane trafficking in neurodegeneration. *Current Biology*, 28(8):R471–R486, 2018.
- [30] Carlos Rosales and Eileen Uribe-Querol. Phagocytosis: a fundamental process in immunity. *BioMed research international*, 2017, 2017.
- [31] Harald Husebye, Marie Hjelmseth Aune, Jørgen Stenvik, Eivind Samstad, Frode Skjeldal, Øyvind Halaas, Nadra J Nilsen, Harald Stenmark, Eicke Latz, Egil Lien, et al. The rab11a gtpase controls toll-like receptor 4-induced activation of interferon regulatory factor-3 on phagosomes. *Immunity*, 33(4):583–596, 2010.
- [32] Chadwick M Hales, Richard Griner, Karen C Hobdy-Henderson, Matthew C Dorn, David Hardy, Ravindra Kumar, Jennifer Navarre, Edward KL Chan, Lynne A Lapierre, and James R Goldenring. Identification and characterization of a family of rab11-interacting proteins. *Journal of Biological Chemistry*, 276(42):39067–39075, 2001.
- [33] Huan-Hong Ji, Lin-Lin Yao, Chang Liu, and Xiang-dong Li. Regulation of myosin-5b by rab11a and the rab11 family interacting protein 2. *Bioscience reports*, 39(1), 2019.
- [34] Thomas C. Südhof and Josep Rizo. Chapter 139 - c2-domains in ca²⁺-signaling. In Ralph A. Bradshaw and Edward A. Dennis, editors, *Handbook of Cell Signaling*, pages 95–100. Academic Press, Burlington, 2003. ISBN 978-0-12-124546-7. doi: <https://doi.org/10.1016/B978-012124546-7/50500-3>. URL <https://www.sciencedirect.com/science/article/pii/B9780121245467505003>.
- [35] Petr Broz and Vishva M Dixit. Inflammasomes: mechanism of assembly, regulation and signalling. *Nature Reviews Immunology*, 16(7):407–420, 2016.
-

-
- [36] Sean P Cullen, Conor J Kearney, Danielle M Clancy, and Seamus J Martin. Diverse activators of the nlrp3 inflammasome promote il-1 β secretion by triggering necrosis. *Cell reports*, 11(10):1535–1548, 2015.
- [37] Karen V Swanson, Meng Deng, and Jenny P-Y Ting. The nlrp3 inflammasome: molecular activation and regulation to therapeutics. *Nature Reviews Immunology*, 19(8):477–489, 2019.
- [38] Nan Song and Tao Li. Regulation of nlrp3 inflammasome by phosphorylation. *Frontiers in immunology*, 9:2305, 2018.
- [39] Zhirong Zhang, Gergö Meszaros, Wan-ting He, Yanfang Xu, Helena de Fatima Magliarelli, Laurent Mailly, Michael Mihlan, Yansheng Liu, Marta Puig Gámez, Alexander Goginashvili, et al. Protein kinase d at the golgi controls nlrp3 inflammasome activation. *Journal of Experimental Medicine*, 214(9):2671–2693, 2017.
- [40] Jueqi Chen and Zhijian J Chen. Ptdins4p on dispersed trans-golgi network mediates nlrp3 inflammasome activation. *Nature*, 564(7734):71–76, 2018.
- [41] Venkat Giri Magupalli, Roberto Negro, Yuzi Tian, Arthur V Hauenstein, Giuseppe Di Caprio, Wesley Skillern, Qiufang Deng, Pontus Orning, Hasan B Alam, Zoltan Maliga, et al. Hdac6 mediates an aggresome-like mechanism for nlrp3 and pyrin inflammasome activation. *Science*, 369(6510), 2020.
- [42] Harald Husebye, Caroline Gravastrand, Astrid Skjesol, Mariia Yurchenko, Aleksandra Jakovljevic, Jan Egil Afset, and Terje Espevik. The rab11-family interacting protein 2 is an important regulator of inflammatory cell death in human macrophages. Unpublished.
- [43] Yogesh K Dhuriya and Divakar Sharma. Necroptosis: a regulated inflammatory mode of cell death. *Journal of neuroinflammation*, 15(1):1–9, 2018.
- [44] Peter Vandenabeele, Lorenzo Galluzzi, Tom Vanden Berghe, and Guido Kroemer. Molecular mechanisms of necroptosis: an ordered cellular explosion. *Nature reviews Molecular cell biology*, 11(10):700–714, 2010.
- [45] Pontus Orning and Egil Lien. Multiple roles of caspase-8 in cell death, inflammation, and innate immunity. *Journal of Leukocyte Biology*, 109(1):121–141, 2021.
- [46] Blake Bertani and Natividad Ruiz. Function and biogenesis of lipopolysaccharides. *EcoSal Plus*, 8(1), 2018.
- [47] Gudula Schmidt, Jörg Selzer, Maria Lerm, and Klaus Aktories. The rho-deamidating cytotoxic necrotizing factor 1 from *Escherichia coli* possesses transglutaminase activity cysteine 866 and histidine 881 are essential for enzyme activity. *Journal of Biological Chemistry*, 273(22):13669–13674, 1998.
-

-
- [48] Anne Doye, Amel Mettouchi, Guillaume Bossis, René Clément, Caroline Buisson-Touati, Gilles Flatau, Laurent Gagnoux, Marc Piechaczyk, Patrice Boquet, and Emmanuel Lemichez. Cnf1 exploits the ubiquitin-proteasome machinery to restrict rho gtpase activation for bacterial host cell invasion. *Cell*, 111(4):553–564, 2002.
- [49] Emmanuel Lemichez, Gilles Flatau, Marc Bruzzone, Patrice Boquet, and Michel Gauthier. Molecular localization of the escherichia coli cytotoxic necrotizing factor cnf1 cell-binding and catalytic domains. *Molecular microbiology*, 24(5):1061–1070, 1997.
- [50] Silvia Pei, Anne Doye, and Patrice Boquet. Mutation of specific acidic residues of the cnf1 t domain into lysine alters cell membrane translocation of the toxin. *Molecular microbiology*, 41(6):1237–1247, 2001.
- [51] Océane Dufies, Anne Doye, Johan Courjon, Cédric Torre, Gregory Michel, Celine Loubatier, Arnaud Jacquél, Paul Chaintreuil, Alissa Majoor, Rodolphe R Guinamard, et al. Escherichia coli rho gtpase-activating toxin cnf1 mediates nlrp3 inflammasome activation via p21-activated kinases-1/2 during bacteraemia in mice. *Nature Microbiology*, 6(3):401–412, 2021.
- [52] Luce Landraud, Maryse Gibert, Michel R Popoff, Patrice Boquet, and Michel Gauthier. Expression of cnf1 by escherichia coli j96 involves a large upstream dna region including the hlycabd operon, and is regulated by the rfah protein. *Molecular microbiology*, 47(6):1653–1667, 2003.
- [53] Alexandre Chenal, AC Sotomayor-Perez, and Daniel Ladant. *The Comprehensive Sourcebook of Bacterial Protein Toxins*. Elsevier Amsterdam, 4th edition, 2015.
- [54] Albrecht Ludwig, Angela Schmid, Roland Benz, and Werner Goebel. Mutations affecting pore formation by haemolysin from escherichia coli. *Molecular and General Genetics MGG*, 226(1):198–208, 1991.
- [55] Mamady Diabate, Patrick Munro, Elsa Garcia, Arnaud Jacquél, Gregory Michel, Sandrine Obba, Diogo Goncalves, Carmelo Luci, Sandrine Marchetti, Dieter Demon, et al. Escherichia coli α -hemolysin counteracts the anti-virulence innate immune response triggered by the rho gtpase activating toxin cnf1 during bacteremia. *PLoS Pathog*, 11(3):e1004732, 2015.
- [56] Brian T Ho, Tao G Dong, and John J Mekalanos. A view to a kill: the bacterial type vi secretion system. *Cell host & microbe*, 15(1):9–21, 2014.
- [57] Amy T Ma, Steven McAuley, Stefan Pukatzki, and John J Mekalanos. Translocation of a vibrio cholerae type vi secretion effector requires bacterial endocytosis by host cells. *Cell host & microbe*, 5(3):234–243, 2009.

-
- [58] Giovanni Suarez, Johanna C Sierra, Michelle L Kirtley, and Ashok K Chopra. Role of hcp, a type 6 secretion system effector, of aeromonas hydrophila in modulating activation of host immune cells. *Microbiology*, 156(Pt 12):3678, 2010.
- [59] Yan Zhou, Jing Tao, Hao Yu, Jinjing Ni, Lingbing Zeng, Qihui Teng, Kwang Sik Kim, Guo-Ping Zhao, Xiaokui Guo, and Yufeng Yao. Hcp family proteins secreted via the type vi secretion system coordinately regulate escherichia coli k1 interaction with human brain microvascular endothelial cells. *Infection and immunity*, 80(3):1243–1251, 2012.
- [60] Mark A Schell, Ricky L Ulrich, Wilson J Ribot, Ernst E Brueggemann, Harry B Hines, Dan Chen, Lyla Lipscomb, H Stanley Kim, Jan Mrázek, William C Nierman, et al. Type vi secretion is a major virulence determinant in burkholderia mallei. *Molecular microbiology*, 64(6):1466–1485, 2007.
- [61] Manisha Yadav, Jingyao Zhang, Hans Fischer, Wen Huang, Nataliya Lutay, Christine Cirl, Josephine Lum, Thomas Miethke, and Catharina Svanborg. Inhibition of tir domain signaling by tcpc: Myd88-dependent and independent effects on escherichia coli virulence. *PLoS Pathog*, 6(9):e1001120, 2010.
- [62] Anna Waldhuber, Manoj Puthia, Andreas Wieser, Christine Cirl, Susanne Dürr, Silke Neumann-Pfeifer, Simone Albrecht, Franziska Römmler, Tina Müller, Yunji Zheng, et al. Uropathogenic escherichia coli strain cft073 disrupts nlrp3 inflammasome activation. *The Journal of clinical investigation*, 126(7):2425–2436, 2016.
- [63] Arif Tasleem Jan. Outer membrane vesicles (omvs) of gram-negative bacteria: a perspective update. *Frontiers in microbiology*, 8:1053, 2017.
- [64] Veena Premjani, Derek Tilley, Samantha Gruenheid, Hervé Le Moual, and John A Samis. Enterohemorrhagic escherichia coli ompt regulates outer membrane vesicle biogenesis. *FEMS microbiology letters*, 355(2):185–192, 2014.
- [65] Carmen Schwechheimer and Meta J Kuehn. Synthetic effect between envelope stress and lack of outer membrane vesicle production in escherichia coli. *Journal of bacteriology*, 195(18):4161–4173, 2013.
- [66] Pascal Belin and Paul Louis Boquet. The escherichia coli dsb gene is partly transcribed from the promoter of a weakly expressed upstream gene. *Microbiology*, 140(12):3337–3348, 1994.
- [67] Jon M Davis, Humberto M Carvalho, Susan B Rasmussen, and Alison D O’Brien. Cytotoxic necrotizing factor type 1 delivered by outer membrane vesicles of uropathogenic escherichia coli attenuates polymorphonuclear leukocyte antimicrobial activity and chemotaxis. *Infection and immunity*, 74(8):4401–4408, 2006.
-

-
- [68] Shouwen Chen, Dahai Yang, Ying Wen, Zhiwei Jiang, Lingzhi Zhang, Jiatiao Jiang, Yaozhen Chen, Tianjian Hu, Qiyao Wang, Yuanxing Zhang, et al. Dysregulated hemolysin liberates bacterial outer membrane vesicles for cytosolic lipopolysaccharide sensing. *PLoS pathogens*, 14(8):e1007240, 2018.
- [69] Sivapriya Kailasan Vanaja, Ashley J Russo, Bharat Behl, Ishita Banerjee, Maya Yankova, Sachin D Deshmukh, and Vijay AK Rathinam. Bacterial outer membrane vesicles mediate cytosolic localization of lps and caspase-11 activation. *Cell*, 165(5):1106–1119, 2016.
- [70] Jennifer A Doudna and Emmanuelle Charpentier. The new frontier of genome engineering with crispr-cas9. *Science*, 346(6213), 2014.
- [71] Dongdong Zhao, Shenli Yuan, Bin Xiong, Hongnian Sun, Lijun Ye, Jing Li, Xueli Zhang, and Changhao Bi. Development of a fast and easy method for escherichia coli genome editing with crispr/cas9. *Microbial cell factories*, 15(1):1–9, 2016.
- [72] Marius Rütering, Brady F Cress, Martin Schilling, Broder Rühmann, Mattheos AG Koffas, Volker Sieber, and Jochen Schmid. Tailor-made exopolysaccharides—crispr-cas9 mediated genome editing in paenibacillus polymyxa. *Synthetic Biology*, 2(1):ysx007, 2017.
- [73] He Huang, Changsheng Chai, Ning Li, Pete Rowe, Nigel P Minton, Sheng Yang, Weihong Jiang, and Yang Gu. Crispr/cas9-based efficient genome editing in clostridium ljungdahlii, an autotrophic gas-fermenting bacterium. *ACS synthetic biology*, 5(12):1355–1361, 2016.
- [74] Fengrui Ren, Chong Ren, Zhan Zhang, Wei Duan, David Lecourieux, Shaohua Li, and Zhenchang Liang. Efficiency optimization of crispr/cas9-mediated targeted mutagenesis in grape. *Frontiers in plant science*, 10:612, 2019.
- [75] Gernot Bonkat, Tomasso Cai, Rajan Veeratterapillay, Franck Bruyere, Riccardo Bartoletti, Adrian Pilatz, Béla Köves, Suzanne E Geerlings, Benjamin Pradere, Robert Pickard, et al. Management of urosepsis in 2018. *European urology focus*, 5(1):5–9, 2019.
- [76] FME Wagenlehner, A Pilatz, KG Naber, and W Weidner. Therapeutic challenges of urosepsis. *European Journal of Clinical Investigation*, 38:45–49, 2008.
- [77] Om Prakash Kalra and Alpana Raizada. Approach to a patient with urosepsis. *Journal of Global Infectious Diseases*, 1(1):57, 2009.
- [78] Stephen F Altschul, Warren Gish, Webb Miller, Eugene W Myers, and David J Lipman. Basic local alignment search tool. *Journal of molecular biology*, 215(3):403–410, 1990.
-

-
- [79] Aron Marchler-Bauer and Stephen H Bryant. Cd-search: protein domain annotations on the fly. *Nucleic acids research*, 32(suppl_2):W327–W331, 2004.
- [80] Lawrence A Kelley, Stefans Mezulis, Christopher M Yates, Mark N Wass, and Michael JE Sternberg. The phyre2 web portal for protein modeling, prediction and analysis. *Nature protocols*, 10(6):845–858, 2015.
- [81] Paulina Balbás, Xavier Soberón, Enrique Merino, Mario Zurita, Hilda Lomeli, Fernando Valle, Noemi Flores, and Francisco Bolivar. Plasmid vector pbr322 and its special-purpose derivatives — a review. *Gene*, 50(1):3–40, 1986. ISSN 0378-1119. doi: [https://doi.org/10.1016/0378-1119\(86\)90307-0](https://doi.org/10.1016/0378-1119(86)90307-0). URL <https://www.sciencedirect.com/science/article/pii/0378111986903070>.
- [82] H.D. Jones. Genetic modification — transformation, general principles. In Brian Thomas, editor, *Encyclopedia of Applied Plant Sciences*, pages 377–382. Elsevier, Oxford, 2003. ISBN 978-0-12-227050-5. doi: <https://doi.org/10.1016/B012-227050-9/00197-6>. URL <https://www.sciencedirect.com/science/article/pii/B0122270509001976>.
- [83] Haruka Hasegawa, Erika Suzuki, and Sumio Maeda. Horizontal plasmid transfer by transformation in escherichia coli: Environmental factors and possible mechanisms. *Frontiers in Microbiology*, 9:2365, 2018. ISSN 1664-302X. doi: 10.3389/fmicb.2018.02365. URL <https://www.frontiersin.org/article/10.3389/fmicb.2018.02365>.
- [84] Alexandrine Froger and James E Hall. Transformation of plasmid dna into e. coli using the heat shock method. *Journal of visualized experiments: JoVE*, (6), 2007.
- [85] Claire A Woodall. Electroporation of e. coli. In *E. coli Plasmid Vectors*, pages 55–59. Springer, 2003.
- [86] Lilit Garibyan and Nidhi Avashia. Research techniques made simple: polymerase chain reaction (pcr). *The Journal of investigative dermatology*, 133(3):e6, 2013.
- [87] Richard J Roberts. How restriction enzymes became the workhorses of molecular biology. *Proceedings of the National Academy of Sciences*, 102(17):5905–5908, 2005.
- [88] Wei Xu, Xuezhen Jiang, and Linfeng Huang. Rna interference technology. *Comprehensive Biotechnology*, page 560, 2019.
- [89] Philip L Felgner, Thomas R Gadek, Marilyn Holm, Richard Roman, Hardy W Chan, Michael Wenz, Jeffrey P Northrop, Gordon M Ringold, and Mark Danielsen. Lipofec-tion: a highly efficient, lipid-mediated dna-transfection procedure. *Proceedings of the National Academy of Sciences*, 84(21):7413–7417, 1987.

-
- [90] Priti Kumar, Arvindhan Nagarajan, and Pradeep D Uchil. Analysis of cell viability by the lactate dehydrogenase assay. *Cold Spring Harbor Protocols*, 2018(6):pdb-prot095497, 2018.
- [91] C A Heid, J Stevens, K J Livak, and P M Williams. Real time quantitative pcr. *Genome research*, 6(10):986–994, 1996. ISSN 1088-9051.
- [92] John W. Pelley. 18 - recombinant dna and biotechnology. In John W. Pelley, editor, *Elsevier's Integrated Review Biochemistry*, pages 161–169. W.B. Saunders, Philadelphia, 2nd edition, 2012. ISBN 978-0-323-07446-9. doi: <https://doi.org/10.1016/B978-0-323-07446-9.00018-0>. URL <https://www.sciencedirect.com/science/article/pii/B9780323074469000180>.
- [93] Ana M Azevedo, Veronica C Martins, Duarte MF Prazeres, Vojislav Vojinovic, Joaquim MS Cabral, and Luis P Fonseca. Horseradish peroxidase: a valuable tool in biotechnology. *Biotechnology annual review*, 9(3):1387–2656, 2003.
- [94] Kanna Nagamatsu, Thomas J Hannan, Randi L Guest, Maria Kostakioti, Maria Hadjifrangiskou, Jana Binkley, Karen Dodson, Tracy L Raivio, and Scott J Hultgren. Dysregulation of escherichia coli α -hemolysin expression alters the course of acute and persistent urinary tract infection. *Proceedings of the National Academy of Sciences*, 112(8):E871–E880, 2015.
- [95] Bijaya K Dhakal and Matthew A Mulvey. The upec pore-forming toxin α -hemolysin triggers proteolysis of host proteins to disrupt cell adhesion, inflammatory, and survival pathways. *Cell host & microbe*, 11(1):58–69, 2012.
- [96] Christine Cirl, Andreas Wieser, Manisha Yadav, Susanne Duerr, Sören Schubert, Hans Fischer, Dominik Stappert, Nina Wantia, Nuria Rodriguez, Hermann Wagner, et al. Subversion of toll-like receptor signaling by a unique family of bacterial toll/interleukin-1 receptor domain-containing proteins. *Nature medicine*, 14(4):399–406, 2008.
- [97] Michael Y Galperin, Yuri I Wolf, Kira S Makarova, Roberto Vera Alvarez, David Landsman, and Eugene V Koonin. COG database update: focus on microbial diversity, model organisms, and widespread pathogens. *Nucleic Acids Research*, 49(D1):D274–D281, 11 2020. ISSN 0305-1048. doi: 10.1093/nar/gkaa1018. URL <https://doi.org/10.1093/nar/gkaa1018>.
- [98] David R McIlwain, Thorsten Berger, and Tak W Mak. Caspase functions in cell death and disease. *Cold Spring Harbor perspectives in biology*, 5(4):a008656, 2013.
- [99] Sandrine M Soh, Hyochan Jang, and Robert J Mitchell. Loss of the lipopolysaccharide (lps) inner core increases the electrocompetence of escherichia coli. *Applied Microbiology and Biotechnology*, 104(17):7427–7435, 2020.
-

-
- [100] Vicky Chang, Ling-Yi Chen, Aileen Wang, and Xiao Yuan. The effect of lipopolysaccharide core structure defects on transformation efficiency in isogenic escherichia coli bw25113 rfag, rfap, and rfac mutants. *J. Exp. Microbiol. Immunol*, 14:101–107, 2010.
- [101] Roland Stenutz, Andrej Weintraub, and Göran Widmalm. The structures of escherichia coli o-polysaccharide antigens. *FEMS microbiology reviews*, 30(3):382–403, 2006.
- [102] Zhijun Wang, Li Xiang, Junjie Shao, Alicja Wegrzyn, and Grzegorz Wegrzyn. Effects of the presence of cole1 plasmid dna in escherichia coli on the host cell metabolism. *Microbial Cell Factories*, 5(1):1–18, 2006.
- [103] *Brock biology of microorganisms*. Pearson, Harlow, 14th ed., global ed. edition, 2015. ISBN 9781292018317.
- [104] Juan C Diaz Ricci and Marriá Eugenia Hernández. Plasmid effects on escherichia coli metabolism. *Critical reviews in biotechnology*, 20(2):79–108, 2000.
- [105] William E Bentley, Noushin Mirjalili, Dana C Andersen, Robert H Davis, and Dhinakar S Kompala. Plasmid-encoded protein: the principal factor in the “metabolic burden” associated with recombinant bacteria. *Biotechnology and bioengineering*, 35(7):668–681, 1990.
- [106] Marcus A Horwitz, Samuel C Silverstein, et al. Influence of the escherichia coli capsule on complement fixation and on phagocytosis and killing by human phagocytes. *The Journal of clinical investigation*, 65(1):82–94, 1980.
- [107] Brady F Cress, Jacob A Englaender, Wenqin He, Dennis Kasper, Robert J Linhardt, and Mattheos AG Koffas. Masquerading microbial pathogens: capsular polysaccharides mimic host-tissue molecules. *FEMS microbiology reviews*, 38(4):660–697, 2014.
- [108] Andre L Samson, Ying Zhang, Niall D Geoghegan, Xavier J Gavin, Katherine A Davies, Michael J Mlodzianoski, Lachlan W Whitehead, Daniel Frank, Sarah E Garnish, Cheree Fitzgibbon, et al. Mkl1 trafficking and accumulation at the plasma membrane control the kinetics and threshold for necroptosis. *Nature communications*, 11(1):1–17, 2020.
- [109] Eva Hadadi, Biyan Zhang, Kajus Baidžajevs, Nurhashikin Yusof, Kia Joo Puan, Siew Min Ong, Wei Hseun Yeap, Olaf Rotzschke, Endre Kiss-Toth, Heather Wilson, et al. Differential il-1 β secretion by monocyte subsets is regulated by hsp27 through modulating mrna stability. *Scientific reports*, 6(1):1–13, 2016.
- [110] Takato Takenouchi, Yoshifumi Iwamaru, Shuei Sugama, Mitsutoshi Tsukimoto, Masayo Fujita, Akio Sekigawa, Kazunari Sekiyama, Mitsuru Sato, Shuji Kojima, Bruno Conti, et al. The activation of p2x7 receptor induces cathepsin d-dependent production
-

-
- of a 20-kda form of il-1 β under acidic extracellular ph in lps-primed microglial cells. *Journal of neurochemistry*, 117(4):712–723, 2011.
- [111] Mabruka Alfaidi, Heather Wilson, Marc Daigneault, Amanda Burnett, Victoria Ridger, Janet Chamberlain, and Sheila Francis. Neutrophil elastase promotes interleukin-1 β secretion from human coronary endothelium. *Journal of Biological Chemistry*, 290(40): 24067–24078, 2015.
- [112] Roy A Black, Shirley R Kronheim, Michael Cantrell, Michael C Deeley, Carl J March, Kathryn S Prickett, Janis Wignall, Paul J Conlon, David Cosman, and Thomas P Hopp. Generation of biologically active interleukin-1 beta by proteolytic cleavage of the inactive precursor. *Journal of Biological Chemistry*, 263(19):9437–9442, 1988.
- [113] GP Ellis. The maillard reaction. In *Advances in carbohydrate chemistry*, volume 14, pages 63–134. Elsevier, 1959.
- [114] T.P Coultate. *Food : the chemistry of its components*. Royal Society of Chemistry, Cambridge, 6th edition, 2016. ISBN 9781849738804.

Appendix - Supplementary materials

A Materials

A.1 Kits and reagents

All kits, reagents, plasmids and primers used in this study are summarised in the tables below.

Table A.1: Reagents

Product	Distributor	Catalog number
A ⁺ serum	St. Olavs Hospital	
AllStars Negative Control siRNA	QIAGEN	SI03650318
Antarctic Phosphatase	New England BioLabs	M0289
β -mercaptoethanol	Sigma Aldrich	M6250
Bovine Serum Albumin (BSA)	Sigma-Aldrich	
BsaI-HFv2	New England BioLabs	R3733
Chloramphenicol	Sigma Aldrich	C3175
CutSmart Buffer	New England BioLabs	B7204
Dimethyl sulfoxide (DMSO)	Sigma Aldrich	D2660
Dithiothreitol (DTT)	PanReac AppliChem	A3668.0050
Fetal Bovine Serum (FBS)	Gibco	10270106
FIP2 siRNA oligo 5 (Hs_RAB11FIP2_5)	QIAGEN	
GelGreen Nucleic Acid Gel Stain	Biotium	41005
GelRed Nucleic Acid Gel Stain	Biotium	41003
GeneRuler 1 kb Plus DNA Ladder 6x Loading Dye	Thermo Scientific™	FERSM1331
Kanamycine	Sigma Aldrich	60615
KOD Hot Start Master Mix	Sigma-Aldrich	D85236
L-Glutamine	Sigma Aldrich	G7513
Lipofectamine RNAi Max	Invitrogen™	13778-150
Magic Mark	Invitrogen	LC5602
Nigericin	Invivogen	t1rl-nig
NLRP3 inhibitor MCC950	Invivogen	inh-mcc
NuPAGE™ LDS Sample Buffer (4×)	Invitrogen™	NP0007
NuPAGE™ MES SDS Running Buffer (20×)	Invitrogen™	NP0002
NuPAGE™ MOPS SDS Running Buffer (20×)	Invitrogen™	NP0001
OneTaq 2× Master Mix with Standard Buffer	New England BioLabs	M0482
Opti-MEM	Gibco	
Phosphate buffered saline (PBS) tablets	Oxoid	BR0014G
Phosphate buffered saline (PBS)	Sigma Aldrich	D8537
Phorbol 12-myristate 13-acetate (PMA)	Sigma Aldrich	P8139
Q5 Hot Start High-Fidelity 2× Master Mix	New England BioLabs	M0494
QIAzol Lysis Reagent	QIAGEN	79306
RNase-Free DNase Set	QIAGEN	79254
RPMI-1640	Gibco, Sigma	11875085, R8758
SeaKem LE Agarose	Lonza	50004
SeeBlue Plus 2 Prestained Standard	Invitrogen™	LC5925
SpeI-HF	New England BioLabs	R3133
SuperSignal™ West Femto Maximum Sensitivity Substrate	Thermo Scientific™	34096
T4 DNA Ligase and Reaction Buffer (10×)	New England BioLabs	M0202
T4 Polynucleotide Kinase and Reaction Buffer (10×)	New England BioLabs	M0201
Ultrapure LPS from <i>E.coli</i> K12	InvivogenT4 Polynucleotide Kinase	t1rl-eklps
XbaI	New England BioLabs	R0145

Table A.2: Kits

Products	Distributor	Catalog number
CyQUANT™ LDH Cytotoxicity Assay Kit	Invitrogen	C20300
DNeasy Blood Tissue Kits	QIAGEN	69504
Human IL-1 beta/IL-1F2 DuoSet ELISA	RD Systems	DY201
iBlot™ 2 Transfer Stack, nitrocellulose	Invitrogen	IB23001
Maxima First Strand cDNA Synthesis Kit for RT-qPCR	Thermo Scientific™	K1641
NuPAGE Novex 4-12% Bis Tris gels	Invitrogen™	WG1402A
QIAquick Gel Extraction Kit	QIAGEN	28704
PerfeCTa qPCR FastMix UNG	Quanta Biosciences	95076-250
PureYield™ Plasmid Miniprep System	Promega	A1223
RNeasy Kits	QIAGEN	74004

Table A.3: Primary antibodies

Antibody	Isotype	Distributor	Catalog number
Human caspase-1 (p20), Bally-1	Mouse	Adipogen	AG-20B-0048-C100
Caspase-3 (5A1E)	Rabbit	Cell Signal Technology	9664S
Caspase-8 (1C12)	Mouse	Cell Signal Technology	9746S
β -Tubulin	Rabbit	Abcam	Ab15568
Human IL-1 β / IL-1F2	Mouse	Biotechne RD systems	AF-201-NA
GSDMD (E8G3F)	Rabbit	Cell Signal Technology	97558
NF- κ B p65 (D14E12) XP	Rabbit	Cell Signal Technology	8242
NF- κ B p65 (L8F6)	Mouse	Cell Signal Technology	9656
anti-NLRP3 (Cryo-2)	Mouse	Adipogen	AG-20B-0014-C100
Rac1/2/3	Rabbit	Cell Signal Technology	2465S
Rab11/FIP2	Rabbit	Abcam	EPR12294-85, ab180504
CNF1 (NG8)	Mouse	Santa Cruz	sc-52655
<i>Escherichia coli</i> OmpT	Rabbit	MyBioSource	MBS7049919
Phospho-MLKL (Ser358) (D6H3V)	Rabbit	Cell Signal Technology	91689
Phospho-PAK1 (Ser199/204)/ PAK2 (Ser192/197)	Rabbit	Cell Signal Technology	2605

Table A.4: Secondary antibodies

Antibody	Distributor	Catalog number
Polyclonal Swine anti-rabbit immunoglobulins/HRP	Dako	P0399
Polyclonal Goat anti-Mouse immunoglobulins/HRP	Dako	P0447

Table A.5: TaqMan primers. All TaqMan primers were ordered from Thermo Fisher

TaqMan primers	Catalog number
TNF (Hs00174128_m1)	4331182
TBP (Hs00427620_m1)	4331182
Rab11FIP2 (Hs00208593_m1)	4331182
NLRP3 (Hs00918082_m1)	4331182
IL1 β (Hs01555410_m1)	4351370
IFN β (Hs01077958_s1)	4351368

Plasmids used in this study are summarised in [Table A.6](#). All of the listed primers in ([Table A.7](#)) were designed with the online software [Benchling](#) and ordered from Eurofins Genomics. The primers were used for cloning CRISPR-constructs which target the virulence genes *cnf1*, *dsbA*, *hlyA*, *ompT* and *tcpC* in a clinically isolated uropathogenic *Escherichia coli* strain 3 (UPEC3). Additional primers for sequencing the complete CRISPR-plasmids and screening for UPEC3 colonies with the deleted genes of interest are also provided in the same table.

Table A.6: Plasmids

Plasmid	Distributor	Catalog number
pCas9	Addgene	42876
pCRISPR	Addgene	42875

Table A.7: Designed primers and guide sequences for cloning CRISPR-constructs and sequence verification. All of the primers were designed in [Benchling](#) and ordered from Eurofins Genomics.

Name	Sequence (left to right: 5' – 3')	Note
cnf1_sgRNA_2.For	AAACGCACTTGAGGAAGTCCAGGAG	sgRNA
cnf1_sgRNA_2.Rev	AAAACCTCCTGGACTTCCTCAAGTGC	sgRNA
cnf1_sgRNA_1.For	AAAACCTCATTATTCCCTCCACGCGG	sgRNA
cnf1_sgRNA_1.Rev	AAAACCGCGTGGAGGAATAATGAG	sgRNA
cnf1_sgDNA_3.For	AAAACGCTCTTATCATAAGGCTGGG	sgRNA
cnf1_sgDNA_3.Rev	AAAACCCAGCCGTATGATAAGAGGC	sgRNA
cnf1_sgDNA_4.For	AAACTGAAGAAAAAATGCTCCCGTG	sgRNA
cnf1_sgDNA_4.Rev	AAAACACGGGAGCATTCTTTCTTCA	sgRNA
cnf_OE_FOR	CTTCACAGAGGAGTTAAAAATATTTTCGGGAAATTATTTATGGCC	homologous arms
cnf_DS_XbaI_REV	TTATTGCTTAGAGTAAAGCCAGTGATGACGA	homologous arms
cnf_OE_REV	GCCAATAAATAATTTCCCGAAAAATATTTTAACTCCTCTGTGAAGA	homologous arms
cnf_US_XbaI_FOR	TAGCTATCTAGAGAGGAAGAGGTAAGCTTCAG	homologous arms
dsbA_gRNA1.For	AAACGCCAGCAACTTGTTTTTCCAG	sgRNA
dsbA_gRNA1.Rev	AAAACCTGGAAAAACAAGTTGCTGGC	sgRNA
dsbA_gRNA2.For	AAACTTGCCTGGTATCCATACCCTGG	sgRNA
dsbA_gRNA2.Rev	AAAACACAGGGTATGGATACCAGCAA	sgRNA
dsbA_gRNA3.For	AAACATACCACGTCAACTTCATGGG	sgRNA
dsbA_gRNA3.Rev	AAAACCCATGAAGTTGACGTGGTAT	sgRNA
dsbA_gRNA4.For	AAACTAAAGGTGAAGAGTACGACGG	sgRNA
dsbA_gRNA4.Rev	AAAACCGTCTACTCTTCACTTTA	sgRNA
dsbA_US_XbaI_For	TTATATTCTAGAATCTCATTGACCCAGCAAG	homologous arms
dsbA_OE_Rev	GTAATTTACATTGAAGATCTACTCTCCGATTAATACA	homologous arms
dsbA_OE_For	ATCGGAGAGAGTAGATCTTCAATGTAATACATAAAGCCCG	homologous arms
dsbA_DS_XbaI_Rev	ATAATATCTAGAGCGGTTGTGTACAGTCATTAT	homologous arms
hlyA_sgDNA_1.For	AAACGGACAACCTGCAATAAAGAAGG	sgRNA
hlyA_sgDNA_1.Rev	AAAACCTTCTTTATTGCAAGTTGTCC	sgRNA
hlyA_sgDNA_2.For	AAACCTCGCTTAAAGGCAACGTC	sgRNA
hlyA_sgDNA_2.Rev	AAAACGGACGTTGCCTTTAAGCGAG	sgRNA
hlyA_sgDNA_3.For	AAACTGCATCAACTTATGGGAGCCG	sgRNA
hlyA_sgDNA_3.Rev	AAAACGGCTCCATAAGTTGATGCG	sgRNA
hlyA_sgDNA_4.For	AAAACCACTGGTAGGTGCTGTTACGG	sgRNA
hlyA_sgDNA_4.Rev	AAAACCGTAAACAGCACCTACCAGTG	sgRNA
hlyA_DS_XbaI_Rev	ATTATATCTAGACCACCACAACAGATAATGGC	homologous arms
hlyA_OE_FOR	GGTTAAGAGGTAATTAATATATTAATTTAAATGATAGCAATCTTACTG	homologous arms
hlyA_OE_Rev	GCTATCATTTAAATTAATATATTAATTTACCTCTTAACTGTTAATG	homologous arms
hlyA_US_XbaI_For	ATTAATTTCTAGAGCGTTATGAACTAAATGCAAG	homologous arms
ompT_gRNA1.For	AAACGTAGATATAGGAACACCTCG	sgRNA
ompT_gRNA1.Rev	AAAACGAGGTGGTTCCTATATCTAC	sgRNA
ompT_gRNA2.For	AAAACAAAAGAGCTGATCGCAATAGG	sgRNA
ompT_gRNA2.Rev	AAAACCTATTCGGATCAGCTCTTTT	sgRNA
ompT_gRNA3.For	AAAACATTAGTCTTGGAACTCTGAGG	sgRNA
ompT_gRNA3.Rev	AAAACCTCAGAGTTCCAAGACTAAT	sgRNA
ompT_gRNA4.For	AAAACGGTGGCACATTTAAATACAGG	sgRNA
ompT_gRNA4.Rev	AAAACCTGTATTTAAATGTGCCACC	sgRNA
ompT_DS_XbaI_For	TATAATTTCTAGACTCCGTATAGAGTTCCATCG	homologous arms
ompT_OE_Rev	TTGAATGGAGACCTTTTCAACGTTAAATAGATTTTCTCCC	homologous arms
ompT_OE_For	GAGAAAATCTATTTAAAGGTTGAAAAGGCTCCATTCATCG	homologous arms
ompT_US_XbaI_Rev	TATTATTTCTAGAGATTAAGGGAGCAACTTAGC	homologous arms
tcpC_sgDNA_1.For	AAACGATGAACAGACACTTGAAGTG	sgRNA
tcpC_sgDNA_1.Rev	AAAACACTTCAAGTCTCTGTTCATC	sgRNA
tcpC_sgDNA_2.For	AAAACCTATTTAACTCGTCTACCAGG	sgRNA
tcpC_sgDNA_2.Rev	AAAACCTGGTAGACGAGTTAAATAG	sgRNA
tcpC_sgDNA_3.For	AAACAGTAATGGCACATTTCCGCGG	sgRNA
tcpC_sgDNA_3.Rev	AAAACGCGCGAAATGTCCGATTACT	sgRNA
tcpC_sgDNA_4.For	AAACTCCACTCCCATCTATAATCGG	sgRNA
tcpC_sgDNA_4.Rev	AAAACCGATTATAGATGGGAGTGGG	sgRNA
tcpC_OE_For	GTTACATAGGCTCAAAATAGCAATAAATCATAAGTGCTTAATATC	homologous arms
tcpC_OE_Rev	TTAAGCACTTATGATTTATTGCTATTTTGAGCCTATGTAACATGC	homologous arms
tcpC_US_XbaI_For	TGTATCTCTAGATATCAGAAAGCAGACCAAGC	homologous arms
tcpC_DS_XbaI_Rev	ATGATCTCTAGAACCTGAAACCATAAAGCGA	homologous arms
cnf1_For	CTTAGTCCTCTGGAAGAGTCTGT	screening primers
cnf1_Rev	GGTAAGATCACTCAGCAACGTA	screening primers
dsbA_For	AACGATGAAGTTCCGGTCCG	screening primers
dsbA_Rev	ACTCGCTTTCACCAACCGGA	screening primers
hlyA_For	AACTCACAGGTCATCATTCCGGCA	screening primers
hlyA_Rev	TGCAGCATAACAAGGCAGCGAA	screening primers
ompT_For	TGATATTGAGTGGCCTGTGAAC	screening primers
ompT_Rev	CGTGGATAAACTGACCGTGAA	screening primers
tcpC_For	ATCTTGCTGAACCCGAAGAGATC	screening primers
tcpC_Rev	AATGTTGACTGCTTCATGGGGACTA	screening primers
sgDNA_Rev	CTGGCAATTCGACGCTAAGAAACC	sequencing primers
CRISPR_FF_Rev	TCGCCTTCTATCGCCTTCTTGACG	sequencing primers
CRISPR_FF_For	CTGCTGAAGCCAGTTACCTTCGGA	sequencing primers

A.2 Lysogeny broth (LB)

Lysogeny broth (LB) used to cultivate *E. coli* in this study was prepared according to [Table A.8](#). To make LB plates, agar was added to the medium. The medium was sterilised by autoclave. After the medium was cooled down, kanamycin or chloramphenicol were added to the medium to a final concentration of 50 µg/mL and 25 µg/mL, respectively.

Table A.8: Lysogeny broth (LB). To make LB plates agar was added to the medium.

Reagent	Amount	Distributor	Catalog number
NaCl	10 g	Merck	1064041000
Tryptone	10 g	Thermo Scientific™	LP0042
Yeast extract	5 g	Thermo Scientific™	LP0021
Deionised water	1 L		
Agar	7.5 g	Thermo Scientific™	LP0011B

A.3 Minimal A medium

To avoid glucosamine formation through Millard reaction due to the presence of glucose and tryptone [[113](#), [114](#)], minimal A medium was prepared in two parts ([Table A.9](#) and [Table A.10](#)) and were sterilised by autoclave. To complete the Minimal A medium, 10 mL of the glucose solution ([Table A.10](#)) was added to the Minimal A medium part 1 ([Table A.9](#)). The final glucose concentration in Minimal A medium is 2 mg/mL. Suitable antibiotics ([section A.2](#)) were also added to the medium for bacteria cultivation.

Table A.9: Minimal A medium - Part 1. Minimal medium was partially made by preparing the following ingredients.

Reagent	Amount	Final concentration	Distributor	Catalog number
K ₂ HPO ₄	5.23 g	60 mM	Sigma-Aldrich	60353
KH ₂ PO ₄	2.25 g	33 mM	Sigma-Aldrich	795488
(NH ₄) ₂ SO ₄	496 mg	7.5 mM	Merck	101217
Trisodium citrate	250 mg	1.7 mM	Merck	106448
MgSO ₄ x 7H ₂ O	123 mg	1 mM	Merck	105886
Tryptone	30 mg	60 µg/mL	Thermo Scientific™	LP0042
Deionised water	490 mL			

Table A.10: Minimal A medium - Part 2. Minimal medium was partially made by preparing the following ingredients.

Reagent	Amount	Final concentration	Distributor	Catalog number
D-(+)-Glucose	5 g	100 g/mL	Sigma-Aldrich	G7021
Deionised water	50 mL			

A.4 Electrophoresis buffer and gel preparation

All DNA were separated in 1 % agarose with $1 \times$ Tris-Acetate-EDTA (TAE) buffer, which was diluted from $50 \times$ TAE buffer (Table A.11). Briefly, $50 \times$ TAE buffer was prepared by dissolving Tris-base and disodium EDTA in 700 mL deionised water. Glacial acetic acid was added to the buffer solution before the volume was adjusted to 1 L. If necessary, the pH in $1 \times$ TAE was adjusted to 8.6. 1 % agarose was made by heating 1 g agarose per 100 mL of $1 \times$ TAE buffer. All DNA fragments were separated at 90 V for 45 min.

Table A.11: $50 \times$ TAE buffer for electrophoresis.

Reagent	Amount	Distributor	Catalog number
Tris-base	242 g	Sigma Aldrich	T1503
Disodium EDTA	18.61 g	Sigma Aldrich	E6758
Glacial Acetic Acid	57.1 mL	VWR Chemicals	20104.243
Deionised water	to 1 L		

A.5 Tris buffered saline-tween (TBS-T) buffer

$1 \times$ Tris buffered saline-tween (TBS-T) buffer used to wash membranes in Western blotting was prepared according to Table A.12.

Table A.12: $1 \times$ TBS-T buffer for membrane washing in Western blot.

Reagent	Volume [L]	Distributor	Catalog number
Tris-HCl (1 M, pH 7.5)	1	Sigma-Aldrich	T3253
NaCl (5 M)	0.6	Merck	1064041000
Tween (10 %)	0.2	Sigma-Aldrich	P1379
Dionised water	to 20		

B Methods

B.1 Database and software

Databases and software that were used in this study are summarised [Table B.13](#) and [Table B.14](#).

Table B.13: Summary of databases. Databases that were used in this study are given with their respective link.

Database	Link
NCBI COG	https://www.ncbi.nlm.nih.gov/research/cog
UniProt	https://www.uniprot.org/
Protein Data Bank	https://www.rcsb.org/
PATRIC	https://www.patricbrc.org/

Table B.14: summary of software. Software that were used in this study are summarised with their respective link.

Bioinformatic software	Link
Benchling	https://www.benchling.com/
BLASTP	https://blast.ncbi.nlm.nih.gov/Blast.cgi
BioRender	https://biorender.com/
Conserved Domain Search	https://www.ncbi.nlm.nih.gov/Structure/cdd/wrpsb.cgi
EMBOSS Transeq	https://www.ebi.ac.uk/Tools/st/emboss_transeq/
iC3D	https://www.ncbi.nlm.nih.gov/Structure/icn3d/full.html
LALIGN	https://embnet.vital-it.ch/software/LALIGN_form.html
ProtParam	https://web.expasy.org/protparam/
Phyre2	http://www.sbg.bio.ic.ac.uk/~phyre2/html/page.cgi?id=index
Softberry FGENSES	http://www.softberry.com/berry.phtml?topic=fgenesbgroup=programssubgroup=gfindb

B.2 Cloning CRISPR-Cas9 constructs

The single guide oligonucleotides (Table A.7) were annealed and phosphorylated after preparing the solution given in Table B.15 and incubated in a thermocycler (C1000 Touch™, Bio-Rad) at 37°C for 30 min, then heated to 95°C for 5 min and cooled down to 4°C with a ramp rate of 0.1°C/s.

Table B.15: Reagents for annealing and phosphorylating guide oligonucleotides. The guide oligonucleotides were designed in [Benchling](#) and named with the suffixes sgDNA_For and sgDNA_Rev.

Reagents	Volume [μ L]
sgDNA_For (100 μ M)	1
sgDNA_Rev (100 μ M)	1
T4 polynucleotide kinase	1
T4 polynucleotide kinase buffer (10 \times)	1
Deionised water	6

The annealed and phosphorylated single guide oligonucleotides were diluted hundred times before they were inserted into the vector, pCRISPR, via Golden Gate Assembly. The reagents in the solution of Golden Gate Assembly are listed in Table B.16 and the single guide oligonucleotides were cloned into the pCRISPR after incubating the solution in a thermocycler with the settings given in Table B.17.

Table B.16: Reagents for Golden Gate Assembly of guide oligonucleotides and pCRISPR. The final volume of the reaction mixture was 10 μ L. sgDNA: Single guide oligonucleotides. X: required volume of pCRISPR for obtaining 28 ng.

Reagents	Volume [μ L]
BsaI	0.75
T4 ligase	0.25
T4 ligase buffer (10 \times)	1
Diluted sgDNA	1
pCRISPR (28 ng)	X
Deionised water	7 - X

Table B.17: Thermocycler settings for Golden Gate Assembly of single guide oligonucleotides and pCRISPR.

Temperature [°C]	Time [min]	Cycle
37	5	20
20	5	
80	20	1
4	∞	

Golden Gate Assembly products (5 μ L) were used to transform chemical competent *E. coli* DH5 α as described in [section 3.4.1](#). To verify successful insertion of single guide oligonucleotides into the vector, colony PCR was performed by using the primer pairs sgDNA_Rev and CRISPR_FF_For ([Table B.18](#)) and the settings given in [Table B.19](#). Alternatively, isolated plasmids from overnight cultures were digested with *Bsa*I and *Spe*I ([Table B.20](#)) and compared with the expected sizes of restricted plasmids after electrophoresis. Digested plasmids with correct sizes, were further dephosphorylated with Antarctic Phosphatase (1 μ L) at 37°C for 1 h.

Table B.18: Composition of colony PCR reagents Colony PCR for screening insertion of guide oligonucleotides (sgDNA) or homology arms. Transformed *E. coli* DH5 α colony was inoculated into 10 μ L of PCR reaction mixture. The volumes of the reagents were scaled according to number of samples that was prepared. For screening insert of sgDNA the primers CRISPR_FF_For and sgDNA_Rev were used, whereas CRISPR_FF_For and CRISPR_FF_Rev were used for verification of insertion of homology arms.

Reagents	Volume [μ L]
OneTaq 2 Master Mix with Standard Buffer	5
Primer For (10 μ M)	0.2
Primer Rev (10 μ M)	0.2
DMSO	0.4
Deionised water	4.2

Table B.19: Thermocycler settings for colony PCR. The following program was used to verify insertion of single guide oligonucleotides and homology arms.

Step	Temperature [°C]	Time	Cycle
Initial denaturation	94	5 min	1
Denaturation	94	30 s	
Annealing	60	60 s	30
Elongation	68	60 s/kbp	
Final elongation	72	5 min	1
Hold	4	∞	-

Table B.20: Composition of reagents for restriction digestion. The reaction mixture (50 μ L) was incubated at 37°C for 30 min. X: Required volume of DNA to obtain the desired amount.

Reagents	Volume [μ L]
<i>Spe</i> I	1
CutSmart buffer (10 \times)	5
DNA (100-1000 ng)	X
Deionised water	44 - X

To generate the homology arms in the CRIPSR-Cas9 systems, upstream and downstream fragments to the target genes were amplified (Table B.21). The size of each fragments were between 465 and 769 bp. To amplify the upstream and downstream regions to *cnf1* and *tcpC* the thermocycler was programmed with the settings given in Table B.22. The annealing step was modified to temperature 52°C for 30 s in order to amplify the upstream and downstream regions to *hlyA*.

Table B.21: Reagents for amplification of upstream and downstream regions to target genes. The genomic DNA (gDNA) of *E. coli* UPEC 3 was used as template DNA. To amplify the downstream regions, primers with the suffixes DS_XbaI_Rev and OE_For were used, whereas primers with US_XbaI_For and OE_Rev suffixes were utilised to amplify the upstream regions. The final volume of the reaction mixture was 20 μ L.

Reagents	Volume [μ L]
Forward primer (10 μ M)	0.6
Reverse primer (10 μ M)	0.6
KOD hot start master mix	10
gDNA (40 ng \leq)	X
Deionised water	8.8 - X

Table B.22: Thermocycler setting for amplification of downstream and upstream regions to *cnf1* and *tcpC*.

Step	Temperature [°C]	Time	Cycle
Polymerase Activation	95	2 min	1
Denaturation	95	20 s	
Annealing	55	10 s	35
Elongation	70	15 s/kbp	
Hold	4	∞	-

To amplify the downstream and upstream region to *ompT* and *dsbA*, Q5 hot start master mix was used. The reaction mixtures were prepared as given in Table B.23 and amplified with the settings given in Table B.30.

Table B.23: Reagents for amplification of upstream and downstream regions to *dsbA* and *ompT*.

Reagent	Volume [μ L]
Forward primer (10 μ M)	1.25
Reverse primer (10 μ M)	1.25
Q5 Hot Start High-Fidelity 2 \times Master Mix	12.5
gDNA (43 ng/ μ L)	3
Deionised water	7

Table B.24: Thermocycler settings cloning upstream and downstream regions to *dsbA* and *ompT*.

Step	Temperature [°C]	Time	Cycle
Polymerase Activation	98	30 s	1
Denaturation	98	10 s	
Annealing	61.5	30 s	30
Elongation	72	30 s	
Final elongation	72	2 min	1
Hold	4	∞	-

The PCR products of upstream and downstream regions were separated and isolated from gel with QIAquick Gel Extraction Kit (QIAGEN) after following the protocol provided by the manufacturer. Briefly, three volumes of QG buffer was added to 1 volume of the sliced gel with DNA (100 mg gel approx. 100 μ L) and incubate at 50°C for 10 min until the gel

was completely dissolved. If the colour of the dissolved gel solution was orange, the pH of the solution was adjusted with 10 μL of 3M sodium acetate. 1 gel volume of isopropanol was added to the gel solution and mixed by inverting and the samples were loaded to a spin column. After centrifuging at 17 900 $\times g$ for 1 min, the flow-through was discarded. This step was repeated until all samples were loaded onto the column. 500 μL of QG buffer was added to the column and centrifuged at 17 900 $\times g$ for 1 min. DNA was washed with 750 μL of PE buffer and the column was centrifuged at 17 900 $\times g$ for 1 min. The empty column placed to a new 2 mL collection tube and was centrifuged for 1 min to remove residual ethanol. 50 μL of EB buffer was added to the column and incubated at room temperature for 1 min, before the DNA was eluted by centrifuging at 17 900 $\times g$ for 1 min.

Isolated upstream and downstream DNA fragments were fused together via overlap extension PCR by preparing the solution given in [Table B.25](#). The upstream and downstream fragments to *cnf1* and *tcpC* were fused after incubating the reaction mixtures in a thermocycler with the same settings given in [Table B.22](#). For fusion of the upstream and downstream regions to *hlyA*, the temperature and the duration of the annealing step were set to 49°C and 30 s, respectively. The annealing temperature was set to 54°C for fusing the upstream and downstream sequences of *ompT*.

Table B.25: Composition of reagents for overlap extension PCR. Reaction mixture (30 μL) for fusion of upstream and downstream regions to target genes via overlap extension PCR. X: Required volume of downstream fragment. Y: Required volume of upstream fragment.

Reagents	Volume [μL]
KOD hot start master mix	15
Downstream fragment (50 ng)	X
Upstream fragment (50 ng)	Y
Deionised water	15 - X - Y

Finally, the fused fragments were enriched by adding 0.6 μL of each primers with the suffixes US_XbaI_For and DS_XbaI_Rev, 10 μL KOD hot start master mix and 8.8 μL deionised water directly into the previous reaction mixture, which gives a total reaction volume of 50 μL . The thermocycler was programmed according to [Table B.26](#) to enrich the fused upstream and downstream fragments to *cnf1* and *tcpC*, whereas the annealing step was modified to 60°C for 30 s for enriching the fused fragments to *hlyA*. The fused upstream and downstream fragments of *ompT* were amplified after the annealing temperature was set to 65.5°C for 30 s.

Table B.26: Settings for enrichment of overlap extension PCR products.

Step	Temperature [°C]	Time	Cycle
Polymerase Activation	95	2 min	1
Denaturation	95	20 s	
Annealing	55	10 s	30
Elongation	70	20 s/kbp	
Hold	4	∞	-

Fusion of the upstream and downstream sequences of *dsbA* was conducted with similar approach, but Q5 polymerase was used instead. The composition of the reagents and thermocycler settings are listed in [Table B.27](#) and [Table B.28](#)

Table B.27: Composition of reagents for fusing upstream and downstream sequences of *dsbA*. Upstream (US) and downstream (DS) sequences of *dsbA* were used with Q5 Hot Start High-Fidelity Master Mix

Reaget	Volume [μ L]
US (19 ng/ μ L)	2.6
DS (11 ng/ μ L)	4.5
Q5 Hot Start High-Fidelity 2 \times Master Mix	15
Deionised water	7.9

Table B.28: Thermocycler settings for fusing upstream and downstream sequences of *dsbA*.

Step	Temperature [°C]	Time	Cycle
Polymerase Activation	98	30 s	1
Denaturation	98	10 s	
Annealing	67	30 s	30
Elongation	72	20 s	
Final elongation	72	2 min	1
Hold	4	∞	-

The homology arms of *dsbA* were enriched after adding the reagents in [Table B.29](#) and incubated with the settings given in [Table B.30](#).

Table B.29: Reagents for enrichment of homology arms of *dsbA*.

Reagent	Volume [μ L]
dsbA_DS_XbaI_Rev (10 μ M)	1
dsbA_DS_XbaI_For (10 μ M)	1
Q5 Hot Start High-Fidelity 2 \times Master Mix	10
Deionised water	8

Table B.30: Thermocycler settings for enrichment of homology arms of *dsbA*.

Step	Temperature [$^{\circ}$ C]	Time	Cycle
Polymerase Activation	98	30 s	1
Denaturation	98	10 s	
Annealing	68	30 s	30
Elongation	72	33 s	
Final elongation	72	2 min	1
Hold	4	∞	-

The enriched DNA fragments were isolated from gels after gel electrophoresis, followed with digestion of the ends of the fused fragments with restriction enzyme *XbaI* (Table B.31) at 37 $^{\circ}$ C for 1 h.

Table B.31: Restriction digestion of overlap extension PCR product. Restriction digestion of fused upstream and downstream fragment to target genes. The final volume of the reaction mixture was 50 μ L.

Reagents	Volume [μ L]
<i>XbaI</i>	1
CutSmart buffer (10 \times)	5
DNA (100-1000 ng)	X
Deionised water	46 - X

After restriction digestion, the fused fragments (inserts) were inserted into the vector, pCRISPR with single guide oligonucleotides by overnight ligation at 16 $^{\circ}$ C. The amount of insert needed for the ligation reaction was calculated by [NEBioCalculator](#) according to the size of the insert and vector as well as the mass of the vector in the reaction mixture. The molar insert:vector ratio in the reaction mixture was set to 3:1 (Table B.32).

Table B.32: Overnight ligation. Ligation of homology arms (insert) and pCRISPR with single guide nucleotide (vector). The molar ratio between insert and vector was set to 3:1 and the volume of insert that is required in the ligation mixture was calculated by [NEBioCalculator](#). The final volume of the solution was 20 μ L. X: Volume of insert. Y: Volume of vector.

Reagents	Volume [μ L]
T4 DNA ligase	1
T4 DNA ligase buffer (10 \times)	2
Insert	X
Vector (50 ng)	Y
Deionised water	17 - X - Y

After overnight ligation of insert and vector, 5 μ L of the ligation product was used to transform *E. coli* DH5a as described in section [section 3.4.1](#). To verify colonies that harbour plasmids with homology arms, the plasmids were isolated from an overnight culture and digested with the restriction enzyme *EcoRI*. The reaction mixture for digesting the plasmids with *EcoRI* was prepared according to [Table B.31](#), where *XbaI* was exchanged with *EcoRI*. Alternatively, the colonies were verified by PCR as described earlier. Finally, the plasmids were also prepared for LightRun sequencing (Eurofins Genomics).

Unfortunately some of the single guide sequence was not cloned into the plasmids. Since the length of the guide oligonucleotide including the compatible sticky ends for *BsaI* is only 24 bp, the deviation between plasmids with and without insert of guide sequence could not be distinguished by electrophoresis. In stead, the reverse single guide sequences were used together with CRISPR_FF_For primer to verify positive colonies.

C Example calculations

C.1 Transformation efficiency

To investigate which method is most efficient for transforming UPEC3 with plasmids, the transformation efficiency was calculated from number of colony forming unit (cfu), amount of plasmids that was used and the dilution factor, which is the ratio between the total volume of bacteria solution and the actual volume plated on LB plate (Equation 1).

$$\text{Transformation efficiency} = \frac{\text{cfu}}{\mu\text{g plasmids}} \times \text{dilution factor} \quad (1)$$

In this study, 0.15198 μg plasmids were added to 50 μL of chemical or electrocompetent UPEC3. The number of cfu obtained from heat shock was 25. After incubation with 900 μL of LB medium for 1.5 h, the bacteria were pelleted and 800 μL of supernatant was discarded. The pellet was resuspended with the remaining supernatant (150 μL), and all of the bacteria solution was plated on LB plate with antibiotics. Since all of the bacteria were plated, the dilution factor will be 1. Thus, the transformation efficiency will be,

$$\text{Transformation efficiency} = \frac{25 \text{ cfu}}{0.15198 \mu\text{g plasmids}} \times 1 = 164.5 \text{ cfu}/\mu\text{g}$$

C.2 Genome editing efficiency

The genome editing efficiency of pCRISPR constructs with and without homologous arms were compared after UPEC3 harboring pCas9 were transformed with equal mole of either pCRISPR_cnf1_sg2 or pCRISPR_Harm_cnf1_sg2. After 41 to 45 h of incubation, 19 random colonies were picked from each plate with bacteria transformed with pCRISPR_cnf1_sg2 or pCRISPR_Harm_cnf1_sg2 and each colony was prepared for colony PCR. The PCR products were separated with electrophoresis and the DNA fragments were visualized after post-staining the gel with GelRed and exposing the gel to UV light. The expected size of the DNA fragment after successful deletion of *cnf1* is 1859 bp, while colonies with unsuccessful knockout of the gene will obtain a PCR product with a size of 4903 bp. To calculate the genome editing efficiency, the total number of colonies with a 1859 bp DNA fragment was divided with total number of colonies that were picked for screening. For instance eight out of 19 colonies obtained a single 1859 bp fragment, which gives a editing efficiency of 42 %.

C.3 Generation time

In general, when bacteria are grown in flasks, the growth cycle of the bacteria can be described by measuring the growth curve. The growth curve can roughly be divided into four phases, namely the lag phase, exponential phase, stationary phase and death phase. In short, the lag phase is usually the time interval from microbial cultures were inoculated into fresh media and until the microbes reach the exponential phase. In the lag phase, the microbes are growing relatively slowly, and the duration of the lag phase can be affected upon change of growing conditions and the history of the inoculum. In the exponential phase, the population is doubling with regular intervals and is growing exponentially. In addition to growing conditions, the rates of exponential growth may also be affected by genetic characteristics. When the bacteria culture reaches the stationary phase, the growth of bacteria is limited and the growth rate is zero. Hence, the population size neither increases or decreases. Finally, the cells enter the death phase, where the population decreases exponentially, but with a slower rate compared with the exponential growth [103].

To determine the growth rate of a species, the generation time (g), which is the time a population requires to double its size, is estimated during exponential growth. During exponential growth, the number of cells can be expressed mathematically (Equation 2), where N , N_0 and n are respectively the final cell number, initial cell number and number of generations during the exponential growth [103].

$$N = N_0 2^n \quad (2)$$

Given that the generation time is defined as in Equation 3, where t is the duration of exponential growth.

$$g = \frac{t}{n} \quad (3)$$

By solving Equation 2 with regard to n , we can get the relationship as shown in Equation 4

$$n = \frac{\ln N - \ln N_0}{\ln 2} \quad (4)$$

The Equation 4 can also be applied to estimate the generation time of a bacteria species by measuring the turbidity of a bacteria culture.

Given that the duration of the exponential phase is approximately 1.5 hours. The initial optical density of the culture at the beginning of the exponential growth is $N_0 = 0.045$, while the final optical density at the end of the exponential growth phase is $N = 0.295$. Thus, number of generations during the exponential growth is,

$$n = \frac{\ln 0.295 - \ln 0.046}{\ln 2} = 2.681$$

The generation time will be,

$$g = \frac{1.5 \text{ h}}{2.681} = 0.559 \text{ h} = 33 \text{ min}$$

C.4 Number seeded cells

The infection experiments in this study was chosen to 6.0×10^5 cells per well. The volume of seed cells in each well is 2 mL. Thus the concentration of cells per well is,

$$\frac{6.0 \times 10^5 \text{ cells}}{2 \text{ mL}} = 3.0 \times 10^5 \text{ cells/mL}$$

For an experiment which require seeding 24 wells with cells, we will need at least 48 mL of THP-1 cells. Due to mechanical loss under the preparation and seeding process, we make 50 mL of cell solutions. After the THP-1 cells were up-concentrated and counted with profile C, the THP-1 cells in the up-concentrated solution was 2.363×10^6 cells. Thus the volume of cells that are needed to dilute in medium is,

$$\frac{3.0 \times 10^5 \text{ cells} \times 50 \text{ mL}}{2.363 \times 10^6 \text{ cells}} = 6.3 \text{ mL}$$

The volume of RPMI medium with 10 % FBS and L-glutamin is 43.7 mL. Finally, 3 μ L of PMA was added to the diluted cell solutions before equally distributing the cells to the multiwell plate (2 mL/ well).

C.5 Bacteria for cell infection

All of the infection experiments in this study had a multiplicity of infection (MOI) of 2. For two and four hour infection experiment, where THP-1 cells were either treated with non-silencing or FIP2-silencing oligoes, we required a number of bacteria for each strain that is enough for infecting THP-1 cells in four wells. Due to pipetting error, the number of bacteria was increased so the bacteria solution is enough for five wells. In addition, the amount of bacteria was also scaled up ten times for easier detection of bacteria pellet during washing and prevent massive loss of bacteria. Thus the total amount of bacteria that is required for each strain is,

$$6.0 \times 10^5 \text{ cells} \times 2 \times 5 \text{ wells} \times 10 = 6.0 \times 10^7 \text{ bacteria}$$

The concentration of bacteria in fresh diluted bacteria cultures can be estimated by measuring the optical density (OD_{600}). Number of bacteria per mL is converted from OD_{600} by [Agilent Genomics: Tools - Bio Calculators](#). This online calculator for estimating bacteria concentration is based on the relationship between OD_{600} of 1.0 equals to 8×10^8 bacteria cells/mL. For instance when OD_{600} for a bacteria culture is 0.3, the calculated bacteria concentration is 2.4×10^8 . Thus, the volume that is required to take out from the bacteria culture is,

$$\frac{6.0 \times 10^7 \text{ bacteria}}{2.4 \times 10^8 \text{ bacteria/mL}} = 0.25 \text{ mL}$$

C.6 LDH release

The absorbance of each sample was measured at 490 nm (Abs_{490}) and at 680 nm (Abs_{680}). The LDH activity is determined by subtracting the Abs_{680} value from Abs_{490} value. All of the LDH activity values were normalised to the non-silenced cells that were only treated with medium throughout the experiment. Finally, to calculate LDH release in percentage, the average of the positive control for maximum release of LDH was used ([Equation 5](#)).

$$LDH\% = \frac{\text{Sample} - \text{Medium}}{\text{Positivecontrol} - \text{Medium}} \times 100\% \quad (5)$$

For instance the LDH activity of THP-1 cells that were infected with UPEC3 wild type is 0.829 after subtracting Abs_{680} value from Abs_{490} value. The average value of duplicates of medium control after subtracting Abs_{680} value from Abs_{490} value is 0.219. The average of triplicates of the LDH release positive control is 2.73. Therefore the LDH release in THP-1 cells infected with UPEC3 wild type will be,

$$\frac{0.829 - 0.219}{2.73 - 0.219} \times 100\% = 24.3\%$$

C.7 Relative quantification value

The expression level of pro-inflammatory genes, pro-IL-1 β , NLRP3, TNF α and IFN β were measured with TaqMan Q-PCR. The relative quantification (RQ) value is a measure of expression level of a gene of interest in fold change relatively to calibrator, which is the non-silenced THP-1 cells treated with medium. Moreover, we also need to measure the expression

level of an endogenous gene, the TATA-box binding protein (TBP). Each cycle, the Q-PCR machine measures the fluorescence that is emitted from the reporter fluorophore. Reporter fluorophore only emits light when it is released from the probe due to degradation by the DNA polymerase. The fluorescence intensity increases with accumulation of reporter fluorophore. After a certain number of cycles, the real fluorescence signal is detected when the intensity is beyond a threshold value at the exponential phase, this value is also defined as the Ct value.

The Ct values are then used to calculate the RQ values. First, the delta Ct (ΔCt) value is calculated from the Ct values, which is defined in [Equation 6](#), where Ct_x is the Ct value of gene of interest in sample x and $Ct_{E,x}$ is the Ct value of endogenous gene in sample x.

$$\Delta Ct_x = Ct_x - Ct_{E,x} \quad (6)$$

The delta delta Ct ($\Delta\Delta Ct$) is then calculated from ΔCt ([Equation 7](#)), where ΔCt_M is the delta Ct value of the calibrator, which is the medium control in our case.

$$\Delta\Delta Ct = \Delta Ct_x - \Delta Ct_M \quad (7)$$

Given that the RQ value is,

$$RQ = 2^{-\Delta\Delta Ct} \quad (8)$$

we can combine [Equation 6](#), [Equation 7](#) and [Equation 8](#) together to one equation ([Equation 9](#)).

$$RQ = 2^{-\Delta\Delta Ct} = 2^{-(Ct_x - Ct_{E,x} - Ct_M + Ct_{E,M})} = \frac{2^{Ct_M - Ct_x}}{2^{Ct_{E,M} - Ct_{E,x}}} \quad (9)$$

For instance the mean Ct value of pro-IL-1 β from duplicates in non-silenced THP-1 cells stimulated with LPS and nigericin is 19.07, while the medium control has a mean Ct value of 18.89. The mean Ct value of TBP of the medium control and the nigericin stimulated cells are 28.86 and 30.64, respectively. Thus the RQ value is

$$\frac{2^{18.89-19.07}}{2^{28.86-30.64}} = 3.00$$

C.8 Relative protein levels

Quantified blot densities of protein of interest and β -tubulin in cell lysates were used to calculate relative protein levels. As examples, the blot densities given in [Table C.33](#) are used in this calculation.

Table C.33: Blot densities. Quantified blot densities of β -tubulin and NLRP3 in cell lysates of unstimulated NS RNA cells and cells stimulated with $\Delta tcpC$.

Treatment	Density	
	β -tubulin	NLRP3
Medium	0.782	0.415
$\Delta tcpC$	0.501	0.718

NLRP3 densities of unstimulated and $\Delta tcpC$ stimulated cells are normalised according to [Equation 10](#), where \bar{P}_y is the normalised signal of protein of interest, while P_y , T_y and T_x are the quantified blot densities of protein of interest and β -tubulin, respectively. x and y designate unstimulated cells and stimulated cells, respectively.

$$\bar{P}_y = \frac{P_y \times T_x}{T_y} \quad (10)$$

Thus normalised NLRP3 in $\Delta tcpC$ stimulated cells is,

$$\bar{P}_{\Delta tcpC} = \frac{0.718 \times 0.782}{0.501} = 1.12$$

similarly, normalised NLRP3 in unstimulated cells is calculated to be 0.415.

Fold change or relative NLRP3 protein levels in $\Delta tcpC$ stimulated cells is calculated with [Equation 11](#).

$$R_y = \frac{\bar{P}_y}{\bar{P}_x} \quad (11)$$

Thus the relative NLRP3 protein levels in $\Delta tcpC$ stimulated cells is,

$$R_{\Delta tcpC} = \frac{1.12}{0.415} = 2.70$$

Calculation of RQ standard deviation was omitted since the standard deviation of Ct values was small.

C.9 Enzyme-linked immunosorbent assay

The total amount of pro-IL-1 β and IL-1 β in the supernatants was estimated based on the standard curve of the relationship between absorbance and concentration IL-1 β . The standard curve was generated from seven serial diluted samples of IL-1 β as described in [section 3.13](#). The absorbance was measured at 450 nm and 570 nm, and the absorbance value at 570 nm was subtracted from the absorbance value at 450 nm to correct imperfection of the plate. The absorbance of the blank was also subtracted from samples. The average optical density (OD) of duplicates of sample standards were calculated and plotted against the concentration of IL-1 β ([Figure C.1](#)).

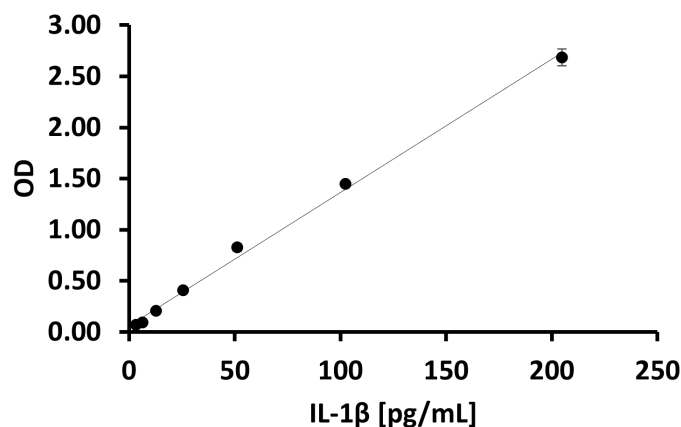


Figure C.1: Standard curve of IL-1 β . The standard curve of IL-1 β was generated from measuring the absorbance of duplicates of sample standards. The optical density (OD) is the the value of absorbance at 570 nm subtracted from the absorbance at 450 nm and blank correction. A curve was fitted through the data points with linear regression. The relationship between OD and the concentration of IL-1 β is $f(x) = 0.013x + 0.0629$, where $f(x)$ and x correspond to OD and the concentration of IL-1 β , respectively. The R^2 value of the fitted model is 0.9966.

Based on the standard curve, the concentration of total pro-IL-1 β and IL-1 β in the supernatants can be graphically estimated when the optical density of the sample is known. Alternative, the concentration can be calculated by solving the fitted model with regard to x ([Equation 12](#)) and the dilution factor of the sample. $f(x)$ and x correspond to OD and the concentration of IL-1 β , respectively.

$$f(x) = 0.013x + 0.0629 \tag{12}$$

For instance the OD value of a hundred times diluted sample is 1.41, then the concentration of IL-1 β is,

$$x = \frac{1.41 - 0.0629}{0.013} \times 100 = 10\,386 \text{ pg/mL}$$

D Results

D.1 Cloning CRISPR-Cas9 constructs

Oligonucleotides for guide annealing (sgRNA) were inserted to pCRISPR via Golden Gate Assembly approach. The product was used to transform DH5 α . DH5 α with the correct construct was verified after plasmids extraction and digestion with the restriction enzymes *Bsa*I and *Spe*I (Figure D.2A) or by PCR with the designed primers sgDNA_Rev and CRISPR_FF_For (Figure D.2B). Either way, the expected sizes of the DNA fragment which indicates insertion of sgDNAs are 2423 bp and 1538 bp after restriction digestion and colony PCR, respectively. Constructs that failed to insert the sgDNAs, had a size of 1822 bp when amplified with the designed primers, whereas four bands with a length of 1285 bp, 1138 bp, 239 bp and 35 bp were obtained after digestion of an empty vector with the restriction enzymes *Bsa*I and *Spe*I. Shown in Figure D.2A, pre-staining the gel with GelRed affected the migration of DNA. This problem was solved by staining the gels after electrophoresis (Figure D.2B). As an example of pCRISPR construct with inserted sgRNA is illustrated in Figure D.7A.

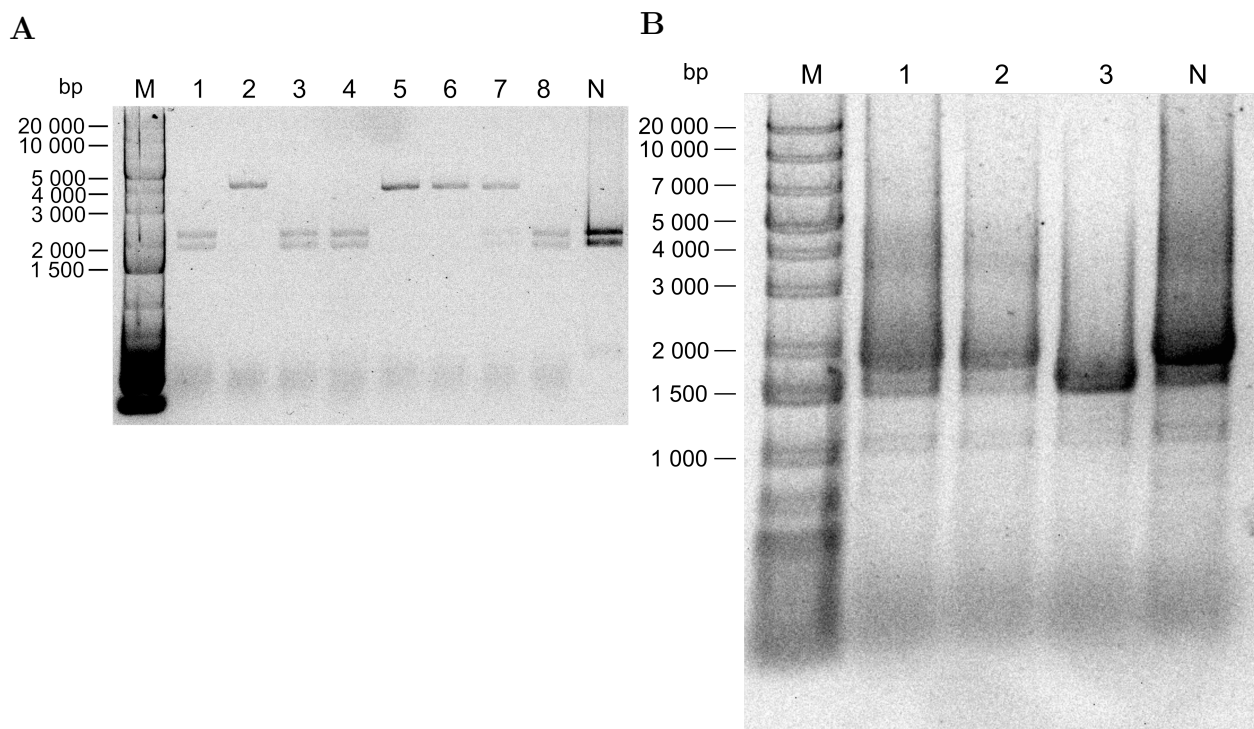


Figure D.2: Verification of insertion of oligonucleotides for guide annealing (sgDNA). Isolated plasmids which potentially have insert of single guide sgDNA were digested with the restriction enzymes *BsaI* and *SpeI*. The expected size of the restricted plasmid with sgDNA is 2423 bp (**A**). Colony PCR of transformed *E. coli* DH5a with pCRISPR and insert of sgDNA. Colonies with correct inserted sgDNAs were screened with the designed primers sgDNA_Rev and CRISPR_FF_For. The expected size of the amplicon is 1538 bp, whereas the size of the DNA fragment amplified from an vector without any sgDNA is 1822 bp (**B**). M: GeneRuler 1kb Plus DNA ladder. N: Negative control (empty pCRISPR).

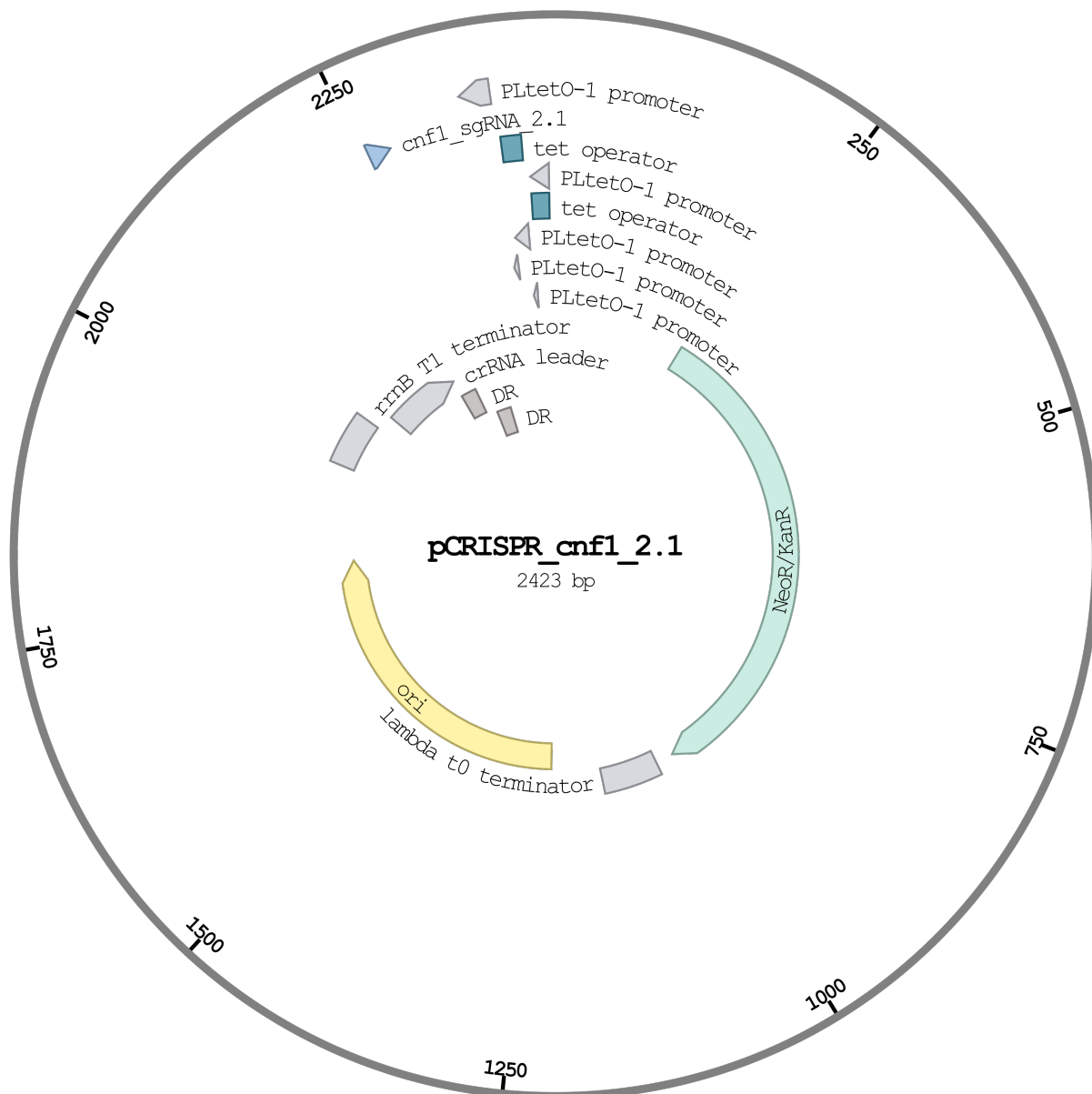


Figure D.3: Designed pCRISPR construct without homology arm. Guide oligo (cnf1_sgRNA.2.1) was designed by the online platform [Benchling](#), and the cloning procedure for generating the pCRISPR-construct was simulated in Benchling.

Similarly, successful insertion of the homology arms into the plasmids were verified by restriction digestion of the plasmids by the enzyme *EcoRI* or by performing colony PCR with the primer pairs CRISPR_FF_For and CRISPR_FF_Rev. After digesting the plasmids with homology arms, the expected size of the *cnf1*, *hlyA* and *tcpC* targeting constructs are 3677 bp, 3737 bp, 3389 bp, respectively. Alternatively, the expected sizes of the DNA fragments obtained from colony PCR with insertion of homology arms are 1633 bp, 1687 bp and 1339 bp for *cnf1*, *hlyA* and *tcpC* targeting constructs, respectively. *dsbA* and *ompT* targeting pCRISPR constructs were verified by colony PCR with expected size of successful insert of homology arms 1470 bp and 1739 bp, respectively. [Figure D.6](#) illustrates pCRISPR construct

with homology arm.

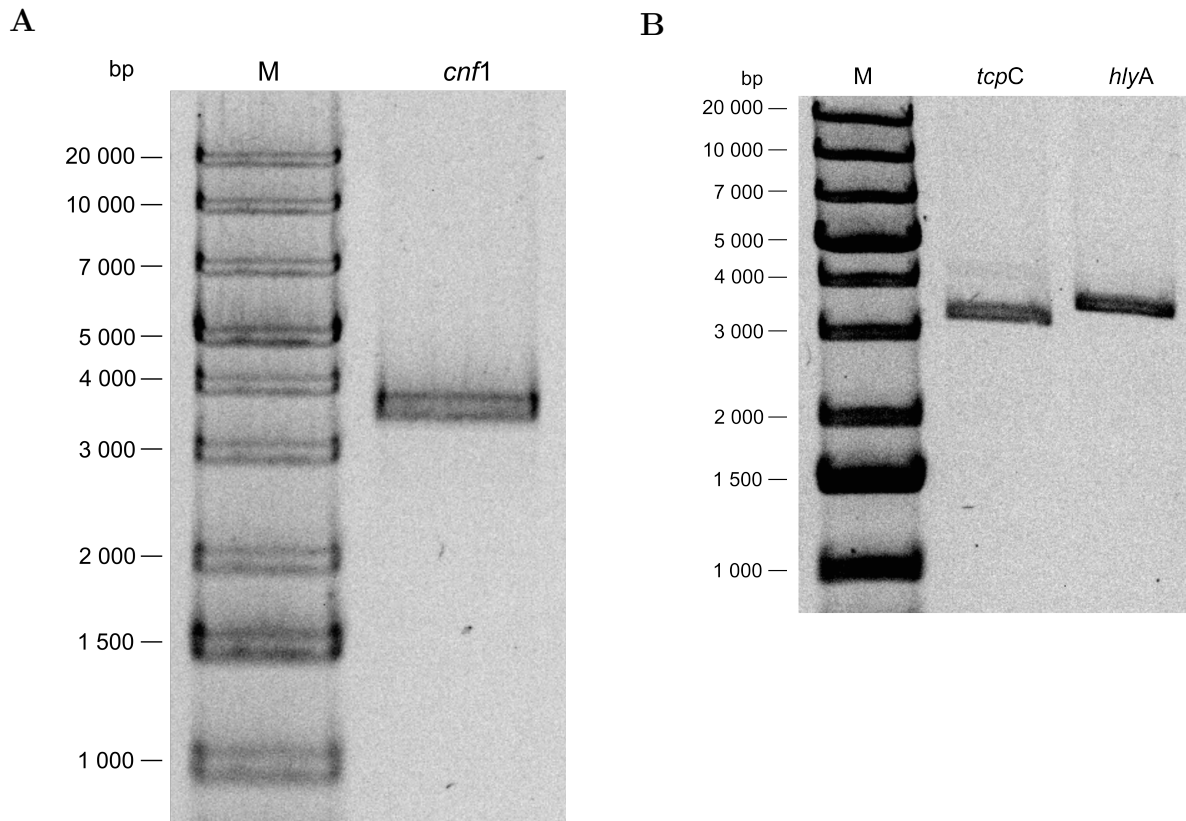


Figure D.4: Verification of insertion of homology arms by restriction digestion. Isolated plasmids which potentially have insert of homology arms were digested with the restriction enzyme *EcoRI*. The expected size of the restricted plasmids which target *cnf1* (**A**), *hlyA* (**B**) or *tcpC* (**B**), have a length of 3677 bp, 3737 bp and 3389 bp, respectively.

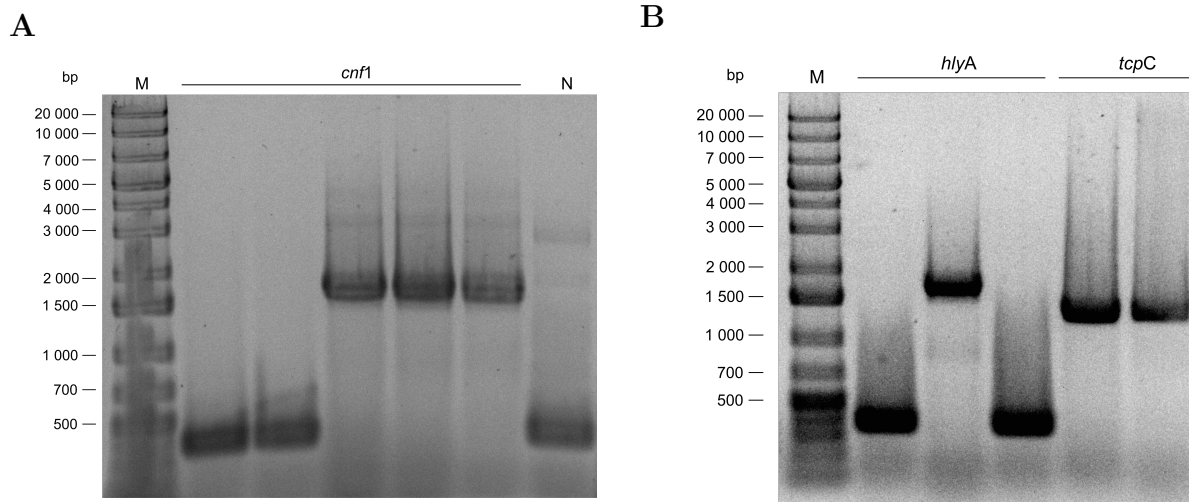


Figure D.5: Verification of homology arms inserted in constructs by colony PCR. The region of insertion of homology arms in pCRISPR were amplified with the designed primer pairs CRISPR_FF_For and CRISPR_FF_Rev. The expected length of the regions where the homology arms are inserted into the plasmids which target *cnf1* (A), *hlyA* or *tcpC* (B) in UPEC3 are 1622 bp, 1687 bp and 1339 bp, respectively.

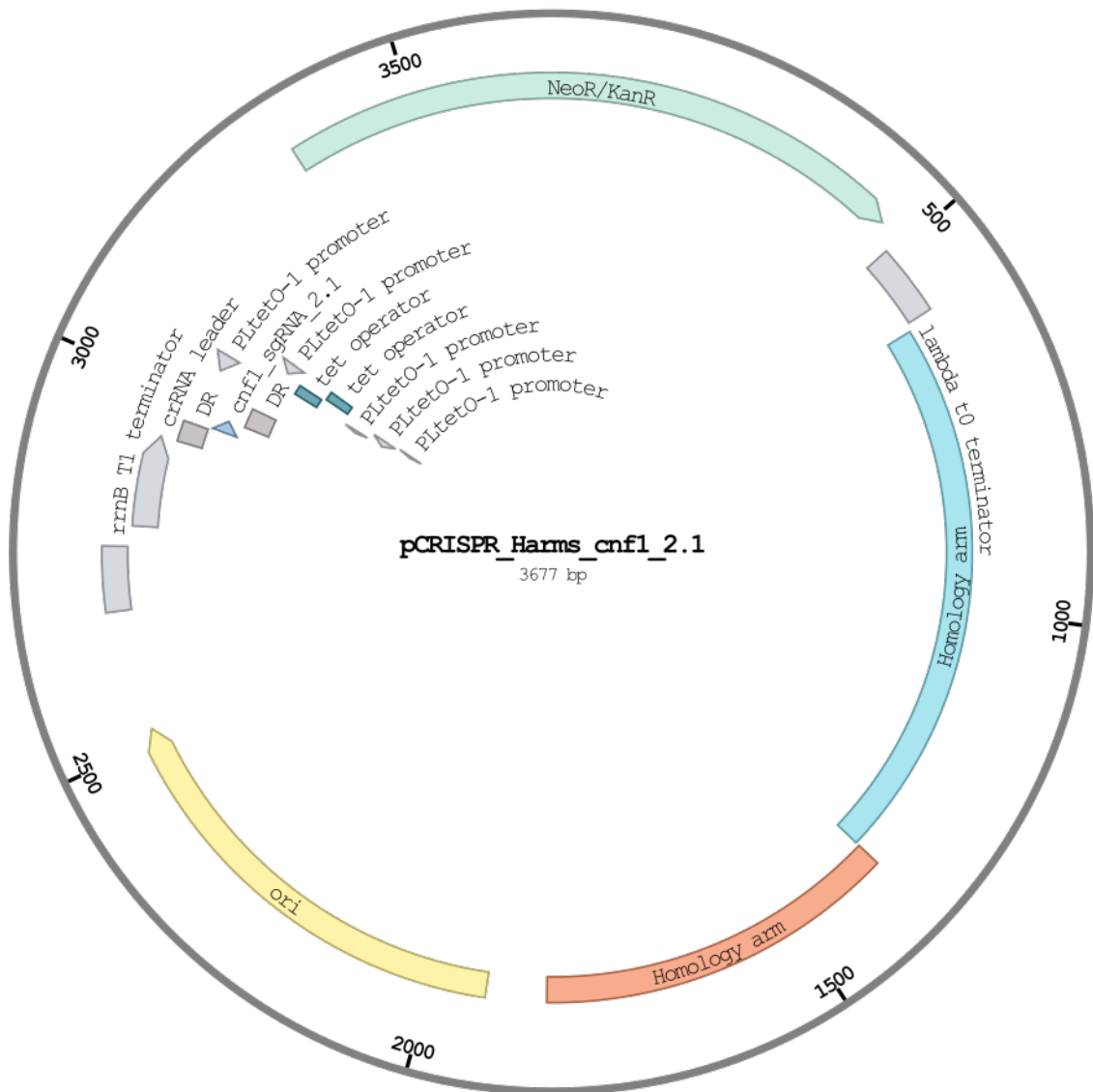
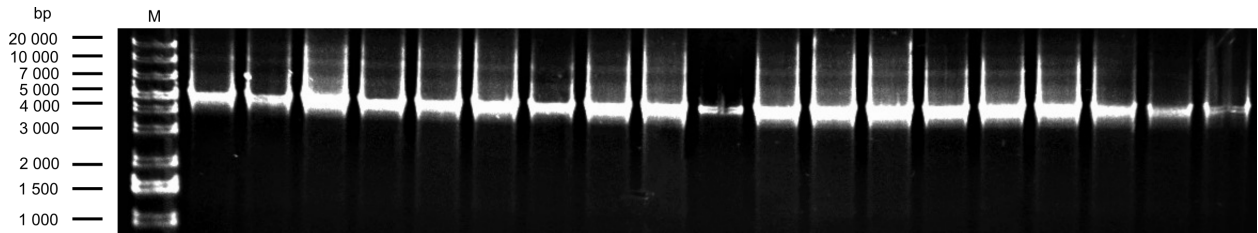


Figure D.6: Designed pCRISPR construct with homology arm. Guide oligo (*cnf1_sgRNA_2.1*) was designed by the online platform [Benchling](#), and the cloning procedure for generating the pCRISPR-construct with homology arms was simulated in Benchling.

D.2 Genome editing efficiency

19 single colonies of UPEC3 transformed with pCas9 and CRISPR constructs targeting *cnf1*, were picked for colony PCR. The PCR primer pairs *seq_cnf1_For* and *seq_cnf1_Rev* were used that either give an 1859 bp amplicon if *cnf1* deletion was successful, or an 4904 bp amplicon if *cnf1* remained intact ([Figure D.7](#)).

A



B

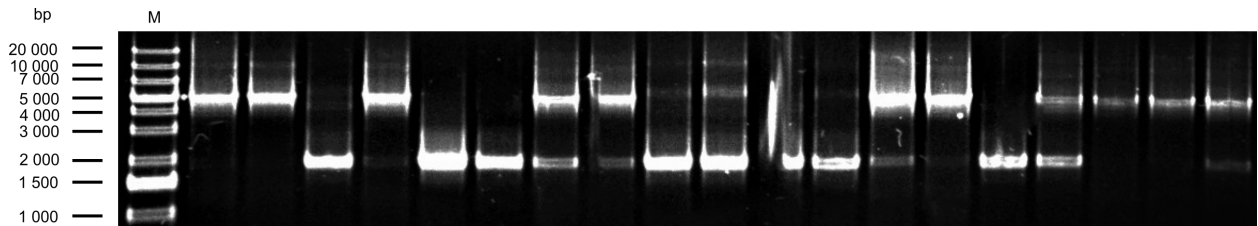


Figure D.7: Colony PCR of transformed UPEC3. Electrocompetent UPEC3 strain harbouring pCas9 was either transformed with pCRISPR_cnf1_sg2, which does not contain homology arms (**A**) or pCRISPR_Harm_cnf1_sg2 with homology arms (**B**). The transformed bacteria, were incubated at 37°C for 41 to 45 hours before picking single colonies for PCR. The primer pairs *cnf1_For* and *cnf1_Rev* were used to amplify the local region of *cnf1*. The expected size of amplicon for successful *cnf1* deletion is 1859 bp, and 4904 bp for unsuccessful deleted *cnf1*.

D.3 Sequence alignment of HlyA expressed in *E. coli* CFT073 and UPEC3 strains

Results from sequence alignment performed by [LALIGN](#) is illustrated in [Figure D.8](#). Local alignment method was selected. Number of reported sub-alignments, E-value threshold, opening gap penalty and extending gap penalty, were respectively set to 3, 10, -12 and -2. By default, BLOSUM50 scoring matrix was used in this alignment.

```

      10      20      30      40      50      60
CFT073 MPTI TTAQI KSTLQSAKQSAANKLHSAQSTKDALKKAEEQTRVAGNRLI LLI PKDYKQ
UPEC3  MPTI TTAQI KSTLQSAKQSAANKLHSAQSTKDALKKAEEQTRVAGNRLI LLI PKDYKQ
      70      80      90     100     110     120
CFT073 GSSLNQLVRTADELGI EVQYDEKNGTAL TKQVFGTAEKLI GLTERGVTI FAPQLDKLLQ
UPEC3  GSSLNQLVRTADELGI EVQYDEKNGTAL TKQVFGTAEKLI GLTERGVTI FAPQLDKLLQ
      130     140     150     160     170     180
CFT073 YQKAGNKGSAENI GDNLGAGSVLSTFQVFLGTALSSMKI DELI KRQKSGSNWSSSEL
UPEC3  YQKAGNKGSAENI GDNLGAGSVLSTFQVFLGTALSSMKI DELI KRQKSGSNWSSSEL
      190     200     210     220     230     240
CFT073 AKASI ELI NQLVDTAASI NNMNSFSQQLNKGSLVSNFKHLTGKVLQNLPLNDI GA
UPEC3  AKASI ELI NQLVDTAASI NNMNSFSQQLNKGSLVSNFKHLTGKVLQNLPLNDI GA
      250     260     270     280     290     300
CFT073 GLDVTSGI LSAI SASFI LSNADADTGTAAAGVELTTKVLGMGKGI SQYII AQRAAQQL
UPEC3  GLDVTSGI LSAI SASFI LSNADADTGTAAAGVELTTKVLGMGKGI SQYII AQRAAQQL
      310     320     330     340     350     360
CFT073 STSAAAAGLI ASWTLAI SPLSFLSI ADKFKRANKI EEYSQRFKLGYDCDSLAAFHKE
UPEC3  STSAAAAGLI ASWTLAI SPLSFLSI ADKFKRANKI EEYSQRFKLGYDCDSLAAFHKE
      370     380     390     400     410     420
CFT073 TGAI DASLTTI STVLASVSSGI SAAATTSLVGAPVSALVAVTGI I SGI LEASKQVFEH
UPEC3  TGAI DASLTTI STVLASVSSGI SAAATTSLVGAPVSALVAVTGI I SGI LEASKQVFEH
      430     440     450     460     470     480
CFT073 VASKMADVI AEVEKHKGNFYFENG/DARHAAPLEDNFKI L SQYNKEYSVERSILI TQQHW
UPEC3  VASKMADVI AEVEKHKGNFYFENG/DARHAAPLEDNFKI L SQYNKEYSVERSILI TQQHW
      490     500     510     520     530     540
CFT073 DTLI GELAGVTRNGDKTL SGSYI DYEEGRLEKPKDEFQKQFDPLKGNL DLSDSKSS
UPEC3  DMLI GELASVTRNGDKTL SGSYI DYEEGRLEKPKDEFQKQFDPLKGNL DLSDSKSS
      550     560     570     580     590     600
CFT073 TLLKFTVPLLTPGEEI RRRRQSGYIEYI TELLVKGMDKVTVKGQDKGSVDYSNLI QHA
UPEC3  TLLKFTVPLLTPGEEI RRRRQSGYIEYI TELLVKGMDKVTVKGQDKGSVDYSNLI QHA
      610     620     630     640     650     660
CFT073 SVGNQYREI RI ESHLGDGDDKVFLSAGSANI YAGKHDMVYDKTDTGYLTI DGTKATE
UPEC3  SVGNQYREI RI ESHLGDGDDKVFLSAGSANI YAGKHDMVYDKTDTGYLTI DGTKATE
      670     680     690     700     710     720
CFT073 AGNYTVTRVLGGDWKI LQEVKKEQSVGKRTKTEKQYRSYEFTHI NGKNTTETDNLYSVE
UPEC3  AGNYTVTRVLGGDWKI LQEVKKEQSVGKRTKTEKQYRSYEFTHI NGKNTTETDNLYSVE
      730     740     750     760     770     780
CFT073 ELI GTTRADKFFGSKFTDI FHGADGDHI EGNDGNDRLYGKGNLTLRGGNGDDQLYGGD
UPEC3  ELI GTTRADKFFGSKFTDI FHGADGDHI EGNDGNDRLYGKGNLTLRGGNGDDQLYGGD
      790     800     810     820     830     840
CFT073 GNDKLI GGTGNMNLNGGEGDELQVQGNLAKNLSGGKGNKLYGSEGADLLDGGEGND
UPEC3  GNDKLI GGTGNMNLNGGEGDELQVQGNLAKNLSGGKGNKLYGSEGADLLDGGEGND
      850     860     870     880     890     900
CFT073 LLLKGGYNDI YRYSQYGHII DDEGGKDKL SLADI DFRDVAFRREGNDLI MYKAEQNV
UPEC3  LLLKGGYNDI YRYSQYGHII DDEGGKDKL SLADI DFRDVAFRREGNDLI MYKAEQNV
      910     920     930     940     950     960
CFT073 LSI GHKNGI TFRNWFBEKESDLSNHQI EQI FDKDGRVI TPDSLKKALEYQSNKASVYV
UPEC3  LSI GHKNGI TFRNWFBEKESDLSNHQI EQI FDKDGRVI TPDSLKKALEYQSNKASVYV
      970     980     990     1000    1010    1020
CFT073 GNDALAYGSDNLI NPLI NEI SKI I SAAGNFDMKEERAAASLLQLSGNASDFSYGRNSI TL
UPEC3  GHDASTYGSQNLINPLI NEI SKI I SAAGNFDMKEERAAASLLQLSGNASDFSYGRNSI TL
      970     980     990     1000    1010    1020
CFT073 TASA
UPEC3  TASA

```

Figure D.8: Sequence alignment of α -hemolysin expressed in *E. coli* CFT073 and UPEC3 strains. The peptide sequences of α -hemolysin were aligned by **LALIGN**. By default, BLUSUM50 scoring matrix was used and number of reported sub-alignments, E-value threshold, opening gap penalty and extendig gap penalty were set to 3, 10, -12 and -2, respectively.

D.4 Post-translational maturation and release of pro-caspase-1 and pro-IL-1 β were affected by bacterial virulence factors

Protein levels of pro-caspase-1 and pro-IL-1 β in the supernatants of THP-1 cells after 2 h and 4 h stimulation with UPEC3 variants (Figure D.9).

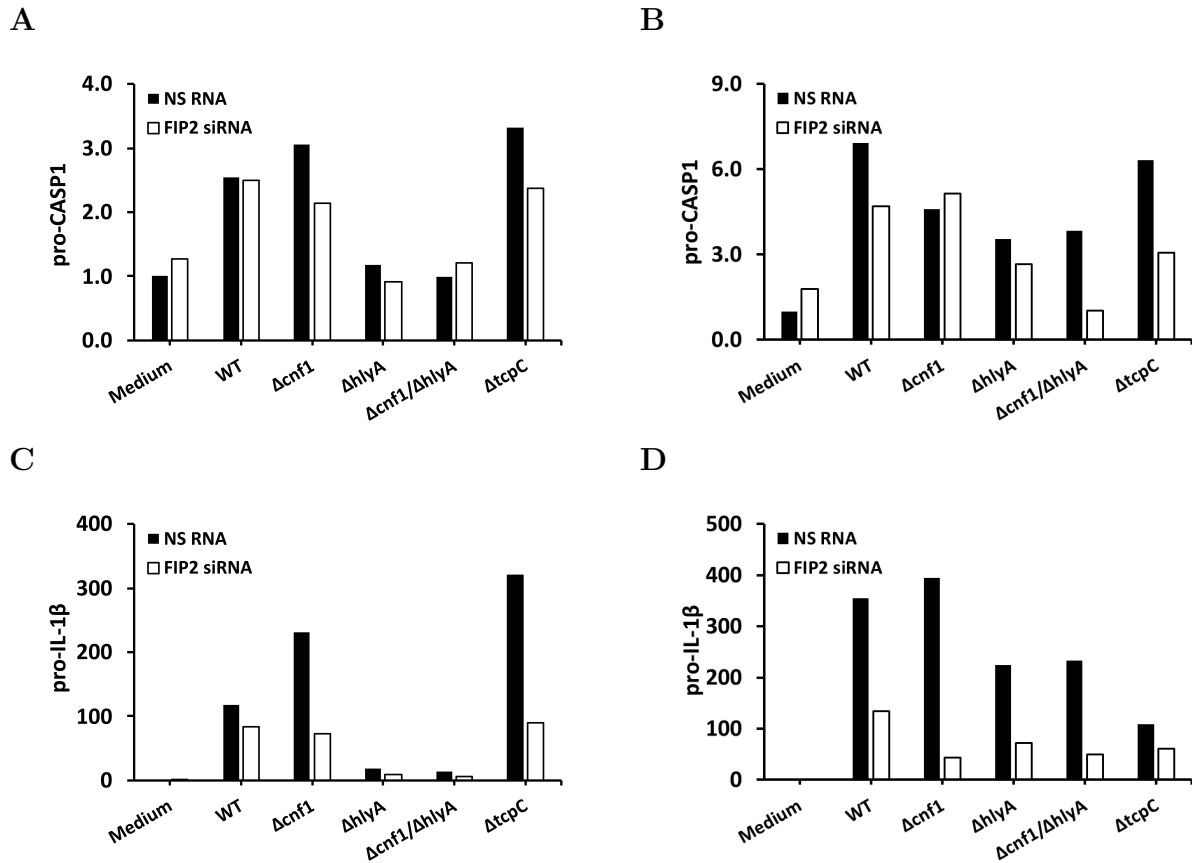


Figure D.9: Pro-IL-1 β and pro-caspase-1 levels in supernatants of THP-1 cells after 2 h and 4 h of stimulation with UPEC3 wild type and mutants. THP-1 cells treated with NS RNA or FIP2 siRNA before stimulation with UPEC3 wild type or mutants for 2 h and 4 h (MOI = 2). Quantification of pro-caspase-1 protein level after 2 h (A) and 4 h (B) stimulation. Quantification of pro-IL-1 β protein level after 2 h (C) and 4 h (D) stimulation.

D.5 LPS priming enhances NLRP3 inflammasome activation

Protein levels of pro-caspase-1 and pro-IL-1 β in the supernatants (Figure D.10) and β -tubulin in lysates (Figure D.11) of LPS primed THP-1 cells stimulated with nigericin, UPEC3 wild type, UPEC3 mutants, CFT073 or DH5 α .

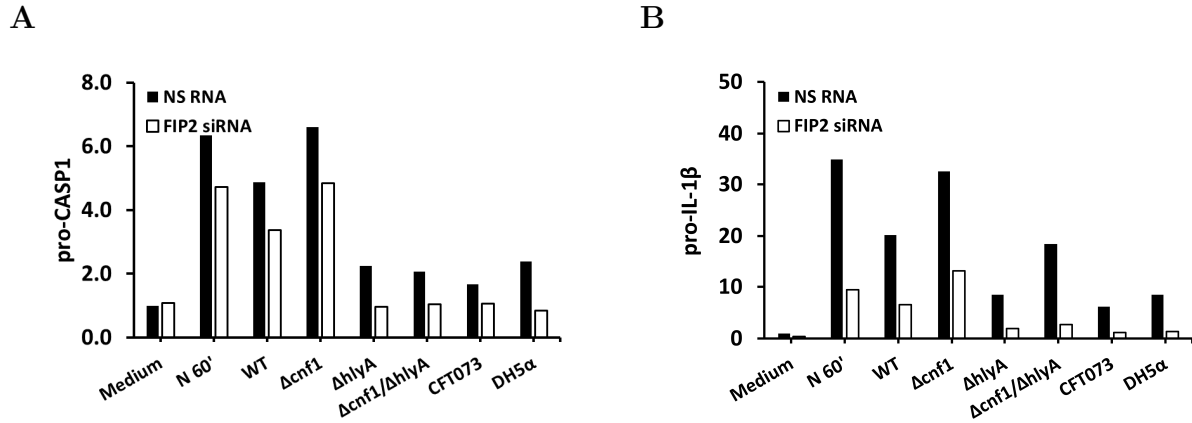


Figure D.10: Quantification of pro-caspase-1 and pro-IL-1 β protein levels in supernatants of THP-1 cells stimulated with nigericin or *E. coli* strains. THP-1 cells were treated with NS RNA or FIP2 siRNA, before LPS priming for 2 h. Primed cells were stimulated with nigericin for 1 h or UPEC3 wild type, UPEC3 mutants, CFT073 and DH5 α for 2 h (MOI = 2). Quantification of pro-caspase-1 protein level (A). Quantification of pro-IL-1 β protein level (B).

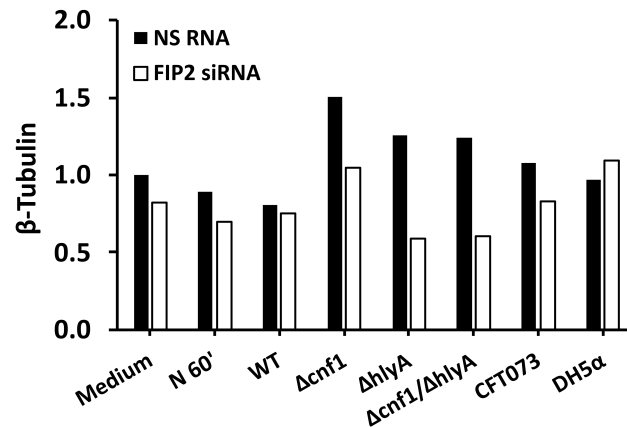


Figure D.11: Quantification of β -tubulin in THP-1 cells stimulated with nigericin, virulent and avirulent *E. coli* strains. THP-1 cells were lipofected with NS RNA or FIP2 siRNA before LPS priming for 2 h (MOI = 2). Primed THP-1 cells were stimulated with nigericin for 1 h or with UPEC3 wild type, UPEC3 mutants, CFT073 or DH5 α for 2 h. β -Tubulin protein levels were normalised to unstimulated NS RNA cells.

